Peristaltic Transport of Realistic Materials in Curved Configurations

By

Farhat Bibi

Reg. No. 90-FBAS/PHDMA/S17

Department of Mathematics and Statistics

Faculty of Basic and Applied Sciences

International Islamic University, Islamabad

2022

PhD
519.23
FAP
c2

curved channel
Mathematics
Numerical analysis

Peristaltic Transport of Realistic Materials in Curved Configurations

By

Farhat Bibi

Supervised By

Dr. Ambreen Afsar Khan

Co-Supervised By

Prof. Dr. Tasawar Hayat

Department of Mathematics and Statistics

Faculty of Basic and Applied Sciences

International Islamic University, Islamabad

2022

Peristaltic Transport of Realistic Materials in Curved Configurations

By

Farhat Bibi

A Thesis
Submitted in the Partial Fulfilment of the
Requirements for the degree of
DOCTOR OF PHILOSOPHY
IN
MATHEMATICS

Supervised By
Dr. Ambreen Afsar Khan

Co-Supervised By
Prof. Dr. Tasawar Hayat

Department of Mathematics and Statistics

Faculty of Basic and Applied Sciences

International Islamic University, Islamabad

2022

Author's Declaration

I, **Farhat Bibi** Reg. No **90-FBAS/PHDMA/S17** hereby state that my Ph.D. thesis titled: **Peristaltic Transport of Realistic Materials in Curved Configurations** is my own work and has not been submitted previously by me for taking any degree from this university, **International Islamic University, Sector H-10, Islamabad, Pakistan** or anywhere else in the country/world.

At any time if my statement is found to be incorrect even after my Graduation the university has the right to withdraw my Ph.D. degree.

Name of Student: **(Farhat Bibi)**
Reg. No. **90-FBAS/PHDMA/S17**
Dated:**31/01/2022**

Plagiarism Undertaking

I solemnly declare that research work presented in the thesis titled: **Peristaltic Transport of Realistic Materials in Curved Configurations** is solely my research work with no significant contribution from any other person. Small contribution/help wherever taken has been duly acknowledged and that complete thesis has been written by me.

I understand the zero tolerance policy of the HEC and University, **International Islamic University, Sector H-10, Islamabad, Pakistan** towards plagiarism. Therefore, I as an Author of the above titled thesis declare that no portion of my thesis has been plagiarized and any material used as reference is properly referred/cited.

I undertake that if I am found guilty of any formal plagiarism in the above titled thesis even after award of Ph.D. degree, the university reserves the rights to withdraw/revoke my Ph.D. degree and that HEC and the University has the right to publish my name on the HEC/University Website on which names of students are placed who submitted plagiarized thesis.

Student/Author Signature: Farhat

Name: **(Farhat Bibi)**

Certificate of Approval

This is to certify that the research work presented in this thesis, entitled: **Peristaltic Transport of Realistic Materials in Curved Configurations** was conducted by **Ms. Farhat Bibi,** Reg. No. **90-FBAS/PHDMA/S17** under the supervision of **Dr. Ambreen Afsar Khan** no part of this thesis has been submitted anywhere else for any other degree. This thesis is submitted to the **Department of Mathematics & Statistics, FBAS, IIU, Islamabad** in partial fulfillment of the requirements for the degree of **Doctor of Philosophy in Mathematics, Department of Mathematics & Statistics, Faculty of Basic & Applied Science, International Islamic University, Sector H-10, Islamabad, Pakistan.**

Student Name: Farhat Bibi **Signature:** Farhat

Examination Committee:

a) **External Examiner 1:**
Name/Designation/Office Address **Signature:**
Dr. Meraj Mustafa
Associate Professor
Department of Mathematics,
School of Natural Sciences, NUST, Islamabad

b) **External Examiner 2:**
Name/Designation/Office Address) **Signature:** qayyub
Dr. Muhammad Ayub
Professor
Department of Mathematics,
Quaid-e-Azam University, Islamabad, Pakistan.

c) **Internal Examiner:**
Name/Designation/Office Address) **Signature:** Khadija
Dr. Khadija Maqbool
Assistant Professor

Supervisor Name:

Dr. Ambreen Afsar Khan **Signature:**

Co-supervisor Name:

Prof. Dr. Tasawar Hayat **Signature:**

Name of HOD:

Dr. Ambreen Afsar Khan **Signature:**

Name of Dean:

Prof. Dr. Muhammad Irfan Khan **Signature:**

Declaration

I hereby declare that this thesis is my work which has been done after admission for the degree of Ph.D. I confirm that I have developed this document on my efforts under the supervision of my supervisor and co-supervisor. This dissertation, as a whole or as a part has not been copied or submitted by others in this or any other university or institute for the completion of the degree.

Signature:----------

Farhat Bibi

PhD Scholar (Mathematics)

Dedicated to

my kids (Fatima, Ibrahim & Qasim)

Acknowledgements

My first and foremost gratitude and thanks goes to **Almighty Allah** for making me enable to proceed in this dissertation successfully. Sure all prays is for Him who created us as best of His creations and granted us strength, health, knowledge, ability and opportunity to achieve our goal. I also extend all affection and devotion to our **Holy Prophet Muhammad (PBUH)** - the beloved of the Almighty and a source of guidance for entire mankind.

Deepest thanks to my valued supervisor **Dr. Ambreen Afsar Khan** who has always been there to help me whenever I needed. This thesis would not have been completed without her sincere and invaluable suggestions, guidance and supervision during the course of my research. Undoubtedly, I learnt a lot from her as she was always ready to extend her sincere help to me. I am also extremely inspired by her as she judiciously maintained the balance in our relation of being ex-class fellows and the supervisor.

I am enormously grateful and indebted to my co-supervisor **Professor Dr. Tasawar Hayat** who has always been a source of inspiration and guidance for me. Without his help and kind support, it would have been impossible to undertake my research. I could start my PhD after a huge gap of 15 years only because of his encouragement and guidance. Despite his extremely busy schedule, he always gave time and provided me the required guidance and his personal support in my academic endeavors.

I am also grateful to **Mr. Asif Iqbal** who was always forthcoming to facilitate me during my PhD. He provided me time and space to do the research despite hectic office routine.

My deepest thanks go to my children - **Fatima, Ibrahim** and **Qasim** as they provided the necessary environment to complete my PhD. A very special gratitude for their love and utmost cooperation as I utilized their valuable time for my research. I am particularly obliged to my loving husband **Nigah Ali** for his untiring support at all levels. At the same time, I am extremely grateful to my highly respected parents

for their prayers and well wishes that kept me working smoothly through all the hard times. I am also thankful to my brothers, sisters and dearest friends **Sara** and **Naheed** for their encouragement and moral support.

I would like to offer my special thanks to my fellows especially **Sidra Shaheen** and **Hira** for their untiring support and an exquisite company throughout. I would like to extend my sincere thanks to all the faculty members specially **Dr. Khadija Maqbool, Dr. Sajida Kausar, Dr. Maliha Rashid** and **Dr. Akbar Zaman** for their assistance at every stage of my course work.

Farhat Bibi

Preface

Peristaltic is an important mechanism in which fluid is transported through successive waves of expansion and contraction propagating together with channel boundaries. This mechanism has widespread applications in physiology and industry. Peristaltic is one of the major mechanisms for transportation of fluid in various biological processes. This is helpful in food swallowing through esophagus, motion of chyme in the gastrointestinal, transportation of urine from kidney to bladder, blood motion in small blood vessels, blood pump via heart and in other reproduction systems etc. In industry, mechanical equipments are designed on this mechanism in order to avoid contamination of outside environment. Its few examples are roller and finger pumps, toxic liquid transport in nuclear industry, tube pumps and hose pumps etc. Many modern medical devices also work on the principle of peristalsis such as the blood in a heart-lung machines and dialysis machines etc. Due to immense application of peristalsis in diversified fields, many researchers explored the peristaltic flow problems while taking into account different conditions and geometries. Maximum work in this field available for straight channels seems not realistic for all situations. Clearly, major chunk of glandular ducts and pipes are found for curved shapes in industrial and physiological systems. This makes it quite attractive and imperative to study the peristalsis in curved configuration.

Further the combined effects of heat and mass transfer result in very complicated mathematical expression between the driving potentials and the fluxes. In these situations the energy flux can be brought not only by the temperature gradient but by composition gradient as well. In view of the above mentioned applications this thesis is organized by taking features of magnetic field, mixed convection, porosity, Soret-Dufour effects, thermal radiation, entropy generation,

variable physical properties of the fluid and electroosmotic effects through curved channel. Boundary conditions for curved channel walls are via physical constraints. This thesis consists of eight chapters and organized in the following fashion.

Chapter one contains brief introduction of peristalsis, literature survey and fundamental equations.

Chapter two addresses the mathematical model of inclined magnetic field for curved geometry. The magneto peristaltic movement of Jeffrey liquids with variable physical characteristics in curved geometry is investigated. Accordingly, the energy expression involves viscous dissipation and variable thermal conductivity. In addition the entropy generation in magneto peristaltic movement of Jeffrey materials together with variable (depending upon temperature) thermal conductivity/ viscosity for curved configurations has been modeled and analyzed. Velocity, heat transfer coefficient, temperature and entropy generation are computed numerically. The graphical analysis is analyzed for pertinent variables. Contents of this work are published in **Part E: Journal of Process Mechanical Engineering (2021) p.09544089211041278.**

Chapter three contains heat and mass transfer in peristalsis of magnetohydrodynamic (MHD) third grade material through curved configuration. Variable characteristics of thermal conductivity and viscosity are taken. Effects of Soret and Dufour are examined. Chemical reaction with activation energy is attended. Compliant properties are subject to channel boundaries. Slip aspects are considered for velocity, temperature and concentration at channel boundaries. Large wavelength and low Reynolds number are invoked. Resulting expressions are computed numerically. The detailed physical interpretations of all the flow quantities are

analyzed for various pertinent parameters. Temperature increases for Dufour parameter whereas concentration reduces for Soret variable. The contents of this chapter are published in **Journal of Thermal Analysis and Calorimetry 143 (2021) 2749-2760.**

Chapter four examined peristaltic transport of Sutterby liquid with temperature dependent thermal conductivity in curved configurations. Inclined magnetic field is considered. Energy expression is modeled with effects of viscous dissipation, non-linear thermal radiation, variable thermal conductivity, Joule heating and heat source/ sink. Lubrication approach in formulation has been implemented. Irregularities are discussed by entropy in the process of heat transfer. Numerical method has been used for velocity and energy equations are solved numerically. Quantities of interest via important parameters are graphically analyzed. Irregularity is minimum via entropy for enhanced thermal conductivity and radiation parameters. Heat transfer rate increases for increased values of Brinkman number. These observations are published in **International Communications in Heat and Mass Transfer 122 (2021):105009.**

Chapter five addresses non-Darcy resistance in peristaltic transport of Sutterby liquid in curved configuration. Variable characteristics of material (i.e. thermal conductivity and viscosity) are taken as temperature-dependent. Soret and Dufour features have also been retained. Problem is modeled by using conservation laws. Long wavelength and small Reynolds number have been invoked. Resulting problems have been solved numerically. Entropy optimization analysis is made. Axial velocity, temperature, concentration, entropy, Bejan number and heat transfer rate are examined for influential variables. Opposite behavior of mass and energy is noted for Soret and Dufour parameters. Entropy enhancement is noticed

for Soret and Dufour parameters. This analysis is published in **Journal of Thermal Analysis and Calorimetry 143 (2021) 2215-2225.**

Chapter six examines entropy generation via thermal radiation, heat absorption coefficient and variable thermal conductivity under magnetic consideration. Third grade material flow by peristalsis in curved configuration has been considered. Modeled problem has been simplified by the lubrication approach. Momentum equation is solved through regular perturbation method and energy equations is solved numerically. Furthermore, physical investigation of pertinent parameters on temperature, velocity, Bejan number, total entropy and pressure gradient has been scrutinized through graphical results. Total entropy enhances for heat absorption coefficient whereas it lessens for thermal conductivity coefficient and thermal radiation parameter. The contents of this chapter are submitted in **International Communications in Heat and Mass Transfer.**

Chapter seven discusses peristaltic flow of Sisko material is modeled with variable characteristics of thermal conductivity and viscosity via curved configuration. Both quantities are taken space and temperature dependent. Conservation laws for mass, momentum and temperature are first modeled and then simplified by taking small wave length and large Reynolds number assumptions. Entropy is also under consideration to study irregularities in heat transfer process. Problem is solved numerically. These solution is utilized to plot the behaviors of quantities of interest against the pertinent parameters. For larger thermal conductivity parameter the temperature decays whereas it increases for Sisko fluid parameter. Irregularity in heat transfer is found minimum through entropy generation for larger viscosity and thermal conductivity. The results of this study are published in **Thermal Analysis and**

Calorimetry 143 (2021) 363-375.

Chapter eight organized modeling of electroosmotic Carreau liquid flow through a microchannel in curved configuration. Fluid flow is because of both the peristaltic pumping and electro osmosis effects. The Carreau liquid flow is governed by Navier–Stokes equations along with electric body force. Heat equation is also modeled. Electric dissipation effects are incorporated. These equations are simplified by assuming lubrication theory. However Poisson–Boltzmann equation is simplified by Debye–Hückel approximation. Resulting expression is solved analytically. Velocity distribution, trapping and temperature are investigated for various pertinent parameters like inverse Electric Double Layer (EDL), ratio of zeta potential, curvature of the channel, electric dissipation and Helmholtz–Smoluchowski velocity etc. Velocity shows dual behavior for different parameters in the curved microchannel and is asymmetric near the centre due to curvature effects. Temperature decreases for EDL thickness however reversed holds for electric dissipation parameter. Contents of this chapter are submitted in **Part E: Journal of Process Mechanical Engineering.**

Chapter Nine presents the conclusion of thesis.

Contents

Chapter 1 1

Literature Survey and Basic Equations 1

1.1 Peristalsis 1

1.2 Literature review 2

1.3 Fundamental Equations 10

1.3.1 Mass Conservation Equation 10

1.3.2 Momentum Conservation Equation 10

1.3.3 Energy Conservation Equation 11

1.3.4 Concentration Equation 11

1.3.5 Maxwell's Equations 12

Chapter 2 13

Entropy Generation Analysis for Peristalsis of Magneto Jeffrey Materials 13

2.1 Mathematical Formulation 13

2.1.1 Entropy 20

2.2 Methodology 22

2.3 Analysis 22

2.3.1 Velocity 22

2.3.2 Temperature 23

2.3.3 Entropy 23

2.3.4 Heat transfer coefficient and isotherm 24

2.3.5 Trapping 24

2.4 Conclusions 39

Chapter 3 ..... **40**

Soret-Dufour Aspects with Activation Energy in Peristaltic Mechanism of Third Grade Material with Variable Features **40**

3.1 Mathematical Formulation 40

3.2 Methodology 46

3.3 Analysis 46

3.3.1 Velocity 46

3.3.2 Temperature 47

3.3.3 Concentration 48

3.4 Conclusions 61

Chapter 4 ..... **62**

Entropy Optimization of MHD Sutterby Fluid Subject to Temperature Dependent Thermal Conductivity and Non-Linear Thermal Radiation **62**

4.1 Mathematical Formulation 62

4.1.1 Entropy 68

4.2 Methodology 69

4.3 Analysis 69

4.3.1 Velocity 70

4.3.2 Temperature 70

4.3.3 Entropy 71

4.3.4 Heat Transfer Rate and Isotherms 72

4.4 Conclusion 89

Chapter 5 ..... **90**

Entropy Production Minimization and Non-Darcy Resistance within Wavy Motion of Sutterby Liquid Subject to Variable Physical Characteristics 90

5.1 Mathematical Formulation 90

5.1.1 Entropy 97

5.2 Methodology 98

5.3 Analysis 98

5.3.1 Velocity 98

5.3.2 Temperature 99

5.3.3 Concentration 99

5.3.4 Entropy and Bejan Number 100

5.3.5 Heat Transfer Coefficient 100

5.4 Conclusion 112

Chapter 6 113

Generation of Entropy in Peristaltic Activity of Third Grade Liquids under Magnetic Field 113

6.1 Mathematical Formulation 113

6.1.1 Entropy 118

6.2 Methodology 119

6.2.1 System at Zeroth Order 120

6.2.2 First Order System 120

6.3 Analysis 121

6.3.1 Velocity 121

6.3.2 Pressure Gradient 122

6.3.3 Temperature 122
6.3.4 Entropy production and Bejan number 124
6.3.5 Trapping 124
6.4 Conclusion 141
Chapter 7 142
Entropy Generation Analysis in Peristalsis of Sisko Fluid Subject to Variable Viscosity and Thermal Conductivity 142
7.1 Mathematical Formulation 142
7.1.1 Entropy 146
7.2 Methodology 147
7.3 Analysis 148
7.3.1 Velocity 148
7.3.2 Temperature 148
7.3.3 Entropy Generation 149
7.3.4 Heat Transfer Rate 150
7.3.5 Trapping and Pumping 150
7.4 Conclusion 164
Chapter 8 165
Electro-Thermal Transportation of Carreau Fluids Through Peristalsis in a Curved Micro-Channel 165
8.1 Mathematical Formulation 165
8.2 Analysis 173
8.2.1 Velocity 174
8.2.2 Trapping 176

8.2.3 Temperature 178

8.3 Conclusions 192

Chapter 9 193

Conclusions 193

References 196

Chapter 1

Literature Survey and Basic Equations

This chapter deals with introduction of peristalsis, literature survey and fundamental equations of fluid flow and mass and heat transfer.

1.1 Peristalsis

Mathematical modeling and analysis of various problems are made to solve the issues associated with industry, engineering and medical sciences. It is well known fact that various materials/ fluids in industrial processes and living organisms are carried out from one point to another through a natural method known as peristaltic pumping. It is a series of wave-like motion that occurs due to contraction and relaxation. Peristalsis has prime importance in the fields of physiology and engineering. For physiologists, it is well known phenomena as it is one of the key mechanisms for transportation of fluid transport in many biological systems. Few examples in this context include urine transport from kidney to bladder, movement of food particles in digestive tract, blood circulation in capillaries, ovum movement in fallopian, vasomotion of small blood vessels and in other reproduction systems etc. Various biological and industrial appliances have also been manufactured by engineers through this concept e.g. finger and hose pumps, heart bypass and dialysis machines, rollers and B.P apparatus are few

pertinent examples in this regard. Peristaltic phenomena is also helpful to transport fluids/ materials where direct contact with the material is avoided e.g. in nuclear industry toxic materials are transported through this mechanism.

1.2 Literature review

Latham [1] is recognized as the pioneer who investigated the peristaltic fluid motion experimentally. Burns and Parkes [2] discussed peristaltic motion through both symmetrical and axially symmetric channels and pipes. In this study two extreme cases are analyzed, one is with peristaltic motion with no pressure gradient and second is fluid flow under pressure along channel. Shapiro and Jaffrin [3] analyzed fluid transport via peristalsis with assumption of small Reynolds number and large wavelength. Yin and Fung [4] carried out a study in which they compared the experimental work and theoretical investigation related to peristaltic motion. Barton and Raynor [5] discussed peristaltic motion in tubes. A mathematical formulation is presented by Lew et al. [6] to present the chyme transport in small intestine. Tong and Vawter [7] adopted numerical technique (finite-element method) to study peristaltic motion. It is concluded that the wavelength and amplitude of the wave affect the flow velocity. Li [8] studied peristaltic motion in cyinderical tubes. Mittra and Prasad [9] discussed the Poiseuille flow of peristaltic motion of the material. Liron [10] investigated the efficiency of peristaltic activity in living bodies. Jaffrin [11] discussed peristaltic pumping theoretically in a tube for the case when effects of inertial and streamline curvature is significant. Fluid flow through peristalsis in non-uniform channels was addressed by Gupta and Seshadri [12] and Vishnyakov et al. [13]. An experimental study was performed by Manero et al. [14] for non-Newtonian fluid flow in oscillating channels. Peristaltic movement of physiological fluid flow

with variable viscosity in a non-uniform channel was discussed by Srivastava et al. [15]. In 1983, Böhme and Friedrich [16] investigated wavy motion for viscoelastic fluids. In this study Reynolds number is taken to be small enough so that inertial forces could be ignored and large wavelength is considered so that pressure could remain constant in the cross-section of the duct. Srivastava and Srivastava [17] studied two-layer fluid flow through a non-uniform duct. Two-dimensional fluid flow through wavy motion was portrayed by Takabatake and Ayukawa [18]. In this work Navier Stokes are solved by using numerical method (finite difference method) for distinct values of wavelength, wave amplitude and Reynolds number. Pozrikidis [19] investigated wavy motion in two-dimensional duct. In this article creeping fluid motion was assumed and impact of width of the channel, amplitude of wave, pressure gradient on pattern of streamlines and characteristics of fluid flow were discussed. Related studies in this context are (see ref. [20-25]).

Initially peristaltic was studied for viscous materials only. Viscous materials are related through linear relationship between strain rate and shear stress. Such materials do not represent realistic materials. For instance, various materials like greases, jellies, gelatin, corn-flour, ketchup, toothpaste, soap, blood, clay coating and various emulsions do not lie in the category of Newtonian materials as these carry non-linear relation amid strain rate and shear stress. These are known as non-Newtonian materials. Non-Newtonian models present different perspective of fluids for better understanding of several dynamical mechanisms. A single material cannot reveal all properties of non-Newtonian fluids. To overcome such facts various non-Newtonian models are proposed in the literature. These materials undertake a vital contribution in daily life, petroleum, geophysics, physiology, chemical industries and

engineering therefore non-Newtonian materials are of much significance. Such significance in various spheres of daily life demands a thorough and comprehensive understanding of these materials making it an ever more attractive field for contemporary. Thus for the first time Raju and Devanathan [26] made a theoretical study to investigate the flow characteristics of physiological fluids in peristalsis. In this study they considered power law fluids in a tube. They discussed in detail the impact of applied pressure gradient coupled with non-Newtonian material parameters on velocity and streamlines. In another study [27], they also extended [26] by taking viscoelastic fluids. Siddiqui et al. [28] examined properties of peristaltic transport of shear-thinning Third grade materials in planner channel. Siddiqui et al. [29] studied the peristaltic motion of second grade fluid via an axi-symmetric conduit. Srivastava [30] analyzed peristaltic transport of couple-stress fluid that is an especial case of non-Newtonian fluids. Hayat et al. [31] presented peristaltic motion of third grade fluid in a circular cylinder tube. This wok presented a model in order to have better understanding of the mechanics of physiological flows. Hayat et al. [32] portrayed peristaltic motion for Johnson-Segalman materials in two-dimensional planner channel. Wang et al. [33] analyzed peristaltic motion for Johnson-Segalman fluid in a sinusoidal deformed tube. In this article wavelength of deformed tube was considered large. Solution for pertinent parameters is calculated for both perturbation and numerical techniques. Haroun [34] studied wavy motion in an asymmetric channel for third grade fluid. In previous works peristaltic motion was considered in straight and planner channel but in this study non-Newtonian fluid was firstly considered in asymmetric channel. Here long wave length is assumed large as comparison to the varying width of the channel. However, amplitude of the wave is not very small as compared to the channel width. After [34], Nasir and Hayat [35] also modeled non-Newtonian fluid in an asymmetric channel. In

this work they considered a four parameters model Carreau fluid as a non-Newtonian fluid. Recent works in this direction can be seen through Ref. [36-41].

Literature survey reveals that reasonable work has been undertaken on material transport through peristaltic mechanism with various conditions and geometric configurations. However, very little work has been done in curved geometry. It is noticed that flow through curved geometry yields rather more realistic applications when compared with flow via straight channel. Obviously various glandular ducts, arteries and pipes in physiological and industrial systems are curved shaped. Peristaltic mechanism in a curved channel was initially investigated by Sato et al. [42] in which they studied viscous fluid in a laboratory frame. They used long wave length and small Reynolds numbers assumptions while solving the equations. Due to the various applications of curved channel, the analysis of [42] has been reviewed by Ali et al. [43]. They presented mathematical formulation of the problem in wave frame for curved geometry for the first time. In these studies it was concluded that flow due to peristaltic motion in curved channel is not symmetric. Due to various applications of non-Newtonian fluids in industry, Ali et al. [44] firstly formulated a mathematical model for non-Newtonian fluid in curved configurations. Here rheology of non-Newtonian fluid was defined by third grade fluid. Hayat et al. [45] discussed impact of magnetic field on wavy motion of third grade fluid in curved configuration. In this article they considered wave frame of reference. Hina et al. [46] investigated wall properties on peristaltic motion of non-Newtonian fluid (third grade fluid) in curved geometry. Ramanamurthy et al. [47] formulated mathematical model for viscous fluid flow in peristaltic motion for curved geometry. In this study they analyzed the flow in laboratory frame of reference. Narla et al. [48] presented exact solution for viscoelastic fluid in

curved channel. In this work they used lubrication approach in order to liberalize the equations. Hayat et al. [49] investigated motion of Carreau-Yasuda liquids through peristalsis in curved configurations. Abbasi et al. [50] considered Eyring-Powell fluid flow via peristaltic transport in curved channel. Problems with different fluids and boundary conditions are investigated in curved channel by different researchers (see Ref. [51-58]).

It is worth mentioning here that application of magnetic field in peristalsis has a lot of significance due to its tremendous applications in various fields of life and thus researchers of different eras have continuously been working in this field (see ref. [59-76]). In these attempts magnetic field is applied either in transverse or in inclined directions for peristaltic flow for different geometries..

Heat transfer is an integral and pivotal element in cooling processes of industries and various other processes. It regularly occurs in the bodies of different temperatures. A number of processes rely on this phenomenon of heat transfer e.g. crystallization, distillation and various boiling operations. Similarly laser therapy, cryosurgery and hyperthermia are considered the most modern ways to destroy unwanted tissues like cancer etc. In peristalsis the food bolus moves in gastrointestinal tract while being immensely affected by the transfer of heat phenomenon. Articles concerning with heat transfer have been presented by many researchers (see refs. [77-84]). It is evident from the available literature that researchers have shown interest in biological and industrial fluid flows with heat transfer. It is a fact that consequences of heat transfer are examined through entropy. In thermo-dynamical systems, frictional forces, viscosity and chemical reactions etc are the main causes of energy degradation that result in entropy production.

In thermodynamics, entropy is stated as thermal irreversibility or depletion of useful energy. One of the major concerns for scientists and researchers, these days, is how to manage the wastage of thermal energy. The analysis of entropy production is considered vital in finding location and origin of irreversibilities. The sources of energy losses are due to friction, heat transfer, expansion and compression, thermal radiation, magnetic field, heat source/ sink and chemical reactions. By minimizing entropy generation, efficiency of thermal systems may be improved. The same may be accomplished through various methods such as by reducing chip components' sizes in computers, introducing porous medium, cooling fans to avoid overheating and heat exchangers. Laws of thermodynamics describe transformation of energy and the first law portrays quantity of energy in the process of heat transfer. Second law describes reduction in quality of energy that is measured as entropy. After working on entropy generation, Bejan [85, 86] was the first one to propose a method that optimizes system's destruction. Afterwards, many other researchers considered irreversibility analysis and ensured its utility in determining the system's efficacy. Souidi et al. [87] analyzed entropy generation for peristaltic flows. Abbas et al. [88] and Rashidi et al. [89] worked on peristaltic flows for nanofluids. Similarly, Hayat et al. [90] discussed entropy in peristalsis with rotating frame. Khan et al. [91] studied entropy for skin friction coefficient and Nusselt number. Farooq et al. [92] portrayed entropy generation for peristaltic transport of carbon nanotubes. Afridi et al. [93] described entropy for heat-mass transport. Noreen et al. [94] presented entropy minimization of Carreau materials along with Hall current and Ohmic heating effects via peristalsis. Khan et al. [95] simulated entropy production via peristaltic motion of viscous fluid in asymmetric channel using shooting method. Nawaz et al. [96] analyzed entropy for peristaltic motion of Williamson liquid in curved configuration.

Viscosity affects the capability of propulsion in peristalsis. It plays an important role during the preparation of flow measurements of fluids. In almost all the real fluids, the viscosity varies with thermal effects when viscous dissipations are taken. Viscosity of physiological fluids like honey, syrup, blood and polymer solutions vary with temperature. Available literature reflects that previously majority works on peristalsis are done for constant viscosity of fluid. Little has been organized for peristalsis by considering the variable viscosity. In several engineering applications, both viscosity and thermal conductivity are temperature dependent with high temperature such as nuclear power plants, missile technologies, rockets and space vehicles, turbines pumps etc. Further in many other procedures the irreversible damage are followed by small change in temperature for example during dialysis and heart lung equipment. Keeping in mind such importance of variable viscosity and thermal conductivity only few investigations have been yet organized. Keeping in view its vitality, few researchers have analyzed the effects of variable viscosity of peristaltic flow. Reddy and Reddy [97] analyzed the peristaltic flow with variable viscosity through a porous medium in a planar channel. Ali et al. [98] considered consequences of slip boundary conditions on the peristaltic flow of MHD fluid while taking variable viscosity. Eldabe et al. [99] analyzed mixed convective heat and mass transfer for a non-Newtonian fluid of peristaltic flow with temperature dependent viscosity. Recently, Tanveer et al. [100] discussed variable viscosity for Sisko fluid in curved channel using compliant wall properties. In most of the investigations constant thermal conductivity has been carried out. However, it has been proved that the thermal conductivity changes linearly with temperature from 0 to 400 °F. Few researchers have also analyzed the combined effects of variable physical properties of peristaltic flow in straight/planner channel. Hussain et al. [101] discussed heat transfer analysis in peristaltic flow of MHD Jeffrey fluid with variable thermal

conductivity. Hussain et al. [102] discusses nonlinear thermal radiation and temperature dependent viscosity for peristaltic flow through porous medium of hydromagnetic fluid in a straight channel. Hayat et al. [103] investigated collective effects of variable viscosity and thermal conductivity for MHD mixed convective peristaltic flow. Hussain et al. [104] studied the influence of temperature dependent viscosity and thermal conductivity for hydromagnetic Jeffrey fluid on peristaltic motion in a straight asymmetric channel. Latif et al. [105] explored combined effects of temperature dependent viscosity and thermal conductivity for MHD third order fluid for symmetric peristaltic channel. Abbasi et al. [106] examined peristaltic flow of electrically conducting fluid through porous medium with temperature dependent viscosity for a planar channel.

Review of the available literature witnesses that advance study is needed for peristaltic movement in micro/nano scale via curved geometry to design devices like kidney-on-a-chip, Gut-on-a-chip and Liver-on-a-chip. These devices work through basic code of electro-kinetic that means interaction of fluid flow in micro channel subject to electrical field. An important element of electro-kinetic flow is electro-osmosis. Tripathi et al. [107] explored electro-osmotic pumping with effects of Soret and Dufour in a microchannel under peristaltic transport of nanofluid through Joule heating. Tripathi et al. [108] extended this model by taking the effects of buoyancy. Narla et al. [109] formulated a model for electro-osmotic and peristaltic pumping in a microchannel. Narla et al. [110] also extended this model to examine uterine hydrodynamics of uterine cavity. Although many researchers have studied electro-osmotic peristaltic flow in different geometries; however, in curved channel Narla et al. [111] explored the electro-osmotic flow of viscous liquid for first time ever and presented its mathematical model. This mathematical model was exclusively derived for blood flow. Results of this study

revealed that peristaltic pumping could be controlled by electro-osmotic phenomenon. In another study, Narla et al. [112] analyzed entropy generation in biomimetic nanofluids via curved geometry with Joule dissipation.

1.3 Fundamental Equations

1.3.1 Mass Conservation Equation

Concept of mass conservation is extensively used in various fields such as mechanics, chemistry and fluid dynamics. It was established in chemical reactions by Mikhail Lomonosov and after that it was revived by Antoine Lavoisier. According to this law, in a closed system mass remained conserved or unchanged that is it can neither be formed nor destroyed by any chemical reaction or physical transformation. Mathematically, it is expressed by equation of continuity as follows:

$$\frac{\partial \rho}{\partial t} + \nabla.(\rho \mathbf{W}) = 0, \tag{1.1}$$

where ρ denotes the density of the material, t time and $\mathbf{W}$ velocity of fluid. The above equation is for the compressible fluid. For incompressible fluid, where density of the fluid remains constant, Eqn. (1.1) reduced to

$$\nabla.\mathbf{W} = 0. \tag{1.2}$$

1.3.2 Momentum Conservation Equation

Momentum conservation is directly followed by Newton's third law motion. According to this law, momentum of an isolated system remains unaltered unless an external force act upon it. Mathematically

$$\rho\frac{d\mathbf{W}}{dt}=\nabla.\boldsymbol{\tau}+\rho\mathbf{f}, \tag{1.3}$$

where $\boldsymbol{\tau}=-p\mathbf{I}+\mathbf{S}$ represents Cauchy Stress tensor, p pressure, $\mathbf{I}$ identity matrix, $\mathbf{S}$ extra stress tensor, $\rho\mathbf{f}$ body force, $\frac{d}{dt}=\frac{\partial}{\partial t}+\mathbf{W}.\nabla$ total derivative and ∇ del operator.

1.3.3 Energy Conservation Equation

The law of conservation of energy states that the total energy remains constant in any process. It may transfer from one to the other system or may change its form but the total quantity of energy remains the same. Mathematically, we write

$$\rho c_p\frac{dT}{dt}=\nabla.\left(\kappa\nabla T\right)+E_T, \tag{1.4}$$

in which ρ shows fluid density, c_p specific heat, T temperature, κ thermal conductivity, E_T energy transfer by viscous dissipation, radiative heat flux, Joule heating, surface cooling\ heating and Dufour effects etc.

1.3.4 Concentration Equation

The equation of concentration can be deduced by considering the assumption of mass conservation within moving material/ fluid. Molecular diffusion and convection are responsible for mass transportation.

$$\frac{dC}{dt}=D_B\nabla^2C+\frac{D_Bk_T}{T_m}\nabla^2T. \tag{1.5}$$

where C represents concentration, D_B represents mass diffusion coefficient, k_T thermal diffusion ratio and T_{mean} mean material temperature.

1.3.5 Maxwell's Equations

Four equations illustrating a relationship between electric and magnetic fields behavior in view of electromagnetism laws are named as Maxwell's equations. These equations are

$$\nabla.\mathbf{E} = \frac{\rho_e}{\varepsilon_0}, \tag{1.6}$$

$$\nabla.\mathbf{B} = 0, \tag{1.7}$$

$$\nabla \times \mathbf{E} = -\frac{\partial \mathbf{B}}{\partial t}, \tag{1.8}$$

$$\nabla \times \mathbf{B} = \mu_0 \mathbf{J} + \mu_0 \varepsilon_0 \frac{\partial \mathbf{E}}{\partial t}, \tag{1.9}$$

in which $\mathbf{E}$ represents electric filed, $\mathbf{B}$ total magnetic field, $\mathbf{J}$ current density, ρ_e charge density, ε_0 permittivity of free space and μ_0 electric quantity.

Chapter 2

Entropy Generation Analysis for Peristalsis of Magneto Jeffrey Materials

This chapter discusses magneto peristaltic movement of Jeffrey liquids with variable physical characteristics in curved geometry. Energy expression involves viscous dissipation and variable thermal conductivity. Entropy generation together with variable (depending upon temperature) thermal conductivity/ viscosity and effects of inclined magnetic field has been modeled and analyzed. Slip boundary conditions for temperature and velocity are invoked. Velocity, heat transfer coefficient, temperature, entropy generation and trapping are computed numerically by using Mathematica 11 software. The graphical results are analyzed for influential variables.

2.1 Mathematical Formulation

We intend to investigate entropy in peristalsis of Jeffrey liquids within curved channel. Channel width is $2a$, radius R' and centre O. Velocity components (W_1, W_2) are taken along radial and axial (R, X) directions respectively. Inclined magnetic field B_0 is applied with an inclination ϑ_0. Fluid viscosity and thermal conductivity are temperature dependent. Flow is induced due to wave propagation having amplitude b, wavelength λ and speed s. The

wavelength λ of curved channel is supposed to be much larger than half width of channel such that $\frac{a}{\lambda} \rightrightarrows 1$. Geometry related to this context is given in Fig. (2.1). Wave shape is taken as:

$$\bar{r} = \pm\chi(X,t) = \pm\left[a + b\sin\left(\frac{2\pi}{\lambda}(X - st)\right)\right], \tag{2.1}$$

where χ represents radial distance of wave from centre line. Heat transfer occurs because of different wall temperatures (T_0, T_1) at upper wall and lower wall respectively such that $(T_1 > T_o)$.

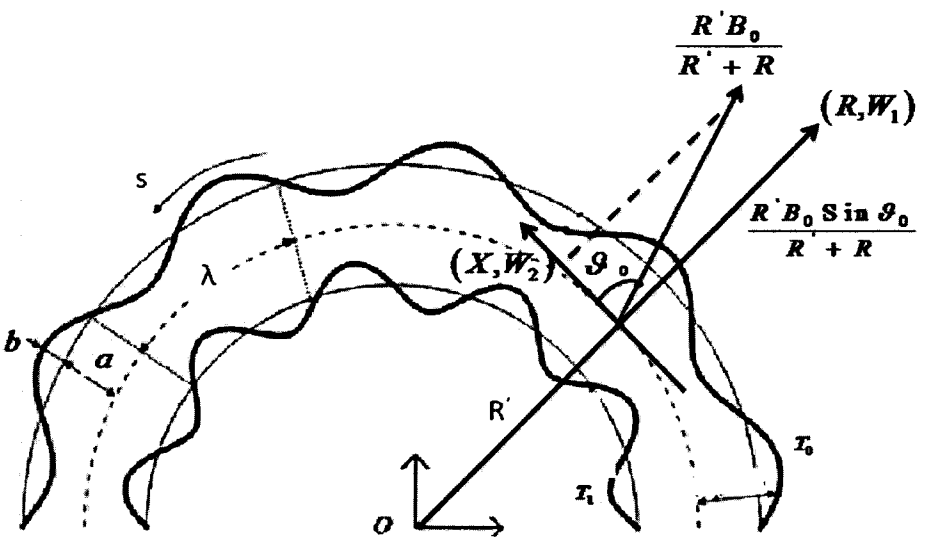

Fig. 2.1: Sketch of considered problem

In curved geometry inclined magnetic field is written as:

$$\mathbf{B} = \left(\frac{R' B_0 \sin\vartheta_0}{R' + R}, \frac{R' B_0 \cos\vartheta_0}{R' + R}, 0\right). \tag{2.2}$$

From Eqn. (2.2), it is clear that for magnetic field is in radial direction when $\vartheta_0 = 90^o$.

By Ohm's law, we can write without electric field

$$\mathbf{J} = -\sigma[\mathbf{B} \times \mathbf{W}], \tag{2.3}$$

and Lorentz force $\mathbf{F}$,

$$\mathbf{F} = \mathbf{B} \times \mathbf{J}, \tag{2.4}$$

in which $\mathbf{J}$ shows current density and σ electrical conductivity.

From Eqns. (2.2) to (2.4), we arrive at

$$\mathbf{F} = \sigma\left(\frac{R'B_0}{R'+R}\right)^2 \left(-W_1 \cos^2\vartheta_0 + W_2 \sin\vartheta_0 \cos\vartheta_0, W_1 \sin\vartheta_0 \cos\vartheta_0 - W_2 \sin^2\vartheta_0, 0\right), \tag{2.5}$$

$$\mathbf{J}.\mathbf{J} = \left(\sigma\frac{R'B_0}{R'+R}\right)^2 \left(W_1 \cos\vartheta_0 - W_2 \sin\vartheta_0\right)^2. \tag{2.6}$$

By Reynolds model we have following expression of temperature dependent viscosity [103-104]:

$$\mu(T) = \mu_o \exp\left\{-\alpha^{'}\left(T - T_0\right)\right\} \approx \mu_o\left(1 - \alpha^{'}\left(T - T_0\right)\right), \tag{2.7}$$

in which μ_0 represents constant fluid dynamic viscosity and $\alpha^{'}$ variable viscosity coefficient. Clearly $\alpha^{'} = 0$ reduces this problem to constant viscosity situation. Temperature dependent thermal conductivity is [101]:

$$\kappa(T) = \kappa_o\left(1 + \beta'\left(T - T_0\right)\right), \tag{2.8}$$

where κ_o shows constant thermal conductivity of material and β' represents variable thermal conductivity coefficient.

Cauchy stress tensor $(\boldsymbol{\tau})$ for Jeffrey materials is [36]:

$$\boldsymbol{\tau} = \mathbf{S} - P\mathbf{I},$$
$$\mathbf{S} = \frac{\mu(T)}{\lambda_1 + 1}\left(\lambda_2 \frac{d\mathbf{A}_1}{dt} + \mathbf{A}_1\right), \tag{2.9}$$

here I denotes identity tensor, P pressure, $\mu(T)$ temperature dependent viscosity, $\lambda_1\left(= \frac{\text{Relaxation time}}{\text{Retardation time}}\right)$, λ_2 retardation time, $\frac{d}{dt}$ material derivative and

$$\mathbf{A}_1 = (\nabla \mathbf{W})' + \nabla \mathbf{W}. \tag{2.10}$$

Elementary equations of present work are [43-46]:

$$R'\frac{\partial W_2}{\partial X} + \frac{\partial}{\partial R}\left((R'+R)W_1\right) = 0, \tag{2.11}$$

$$\rho\left(\frac{\partial W_2}{\partial t} + W_1\frac{\partial W_2}{\partial R} - \frac{W_1 W_2}{R'+R} + \frac{W_2 R'}{(R'+R)}\frac{\partial W_2}{\partial X}\right) = -\frac{R'}{(R'+R)}\frac{\partial P}{\partial X} + \frac{1}{(R'+R)^2}\frac{\partial}{\partial \bar{R}}\left(S_{XR}(R'+V)^2\right)$$
$$+\frac{R'}{(R'+R)}\frac{\partial S_{XX}}{\partial X} + \sigma\left(\frac{R'B_0}{R'+R}\right)^2\left(-W_2\sin^2\vartheta_0 + W_1\sin\vartheta_0\cos\vartheta_0\right), \tag{2.12}$$

$$\rho\left(\frac{\partial W_1}{\partial t} + W_1\frac{\partial W_1}{\partial R} + \frac{R'W_2}{(R'+R)}\frac{\partial W_1}{\partial X} - \frac{{W_2}^2}{R'+R}\right) = -\frac{\partial P}{\partial R} - \frac{S_{XX}}{(R'+R)} + \frac{R'}{(R'+R)}\frac{\partial S_{XR}}{\partial X}$$
$$+\frac{1}{R'+R}\frac{\partial}{\partial R}\left((R'+R)S_{RR}\right) - \sigma\left(\frac{B_0 R'}{R'+R}\right)^2\left(-W_2\sin\vartheta_0\cos\vartheta_0 + W_1\cos^2\vartheta_0\right), \tag{2.13}$$

$$\rho C_p\left(\frac{\partial T}{\partial t}+W_1\frac{\partial T}{\partial R}+\frac{R'W_2}{(R'+R)}\frac{\partial T}{\partial \bar{X}}\right)=-\nabla.\left(-\kappa(T)\nabla T\right)-\frac{\partial W_2}{\partial R}\left(S_{XX}-S_{RR}\right)$$
$$+\left(\frac{\partial W_2}{\partial R}-\frac{W_2}{(R'+R)}+\frac{R'}{(R'+R)}\frac{\partial W_1}{\partial \bar{X}}\right)S_{XR}+\sigma\left(\frac{R'B_0}{R'+R}\right)^2\left(W_1\cos\vartheta_0-W_2\sin\vartheta_0\right)^2, \tag{2.14}$$

with

$$\nabla.\left(-\kappa(T)\nabla T\right)=-\frac{\partial}{\partial R}\left(\kappa(T)\frac{\partial T}{\partial R}\right)-\frac{\kappa(T)}{R'+R}\frac{\partial T}{\partial R}-\frac{\partial}{\partial X}\left(\frac{\kappa(T)R'^2}{(R'+R)^2}\frac{\partial T}{\partial X}\right). \tag{2.15}$$

Here ρ denotes density, S_{XX}, S_{XR}, S_{RR} the extra stress tensor $\mathbf{S}$ components, C_p specific heat and T material temperature.

The boundaries conditions are

$$\begin{aligned} &W_2-\alpha_1'S_{XR}=0,\quad T-\beta_1'\frac{\partial T}{\partial R}=T_1 \quad \text{at} \quad R=-\chi,\\ &W_2+\alpha_1'S_{XR}=0,\quad T+\beta_1'\frac{\partial T}{\partial R}=T_0 \quad \text{at} \quad R=\chi, \end{aligned} \tag{2.16}$$

where α_1' and β_1' stand for slip parameters.

We considered transformation between wave $(\bar{x},\bar{r})$ and laboratory (X,R) frames as:

$$\begin{aligned} &\bar{x}=X-st, \bar{r}=R,\quad \bar{w}_2(\bar{x},\bar{r})=W_2(X,R,t)-s,\quad \bar{w}_1(\bar{x},\bar{r})=W_1(X,R,t),\\ &\bar{T}(\bar{x},\bar{r})=T(X,R,t), \bar{p}(\bar{x},\bar{r})=P(X,R,t). \end{aligned} \tag{2.17}$$

Applying transformation (2.17) in Eqns. (2.11) to (2.16), we arrived at

$$R'\frac{\partial \bar{w}_2}{\partial \bar{x}}+\frac{\partial}{\partial \bar{r}}\left((R'+\bar{r})\bar{w}_1\right)=0,$$

$$\rho\left(-s\frac{\partial\bar{w}_1}{\partial\bar{x}}+\bar{w}_1\frac{\partial\bar{w}_2}{\partial\bar{r}}-\frac{(\bar{w}_2+s)}{R'+\bar{r}}+\frac{(\bar{w}_2+s)R'}{R'+\bar{r}}\frac{\partial\bar{w}_1}{\partial\bar{x}}\right)=$$

$$-\frac{R'}{R'+\bar{r}}\left[\begin{array}{l}\dfrac{\partial\bar{p}}{\partial\bar{x}}+\dfrac{\partial S_{\bar{x}\bar{x}}}{\partial\bar{x}}+\dfrac{1}{R'(R'+\bar{r})}\dfrac{\partial}{\partial\bar{r}}\left(S_{\bar{x}\bar{r}}(R'+\bar{r})^2\right)\\ +\sigma\dfrac{R'}{R'+\bar{r}}B_0^2\left(-(\bar{w}_2+s)\sin^2\vartheta_0+\bar{w}_1\sin\vartheta_0\cos\vartheta_0\right)\end{array}\right],$$

$$\rho\left(-s\frac{\partial\bar{w}_1}{\partial\bar{x}}+\bar{w}_1\frac{\partial\bar{w}_2}{\partial\bar{r}}+\frac{R'(\bar{w}_2+s)}{(R'+\bar{r})}\frac{\partial\bar{w}_1}{\partial\bar{x}}-\frac{(\bar{w}_2+s)^2}{R'+\bar{r}}\right)=-\frac{\partial\bar{p}}{\partial\bar{r}}-\frac{S_{\bar{x}\bar{x}}}{(R'+\bar{r})}+\frac{R'}{(R'+\bar{r})}\frac{\partial S_{\bar{x}\bar{r}}}{\partial\bar{x}}$$

$$+\frac{1}{R'+\bar{r}}\frac{\partial}{\partial\bar{r}}\left((R'+\bar{r})S_{\bar{r}\bar{r}}\right)-\sigma\left(\frac{B_0R'}{R'+\bar{r}}\right)^2\left(-(\bar{w}_2+s)\sin\vartheta_0\cos\vartheta_0+\bar{w}_1\cos^2\vartheta_0\right),$$

$$\rho C_p\left(-s\frac{\partial\bar{T}}{\partial\bar{x}}+\bar{w}_1\frac{\partial\bar{T}}{\partial\bar{r}}+\frac{R'(\bar{w}_2+s)}{(R'+\bar{r})}\frac{\partial\bar{T}}{\partial\bar{x}}\right)=-\nabla.\left(-\kappa(\bar{T})\nabla\bar{T}\right)-\frac{\partial\bar{w}_2}{\partial\bar{r}}\left(S_{\bar{x}\bar{x}}-S_{\bar{r}\bar{r}}\right)$$

$$+\left(\frac{\partial\bar{w}_2}{\partial\bar{r}}-\frac{(\bar{w}_2+s)}{(R'+\bar{r})}+\frac{R'}{(R'+\bar{r})}\frac{\partial\bar{w}_1}{\partial\bar{x}}\right)S_{\bar{x}\bar{r}}+\sigma\left(\frac{R'B_0}{R'+\bar{r}}\right)^2\left(\bar{w}_1\cos\vartheta_0-(\bar{w}_2+s)\sin\vartheta_0\right)^2,$$

where $\nabla.\left(-\kappa(\bar{T})\nabla\bar{T}\right)$ in curved channel is computed as

$$\nabla.\left(-\kappa(\bar{T})\nabla\bar{T}\right)=-\frac{\partial}{\partial\bar{r}}\left(\kappa(\bar{T})\frac{\partial\bar{T}}{\partial\bar{r}}\right)-\frac{\kappa(\bar{T})}{R'+\bar{r}}\frac{\partial\bar{T}}{\partial\bar{r}}-\frac{\partial}{\partial\bar{x}}\left(\frac{\kappa(\bar{T})R'^2}{(R'+\bar{r})^2}\frac{\partial\bar{T}}{\partial\bar{x}}\right).$$

We now define dimensionless variables (x,r), pressure p, velocity components $(\bar{w}_2,\bar{w}_1)$, wave number δ, amplitude b_1, temperature θ, Reynolds number Re, peristaltic wall h, viscosity parameter α, Brinkman number Br, thermal conductivity parameter β, curvature k, Prandtl number Pr, thermal slip parameters (α_1,β_1) and Hartmann number H as follows:

$$(r,x)=\left(\frac{\bar{r}}{a},\frac{\bar{x}}{\lambda}\right),\qquad p=\frac{a^2\bar{p}}{s\mu_o\lambda},\qquad (w_2,w_1)=\left(\frac{\bar{w}_2}{s},\frac{\bar{w}_1}{s}\right),\qquad \delta=\frac{a}{\lambda},$$

$$b_1=\frac{b}{a},\qquad \theta=\frac{T-T_o}{T_1-T_o},\qquad \mathrm{Re}=\frac{\rho sa}{\mu_o},\qquad h=\frac{\chi}{a},$$

$$\alpha=\alpha'(T_1-T_o),\quad Br=\frac{\mu_o s^2}{\kappa_o(T_1-T_o)},\qquad \beta=\beta'(T_1-T_o),\qquad k=\frac{R'}{a},$$

$$\mathrm{Pr}=\frac{\mu_o C_p}{\kappa_o},\qquad \alpha_1=\frac{\alpha_1'}{a},\qquad \beta_1=\frac{(T_1-T_o)\beta_1'}{a},\qquad H=\sqrt{\frac{\sigma B_0^2 a^2}{\mu_0}}. \tag{2.18}$$

Velocities (w_1,w_2) via stream function (ψ) can be presented below

$$(w_1,w_2)=\left(-\frac{k\delta}{k+r}\frac{\partial\psi}{\partial x},\frac{\partial\psi}{\partial r}\right). \tag{2.19}$$

By low Reynolds number and long wavelength we get

$$\frac{k}{r+k}\frac{\partial p}{\partial x}=\frac{1}{(\lambda_1+1)(r+k)^2}\frac{\partial}{\partial r}\left((1-\alpha\theta)(r+k)^2\left\{-\frac{1}{(r+k)}\left(1+\frac{\partial\psi}{\partial r}\right)+\frac{\partial^2\psi}{\partial r^2}\right\}\right)$$
$$-\frac{k^2H^2\sin^2\vartheta_0}{(k+r)^2}\left(1+\frac{\partial\psi}{\partial r}\right), \tag{2.20}$$

$$\frac{\partial p}{\partial r}=0, \tag{2.21}$$

$$\beta\left(\frac{\partial\theta}{\partial r}\right)^2+(1+\beta\theta)\left(\frac{\partial^2\theta}{\partial r^2}+\frac{1}{r+k}\frac{\partial\theta}{\partial r}\right)+Br\frac{(1-\alpha\theta)}{\lambda_1+1}\left[-\frac{1}{(r+k)}\left(1+\frac{\partial\psi}{\partial r}\right)+\frac{\partial^2\psi}{\partial r^2}\right]^2$$
$$+Br\frac{k^2(H\sin\vartheta_0)^2}{(k+r)^2}\left(1+\frac{\partial\psi}{\partial r}\right)^2=0, \tag{2.22}$$

$$S_{rx}=\frac{(1-\alpha\theta)}{1+\lambda_1}\left(-\frac{1}{(r+k)}\left(1+\frac{\partial\psi}{\partial r}\right)+\frac{\partial^2\psi}{\partial r^2}\right). \tag{2.23}$$

Eqns. (2.20) and (2.21) imply that

$$\frac{\partial}{\partial r}\left[\begin{array}{l}\dfrac{1}{(r+k)(1+\lambda_1)}\dfrac{\partial}{\partial r}\left((1-\alpha\theta)\left\{-(r+k)\left(1+\dfrac{\partial\psi}{\partial r}\right)+(r+k)^2\dfrac{\partial^2\psi}{\partial r^2}\right\}\right)\\ -\dfrac{k^2(H\sin\vartheta_0)^2}{(k+r)}\left(1+\dfrac{\partial\psi}{\partial r}\right)\end{array}\right]=0, \tag{2.24}$$

with boundary conditions in dimensionless form

$$\begin{aligned}&\psi(r)=-\frac{F}{2},\quad -\alpha_1 Sxr+\psi'(r)+1=0,\quad -\beta_1\theta'(r)+\theta(r)-1=0 \quad \text{at} \quad r=-h,\\ &\psi(r)=\frac{F}{2},\qquad \alpha_1 Sxr+\psi'(r)+1=0,\qquad \beta_1\theta'(r)+\theta(r)=0 \qquad \text{at} \quad r=h,\end{aligned} \tag{2.25}$$

$$F=\int_{-h}^{h}\psi_r dr=\psi(h)-\psi(-h), \tag{2.26}$$

$$h=(1+b_1\sin(2\pi x)). \tag{2.27}$$

Heat transfer coefficient at $r=h(x)$ is

$$z=\frac{\partial h}{\partial x}\times\frac{\partial\theta}{\partial r}. \tag{2.28}$$

2.1.1 Entropy

Entropy generation [75] in fixed frame is given by

$$S_{gen}=\frac{\kappa(T)}{\Theta_o^2}\left(\frac{dT}{dR}\right)^2+\frac{\sigma}{\Theta_o}\left(\frac{R'B_0}{R'+R}\right)^2\left(W_1\cos\vartheta_0-W_2\sin\vartheta_0\right)^2$$
$$+\frac{1}{\Theta_o}\left(\left(\frac{\partial W_2}{\partial R}+\frac{R'}{R'+R}\frac{\partial W_1}{\partial X}-\frac{W_2}{R'+R}\right)S_{XR}+\left(-S_{XX}+S_{RR}\right)\frac{\partial W_2}{\partial R}\right), \tag{2.29}$$

where Θ_o denotes reference temperature. Above equation is combination of three parts. First part represents entropy generation caused by heat transfer, second part shows entropy because of effects of inclined magnetic field and third part due to fluid friction.

Entropy production in dimensionless form becomes

$$N_s=\frac{S_{gen}}{S_G}=\left(\frac{\partial\theta}{\partial r}\right)^2+\frac{\Lambda Br}{1+\beta\theta}\left[\begin{array}{c}\frac{(1-\alpha\theta)}{(\lambda_1+1)}\left(-\frac{1}{r+k}\left(1+\frac{\partial\psi}{\partial r}\right)+\frac{\partial^2\psi}{\partial r^2}\right)^2\\+\frac{k^2\left(H\sin\vartheta_0\right)^2}{\left(k+r\right)^2}\left(1+\frac{\partial\psi}{\partial r}\right)\end{array}\right], \tag{2.30}$$

in which Λ defines temperature difference parameter and S_G entropy generation characteristic as

$$\Lambda=\frac{\Theta_o}{\left(T_1-T_o\right)},\quad S_G=\frac{\kappa(T)\left(T_1-T_o\right)^2}{a^2\Theta_o^2}. \tag{2.31}$$

Bejan number (Be) is

$$\mathrm{Be}=\frac{\left(\frac{\partial\theta}{\partial r}\right)^2}{\left(\frac{\partial\theta}{\partial r}\right)^2+\Lambda Br\,\frac{1}{1+\beta\theta}\left[\frac{1-\alpha\theta}{(1+\lambda_1)}\left(\frac{\partial^2\psi}{\partial r^2}-\frac{1}{r+k}\left(\frac{\partial\psi}{\partial r}+1\right)\right)^2+\left(\frac{k}{r+k}H\sin\vartheta_0\right)^2\left(\frac{\partial\psi}{\partial r}+1\right)\right]}. \tag{2.32}$$

From (2.32), it is clear that $Be \in [0,1]$.

2.2 Methodology

Eqns. (2.22) and (2.24) subject to the boundary condition (2.25) are solved numerically to solve boundary value problems.

2.3 Analysis

In this section we analyze responses of axial velocity, entropy generation, temperature and heat transfer coefficient versus pertinent parameters.

2.3.1 Velocity

Effects of axial velocity are illustrated through Figs. (2.2) to (2.5) against r for different parameters (α, k, ϑ_o and λ_1). In Fig. (2.2), it is seen that maximum velocity occurs near centre of the channel and it decays for higher α in the vicinity of upper wall where temperature of wall being $T_0 (< T_1)$. Enhancement in wave amplitude is observed for larger α. It is because of inverse relation between μ and α. For higher values of α viscosity decreases and thus fluid velocity increases. Fig. (2.3) shows behavior of w_2 for k. An increase in k velocity is decreased near the lower wall and it is higher near upper channel wall. When k increased, curved channel is converts to straight channel and for straight channel velocity amplitude is symmetric at centre of channel. Fig. (2.4) shows impact of inclination ϑ_o on velocity. For ϑ_o from 0^o to 90^o, material velocity decreases. For $\vartheta_o = 0^o$ magnetic field is in the direction of flow with maximum velocity. However for $\vartheta_o = 90^o$ the fluid velocity is least

due to maximum magnetic field strength. From Fig. (2.5), it is observed that w_2 decreases in half of the channel width for larger values of λ_1. In all these figures, it can also be noticed that trend of velocity is dual due to curved geometry.

2.3.2 Temperature

Figs. (2.6) to (2.10) exhibit temperature distribution θ via r for various pertinent parameters. Fig. (2.6) reveals that by increasing viscosity coefficient (α), temperature is decreased. Fig. (2.7) illustrates that for increased value of thermal conductivity coefficient (β) the fluid temperature decreases. In fact an enhancement in β intensifies the fluid ability for soaking up or dispersion heat. Fig. (2.8) depicts influence of Br on θ. Temperature is found increasing for higher Br. It shows that for higher Brinkman number the effect of viscosity dominates and it opposes flow field. Because of flow resistance, an increase in the collision occurs for fluid particles and consequently the temperature rises. Fig. (2.9) explains behavior of λ_1 on θ. It elucidates that temperature decreases with higher λ_1. Fig. (2.10) shows that when inclination ϑ_o of magnetic field is increased from 0^o to 90^o, θ also increases.

2.3.3 Entropy

Figs. (2.11) to (2.18) are drawn to observe outcome of entropy generation (Ns) and Bejan number versus various parameters $(\beta, Br, \vartheta_o$ and $\alpha)$. Figs. (2.11) and (2.12) demonstrate influence of β on Ns and Bejan number. Increase in β shows similar behavior for both quantities. Effect of $\Lambda.Br$ can be revealed from Figs. (2.13) and (2.14). Br has direct relation with viscosity and square of the wave propagation speed. An enhancement in $\Lambda.Br$

corresponds to more temperature rise thus entropy also increases (see Fig. (2.13)). Fig. (2.14) explains the dominant effects of heat transfer for increasing $\Lambda.Br$. Figs. (2.15) and (2.16) show influence of ϑ_0 on Ns and Bejan number. Opposite trend is noticed for both. Entropy increases near the channel walls for higher inclination (ϑ_0) whereas Bejan number decreases due to dominating effects of magnetic field strength. Figs. (2.17) and (2.18) show the effect of α on dimensionless quantities Ns and Bejan number. Clearly, both decrease by increasing viscosity coefficient. It is also noticed that Ns does not change significantly in the central region of the channel.

2.3.4 Heat transfer coefficient and isotherm

Figs. (2.19) and (2.20) are sketched to show the impact of β and H respectively on heat transfer coefficient. These figures revealed similar behavior i.e. increasing response of heat transfer coefficient for larger β and H. In these figures oscillatory behavior is observed because of wavy motion of channel walls

Figs. 2.21a and 2.21b are sketched to show the contours of temperature for curved and straight channels respectively. It is observed that distribution of temperature is high for curved configuration in comparison with straight channel. In these figures thermal conductivity and viscosity are assumed constant.

2.3.5 Trapping

In the fluid model, it is vital and significant to investigate the pattern of stream lines. Sketch of stream function reveals a very clear visualization of flow behavior. In the flow of physiological fluids, contour plots of stream lines depict the intrinsic flow properties which are referred as

trapping. Trapping phenomenon for non-Newtonian fluid model is presented through Figs. (2.22) to (2.24).

The consequences of curvature on trapping can be illustrated through Figs. (2.22a-2.22c). For small values of curvature parameter $(k = 2, 4)$ more streamlines are trapped in upper half than the lower half of channel. Moreover, bolus size in upper and lower half is asymmetric. When curvature parameter is increased to infinity i.e. $(k \to \infty)$, then trapping phenomenon in the channel seems to be symmetric. Effect of viscosity parameter (α) on trapping is observed through Figs. (2.23a-2.23c). In Fig. (2.23a), when viscosity is considered to be constant i.e. $(\alpha = 0)$, more streamlines are trapped in central and upper half of channel. When viscosity of the fluid is taken to be temperature dependent i.e. $(\alpha \neq 0)$ and by increasing (α), size of the bolus expands in central and upper half while it shrinks in lower half of the curved channel. The effect of Hartmann number on trapping phenomenon is portrayed through Figs. (2.24a-2.24c). It is noted that as Hartmann number (H) enhances, symmetry at both halves also increases.

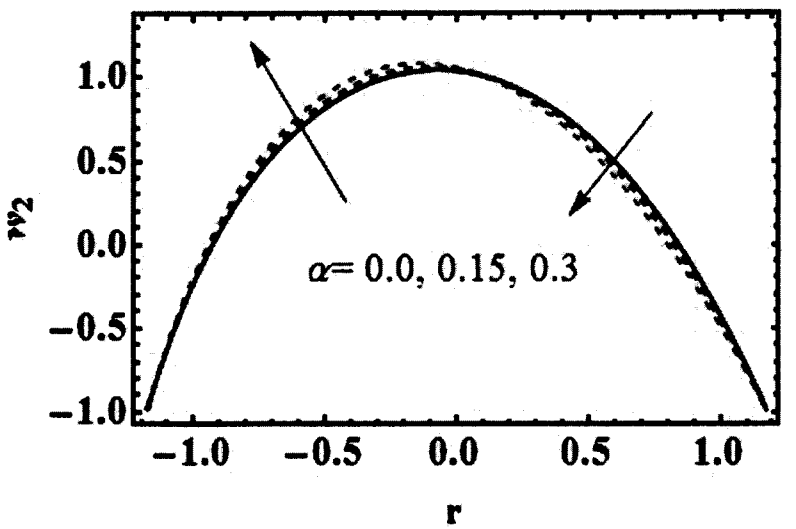

Fig. (2.2): Velocity for viscosity parameter (α)

with x=0.1, β=0.1, k = 3, Br=0.5,$\vartheta_0 = \pi/4$, H=1.2, λ_1=1.5.

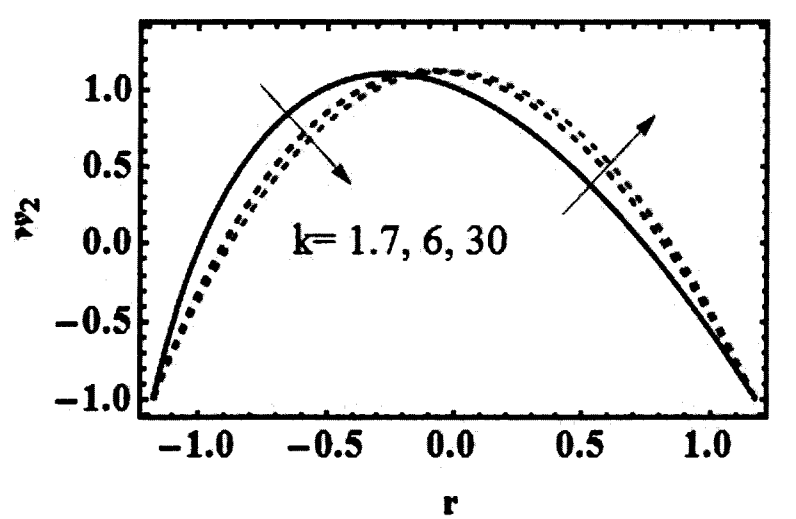

Fig. (2.3): Velocity for curvature parameter (k)

with x=0.1, α=0 β=0.1, Br=0.5,$\vartheta_0 = \pi/4$, H=1.2, λ_1=1.5.

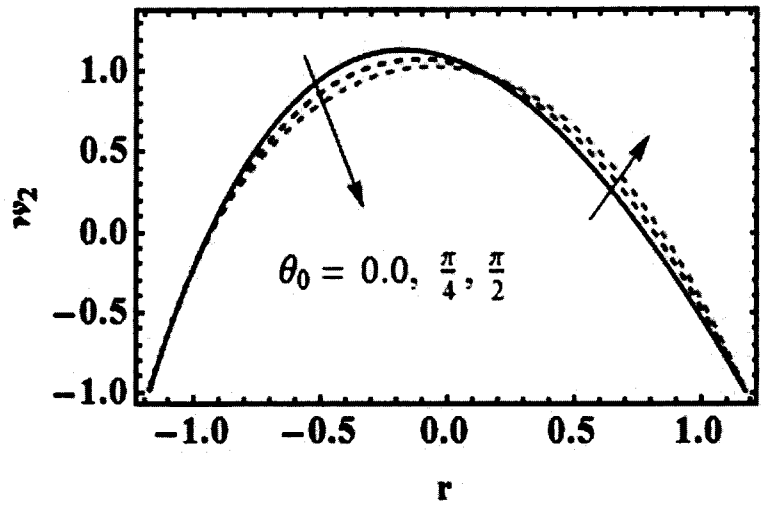

Fig. (2.4): Velocity for inclination parameters

with x=0.1, α=0 β=0.1, k = 1.7, Br=0.5, H=1.2, λ_1=1.5.

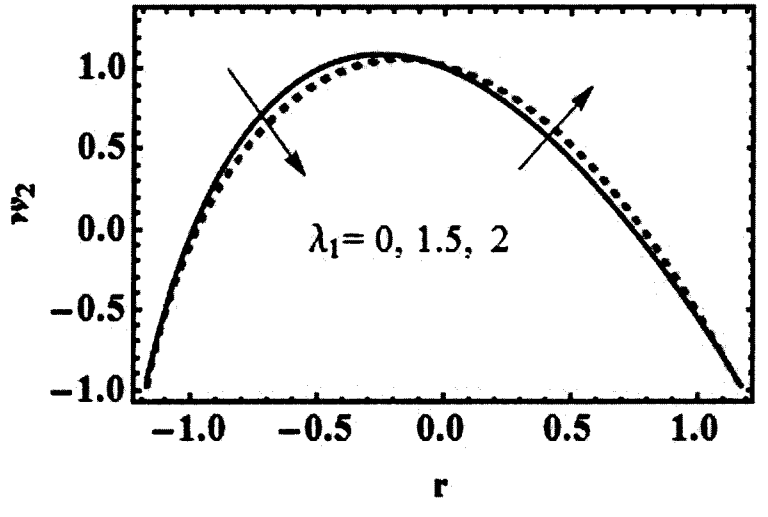

Fig. (2.5): Velocity for ratio of relaxation to retardation time

with x=0.1, α=0 β=0.1, k = 1.7, Br=0.5, ϑ_0 =π/4, H=1.2.

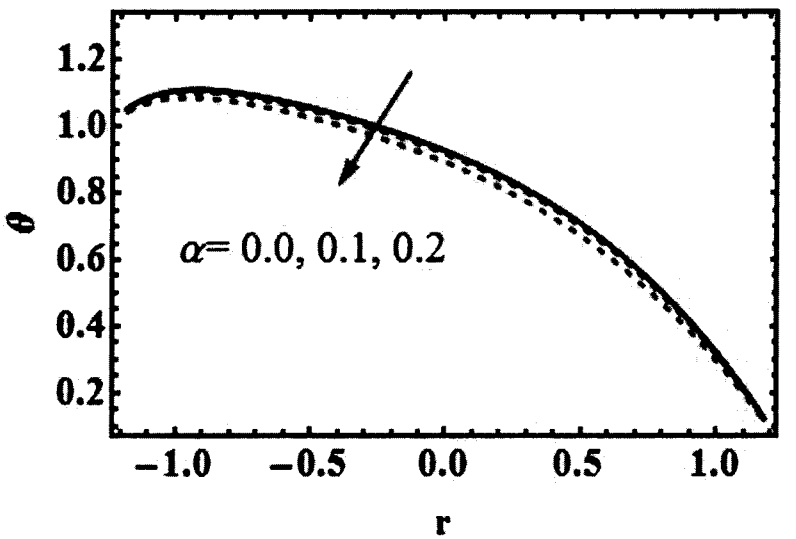

Fig. (2.6): Temperature for viscosity parameter

with β=0.1, k = 3, Br=0.5, $\vartheta_0 = \pi/4$, H=0.5, λ_1=1.5.

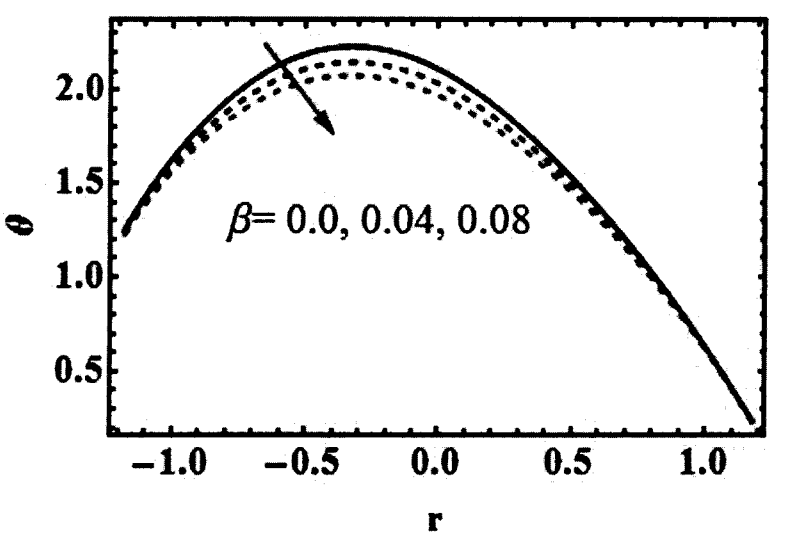

Fig. (2.7): Temperature for thermal conductivity parameter

with α=0.05, k = 3, Br=0.5, $\vartheta_0 = \pi/4$, H=0.5, λ_1=1.5.

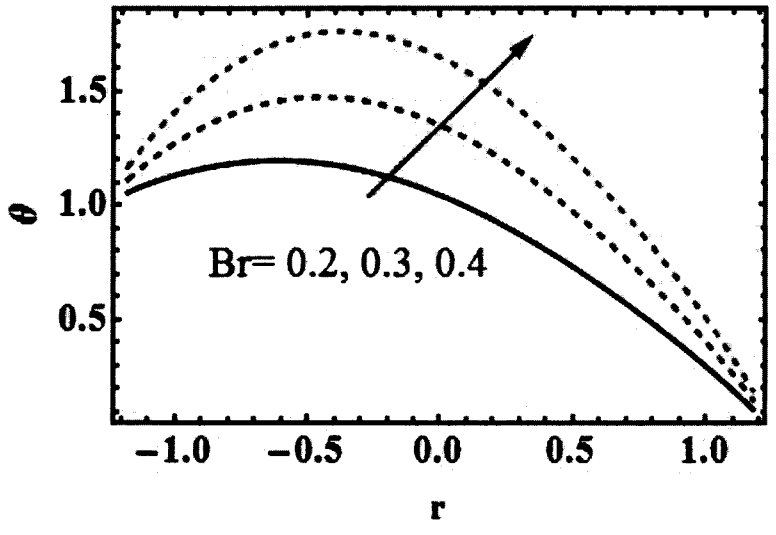

Fig. (2.8): Temperature for Brinkman number

with $\alpha=\beta=0.1$, $k = 3$, $\vartheta_0=\pi/4$, H=0.5, $\lambda_1=1.5$.

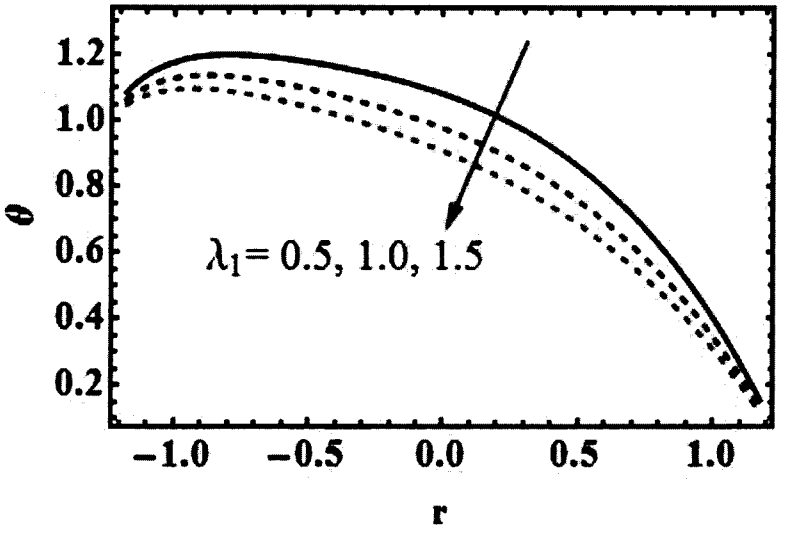

Fig. (2.9): Temperature for ratio of relax tion to retardation time with

with $\alpha=\beta=0.1$, $k = 3$, Br=0.5, $\vartheta_0=\pi/4$, H=0.5.

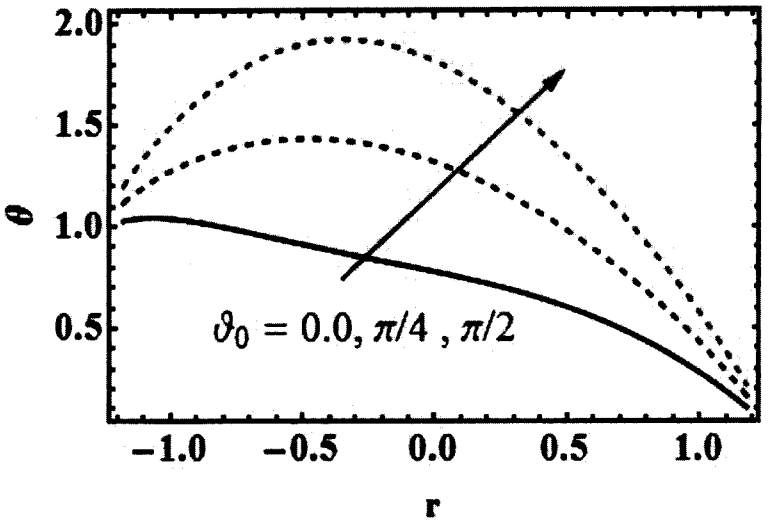

Fig. (2.10): Temperature for inclination of magnetic field with α=0.05, β=0.1, k = 3, Br=0.5, H=1, λ_1=1.5.

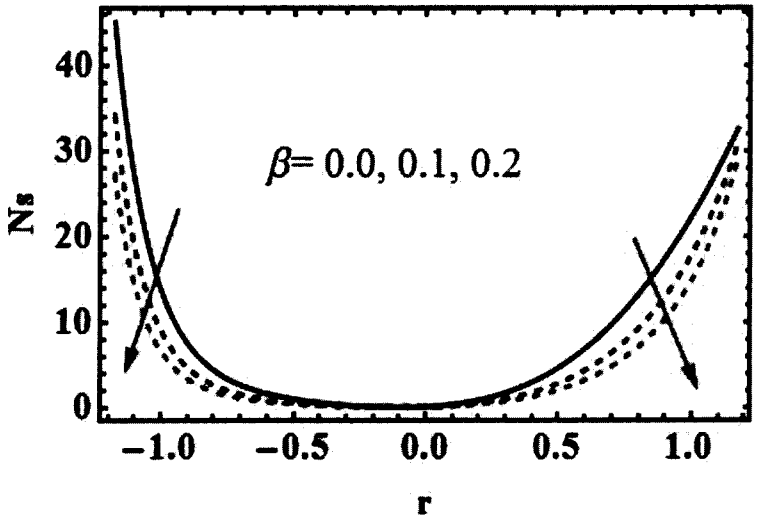

Figs. (2.11): Entropy for thermal conductivity parameter with α=0.1, k = 3, Br=3, ϑ_0 =π/4, H=0.5, λ_1=1, Λ=0.01.

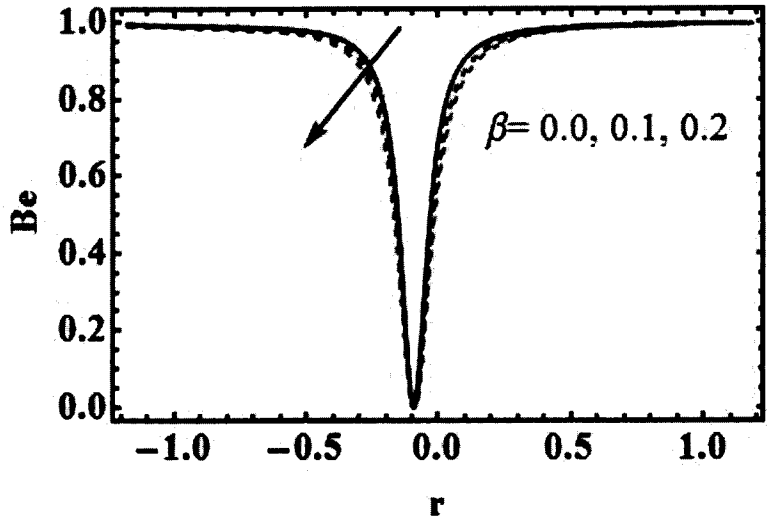

Fig. (2.12): Bejan number for thermal conductivity parameter

with α=0.1, k = 3, Br=3, $\vartheta_0 = \pi/4$, H=0.5, λ_1=1, Λ=0.01.

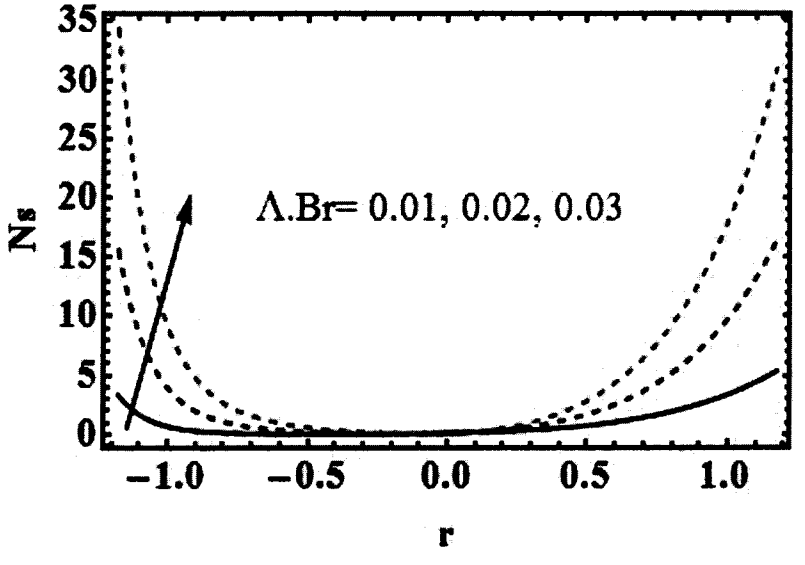

Fig. (2.13): Entropy for Brinkman number

with α=β=0.1, k = 3, $\vartheta_0 = \pi/4$, H=0.5, λ_1=1.

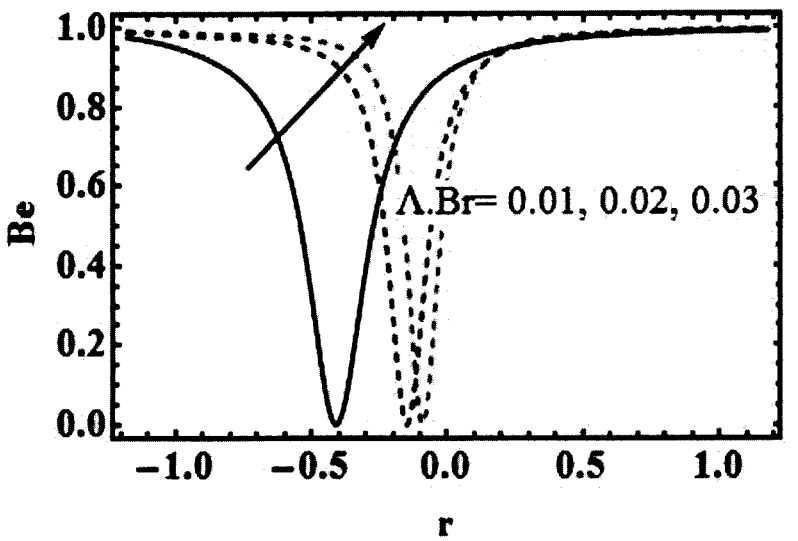

Fig. (2.14): Bejan number for Brinkman number

with $\alpha=\beta=0.1$, $k = 3$, $\vartheta_0=\pi/4$, H=0.5, $\lambda_1=1$.

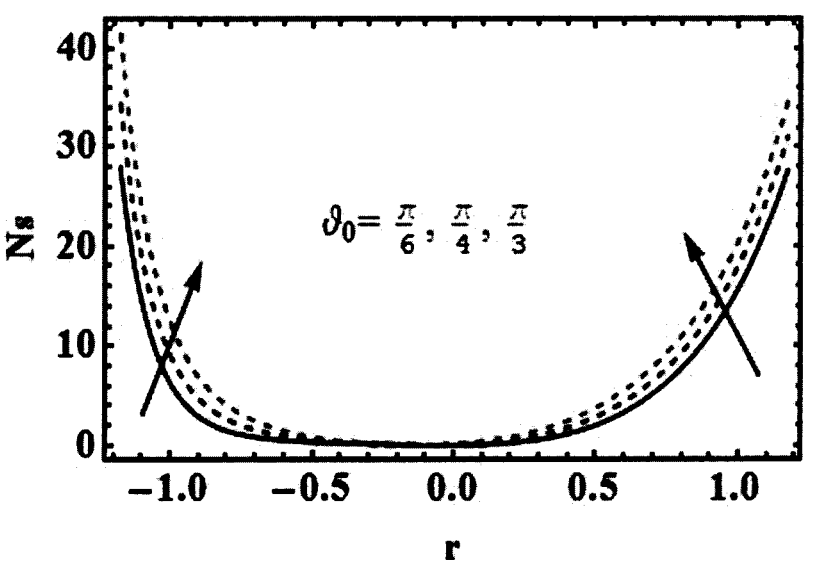

Fig. (2.15): Entropy for inclination of magnetic field

with $\alpha=\beta=0.1$, $k = 3$, Br=3, H=0.5, $\lambda_1=1$, $\Lambda=0.01$.

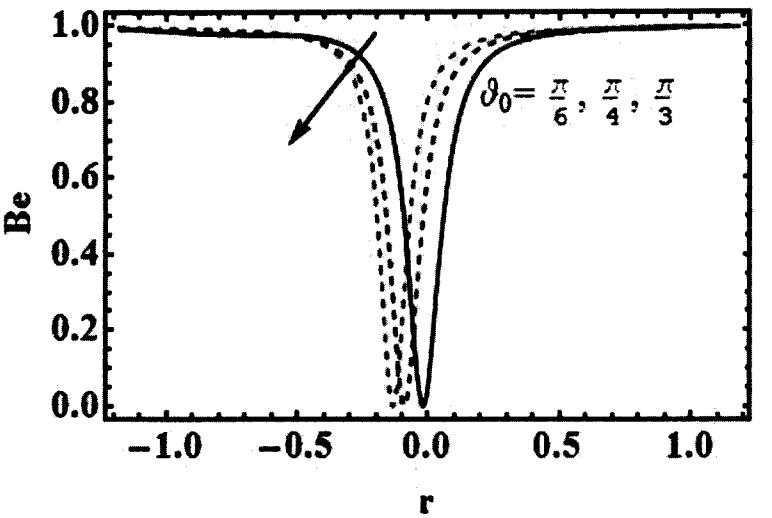

Fig. (2.16): Bejan number for inclination of magnetic field with $\alpha=\beta=0.1$, $k = 3$, Br=3, H=0.5, $\lambda_1=1$, $\Lambda=0.01$.

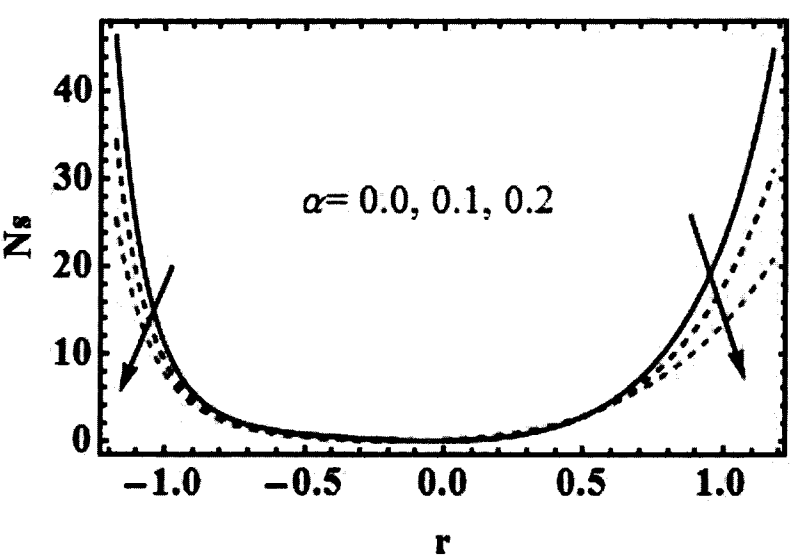

Fig. (2.17): Entropy for thermal conductivity parameter with $\beta=0.1$, $k = 3$, Br=3, $\vartheta_0=\pi/6$, H=0.5, $\lambda_1=1$, $\Lambda=0.01$.

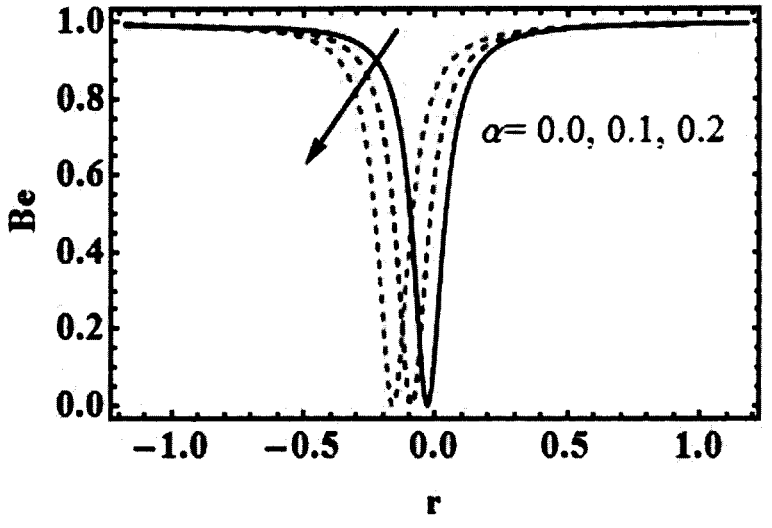

Fig. (2.18): Bejan number for thermal conductivity parameter with β=0.1, k = 3, Br=3, $\vartheta_0 = \pi/6$, H=0.5, λ_1=1, Λ=0.01.

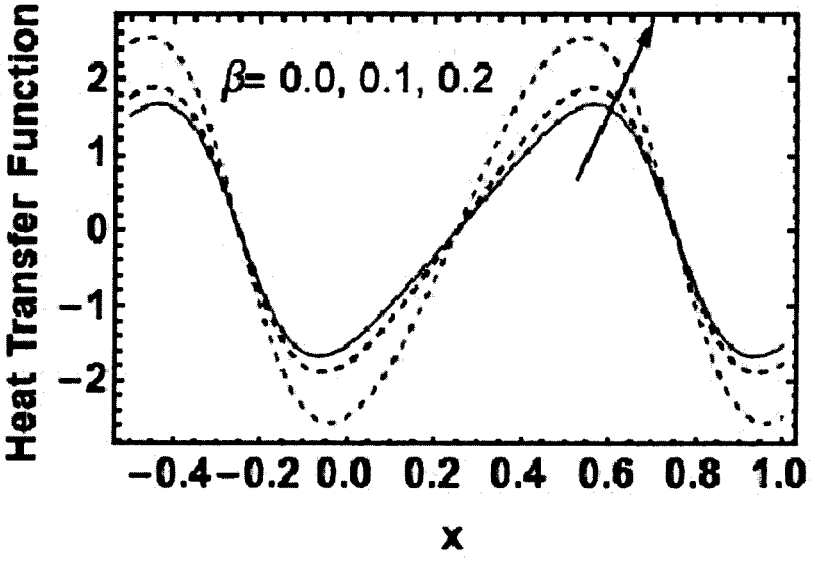

Fig. (2.19): Heat transfer function for thermal conductivity parameter with α= 0.1, k = 3, Br=0.5, $\vartheta_0 = \pi/4$, H=1.5, λ_1=1, Λ=0.01.

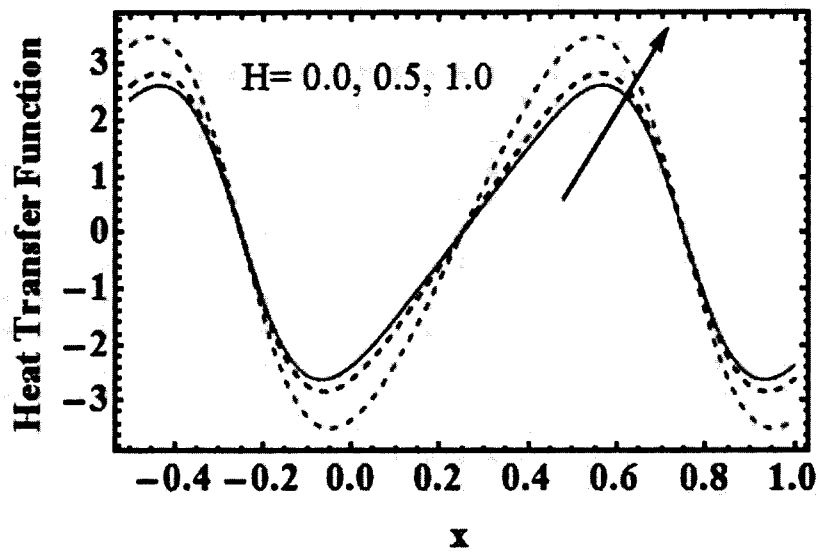

Fig. (2.20): Heat transfer function for Hartmann number

with $\alpha=\beta=0.1$, $k = 3$, Br=0.5, $\vartheta_0=\pi/4$, $\lambda_1=1$, $\Lambda=0.01$.

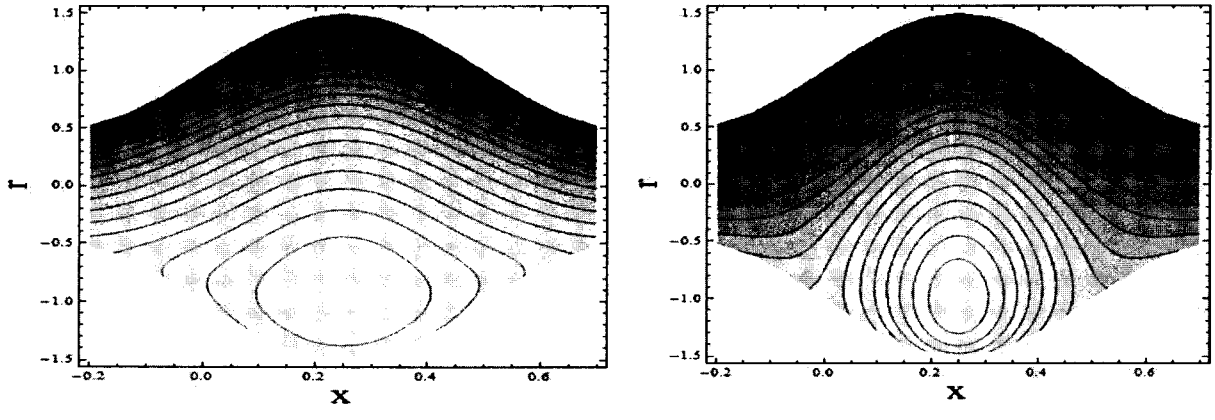

(a): k= 1.7

(b): k=100

Figs. (2.21a, 2.21b): Temperature contours for curvature parameters

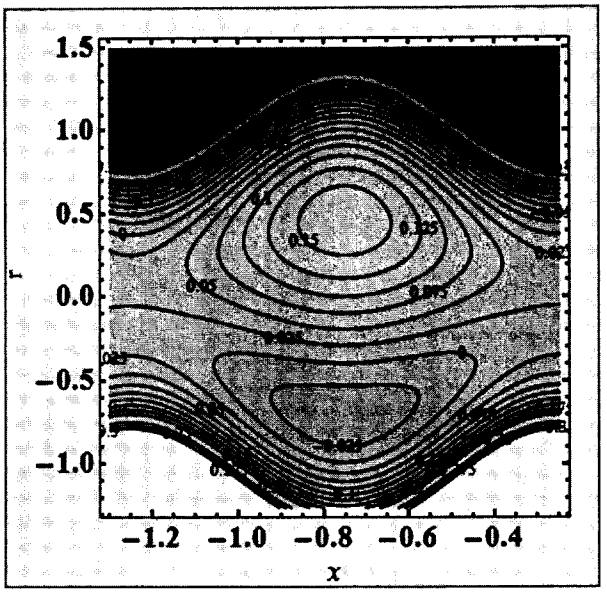

(a): $k = 2$

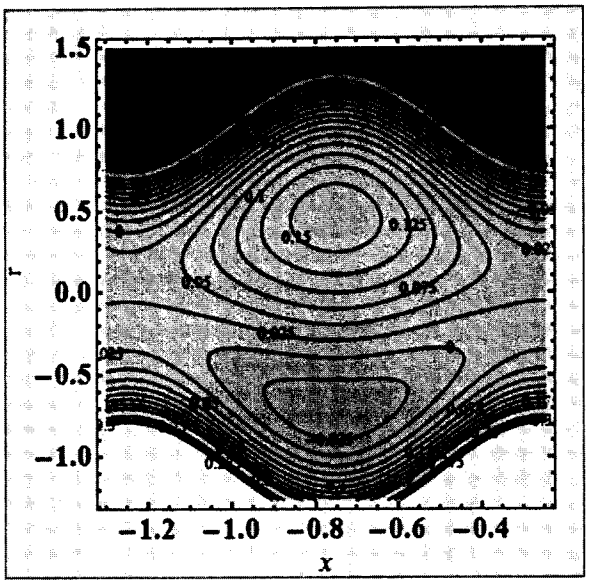

(b): $k = 4$

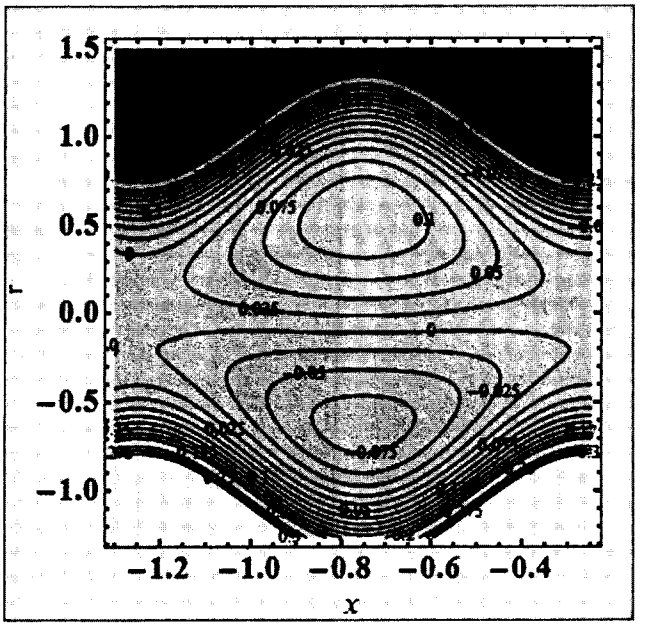

(c): $(k \to \infty)$

Figs. (2.22a-2.22c): Stream lines for curvature parameter k

with α=0.1, β=0.1, $\vartheta_0 = \pi/4$, H=0.3, λ_1=1.5.

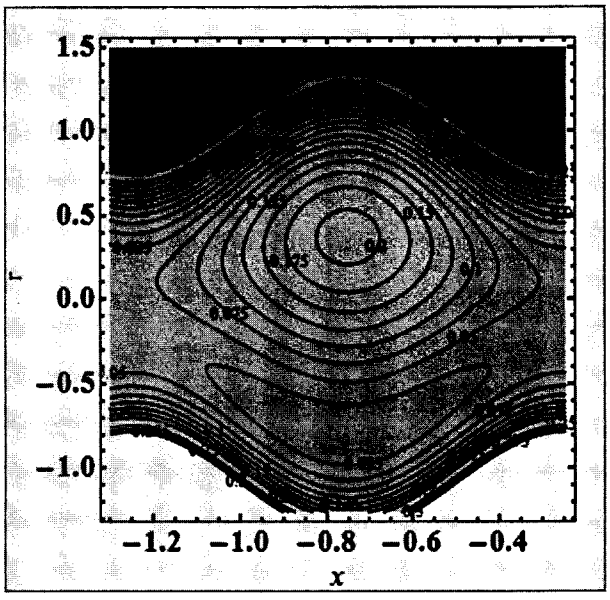

(a): α= 0.0

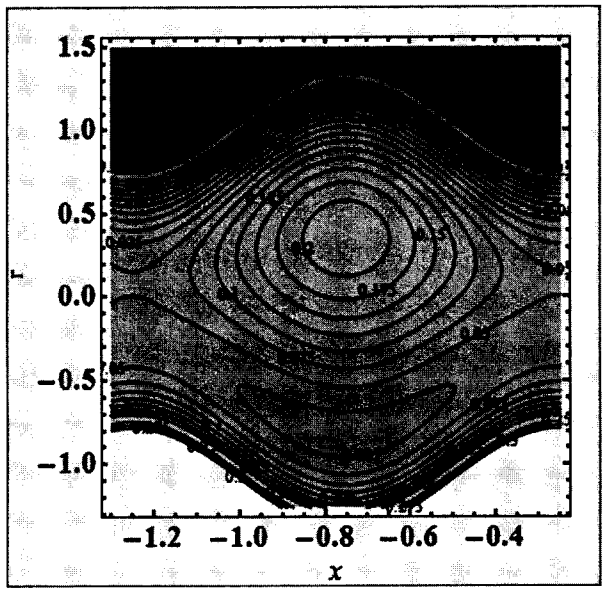

(b): α = 0.1

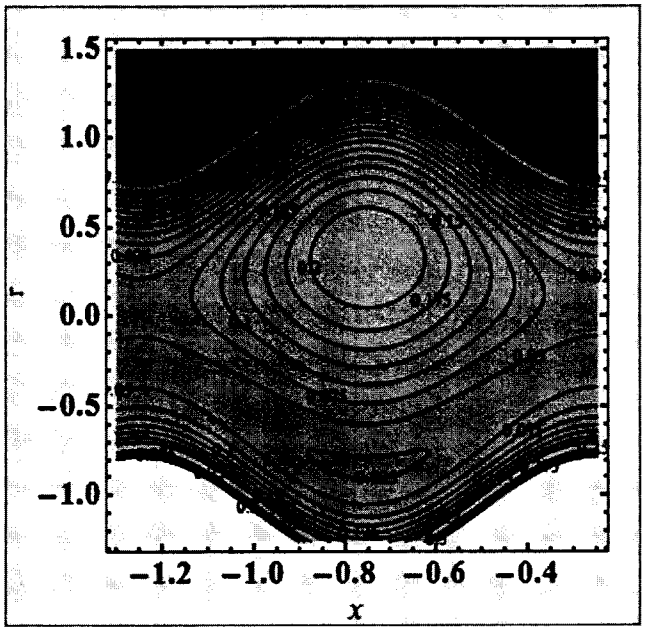

(c):α = 0.2

Figs. (2.23a-2.23c): Stream lines for viscosity parameter

with *H=0.3*, β=0.1, $\vartheta_0=\pi/4$, *k* =2, λ_1=1.5.

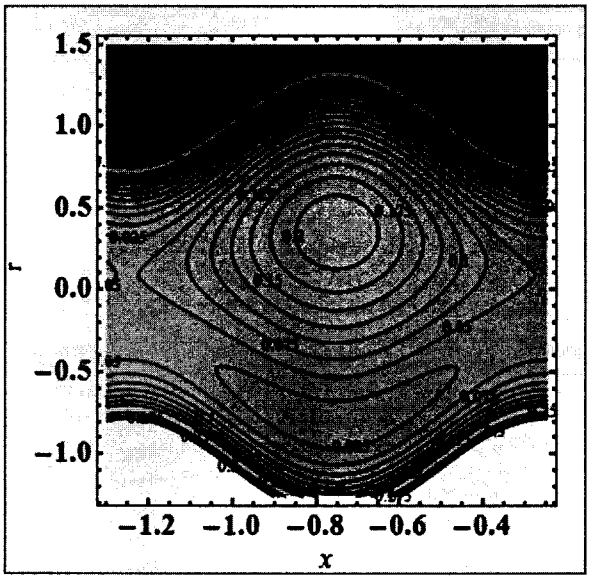

(a) H= 0.2

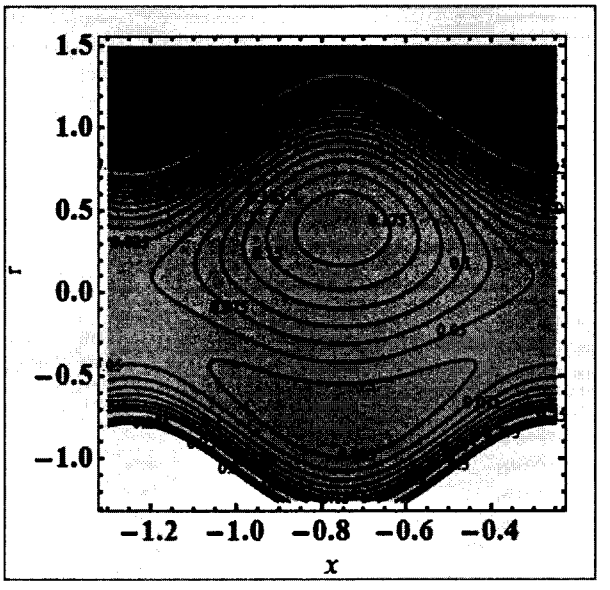

(b) H= 0.6

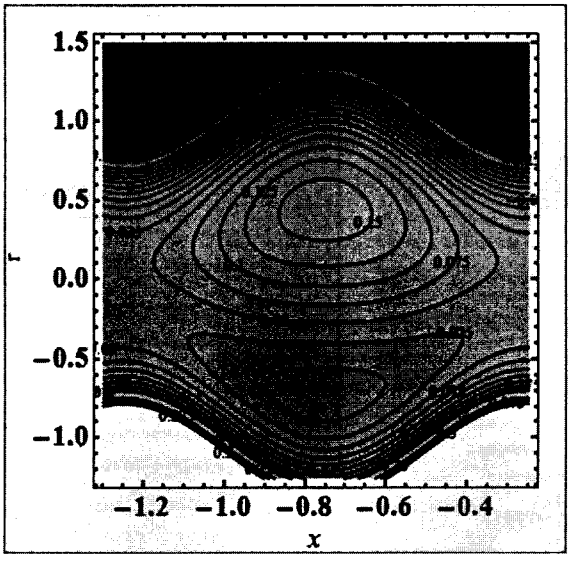

(c) H= 0.9

Figs. (2.24a-2.24c): Stream lines for Hartmann number H

with β=0.1, $\vartheta_0 = \pi/4$, k =2, λ_1=1.5.

2.4 Conclusions

In this chapter, peristaltic flow of Jeffrey liquids has been taken. Physical properties of the material are modeled as variables. Inclined magnetic field is formulated mathematically for curved geometry. Velocity, temperature, entropy and isotherms of the flow are analyzed. Key points are as follow:

- There is opposite response for α and ϑ_0 for axial velocity.
- Temperature is decreased by higher α and β.
- Rate of heat transfer shows similar response for β and H.
- Response of entropy is found parabolic for considered parameters.
- Entropy is higher for ϑ_0 and $\Lambda.Br$.
- Entropy minimizes for α and β.
- Temperature distribution is higher for curved channel in contrast to straight channel.

Chapter 3

Soret-Dufour impacts with Activation Energy in Peristaltic Mechanism of Third Grade Material

In this chapter heat and mass transfer in peristalsis of MHD third grade material are addressed. Soret and Dufour contributions are examined. Variable properties of thermal conductivity and viscosity are considered. Compliant wall properties are taken. Thermal radiation is present. Furthermore, non-linear activation energy through chemical reaction is also considered. Slip boundary conditions are taken for momentum, energy and concentration flow. Numerical solutions to the considered problems are developed and analyzed.

3.1 Mathematical Formulation

Effects of Soret and Dufour in peristalsis of electrically conducting third grade material are analyzed in curved geometry. Width of channel is $2a$. It is coiled in circle $\left(O,R^{'}\right)$. Components $\left(W_1,W_2\right)$ of velocity $\mathbf{W}$ are along radial and axial directions (R,X) respectively. Thermal conductivity and viscosity are taken as functions of temperature. Waves are traveling along with channel walls with wavelength λ, speed s and amplitude b as in Fig. (2.1). Geometry of such waves satisfies

$$\bar{r} = \pm\chi(X,t) = \pm\left[a + b\sin\left(\frac{2\pi}{\lambda}(X - st)\right)\right], \tag{3.1}$$

Conservation of energy and concentration laws with thermal radiation, viscous dissipation, Soret and Dufour impacts and activation energy with chemical reaction are considered. Compliant wall properties at the boundaries of curved channel are taken. Velocity, heat and mass transfer for slip effects are applied at channel walls. Magnetic field having strength (B_0) is exerted radially direction for $\vartheta_0 = 90^o$ (see Eqn. (2.2)). Impact of induced magnetic field is not taken into account because of low magnetic Reynolds number. We write

$$\mathbf{B} = \left(\frac{R'}{R'+R}B_0, 0, 0\right). \tag{3.2}$$

By Ohm's law and Lorentz force as defined in Eqns. (2.3) and (2.4), we arrived at

$$\mathbf{F} = \left(0, -\sigma\left(\frac{R'B_0}{R'+R}\right)^2 W_2, 0\right), \tag{3.3}$$

in which $\mathbf{F}$ denotes body force due to magnetic field along radial direction and σ electric conductivity. According to Rosseland approximation radiative heat flux $(\mathbf{q}_r)$ [74] is:

$$\mathbf{q}_r = -\frac{16T_0^3\sigma^*}{3k^*}(\nabla T), \tag{3.4}$$

in which k^* and $\sigma^*\left(=5.6697\times10^{-8}Wm^{-2}K^{-4}\right)$ represent mean absorption coefficient and Stephan-Boltzmann constant respectively and

$$\nabla T = \left(\frac{\partial T}{\partial R}, \frac{R'}{R'+R}\frac{\partial T}{\partial X}\right). \tag{3.5}$$

Governing equations with considered assumptions are as under

$$\frac{R^{'}}{R^{'}+R}\frac{\partial W_2}{\partial X}+\frac{\partial W_1}{\partial R}+\frac{W_1}{R^{'}+R}=0, \tag{3.6}$$

$$\rho\left(\frac{dW_2}{dt}+\frac{W_1W_2}{R+R^{'}}\right)=\frac{R^{'}}{R+R^{'}}\left(\begin{array}{l}-\dfrac{\partial P}{\partial X}+\dfrac{\partial S_{XX}}{\partial X}-\sigma\dfrac{R^{'}B_0^2}{R+R^{'}}W_2\\ +\dfrac{1}{R^{'}\left(R+R^{'}\right)}\dfrac{\partial}{\partial R}\left(\left(R+R^{'}\right)^2S_{XR}\right)\end{array}\right), \tag{3.7}$$

$$\rho\left(\frac{dW_1}{dt}-\frac{W_2^2}{R+R^{'}}\right)=-\frac{\partial P}{\partial R}-\frac{S_{XX}}{R+R^{'}}+\frac{1}{R+R^{'}}\frac{\partial}{\partial R}\left(\left(R+R^{'}\right)S_{RR}\right)+\frac{R^{'}}{R+R^{'}}\frac{\partial S_{XR}}{\partial X}, \tag{3.8}$$

$$\begin{aligned}\rho C_p\frac{dT}{dt}&=\frac{\partial}{\partial R}\left(\kappa(T)\frac{\partial T}{\partial R}\right)-\frac{\kappa(T)}{R+R^{'}}\frac{\partial T}{\partial R}+\frac{\partial}{\partial X}\left(\frac{\kappa(T)R^{'2}}{\left(R+R^{'}\right)^2}\frac{\partial T}{\partial X}\right)-\frac{\partial W_2}{\partial R}\left(-S_{RR}+S_{XX}\right)\\&-\left(-\frac{R^{'}}{R+R^{'}}\frac{\partial W_1}{\partial X}-\frac{\partial W_2}{\partial R}+\frac{W_2}{R+R^{'}}\right)S_{RX}-\frac{D_Bk_T}{c_s}\left(-\frac{\partial^2}{\partial X^2}-\frac{\partial^2}{\partial R^2}-\frac{1}{R+R^{'}}\frac{\partial}{\partial R}\right)C\\&+\sigma\left(\frac{R^{'}B_0}{R^{'}+R}\right)^2\left(W_1^2+W_2^2\right)-\frac{16\sigma^*T_0^3}{3k^*}\left(-\frac{\partial^2}{\partial X^2}-\frac{1}{R+R^{'}}\frac{\partial}{\partial R}-\frac{\partial^2}{\partial R^2}\right)T,\end{aligned} \tag{3.9}$$

$$\begin{aligned}\frac{dC}{dt}&=-D_B\left[-\frac{\partial^2}{\partial X^2}-\frac{1}{R+R^{'}}\frac{\partial}{\partial R}-\frac{\partial^2}{\partial R^2}\right]C-\frac{D_Bk_T}{T_m}\left[-\frac{\partial^2}{\partial X^2}-\frac{1}{R+R^{'}}\frac{\partial}{\partial R}-\frac{\partial^2}{\partial R^2}\right]T\\&-k_r^2\left(\frac{T}{T_0}\right)^n(-C_0+C)\exp\left(-\frac{E_a}{\Upsilon^*T}\right),\end{aligned} \tag{3.10}$$

where T represents temperature of fluid, ρ fluid density, C_p specific heat, C concentration, D_B mass diffusion coefficient, k_T thermal diffusion ratio, c_s concentration susceptibility, $\kappa(T)$ temperature dependent thermal conductivity coefficient, k_r^2 chemical reaction rate, E_a activation energy, $\mathbf{L}(=\operatorname{grad}\mathbf{W})$, T_{mean} and

$\Upsilon^*\left(=8.61\times10^{-5}ev/k\right)$ are mean material temperature and Boltzmann respectively.

The imposed boundary conditions are

$$\pm\gamma_1' S_{XR}+W_2=0, \quad \text{at} \quad R=\pm\chi, \tag{3.11}$$

$$\pm\gamma_2'\frac{\partial T}{\partial R}+T=\begin{Bmatrix}T_1\\T_0\end{Bmatrix} \quad \text{at} \quad R=\pm\chi, \tag{3.12}$$

$$\pm\gamma_3'\frac{\partial C}{\partial R}+C=\begin{Bmatrix}C_1\\C_0\end{Bmatrix} \quad \text{at} \quad R=\pm\chi, \tag{3.13}$$

$$\left(m'\frac{\partial^3}{\partial X\partial t^2}-\tau'\frac{\partial^3}{\partial X^3}+d'\frac{\partial^2}{\partial X\partial t}\right)\chi=\frac{\partial P}{\partial X} \quad \text{at} \quad R=\pm\chi, \tag{3.14}$$

Model of third grade fluid is defined as [67]:

$$\boldsymbol{\tau}=-p\mathbf{I}+\mathbf{S}, \tag{3.15}$$

$$\mathbf{S}=\mu(T)\mathbf{B}_1+\beta_1\mathbf{B}_2+\beta_2\mathbf{B}_1^2+\alpha_1\left(tr\mathbf{B}_1^2\right)\mathbf{B}_1, \tag{3.16}$$

$$\mathbf{B}_1=\mathbf{L}'+\mathbf{L}, \tag{3.17}$$

$$\mathbf{B}_2=\left(\frac{\partial}{\partial t}+\mathbf{W}.\nabla\right)\mathbf{B}_1+\mathbf{B}_1\mathbf{L}+\mathbf{L}'\mathbf{B}_1, \tag{3.18}$$

where $\mu(T)$ portrays temperature dependent viscosity, $(\alpha_1,\beta_1,\beta_2)$ material parameters, $(\mathbf{B}_1,\mathbf{B}_2)$ first and second Rivilin-Erickson tensors such that

$$\beta_1\geq 0, \quad \alpha_1\geq 0, \quad |\beta_1+\beta_2|\leq\sqrt{24\mu\alpha_1}. \tag{3.19}$$

In this chapter viscosity and thermal conductivty of the fluid are taken temperature dependent as defined in Eqns. (2.7) and (2.8) in chapter 2.

Let the dimensionless velocities, curvature, amplitude ratio, pressure, temperature, concentration, wave number, peristaltic wall, Reynolds number, variable viscosity

parameter, components of extra stress tensor, variable thermal conductivity parameter, Brinkman number, elasticity parameters, Prandtl number, chemical reaction parameter, third grade fluid parameter, temperature ratio parameter, activation energy parameter, Schmidt number, Dufour number, Hartmann number, radiation parameter, Soret number and velocity, thermal and concentration slip parameters are

$$(w_1, w_2) = \left(\frac{\bar{w}_1}{s}, \frac{\bar{w}_2}{s}\right), \quad k = \frac{R'}{a}, \quad b_1 = \frac{b}{a}, \quad p = \frac{a^2 P}{s\mu_o \lambda}, \quad \theta = \frac{T - T_o}{T_1 - T_o},$$

$$\phi = \frac{C - C_o}{C_1 - C_o}, \quad \delta = \frac{a}{\lambda}, \quad \mathrm{Re} = \frac{\rho s a}{\mu_o}, \quad \alpha = \alpha'(T_1 - T_o), \quad S_{ij} = \frac{a S_{IJ}}{b\mu_o},$$

$$\beta = \beta'(T_1 - T_o), \quad Br = \frac{\mu_0 s^2}{\kappa_o (T_1 - T_o)}, \quad (E_1, E_2, E_3) = \left(-\frac{\tau' a^3}{\mu_o \lambda^3 s}, \frac{m' a^3}{\lambda^3 s}, \frac{d' a^3}{\lambda^2 \mu_o}\right),$$

$$\mathrm{Pr} = \frac{\mu_o c_p}{\kappa_o}, \quad \xi = \frac{\rho k_r^2 a^2}{\mu_0}, \quad \beta_3 = \frac{\alpha_1}{\mu_o}\left(\frac{s}{a}\right)^2, \quad \Omega = \frac{T_1}{T_0}, \quad Sc = \frac{\mu_o}{\rho D_B},$$

$$Du = \frac{D_B (C_1 - C_0) K_T}{C_s C_p \mu (T_1 - T_0)}, \quad H = \sqrt{\frac{\sigma B_0^2 a^2}{\mu_0}}, \quad R_d = \frac{16\sigma^* T_0^3}{3k^*}, \quad Sr = \frac{\rho D_B k_T (T_1 - T_0)}{T_{mean} \mu (C_1 - C_0)},$$

and $\gamma_i = \frac{\gamma_i'}{a}\Big|_{i=1,2,3}$ respectively. (3.21)

Velocities (w_1, w_2) as a stream function (ψ) can be defined as:

$$w_1 = \frac{\delta k}{r + k}\frac{\partial \psi}{\partial x}, w_2 = -\frac{\partial \psi}{\partial r}. \tag{3.22}$$

Substituting Eqn. (3.20) into Eqns. (3.6-3.18) then using Eqns. (3.21) and (3.22) in the resulting expressions; condition of incompressibility is satisfied trivially in Eqn. (3.6) and applying lubrication approach in rests of the expressions give

$$k\frac{\partial p}{\partial x} = \frac{1}{(r + k)}\frac{\partial}{\partial r}\left((r + k)^2 S_{rx}\right) + \frac{H^2 k^2}{k + r}\frac{\partial \psi}{\partial r}, \tag{3.23}$$

$$\frac{\partial p}{\partial r}=0, \tag{3.24}$$

$$(\beta\theta+1)\left(\frac{\partial^2\theta}{\partial r^2}+\frac{1}{r+k}\frac{\partial\theta}{\partial r}\right)+\beta\left(\frac{\partial\theta}{\partial r}\right)^2+Br\left(-\frac{1}{r+k}\frac{\partial\psi}{\partial r}+\frac{\partial^2\psi}{\partial r^2}\right)S_{xr}+Du\,\mathrm{Pr}\left(\frac{1}{r+k}\frac{\partial\phi}{\partial r}+\frac{\partial^2\phi}{\partial r^2}\right)$$
$$+R_d\,\mathrm{Pr}\left(\frac{1}{k+r}\frac{\partial\theta}{\partial r}+\frac{\partial^2\theta}{\partial r^2}\right)+Br\frac{k^2H^2}{(k+r)^2}\left(-\frac{\partial\psi}{\partial r}\right)^2=0, \tag{3.25}$$

$$\frac{1}{r+k}\frac{\partial\phi}{\partial r}+\frac{\partial^2\phi}{\partial r^2}+ScSr\left(\frac{1}{r+k}\frac{\partial\theta}{\partial r}+\frac{\partial^2\theta}{\partial r^2}\right)-Sc\xi\left(1+(\Omega-1)\theta\right)^n\varphi\exp\left(-\frac{E}{1+(\Omega-1)\theta}\right)=0. \tag{3.26}$$

Eqns. (3.23) and (3.24) imply that

$$\frac{\partial}{\partial r}\left[\frac{1}{k(r+k)}\frac{\partial}{\partial r}\left((r+k)^2S_{rx}\right)+\frac{H^2k}{k+r}\frac{\partial\psi}{\partial r}\right]=0, \tag{3.27}$$

$$S_{xr}=S_{rx}=-(1-\alpha\theta)\left(-\frac{1}{r+k}\frac{\partial\psi}{\partial r}+\frac{\partial^2\psi}{\partial r^2}\right)-2\beta_3\left(-\frac{1}{r+k}\frac{\partial\psi}{\partial r}+\frac{\partial^2\psi}{\partial r^2}\right)^3, \tag{3.28}$$

$$h=1+b_1\sin(2\pi x). \tag{3.29}$$

Dimensionless boundary conditions now are

$$-\frac{\partial\psi}{\partial r}\pm\gamma_1S_{xr}=0 \quad \text{at} \quad r=\pm h, \tag{3.30}$$

$$\pm\gamma_2\frac{\partial\theta}{\partial r}+\theta=\begin{Bmatrix}1\\0\end{Bmatrix} \quad \text{at} \quad r=\pm h, \tag{3.31}$$

$$\pm\gamma_3\frac{\partial\phi}{\partial r}+\phi=\begin{Bmatrix}1\\0\end{Bmatrix} \quad \text{at} \quad r=\pm h, \tag{3.32}$$

$$k(r+k)\left(E_2\frac{\partial^3}{\partial x\partial t^{*2}}+E_1\frac{\partial^3}{\partial x^3}+E_3\frac{\partial^2}{\partial x\partial t^*}\right)\eta_1=\frac{\partial}{\partial r}\left((r+k)^2S_{rx}\right)+H^2k^2\frac{\partial\psi}{\partial r} \quad \text{at} \quad r=\pm h. \tag{3.33}$$

3.2 Methodology

Eqns. (3.25-3.29) subject to boundary conditions (3.30-3.33) have been solved numerically by using a built in command (NDSolve) in Mathematics.

3.3 Analysis

Physical interpretations of axial velocity, temperature and concentration against pertinent parameters have been deliberated upon in this section.

3.3.1 Velocity

Fig. (3.1) shows impact of temperature dependent viscosity coefficient (α) on axial velocity. An enhancement is noticed in wave amplitude for larger α. Since μ and α have inverse relationship so for higher α, the viscosity decreases and consequently fluid velocity enhanced. Response of axial velocity for curvature (k) is seen from Fig. (3.2). Here velocity reduces near lower channel wall and it increases in remaining part of channel. Interestingly velocity is more for straight channel in contrast with curved configuration. However velocity is asymmetric about the mean position. Variation in radial magnetic field H on velocity can be observed from Fig. (3.3). Clearly velocity amplitude is decreased for an increased Hartmann number (H). As the applied radial magnetic force behaves as a resistive force that acts in opposite direction to the fluid flow. Fig. (3.4) depicts variation in third grade fluid parameter (β_3). This plot clearly shows that velocity decays for higher β_3. Figs. (3.5) and (3.6) are sketched for compliant walls coefficients (E_2, E_1) and E_3 respectively. It is noticed that velocity is increased for elastic coefficients

(E_2, E_1) and it decreased in case of damping parameter (E_3). Fig. (3.7) is formulated to show the effects of slip parameter for velocity (γ_1). Obviously origin is changing by varying γ_1.

3.3.2 Temperature

This portion describes temperature for pertinent parameters. Fig. (3.8) shows that variable thermal conductivity coefficient (β) has inverse relationship with θ. As β is increased, the temperature of material is decreased. Fig. (3.9) presents influence of Deborah parameter (β_3) on fluid temperature. It is found that temperature drops with rise of β_3. It is also noticed that temperature in third grade material is lower in comparison with viscous fluid. It is shown in Fig. (3.10) that by increasing Brinkman number$(Br)$the temperature is also enhanced due to the viscous dissipation effects. Fig. (3.11) gives Dufour (Du) effects on θ. Temperature against Du is increased. For higher Du the viscosity decreases and hence fluid velocity is increased. As a result fast movement of fluid particles together with increased molecular vibration enhances fluid temperature. Fig. (3.12) shows variation in θ versus R_d. Temperature decreases for higher R_d as it has inverse relation with radiation and k^*. There is decay in absorption parameter for higher radiation. Thus extra heat is transmitted away. Consequently temperature is decreased accordingly. Fig. (3.13) witnessed that temperature increases against higher Schmidt number Sc. Figs. (3.14) and (3.15) are drawn for compliant wall parameters (E_2, E_1) and E_3. Converse behavior of temperature is observed for elastic coefficients (E_2, E_1) and damping parameter (E_3). In

Fig. (3.16), it is shown that response of θ is increasing for increased H. Impact of temperature for slip parameters (γ_2) is change for origin of temperature (see Fig. (3.17)).

3.3.3 Concentration

Figs. (3.18) to (3.24) are plotted for effects of parameters under consideration on concentration (ϕ). Figs. (3.18) and (3.19) show the decreasing behavior of concentration for both Sr and Sc. Mass diffusion decreases for increasing Sr and so concentration decreases accordingly. Fig. (3.20) illustrates ϕ via E. When activation energy parameter (E) is enhanced, the value of expression of Arrhenius form decreases which corresponds to enlarged chemical reaction. As a result the concentration increases. Fig. (3.21) shows slight decrease in concentration for increased n. Fig. (3.22) is prepared to observe concentration behavior for increasing chemical reaction (ξ). This sketch depicts that concentration is reduced for increased destructive chemical reaction parameter (ξ). Fig. (3.23) shows ϕ against β_3. It is evident that concentration is high for third grade material than viscous fluid. Fig. (3.24) gives concentration outcome for slip parameter (γ_3). It is evident that concentration shows dual response near upper and lower channel walls by varying γ_3.

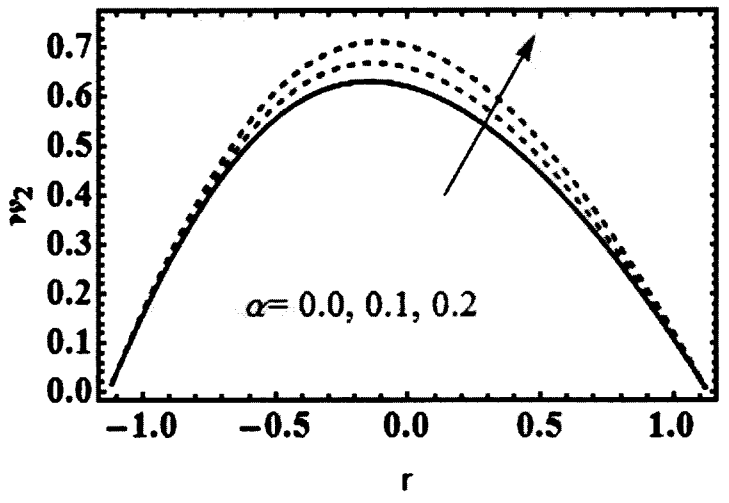

Fig. (3.1): Velocity profile for viscosity coefficient with $k = 3, \xi = 0.1, \beta_3 = \beta = 0.1, Br = 2, H = 0.4,$ $Sr = 1, Du = \Pr = Sc = 0.5, Rd = 0.5.$

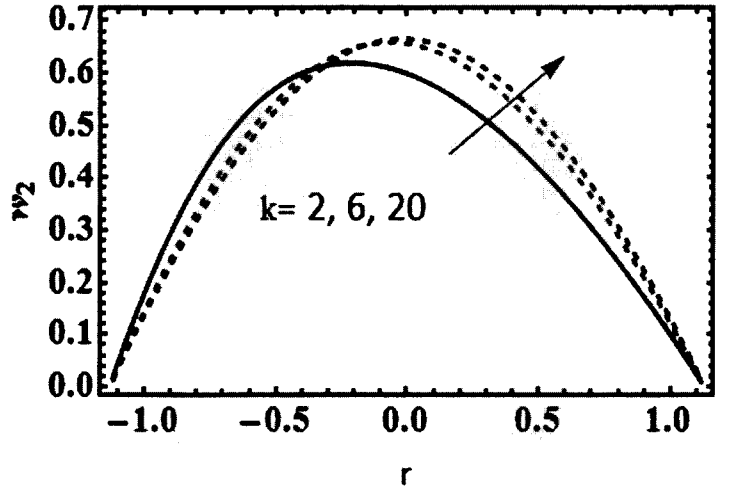

Fig. (3.2): Velocity profile for curvature parameter with $\xi = 0.1, \beta_3 = \beta = 0.1, Br = 2, H = 0.4,$ $Sr = 1, \alpha = 0.03, Du = \Pr = Sc = 0.5, Rd = 0.5.$

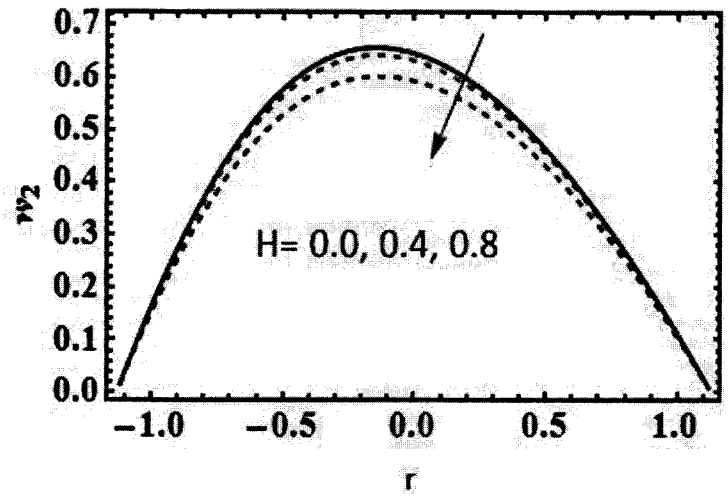

Fig. (3.3): Velocity profile for Hartmann number with $k = 3, \alpha = 0.03, \beta_3 = \beta = 0.1, Br = 2, H = 0.4,$ $Sr = 1, Du = \Pr = Sc = 0.5, \xi = 0.1, Rd = 0.5.$

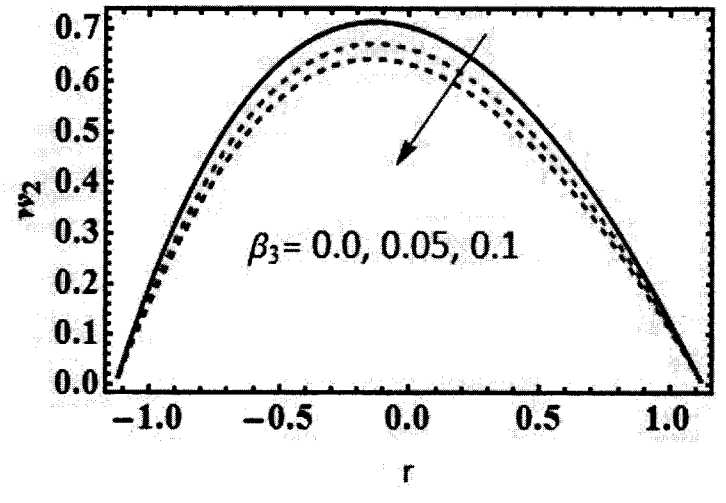

Fig. (3.4): Velocity profile for fluid parameter with $k = 3, \alpha = 0.03, \beta_3 = \beta = 0.1, Br = 2, H = 0.4,$ $Sr = 1, Du = \Pr = Sc = 0.5, \xi = 0.1, Rd = 0.5.$

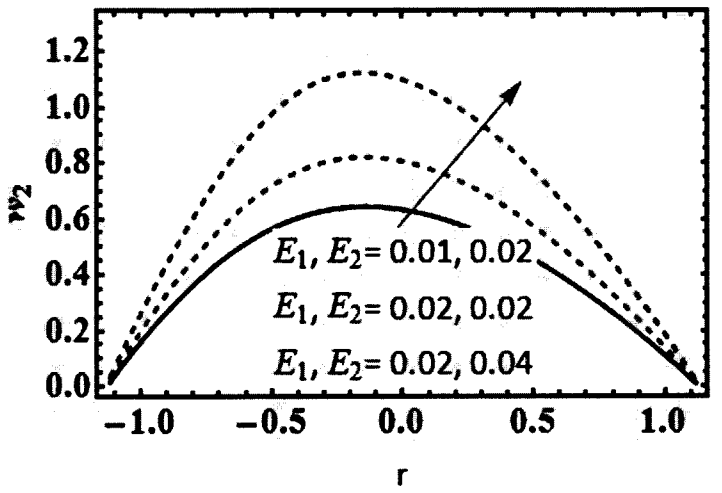

Fig. (3.5): Velocity profile for elastic parameters with $k = 3, \alpha = 0.03, \beta_3 = \beta = 0.1, Br = 2,$ $Sr = 1, H = 0.4, Rd = 0.5, \Pr = Du = Sc = 0.5, \xi = 0.1.$

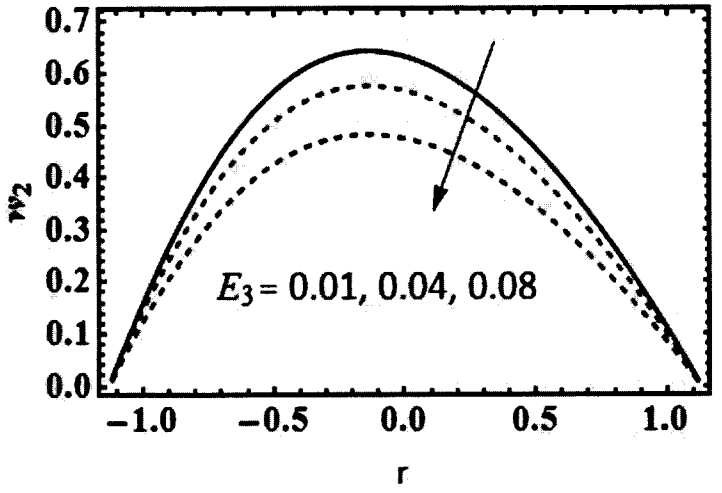

Fig. (3.6): Velocity profile for elastic parameters with $k = 3, \alpha = 0.03, \beta_3 = \beta = 0.1, Br = 2,$ $Sr = 1, H = 0.4, Rd = 0.5, \Pr = Du = Sc = 0.5, \xi = 0.1.$

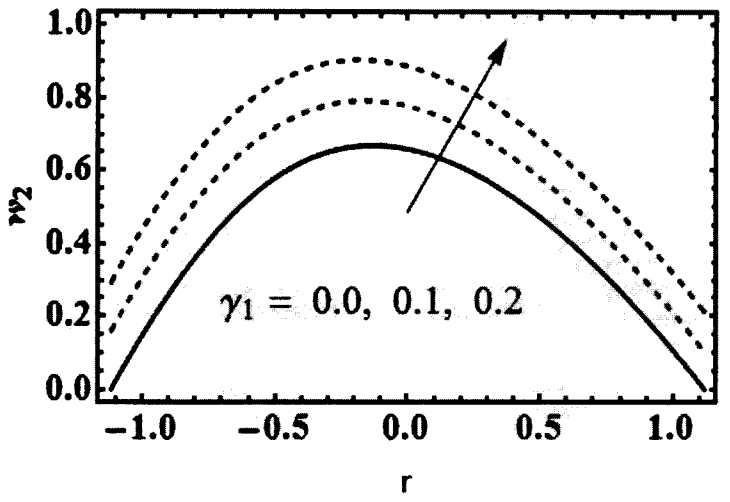

Fig. (3.7) : Velocity profile for slip parameter with $k = 3, \alpha = 0.1, \beta_3 = \beta = 0.1, Br = 1, Rd = 0.5, \xi = 0.1,$ $Sr = 1, H = 0.2, \Pr = Sc = 0.5.$

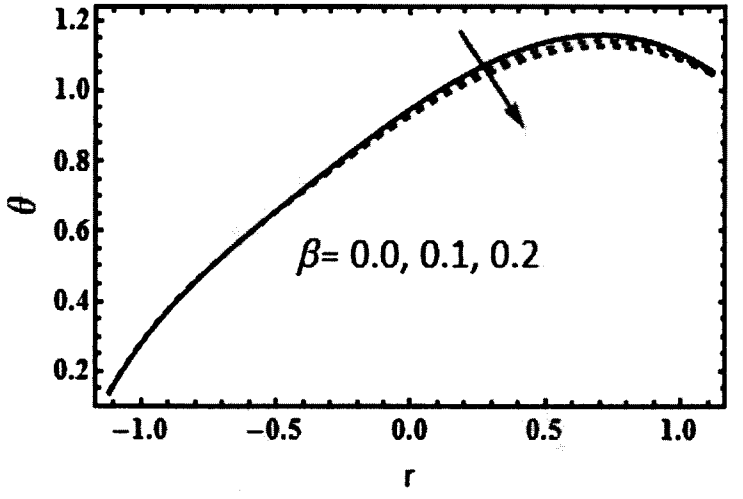

Fig. (3.8): Temperature profile for thermal conductivity coefficient with $k = 3, \alpha = 0.03, \beta_3 = 0.1,$ $Br = 2, Du = 0.8, H = 0.1, Sc = \Pr = 0.5, Sr = 1, Rd = 0.5, \xi = 0.1.$

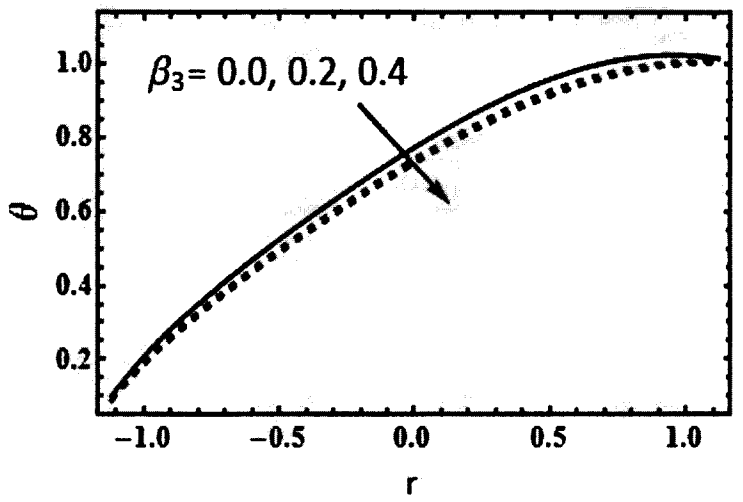

Fig. (3.9): Temperature profile for fluid parameter with $\alpha = 0.03, \beta_3 = \beta = 0.1, Br = 2, Du = 0.8,$ $H = 0.1, Sc = \Pr = 0.5, Sr = 1, Rd = 0.5, \xi = 0.1.$

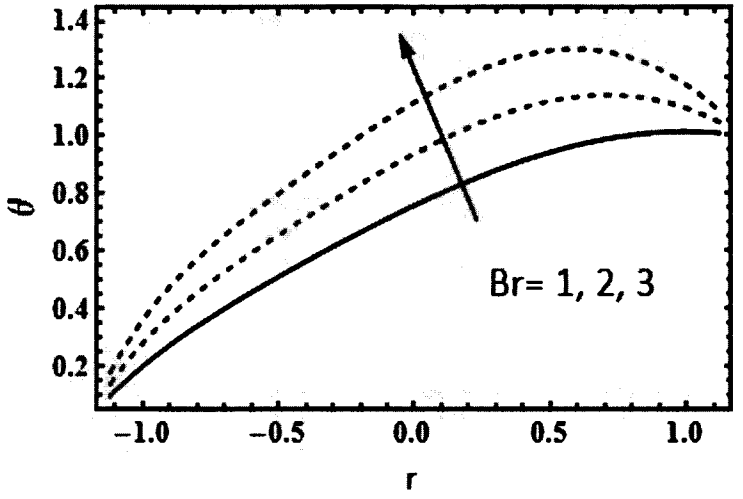

Fig. (3.10): Temperature profile for Brinkman number with $k = 3, \alpha = 0.03, H = 0.1, \beta_3 = \beta = 0.1,$ $Sr = 1, \Pr = Sc = 0.5, Rd = 0.5, \xi = 0.1.$

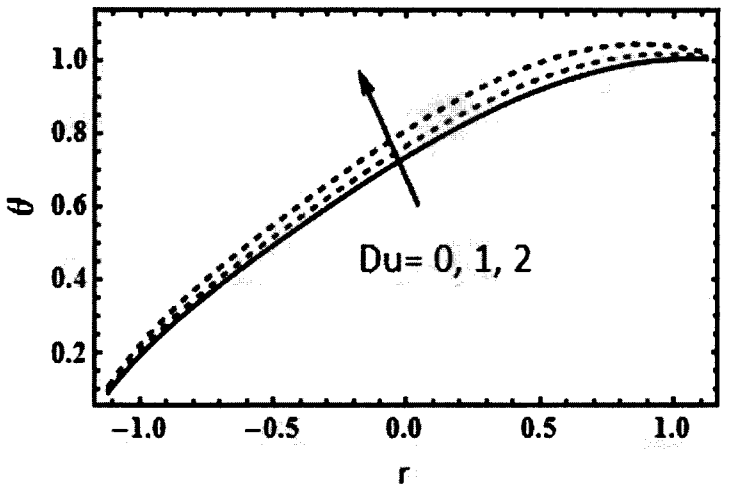

Fig. (3.11) : Temperature profile for Dufour parameter with $k = 3, \alpha = 0.03, H = 0.1, \beta_3 = \beta = 0.1,$ $Sr = 1, Br = 2, \Pr = Sc = 0.5, Rd = 0.5, \xi = 0.1.$

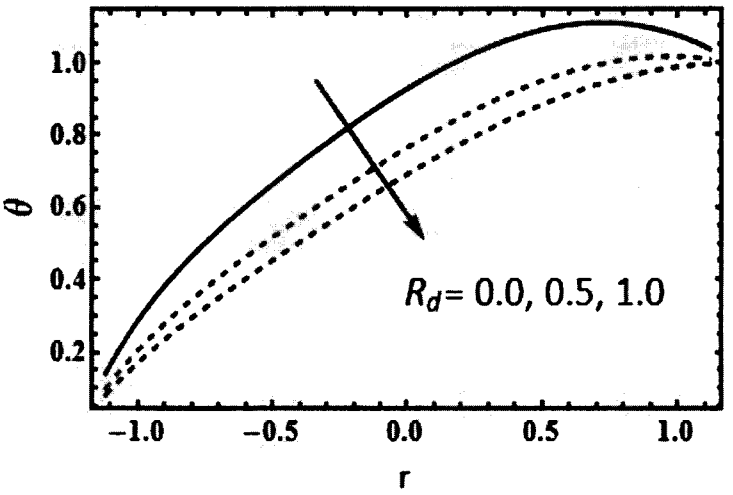

Fig. (3.12): Temperature profile for thermal radiation parameter with $k = 3, Sr = Du = 1, Br = 1,$ $\beta = \beta_3 = 0.1, \alpha = 0.03, H = 0.1, Sc = \Pr = 0.5, \xi = 0.1.$

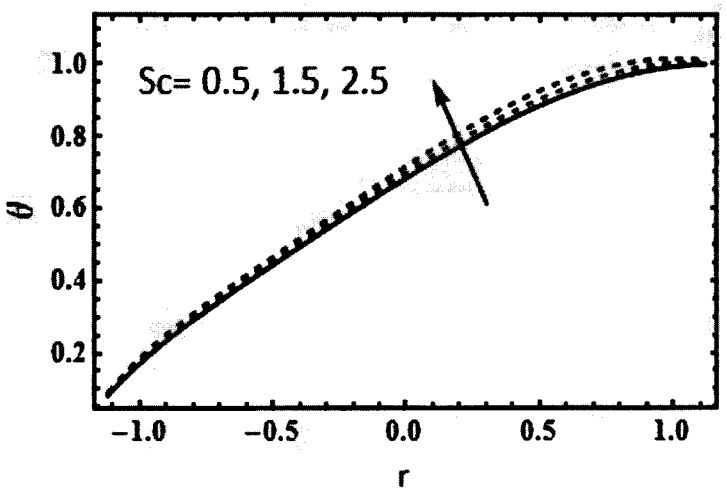

Fig. (3.13) : Temperature profile for Schmidt number with $k = 3, Sr = Du = 1, Br = 1, \beta = \beta_3 = 0.1,$ $\alpha = 0.03, H = 0.1, \Pr = 0.5, Rd = 0.5, \xi = 0.1.$

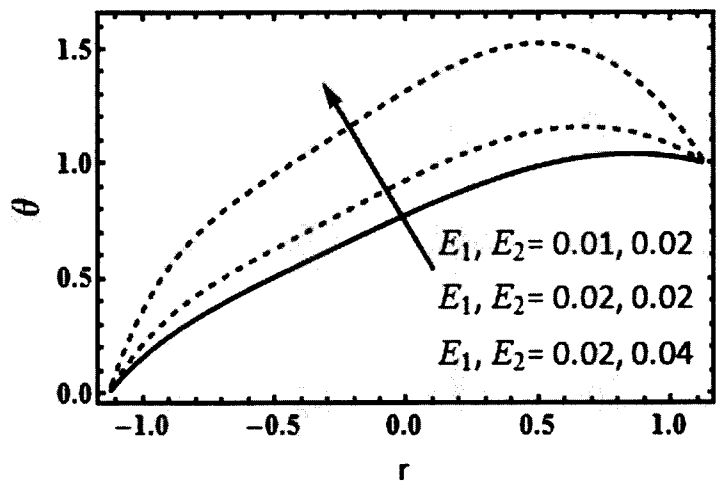

Fig. (3.14): Temperature profile for elastic wall parameters with $k = 3, Br = 2, \xi = 0.1, \alpha = 0.03,$ $Du = 0.5, \beta_3 = \beta = 0.1, Sc = \Pr = 0.5, Rd = 0.5, Sr = 1.$

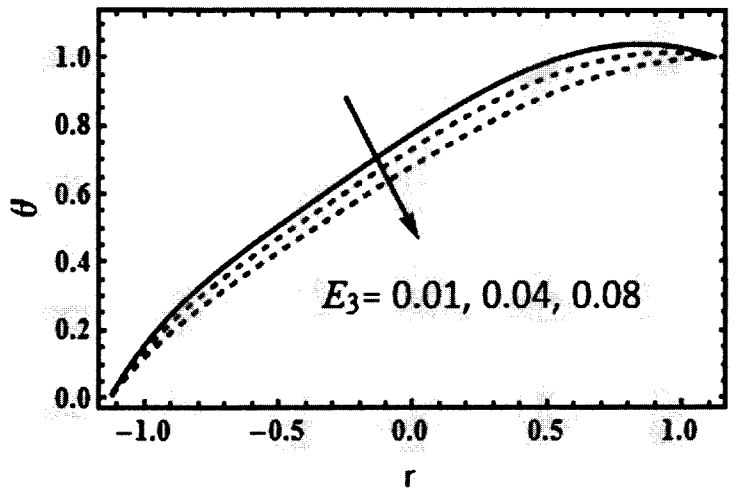

Fig. (3.15) : Temperature profile for elastic wall parameters with $k = 3, Br = 2, \xi = 0.1, \alpha = 0.03,$ $Du = 0.5, \beta_3 = \beta = 0.1, Sc = \Pr = 0.5, Rd = 0.5, Sr = 1.$

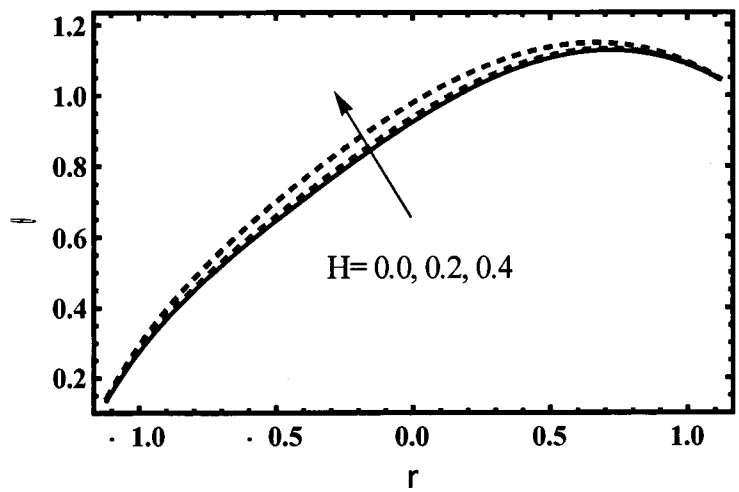

Fig. (3.16): Temperature profile for Hartmann number with k=3,α=0.03,β_3=β=0.1,Sr=1, Br=2,Du=Sc=Pr=0.5,Rd=0.5,ξ=0.1.

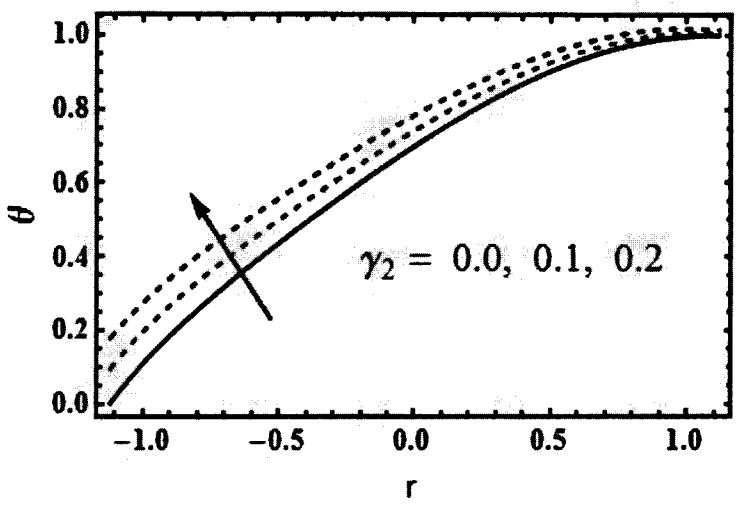

Fig. (3.17): Temperature profile for thermal slip parameter with k=3,α=0.03,β_3=β=0.1, Sr=1,Br=2,H=0.2,Du=Sc=Pr=0.5,Rd=0.5,ξ=0.1.

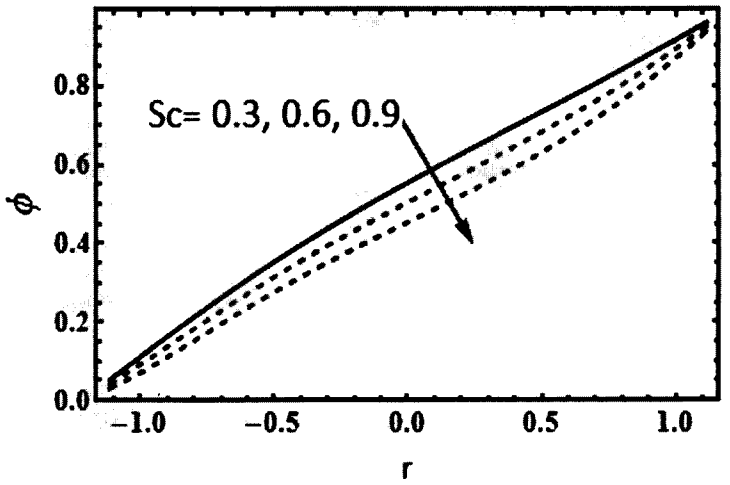

Fig. (3.18): Concentration profile for Soret parameter with $k = 3, Du = 0.8, \alpha = 0.03, \xi = 0.1, H = 0.1,$ $\beta_3 = 0.1, Br = 2, Sc = 0.4, \Pr = 0.5, Rd = 0.5.$

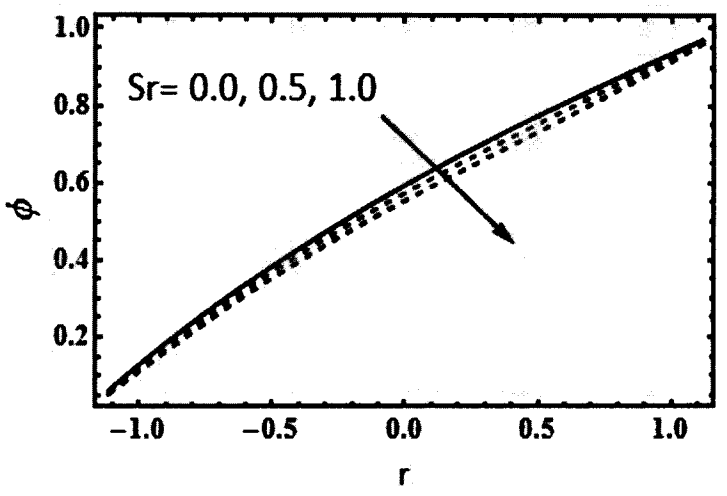

Fig. (3.19) : Concentration profile for Schmidt number with $k = 3, Du = 0.8, \alpha = 0.03, \xi = 0.1, H = 0.1,$ $\beta_3 = 0.1, Br = 2, \Pr = 0.5, Rd = 0.5.$

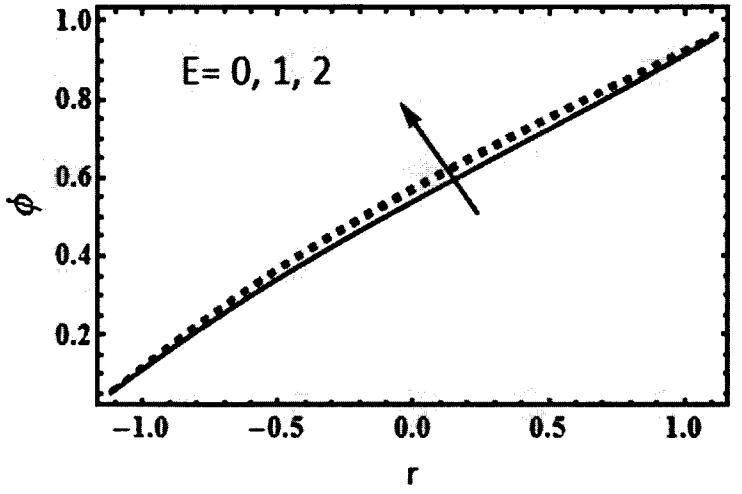

Fig. (3.20): Concentration profile for activation energy parameter with $k = 3, \Pr = 0.5, \alpha = 0.03,$ $H = 0.1, Br = 2, \beta_3 = \beta = 0.1, \Pr = Sr = Sc = 0.3, \xi = 0.1, Rd = 0.5.$

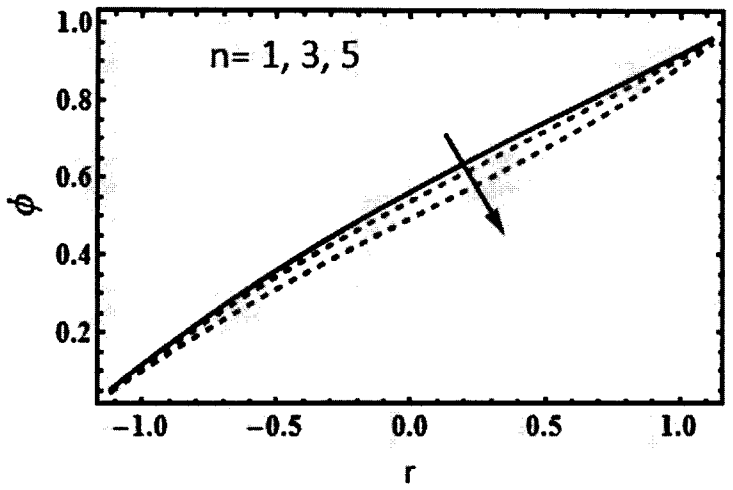

Fig. (3.21) : Concentration profile for n with $k = 3, \Pr = 0.5, \alpha = 0.03, H = 0.1, Br = 2, \beta_3 = \beta = 0.1,$ $\Pr = Sr = Sc = 0.3, \xi = 0.1, Rd = 0.5.$

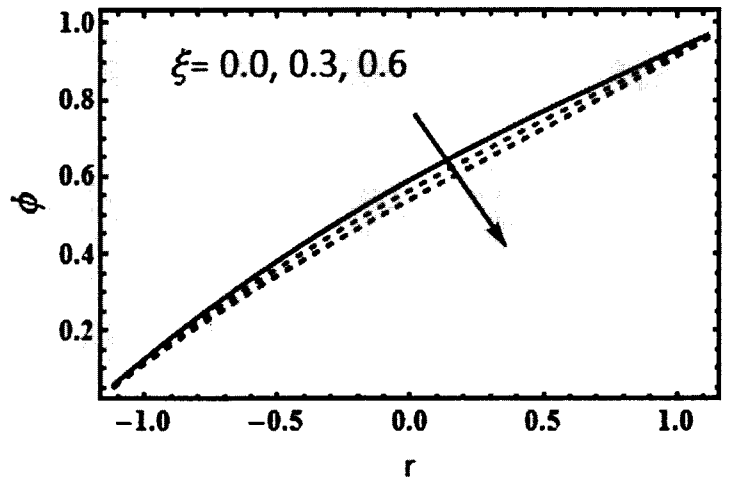

Fig. (3.22): Concentration profile for chemical reaction with $k = 3, \beta = 0.1, Du = 1, \beta_3 = 0.1,$ $\alpha = 0.03, Br = 1, H = 0.1, \Pr = Sc = 0.5, Sr = 1, Rd = 0.5.$

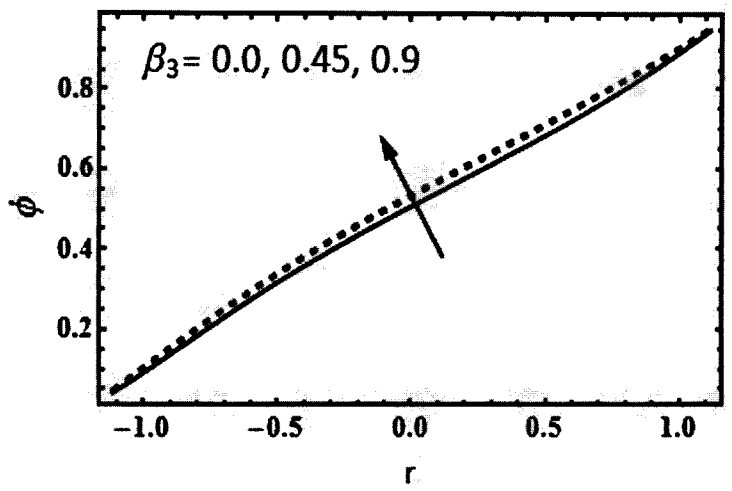

Fig. (3.23) : Concentration profile for fluid parameter with $k = 3, \beta = 0.1, Du = 1, \alpha = 0.03, Br = 1,$ $H = 0.1, \Pr = Sc = 0.5, Sr = 1, Rd = 0.5.$

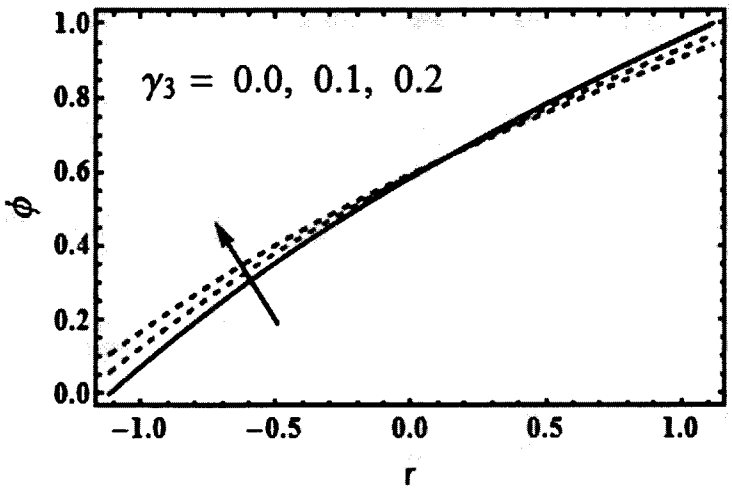

Fig. (3.24) : Concentration profile for concentration slip parameter with $k = 3, \alpha = 0.03, Du = 0.2, \beta = 0.1,$ $Br = 1, H = 0.5, \Pr = 0.5, Sc = Sr = 0.3, Rd = 0.5, \xi = 0.1.$

3.4 Conclusions

Key points are listed below:

- Behavior of velocity is increasing for temperature dependent viscosity parameter α.
- Behavior of temperature is qualitatively same (i.e. decreasing) for both β and β_3.
- Temperature has opposite outcomes for Du and R_d.
- Concentration decreases for Sr.
- Impacts of E and ξ are opposite on concentration.
- The problem is related to viscous fluid when $\alpha = \beta_3 = 0$.

Chapter 4

Entropy Optimization of MHD Sutterby Fluid Subject to Temperature Dependent Thermal Conductivity and Non-Linear Thermal Radiation

Here peristaltic transport of Sutterby liquid with temperature dependent thermal conductivity is addressed. Inclined magnetic field is imposed in curved geometry. Entropy generation with variable thermal conductivity of Sutterby liquids, magnetic field, non-linear thermal radiation and heat absorption is discussed. The system of differential equations by lubrication approach is arranged. The parameters of interest are sketched and analyzed by the plots of velocity, temperature, stream function and entropy production.

4.1 Mathematical Formulation

Here our objective is to discuss entropy production in peristalsis of incompressible Sutterby material in curved geometry. Width of the channel is $2a$. It is coiled in a circle with centre O and radius R'. The velocity components (W_1, W_2) are in radial and axial directions (R, X) respectively. Temperature dependent thermal conductivity of Sutterby material is considered. Heat absorption/ addition coefficient and non-linear thermal radiations are also taken into account. Magnetic field of strength B_0 with an inclination angle ϑ_0 is taken.

Fluid is moving in channel because of propagation of waves with speed s, wavelength λ and amplitude b. The problem addressed is modeled with no-slip boundary conditions for velocity. Convective boundary conditions are taken at boundary of the channel walls with distinct temperature. Fig. (2.1) depicts the physical sketch.

Mathematically, walls of the channel are

$$\bar{r} = \pm\chi(X,t) = \pm\left[a + b\sin\left(\frac{2\pi}{\lambda}(X - st)\right)\right], \tag{4.1}$$

Model of Sutterby fluid is defined as

$$\mathbf{S} = \frac{\mu_0}{2}\left[\frac{\sinh^{-1}\gamma\left|\dot{G}\right|^2}{\gamma\left|\dot{G}\right|^2}\right]^{n_1}\mathbf{A}, \tag{4.2}$$

in which $\mathbf{S}$ extra stress tensor, μ_0 constant dynamic viscosity of the fluid, γ fluid parameter, $\dot{G}\left(=\sqrt{\frac{1}{2}tr\left(\mathbf{A}^2\right)}\right)$ shear rate, n_1 power-law index and $\mathbf{A}\left(=\text{grad}\,\mathbf{W} + \text{grad}\,\mathbf{W}'\right)$ deformation rate tensor. In Eqn. (4.2) if $n_1 = 0$, the model represents Newtonian fluid model and for $n_1 = 1$ the model reduces to Eyring model. Since

$$\sinh^{-1}\gamma\left|\dot{G}\right|^2 = \gamma\left|\dot{G}\right|^2 - \frac{1}{3!}\left(\gamma\left|\dot{G}\right|^2\right)^3 + \frac{1}{5!}\left(\gamma\left|\dot{G}\right|^2\right)^5 - + \ldots, \tag{4.3}$$

Eqn. (4.2) reduces to

$$\mathbf{S} \approx \frac{\mu_0}{2}\left[1 - \frac{1}{3!}\left(\gamma\left|\dot{G}\right|^2\right)^2\right]^{n_1}\mathbf{A}. \tag{4.4}$$

After applying Binomial expansion in above Eqn. (4.4), components of Stress tensor become:

$$S_{XY}=\frac{\mu_0}{2}\left[1-\frac{n_1\gamma^2}{6}\left(\left|\dot{G}\right|^2\right)^2\right]\left(2\frac{\partial W_2}{\partial R}\right),$$

$$S_{RR}=\frac{\mu_0}{2}\left[1-\frac{n_1\gamma^2}{6}\left(\left|\dot{G}\right|^2\right)^2\right]\left(-2\frac{\partial W_2}{\partial R}\right),$$

$$S_{XR}=S_{RX}=\frac{\mu_0}{2}\left[1-\frac{n_1\gamma^2}{6}\left(\left|\dot{G}\right|^2\right)^2\right]\left(\frac{\partial W_1}{\partial R}+\frac{R}{r+R}\frac{\partial W_2}{\partial X}-\frac{W_1}{r+R}\right), \tag{4.5}$$

in which

$$\left|\dot{G}\right|=\sqrt{4\left(\frac{\partial W_2}{\partial R}\right)^2+\left(\frac{\partial W_1}{\partial X}\right)^2+\left(\frac{R}{r+R}\frac{\partial W_2}{\partial X}\right)^2+\frac{2R}{r+R}\frac{\partial W_1}{\partial R}\frac{\partial W_2}{\partial X}+\left(\frac{W_1}{r+R}\right)^2-\frac{2RW_1}{(r+R)^2}\frac{\partial W_2}{\partial X}-\frac{2W_1}{r+R}\frac{\partial W_1}{\partial X}}. \tag{4.6}$$

Inclined magnetic field in curved geometry is:

$$\mathbf{B}=\left(\frac{R'B_0}{R'+R}\sin\vartheta_0,\frac{R'B_0}{R'+R}\cos\vartheta_0,0\right). \tag{4.7}$$

Note that induced magnetic field effects are ignored because of low magnetic Reynolds number. Clearly, for $\vartheta_0=90^o$ the magnetic field is along radial direction as described in chapter 2.

Thus by Ohm's law (2.7) and Lorentz force (2.8), we get

$$\mathbf{F}=\sigma\left(\frac{R'B_0}{R'+R}\right)^2\left(-W_1\cos^2\vartheta_0+W_2\cos\vartheta_0\sin\vartheta_0,W_1\cos\vartheta_0\sin\vartheta_0-W_2\sin^2\vartheta_0,0\right), \tag{4.8}$$

and

$$\mathbf{J}.\mathbf{J}=\left(\frac{R'\sigma B_0}{R'+R}\right)^2\left(W_1\cos\vartheta_0-W_2\sin\vartheta_0\right)^2. \tag{4.9}$$

Thermal conductivity depending upon temperature is taken as

$$\kappa(T)=\kappa_o\left(1+\alpha'\left(T-T_0\right)\right), \tag{4.10}$$

in which κ_o denotes constant thermal conductivity and α' variable thermal conductivity

coefficient.

Fundamental equations of problem are

$$\nabla.\mathbf{W}=0, \tag{4.11}$$

$$\rho\frac{d\mathbf{W}}{dt}=\nabla.\mathbf{S}-\nabla P+\rho\left(\sigma\left[\mathbf{W}\times\mathbf{B}\right]\times\mathbf{B}\right), \tag{4.12}$$

$$\rho c_p\frac{dT}{dt}=-\nabla.\left[-\kappa(T)\nabla T\right]+\mathbf{L}.\mathbf{S}-\nabla.\mathbf{q}_r+\frac{\mathbf{J}.\mathbf{J}}{\sigma}+Q_0(T-T_0), \tag{4.13}$$

in which ρ shows fluid density, c_p specific heat, Q_0 heat addition/ absorption coefficient, $\mathbf{L}=\text{grad}\,\mathbf{W}$, P pressure and $\mathbf{q}_r$ radiative heat flux as defined in Eqn. (3.13).

Component form of Eqns. (4.11) to (4.13) is

$$R'\frac{\partial W_1}{\partial X}+\frac{\partial}{\partial R}\left((R'+R)W_2\right)=0, \tag{4.14}$$

$$\rho\left(\frac{dW_1}{dt}+\frac{W_1W_2}{R+R'}\right)=-\frac{R'}{(R+R')}\frac{\partial P}{\partial X}+\frac{1}{(R+R')^2}\frac{\partial}{\partial R}\left\{(R'+R)^2S_{XR}\right\}+\frac{R'}{(R+R')}\frac{\partial S_{XX}}{\partial X}$$
$$+\sigma\left(\frac{R'B_0}{R+R'}\right)^2\left(W_1\sin\vartheta_0\cos\vartheta_0-W_2\sin^2\vartheta_0\right), \tag{4.15}$$

$$\rho\left(\frac{dW_2}{dt}-\frac{W_1^2}{R+R'}\right)=-\frac{\partial P}{\partial R}+\frac{1}{(R+R')}\frac{\partial}{\partial R}\left\{(R+R')S_{RR}\right\}-\frac{S_{XX}}{(R+R')}+R'\frac{\partial S_{XR}}{\partial X}$$
$$-\sigma\left(\frac{R'B_0}{R+R'}\right)^2\left(W_1\cos^2\vartheta_0-W_2\sin\vartheta_0\cos\vartheta_0\right), \tag{4.16}$$

$$\rho C_p\frac{dT}{dt}=-\nabla.\left(-\kappa(T)\nabla T\right)+\left(\frac{\partial W_2}{\partial R}-\frac{W_2}{(R'+R)}+\frac{R'}{(R'+R)}\frac{\partial W_1}{\partial X}\right)S_{RX}+\frac{\partial W_1}{\partial R}\left(S_{RR}-S_{XX}\right)$$
$$+\frac{16\sigma^*T_0^3}{3k^*}\left(\frac{\partial^2}{\partial R^2}+\frac{1}{R+R'}\frac{\partial}{\partial R}+\frac{\partial^2}{\partial X^2}\right)T+\sigma\left(\frac{R'B_0}{R+R'}\right)^2\left(W_1\cos\vartheta_0-W_2\sin\vartheta_0\right)^2+Q_0(T-T_0), \tag{4.17}$$

where variable thermal conductivity in curved channel is modeled as

$$\nabla.\left(-\kappa(T)\nabla T\right)=\frac{\partial}{\partial R}\left(-\kappa(T)\frac{\partial T}{\partial R}\right)-\frac{\partial}{\partial X}\left(\frac{R'^2\kappa(T)}{\left(R+R'\right)^2}\frac{\partial T}{\partial X}\right)-\frac{\kappa(T)}{\left(R+R'\right)}\frac{\partial T}{\partial R}. \tag{4.18}$$

Boundary conditions are

$$\left.\begin{aligned} &W_2=0 && \text{at } R=\pm\chi,\\ &\kappa_1\frac{\partial T}{\partial R}=-\beta_1'\left(T_1-T\right) && \text{at } R=-\chi,\\ &\kappa_1\frac{\partial T}{\partial R}=-\beta_2'\left(T-T_0\right) && \text{at } R=\chi, \end{aligned}\right\} \tag{4.19}$$

in which T_0 and T_1 denote temperature of upper and lower walls respectively, κ_1 thermal conductivity of the walls and $\left(\beta_1^{'},\beta_2^{'}\right)$ Biot numbers.

Wave and fixed frames can be related through following transformations

$$\bar{r}=R,\quad \bar{x}=X-st,\quad \bar{w}_1=W_1,\quad \bar{w}_2=W_2-s. \tag{4.20}$$

Dimensionless variables velocities, pressure, temperature, wave number, peristaltic wall, Reynolds number, variable thermal conductivity parameter, Eckert number, Prandtl number, Brinkman number, curvature, amplitude ratio, radiation parameter, heat absorption parameter, Hartmann number, thermal Biot parameters and Sutterby fluid parameter are defined as:

$$(r,x)=\left(\frac{\bar{r}}{a},\frac{\bar{x}}{\lambda}\right),\qquad (w_1,w_2)=\left(\frac{\bar{w}_1}{s},\frac{\bar{w}_2}{s}\right),\qquad p\left(=\frac{a^2P}{s\mu_0\lambda}\right),\quad \theta\left(=\frac{T-T_o}{T_1-T_o}\right),$$

$$\delta\left(=\frac{a}{\lambda}\right),\qquad h=\frac{\chi}{a},\qquad \mathrm{Re}\left(=\frac{\rho sa}{\mu_0}\right),\quad \alpha\left(=\alpha'\left(T_1-T_o\right)\right),$$

$$Ec\left(=\frac{s^2}{C_p\left(T_1-T_o\right)}\right),\qquad \mathrm{Pr}\left(=\frac{\mu_0C_p}{\kappa_o}\right),\qquad Br\left(=Ec\ \mathrm{Pr}\right),\quad k\left(=\frac{R'}{a}\right),$$

$$b_1\left(=\frac{b}{a}\right), \qquad R_d\left(=\frac{16\sigma^* T_0^3}{3k^*\kappa_o}\right), \qquad Q\left(=\frac{a^2 Q_0}{\kappa_0}\right), \qquad B=\sqrt{\frac{\sigma B_0^2 a^2}{\mu_0}},$$

$$(\beta_1,\beta_2)=\left(\frac{a\beta_1'}{\kappa_1},\frac{a\beta_2'}{\kappa_1}\right), \quad \gamma^{*2}\left(=\frac{\gamma^2 s^2}{b_1^2}\right).$$

Velocities (w_1, w_2) through stream function (ψ) can be expressed below:

$$w_1=-\frac{k\delta}{r+k}\frac{\partial\psi}{\partial x}, \; w_2=\frac{\partial\psi}{\partial r}. \tag{4.21}$$

Using Eqns. (4.20) and (4.21), above mentioned dimensionless variables and applying lubrication approach (as flow is considered laminar thus $\mathrm{Re}\to 0$ and channel width is very small than wave length), Eqns. (4.14) to (4.19) are reduced in dimensionless form as:

$$\frac{k}{k+r}\frac{\partial p}{\partial x}=\frac{1}{(k+r)^2}\frac{\partial}{\partial r}\left(S_{rx}(k+r)^2\right)-\left(\frac{kB}{k+r}\right)^2\left(1+\frac{\partial\psi}{\partial r}\right)\sin^2\vartheta_0, \tag{4.22}$$

$$\frac{\partial p}{\partial r}=0, \tag{4.23}$$

$$(1+\alpha\theta)\left(\frac{1}{r+k}\frac{\partial\theta}{\partial r}+\frac{\partial^2\theta}{\partial r^2}\right)+\alpha\left(\frac{\partial\theta}{\partial r}\right)^2+Br\left(-\frac{1}{r+k}\left(\frac{\partial\psi}{\partial r}+1\right)+\frac{\partial^2\psi}{\partial r^2}\right)S_{rx}+Br\left(\frac{kB\sin\vartheta_0}{r+k}\right)^2\left(\frac{\partial\psi}{\partial r}+1\right)^2$$
$$+\mathrm{Pr}\,R_d\left(\frac{\partial^2\theta}{\partial r^2}+\frac{1}{r+k}\frac{\partial\theta}{\partial r}\right)+Q\theta=0, \tag{4.24}$$

and incompressibility condition is trivially satisfied.

Eqns. (4.22) and (4.23) imply

$$\frac{\partial}{\partial r}\left[\frac{1}{(k+r)}\frac{\partial}{\partial r}\left(S_{rx}(k+r)^2\right)-\frac{(kB\sin\vartheta_0)^2}{k+r}\left(1+\frac{\partial\psi}{\partial r}\right)\right]=0, \tag{4.25}$$

where

$$S_{rx}=\frac{1}{2}\left(\frac{\partial^2\psi}{\partial r^2}-\frac{1}{(k+r)}\left(1+\frac{\partial\psi}{\partial r}\right)\right)\left[1-\frac{n\gamma^{*2}}{6}\left(\frac{\partial^2\psi}{\partial r^2}-\frac{1}{(k+r)}\left(1+\frac{\partial\psi}{\partial r}\right)\right)^2\right]. \tag{4.26}$$

and $p=p(x)$.

Boundary conditions in non-dimensional form are

$$\left.\begin{aligned}&\psi=\mp\frac{F}{2},\quad w_2=\frac{\partial\psi}{\partial r}=-1 \qquad \text{at } r=\mp h,\\&\beta_1(1-\theta)+\frac{\partial\theta}{\partial r}=0, \qquad \text{at } r=-h,\\&\beta_2\theta+\frac{\partial\theta}{\partial r}=0, \qquad \text{at } r=h,\end{aligned}\right\} \tag{4.27}$$

with

$$F=\int_{-h}^{h}\frac{\partial\psi}{\partial r}dr=\psi(h)-\psi(-h), \tag{4.28}$$

$$h=1+b_1\sin(2\pi x). \tag{4.29}$$

4.1.1 Entropy

Entropy production for Sutterby fluid is defined as

$$Ns=-\frac{1}{\Theta_o^2}\mathbf{q}.\nabla T+\frac{1}{\Theta_o}\left(\begin{aligned}&\frac{\mu_0}{2}\left[1-\frac{n_1\gamma^2}{6}\left(|\dot{G}|^2\right)^2\right]\left(\frac{\partial W_1}{\partial R}+\frac{R}{R'+R}\frac{\partial W_2}{\partial X}-\frac{W_1}{R'+R}\right)^2+Q_0(T-T_0)\\&+\sigma\left(\frac{R'B_0}{R'+R}\right)^2\left(W_1\cos\vartheta_0-W_2\sin\vartheta_0\right)^2+\frac{16\sigma^*T_0^3}{3k^*}\left(\frac{\partial^2}{\partial R^2}+\frac{1}{R'+R}\frac{\partial}{\partial R}+\frac{\partial^2}{\partial X^2}\right)T\end{aligned}\right), \tag{4.30}$$

where Θ_o and $\mathbf{q}\left(=-\kappa(T)\nabla T\right)$ denote reference temperature and heat flux respectively. Eqn. (4.30) comprises of entropy generation due to heat transfer, fluid friction, heat source/ sink coefficient, magnetic field effects and thermal radiation.

Dimensionless form of entropy generation Eqn. (4.30) becomes

$$S=\frac{N_s}{S_G}. \tag{4.31}$$

Thus

$$S=\left(\frac{\partial\theta}{\partial r}\right)^2 + \frac{\Lambda}{(1+\alpha\theta)}\left(Br\left(\begin{array}{c}\frac{1}{2}\left(\frac{\partial^2\psi}{\partial r^2}-\frac{1}{(k+r)}\left(1+\frac{\partial\psi}{\partial r}\right)\right)^2\left(1-\frac{n\gamma^2}{6}\left(\frac{\partial^2\psi}{\partial r^2}-\frac{1}{(k+r)}\left(1+\frac{\partial\psi}{\partial r}\right)\right)^2\right)\\ +\left(\frac{kB\sin\vartheta_0}{k+r}\right)^2\left(1+\frac{\partial\psi}{\partial r}\right)^2\end{array}\right)\right), \\ +\Pr R_d\left(\frac{\partial^2\theta}{\partial r^2}+\frac{1}{k+r}\frac{\partial\theta}{\partial r}\right)+Q\theta \tag{4.32}$$

in which

$$\Lambda\left(=\frac{\Theta_o}{(T_1-T_o)}\right),\quad S_G\left(=\frac{\kappa(T)(T_1-T_0)^2}{\Theta_0^2 a^2}\right). \tag{4.33}$$

4.2 Methodology

The problem under consideration has non-linear system of differential equations. It is not possible to solve these equations exactly. Thus we evaluate momentum Eqns. (4.25), energy equation (4.24) and total entropy generation (4.32) numerically by using Shooting method from NDSolve command in Mathematica.

4.3 Analysis

Here interpretation of axial velocity, temperature, entropy generation and pumping characteristics is arranged for relevant parameters i.e. variable thermal conductivity (α), heat absorption/ addition parameter (Q), magnetic strength (B), inclination (ϑ_0), Biot

numbers (β_1, β_2), thermal radiation parameter (R_d), Brinkman number (Br), Sutterby fluid parameter (γ^{*2}) and curvature (k).

4.3.1 Velocity

Figs. (4.1-4.5) display the effects of pertinent parameters B, ϑ_0, γ^{*2} and k on axial velocity w_2. It is evident from Figs. (4.1-4.2) that behavior of velocity is alike for both parameters B and ϑ_0. Clearly, near lower wall the velocity decreases when it increases in vicinity of upper wall by enhancing B and ϑ_0. Velocity decreases as magnetic force behaves as a resistive force to fluid. Moreover, it is also noticed that velocity decays by rising ϑ_0 and velocity is minimum for $\vartheta_0 = 90^o$ (see Fig. (4.2). Since at $\vartheta_0 = 90^o$ magnetic force is perpendicular to the direction of flow and resists fluid motion the most. Figs. (4.3-4.4) reveal behavior of Sutterby fluid parameter γ^{*2} for $(n < 0)$ and $(n > 0)$ respectively. It is clear that velocity shows opposite behavior for $(n < 0)$ and $(n > 0)$. As axial velocity accelerates for $n < 0$ while it de-accelerates for $n > 0$ at centre of channel.

Fig. (4.5) illustrates the influence of curvature k on the velocity. Here velocity decreases in vicinity of lower wall however it enhances near the upper wall when k is increased. Further the velocity remains symmetric about the central line for straight channel.

4.3.2 Temperature

The recent subsection is devoted to present temperature θ via r for various sundry parameters α, Q, B, ϑ_0, β_1, β_2, R_d and Br through Figs. (4.6-4.13). Fig. (4.6) represents that θ decays by rising α. Effect of Q is exhibited through Fig. (4.7). Heat is

absorbed $(\text{for } Q>0)$ and radiated away $(\text{for } Q<0)$. By increasing heat absorption $(\text{for } Q=0.2,\ 0.4)$, temperature rises obviously. However temperature decays when heat is radiated away as $(\text{for } Q=-0.2,\ -0.4)$. Figs. (4.8) and (4.9) show the response of θ for increasing B and ϑ_0. It is clear from these figures that θ enhances for both parameters B and ϑ_0. Influence of Biot numbers (β_1, β_2) on θ can be revealed through Figs. (4.10) and (4.11). Temperature decreased near the lower and upper walls for increasing β_1 and β_2 respectively. Fig. (4.12) witnesses that temperature decays for higher R_d. As R_d is inversely proportional to heat absorption coefficient k^*. Thus absorption parameter decreases for larger radiation. Clearly additional heat is radiated away and temperature is reduced. Fig. (4.13) represents θ via Br. It is clear from this figure that temperature enhances for higher Br. It is due to the major effect for viscosity in Brinkman number that resists flow of liquid. Because of this resistance in flow, increase in collision of fluid particles takes place and as a result particles lose energy and thus temperature rises.

4.3.3 Entropy

Figs. (4.14-4.19) are presented to portray behavior of total entropy production (S) for important parameters B, ϑ_0, α, Q, R_d and Br. Influences of B and ϑ_0 on S are presented through Figs. (4.14-4.15). Entropy (S) enhances near the channel walls when B and ϑ_0 are enhanced. Effect of α on S is shown in Fig. (4.16). It is noticed that S decays in vicinity of channel walls. Since entropy is directly related to temperature, therefore entropy reduces when temperature decreases. Effect of Br on S is explained from Fig.

(4.17). Brinkman number (Br) elaborates viscous effects and is in direct relation to the square of velocity. Increase in Br leads to enhanced entropy. Opposite behavior of S is observed for R_d and $Q(>0)$ (see Figs. (4.18-4.19). It is clear from these figures that entropy is lesser at centre and it is higher in vicinity of channel walls.

4.3.4 Heat Transfer Rate and Isotherms

Heat transfer rate at the upper wall is $\frac{\partial \eta_1}{\partial r}\theta'(\eta_1)$. Effects of thermal conductivity coefficient, Brinkman number and radiation coefficient on heat transfer are portrayed at a fixed point $(x=0.5)$ through Figs. (4.20) to (4.22). It is quite evident that it is decreasing for thermal conductivity coefficient and radiation while increasing for Brinkman number. Figs. 4.23a and 4.23b represent contours of temperature for channel curvature (k). These figures portray that distribution of temperature is less in straight channel when compared with curved channel.

4.3.5 Trapping

Trapping shows lot of significance in fluid transportation through peristalsis. Because of contraction/ expansion of peristaltic walls, fluid mass in form of bolus circulates inside the channel and it moves forward with the velocity of propagating peristaltic walls. Figs. (4.24) to (4.26) are prepared to show streamlines nature for different quantities considered in this work. Figs. (4.24a-4.24c) depict that with increasing γ^{*2}, bolus size decreases in upper and lower half of curved channel. In lower half, it can also be noticed that bolus stretches in upward direction. Streamlines movement for k is depicted through Figs. (4.25a-4.25c). It

is clear that bolus size and streamlines in both halves of the channel are symmetry for straight channel. Effect of inclination ϑ_0 of magnetic field is shown in Figs. (4.26a-4.26c). When ϑ_0 increases from $0 \rightarrow \frac{\pi}{2}$, strength of magnetic field enhances. For this, bolus and streamlines from the lower portion move in upward direction and bolus presses the streamlines in the upper channel.

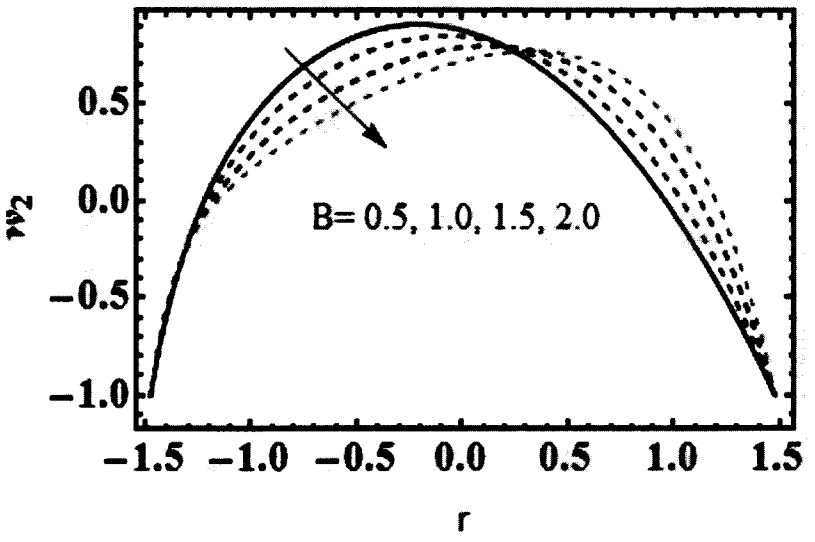

Fig. (4.1): Velocity for magnetic field with $n = k = 3$, $\vartheta_0 = \frac{\pi}{4}, \gamma^{*2} = 0.1$.

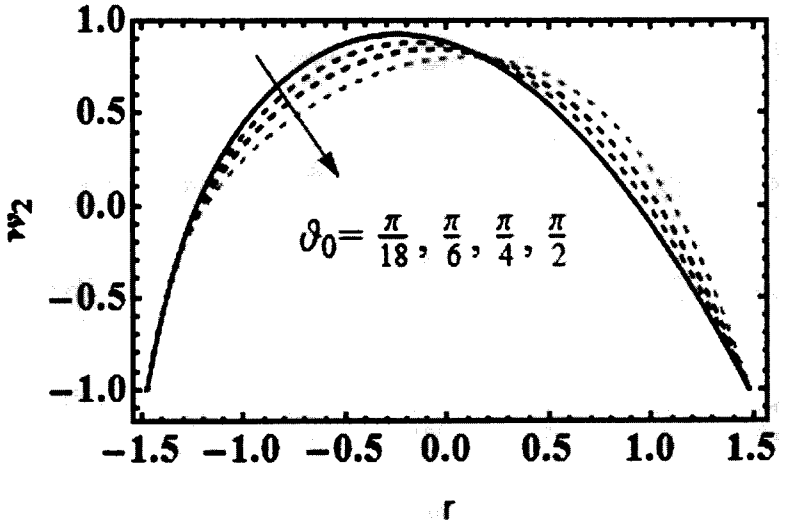

Fig. (4.2): Velocity for inclination of magnetic field with $n = k = 3$, $B = 1$, $\gamma^{*2} = 0.1$.

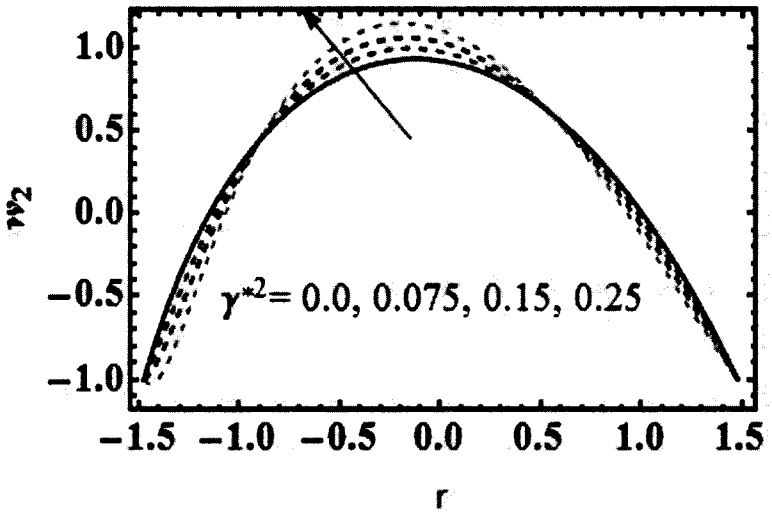

Fig. (4.3): Velocity for fluid parameters for $(n=-3)$ with $n = k = 3$, $B = 1$, $\vartheta_0 = \frac{\pi}{4}$.

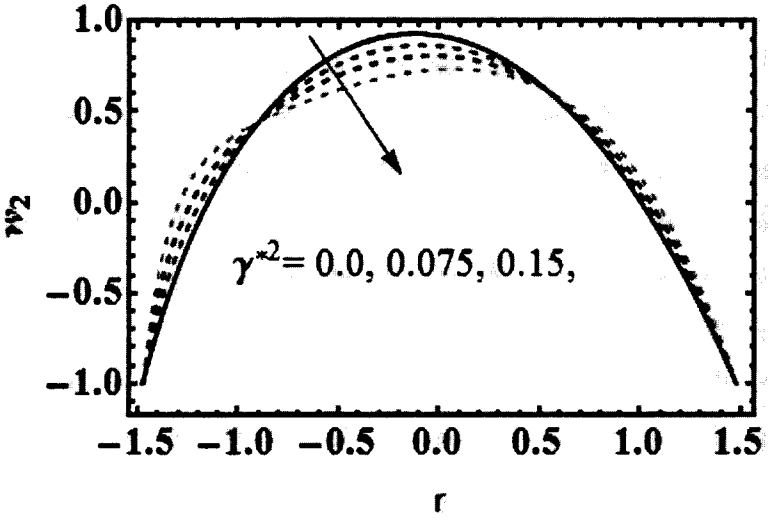

Fig. (4.4): Velocity for fluid parameters for $(n=3)$ with $n = k = 3$, $B = 1$, $\vartheta_0 = \frac{\pi}{4}$.

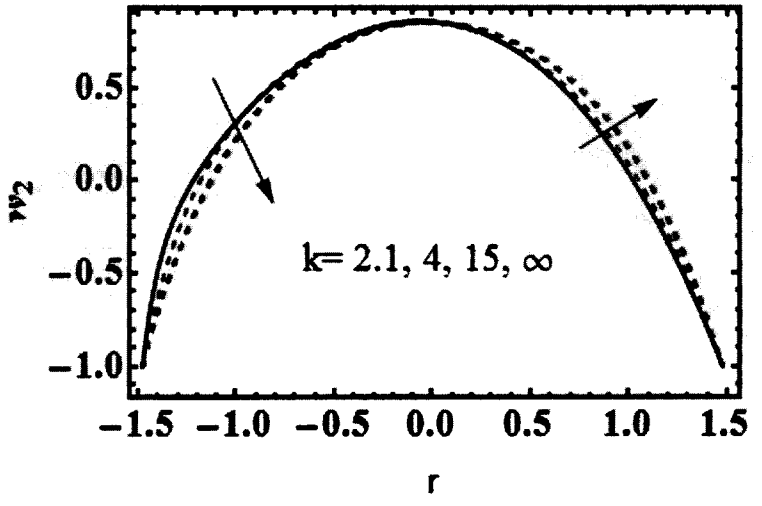

Fig. (4.5): Velocity for curvature parameters with $n = 3, B = 1, \vartheta_0 = \frac{\pi}{4}, \gamma^{*2} = 0.1$.

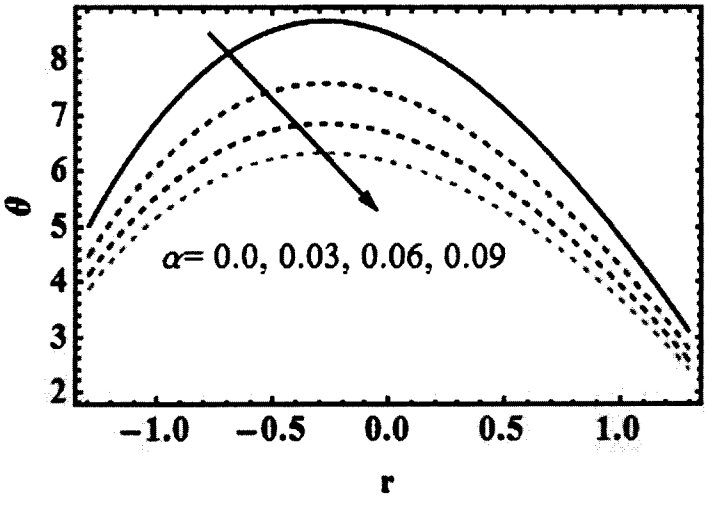

Fig. (4.6): θ for thermal conductivity coefficient with $n = k = 3,\ B = 1.5,\ \vartheta_0 = \frac{\pi}{4}$, $\gamma^{*2} = 0.1, R_d = 0.2, \beta_1 = \beta_2 = 2, Q = 0.4, Br = 0.5$.

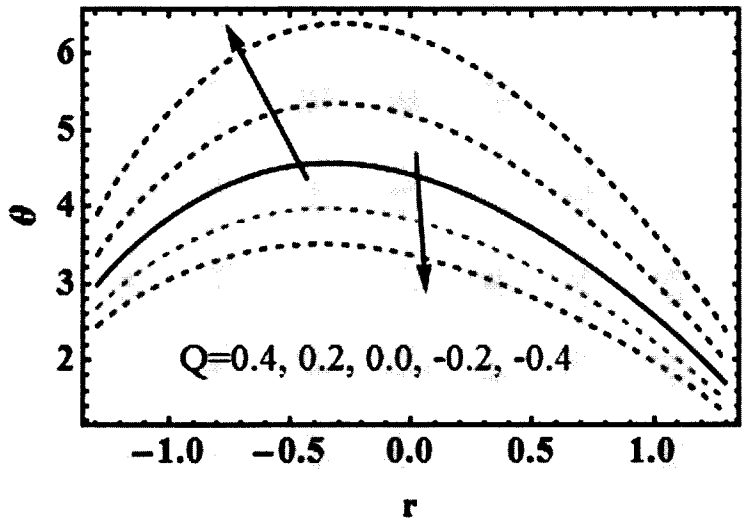

Fig. (4.7): θ for heat absorption parameter with $n = k = 3,\ B = 1.5,\ \vartheta_0 = \frac{\pi}{4}$, $\alpha = \gamma^{*2} = 0.1, R_d = 0.2, \beta_1 = \beta_2 = 2, Br = 0.5.$

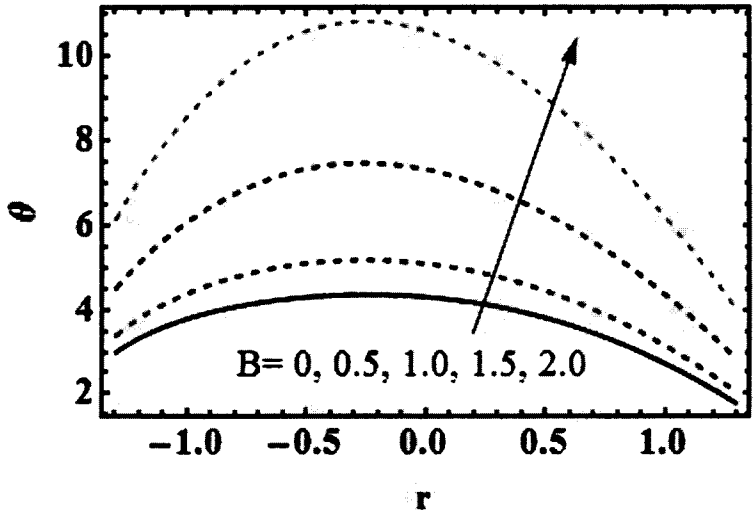

Fig. (4.8): θ for magnetic field with $n = k = 3,\ \vartheta_0 = \frac{\pi}{4}, \alpha = \gamma^{*2} = 0.1,$ $R_d = 0.2, \beta_1 = \beta_2 = 2, Q = 0.4, Br = 0.5.$

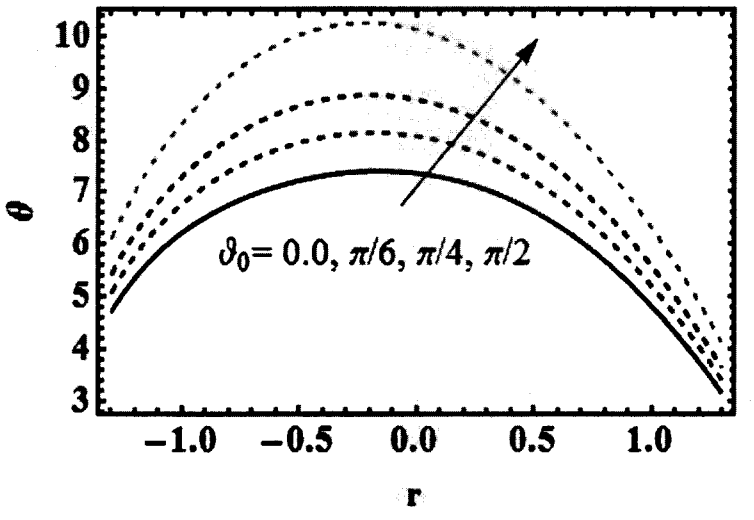

Fig. (4.9): θ for inclination of magnetic with $n = k = 3, B = 1.5,$ $\alpha = \gamma^{*2} = 0.1, R_d = 0.2, \beta_1 = \beta_2 = 2, Q = 0.4, Br = 0.5.$

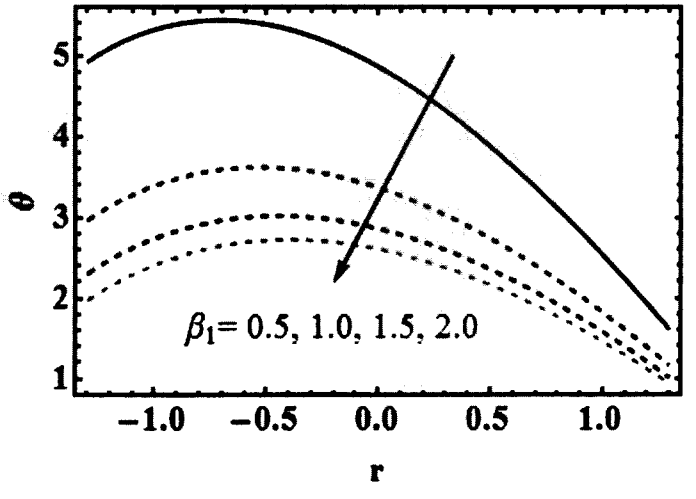

Figs. (4.10): θ for Biot numbers with $n = k = 3,\ B = 1.5,\ \vartheta_0 = \frac{\pi}{4}, \alpha = \gamma^{*2} = 0.1, R_d = 0.2,$ $\beta_1 = 2, Q = 0.4, Br = 0.5.$

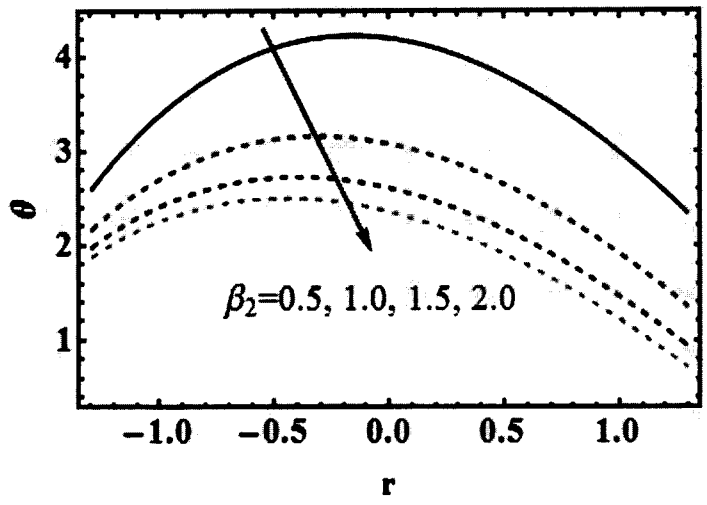

Figs. (4.11): θ for Biot numbers with $n = k = 3,\ B = 1.5,\ \vartheta_0 = \frac{\pi}{4}, \alpha = \gamma^{*2} = 0.1,$ $R_d = 0.2, \beta_1 = 2, Q = 0.4, Br = 0.5.$

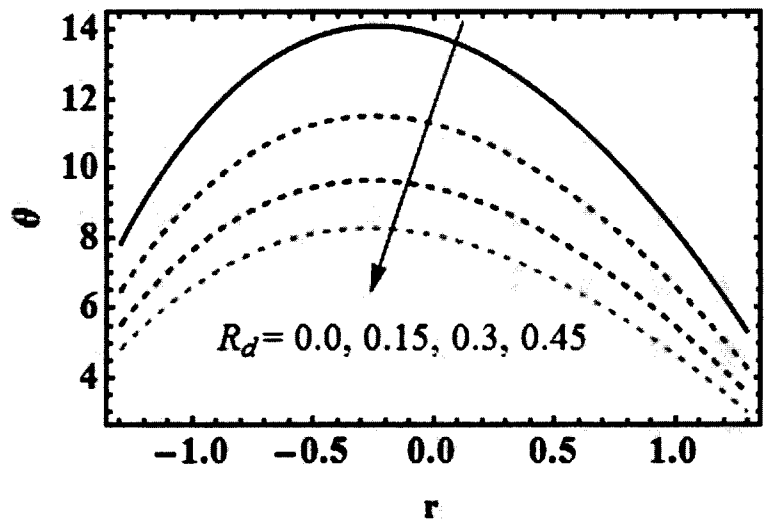

Fig. (4.12): θ for thermal radiation with $n = k = 3,\ B = 1.5, \vartheta_0 = \frac{\pi}{4}, \alpha = \gamma^{*2} = 0.1,$ $\beta_1 = \beta_2 = 2, Q = 0.4, Br = 0.5.$

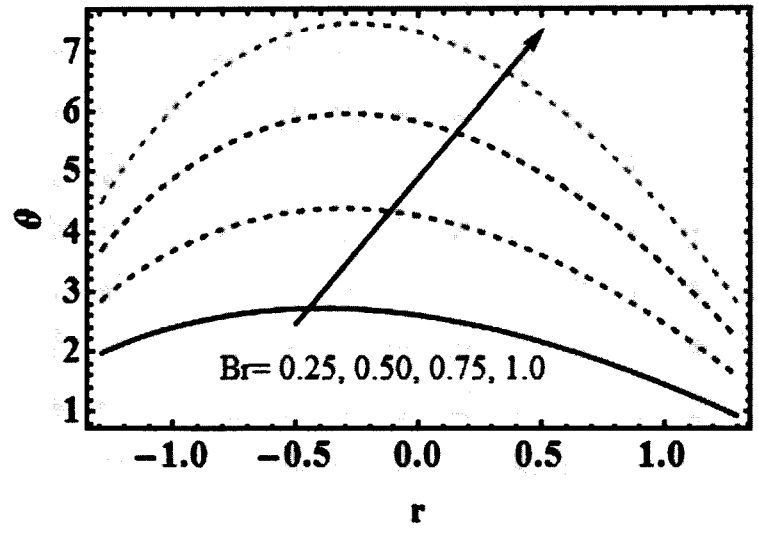

Figs. (4.13): θ for Brinkmann number with $n = k = 3,\ B = 1.5, \vartheta_0 = \frac{\pi}{4}, \alpha = \gamma^{*2} = 0.1,$ $R_d = 0.2, \beta_1 = \beta_2 = 2, Q = 0.4.$

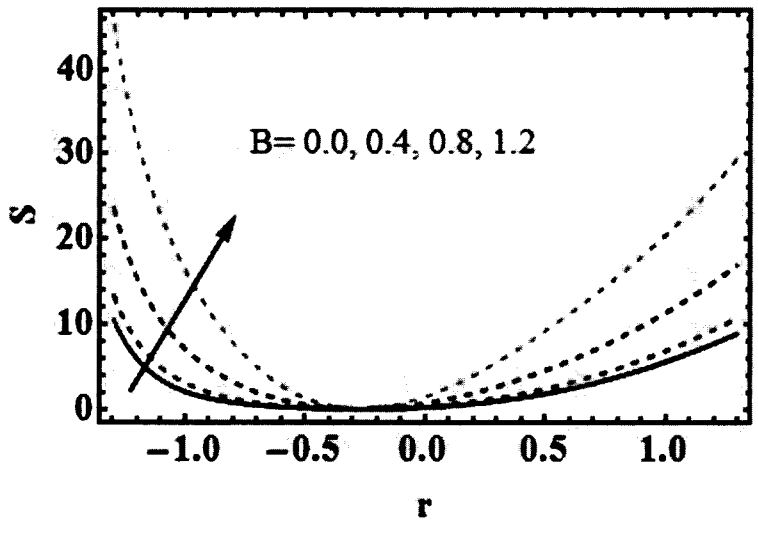

Fig. (4.14): Entropy for magnetic field with $k = 3,\ \vartheta_0 = \frac{\pi}{4}, \alpha = 0.02, \gamma^{*2} = 0.1,$ $n = \beta_1 = \beta_2 = 2, R_d = 0.2, Q = 0.5, Br = 0.8.$

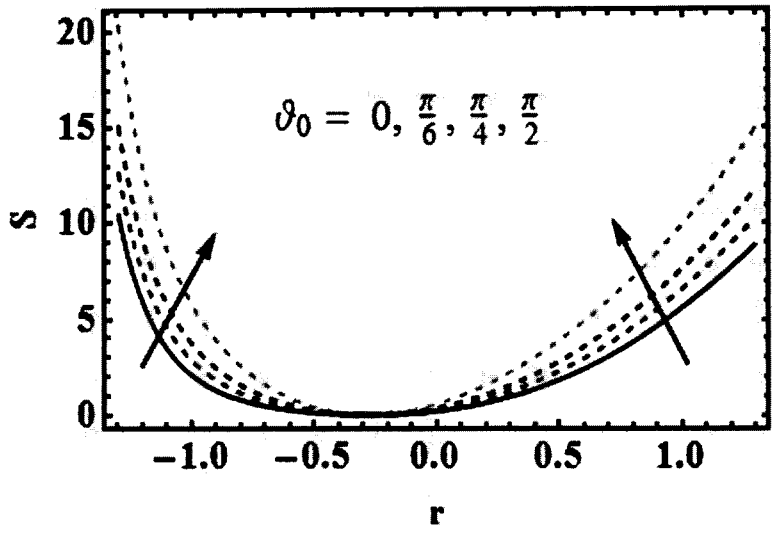

Fig. (4.15): Entropy for inclination of magnetic field with $k = 3$, $\vartheta_0 = \frac{\pi}{4}, \alpha = 0.02$, $\gamma^{*2} = 0.1, n = \beta_1 = \beta_2 = 2, R_d = 0.2, Q = 0.5, Br = 0.8.$

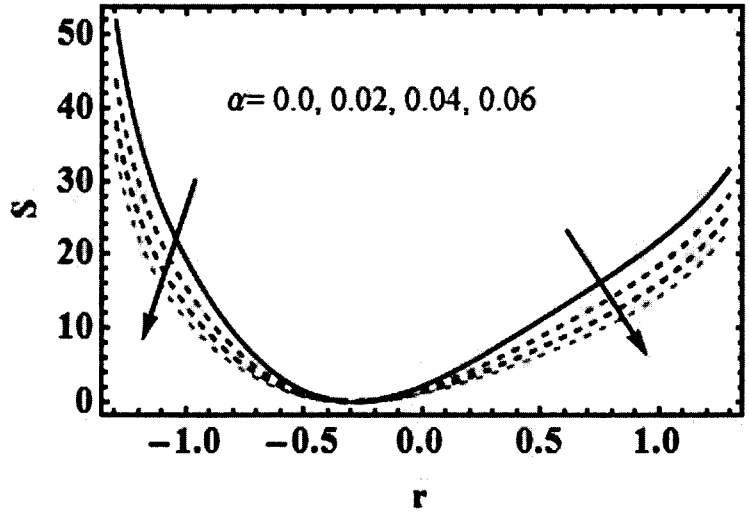

Fig. (4.16): Entropy for thermal conductivty coefficient with $k = 3$, $B = 0.5$, $\vartheta_0 = \frac{\pi}{4}, \alpha = 0.02$, $\gamma^{*2} = 0.1, n = \beta_1 = \beta_2 = 2, R_d = 0.2, Q = 0.5, Br = 0.8.$

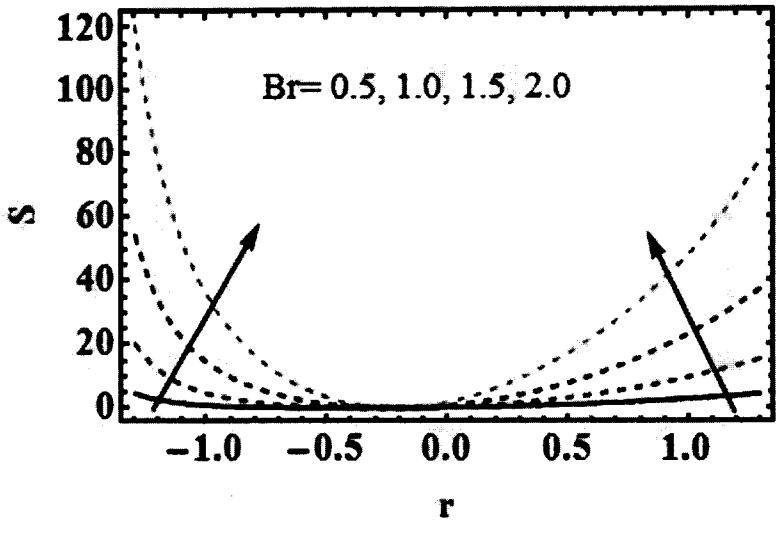

Fig. (4.17): Entropy for Brinkmann number with $k = 3,\ B = 0.5,\ \vartheta_0 = \frac{\pi}{4}, \alpha = 0.02,$ $\gamma^{*2} = 0.1, n = \beta_1 = \beta_2 = 2, R_d = 0.2, Q = 0.5.$

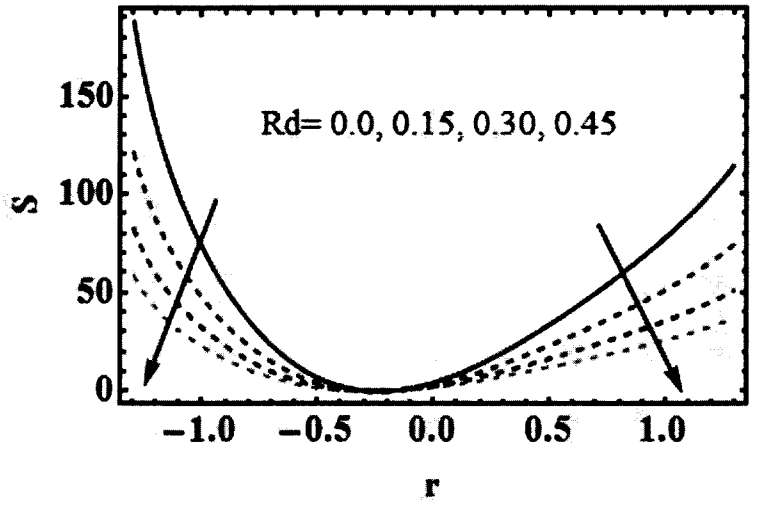

Fig. (4.18): Entropy for thermal radiation with $k = 3,\ B = 0.5,\ \vartheta_0 = \frac{\pi}{4}, \alpha = 0.02, \gamma^{*2} = 0.1,$ $n = \beta_1 = \beta_2 = 2, Q = 0.5, Br = 0.8.$

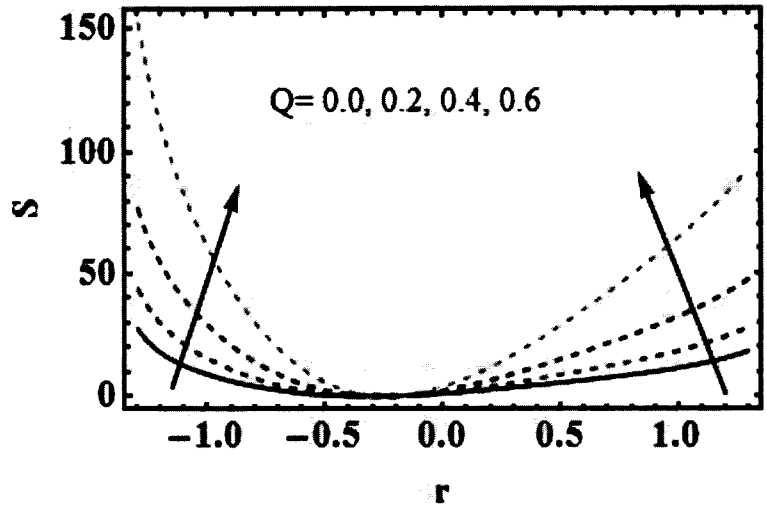

Fig. (4.19): Entropy for heat absorption parameter with $k = 3,\ B = 0.5,\ \vartheta_0 = \frac{\pi}{4}, \alpha = 0.02,$ $\gamma^{*2} = 0.1, n = \beta_1 = \beta_2 = 2, R_d = 0.2, Br = 0.8.$

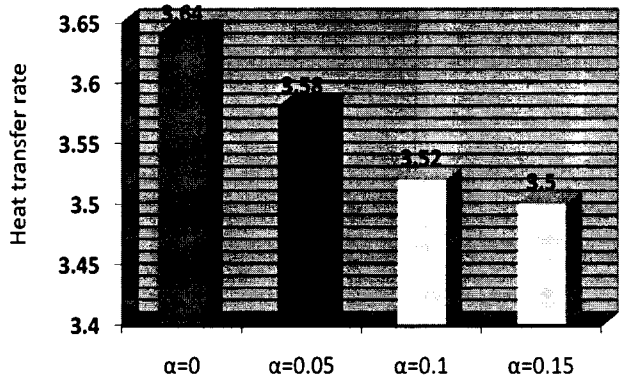

Fig. (4.20): Heat transfer rate for thermal conductivity coefficent with $x = 0.5, R_d = 0.5, Br = 0.2,$ $Q = 0.2, \gamma^{*2} = 0.01, k = 3, \beta_1 = \beta_2 = n = 2, B = 1.5, \vartheta_0 = \frac{\pi}{4}.$

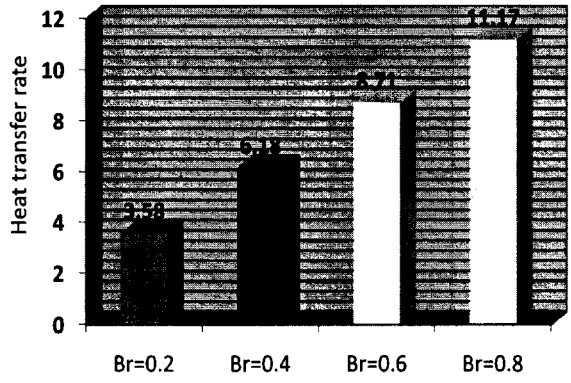

Fig. (4.21): Heat transfer rate for Brinkman number with $x = 0.5, R_d = 0.5, \alpha = 0.1, Q = 0.2, \gamma^{*2} = 0.01,$

$k = 3, \beta_1 = \beta_2 = n = 2, B = 1.5, \vartheta_0 = \frac{\pi}{4}.$

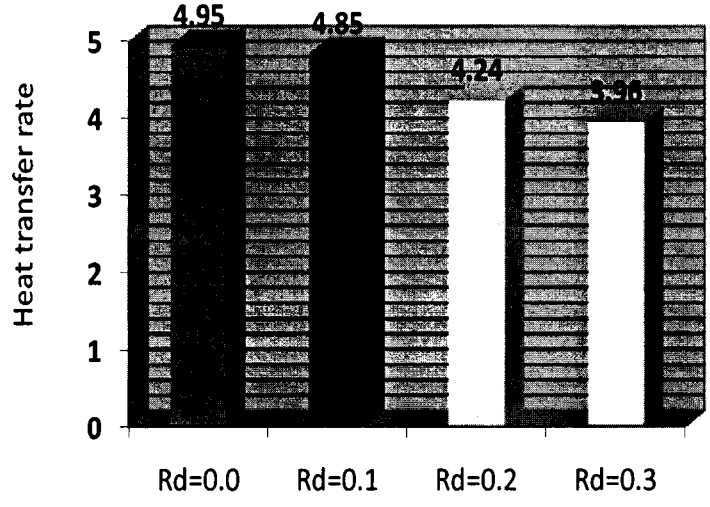

Fig. (4.22): Heat transfer rate for thermal radiation parameter with $x = 0.5, Br = 0.2, \alpha = 0.1, Q = 0.2,$

$\gamma^{*2} = 0.01, k = 3, \beta_1 = \beta_2 = n = 2, B = 1.5, \vartheta_0 = \frac{\pi}{4}.$

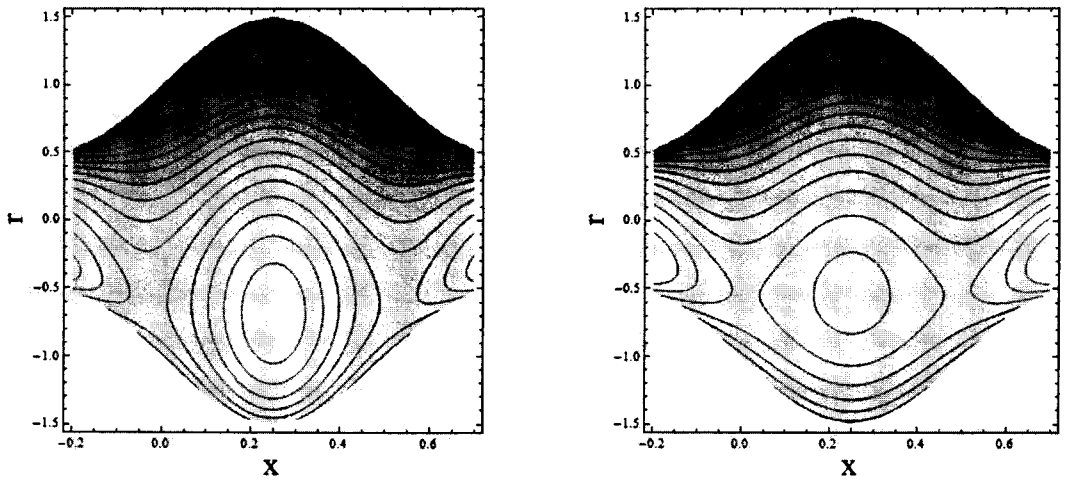

(a): k =2.1 (b): k =100

Figs. (4.23a, b): Contours of temperature for k with $R_d = 0.5, \gamma^{*2} = \alpha = 0, \beta_1 = \beta_2 = 2, B = 1.1, \vartheta_0 = \frac{\pi}{4}$.

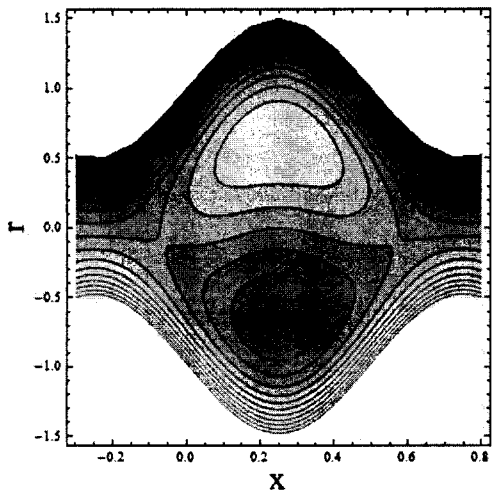

(a): $\gamma^{*2} = 0.0$

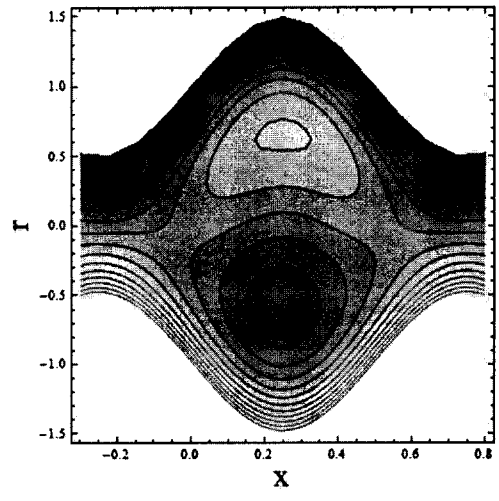

(b): $\gamma^{*2} = 0.2$

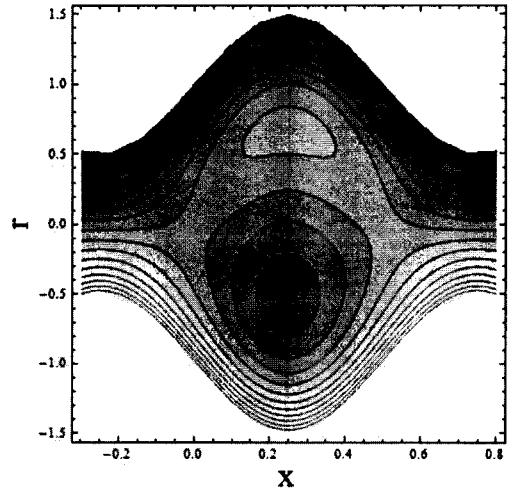

(c): $\gamma^{*2} = 0.4$

Figs. (4.24a-4.24c): Streamlines for Sutterby fluid parameter. The values of other parameters are $k = 3$, $n = 4, B = 1.5, \vartheta_0 = \frac{\pi}{4}$.

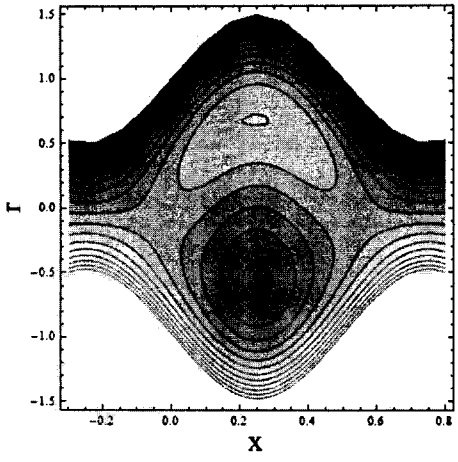

(a): $k = 2.3$

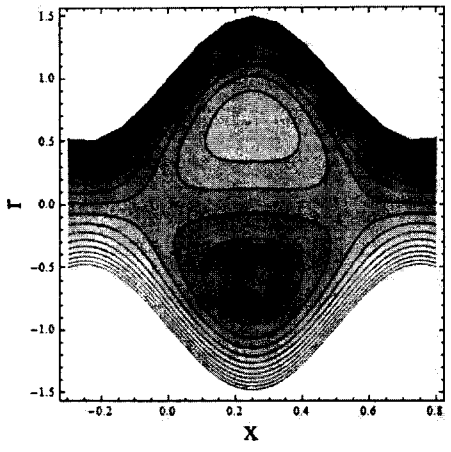

(b): $k = 9$

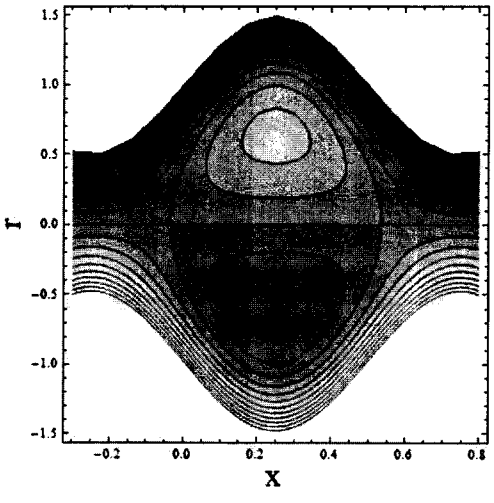

(c): $k = 100$

Figs. (4.25a-4.25c): Streamlines for curvature of the channel. The values of other parameters are $\gamma^{*2} = 0.1, n = 4, B = 1.5, \vartheta_0 = \frac{\pi}{4}$.

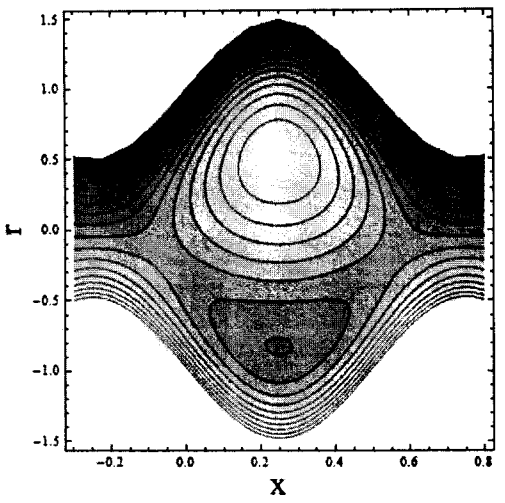

(a): $\vartheta_0 = \frac{\pi}{16}$

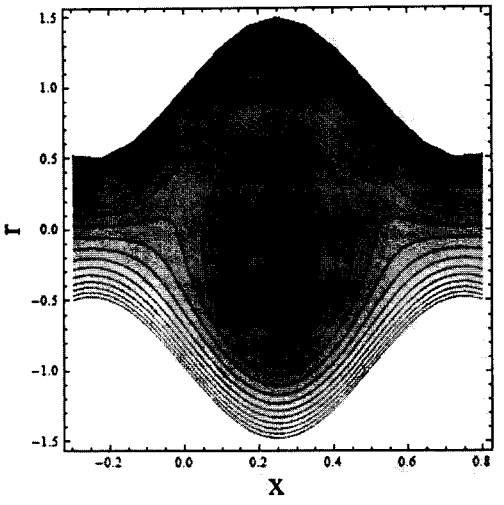

(b): $\vartheta_0 = \frac{\pi}{4}$

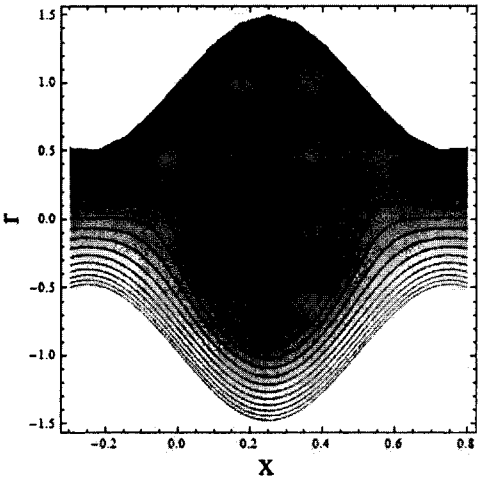

(c): $\vartheta_0 = \frac{\pi}{2}$

Figs. (4.26a-4.26c): Streamlines for inclination of magenetic field. The values of other parameters are $\gamma^{*2} = 0.1$, $n = 4, k = 3, B = 1.5$.

4.4 Conclusion

In this chapter has following key points.

- Opposite behavior of axial velocity is noted for rising fluid parameter (γ^{*2}) for $(n>0 \text{ and } n<0)$.
- Decrease in temperature is seen for variable thermal conductivity coefficient (α) and thermal radiation parameter (R_d) while it rises for heat absorption parameter $Q(>0)$.
- Irreversibility is minimum for variable thermal conductivity parameter β.
- Results of the this chapter are summarized to viscous material when $(n=0)$ and Eyring liquid for $(n=1)$.
- Heat transfer rate decreases for radiation parameters R_d while it is higher for Brinkman number Br.

Chapter 5

Entropy Production Minimization and Non-Darcy Resistance within Wavy Motion of Sutterby Liquid Subject to Variable Physical Characteristics

The objective of this chapter is to analyze peristaltic movement of Sutterby material through porous medium. Modified Darcy's law has been applied. Soret and Dufour effects in energy and concentration processes are retained. Variable physical properties of the material have been included. Investigation of entropy is also made part of the analysis. Total entropy production is inspected for parameters of curiosity like Soret, Dufour, variable viscosity and thermal conductivity coefficients. Modeled equations are solved numerically. Results are presented through graphs.

5.1 Mathematical Formulation

Peristaltic activity of Sutterby liquid in curved geometry is examined. Soret and Dufour impacts are outlined. Variable physical characteristics of the material are under consideration. Thermal conductivity and viscosity are assumed as temperature-dependent. Modified Darcy law for porous medium is taken into account. Width of curved channel is $2a$. It is coiled in a circle. Fluid flow is because of waves propagation with speed s,

wavelength λ and amplitude b. Thus mathematically, we have

$$R = \pm\chi(X,t) = \pm\left[a + b\sin\left(\frac{2\pi}{\lambda}(X - st)\right)\right], \tag{5.1}$$

Here $\bar{r}$ is the radial distance and components (W_1, W_2) of velocity $\mathbf{W}$ are along (R, X) directions respectively. Channel walls are comprised of no-slip effects for momentum, temperature and concentration. Furthermore, we assume that temperatures at upper and lower walls are T_0 and T_1 respectively such that $T_0 (< T_1)$. Similarly concentrations C_0 and C_1 at upper and lower walls being $C_0 (< C_1)$.

Governing equations for considered problem are

$$\nabla.\mathbf{W} = 0, \tag{5.2}$$

$$\rho\frac{d\mathbf{W}}{dt} = \nabla.\boldsymbol{\tau} - \mathbf{D}, \tag{5.3}$$

$$\rho c_p \frac{dT}{dt} = \nabla.(\kappa(T)\nabla T) + \mathbf{S}.\mathbf{A} + \frac{D_B k_T}{c_s}\nabla^2 C, \tag{5.4}$$

$$\frac{dC}{dt} = D_B\nabla^2 C + \frac{D_B k_T}{T_m}\nabla^2 T. \tag{5.5}$$

Where ρ denotes fluid density, $\boldsymbol{\tau}$ Cauchy stress tensor, c_p specific heat, T Temperature, C concentration, D_B mass diffusion coefficient, c_s concentration susceptibility, k_T thermal diffusion ratio, $(\kappa(T), \mu(T))$ thermal conductivity and viscosity as a function of temperature.

Extra stress tensor $\mathbf{S}$, for Sutterby fluid obeys

$$\mathbf{S}=\frac{\mu(T)}{2}\left(\frac{\sinh^{-1}\eta\left|\dot{G}\right|^{2}}{\eta\left|\dot{G}\right|^{2}}\right)^{m}\mathbf{A}, \tag{5.6}$$

In which m, denote power-law index, η Sutterby fluid parameter, $\mathbf{A}=\operatorname{grad}\mathbf{W}+\operatorname{grad}\mathbf{W}$ deformation rate tensor and $\dot{G}=\sqrt{\frac{1}{2}tr\left(\mathbf{A}^{2}\right)}$ trace respectively. Sutterby material has the property of both shear thickening (dilatant materials for $m<0$) and shear thinning (pseudo-plastic materials for $m>0$) characteristics. Eqn. (5.6) represents viscous fluid model for $m=0$ and Eyring fluid model for $m=1$. As

$$\sinh^{-1}\left(\eta\left|\dot{G}\right|^{2}\right)=\eta\left|\dot{G}\right|^{2}-\frac{1}{3!}\left(\eta\left|\dot{G}\right|^{2}\right)^{3}+\frac{1}{5!}\left(\eta\left|\dot{G}\right|^{2}\right)^{5}\ldots \tag{5.7}$$

so the components from Eqn. (5.6) are:

$$\left.\begin{aligned}
S_{XX}&=\frac{\mu(T)}{2}\left(2\frac{\partial W_{1}}{\partial R}\right)\left[1-\frac{m}{3!}\left(\eta\left|\dot{G}\right|^{2}\right)^{2}\right],\\
S_{RR}&=\frac{\mu(T)}{2}\left(-2\frac{\partial W_{1}}{\partial R}\right)\left[1-\frac{m}{3!}\left(\eta\left|\dot{G}\right|^{2}\right)^{2}\right],\\
S_{XR}=S_{RX}&=\frac{\mu(T)}{2}\left(\frac{\partial W_{2}}{\partial R}+\frac{R}{r+R}\frac{\partial W_{1}}{\partial X}-\frac{W_{2}}{r+R}\right)\left[1-\frac{m}{3!}\left(\eta\left|\dot{G}\right|^{2}\right)^{2}\right],
\end{aligned}\right\} \tag{5.8}$$

in which

$$\left|\dot{G}\right|=\sqrt{\begin{aligned}&4\left(\tfrac{\partial W_{1}}{\partial R}\right)^{2}+\left(\tfrac{\partial W_{2}}{\partial X}\right)^{2}+\left(\tfrac{W_{2}}{r+R}\right)^{2}+\left(\tfrac{R}{r+R}\tfrac{\partial W_{1}}{\partial X}\right)^{2}\\&+\tfrac{2R}{r+R}\tfrac{\partial W_{2}}{\partial R}\tfrac{\partial W_{1}}{\partial X}-\tfrac{2W_{2}}{r+R}\tfrac{\partial W_{2}}{\partial X}-\tfrac{2RW_{2}}{(r+R)^{2}}\tfrac{\partial W_{1}}{\partial X}\end{aligned}}.$$

By Reynolds model, the expression for viscosity is

$$\mu(T)=\mu_{o}e^{-\beta'(T-T_{0})}\beth\ \mu_{o}\left(1-\beta'\left(T-T_{0}\right)\right). \tag{5.9}$$

Thermal conductivity depending on temperature is

$$\kappa(T) \cong \kappa_o\left(1+\gamma'\left(T-T_0\right)\right). \tag{5.10}$$

Where κ_0, μ_0 Constant thermal conductivity and viscosity, β', γ' Viscosity and thermal conductivity coefficients.

Modified Darcy's law for Sutterby fluid gives

$$\mathbf{D} = -\frac{\mu(T)}{2K}\left(\frac{\sinh^{-1}\eta\left|\dot{G}\right|^2}{\eta\left|\dot{G}\right|^2}\right)^m \mathbf{W}. \tag{5.11}$$

Now Eqns. (5.2) to (5.5) give

$$\frac{\partial W_1}{\partial R} + \frac{R'}{(R+R')}\frac{\partial W_2}{\partial R} + \frac{W_1}{(R+R')} = 0, \tag{5.12}$$

$$\rho\left(\frac{dW_2}{dt} + \frac{W_1 W_2}{R+R'}\right) = -\frac{R'}{(R+R')}\frac{\partial P}{\partial X} + \frac{1}{(R+R')^2}\frac{\partial}{\partial R}\left((R+R')^2 S_{XR}\right) + \frac{R'}{(R+R')}\frac{\partial S_{XX}}{\partial X}$$
$$-\frac{\mu(T)}{2K}\left(1-\frac{m}{3!}\left(\eta\left|\dot{G}\right|^2\right)^2\right)W_1, \tag{5.13}$$

$$\rho\left(\frac{dW_1}{dt} - \frac{W_2^2}{R+R'}\right) = -\frac{\partial P}{\partial R} + \frac{1}{R+R'}\frac{\partial}{\partial R}\left((R+R')S_{RR}\right) - \frac{S_{XX}}{R+R'} + \frac{R'}{R+R'}\frac{\partial S_{XR}}{\partial X}$$
$$-\frac{\mu(T)}{2K}\left(1-\frac{m}{3!}\left(\eta\left|\dot{G}\right|^2\right)^2\right)W_2, \tag{5.14}$$

$$\rho c_p \frac{dT}{dt} = -\frac{\partial}{\partial R}\left(-\kappa(T)\frac{\partial T}{\partial R}\right) + \frac{\partial}{\partial X}\left(\frac{\kappa(T)R'^2}{(R+R')^2}\frac{\partial T}{\partial X}\right) - \frac{\kappa(T)}{R+R'}\frac{\partial T}{\partial R} - \frac{\partial W_2}{\partial R}\left(S_{XX}-S_{RR}\right)$$
$$+\left(\frac{\partial W_2}{\partial R} - \frac{W_2}{R+R'} + \frac{R'}{R+R'}\frac{\partial W_1}{\partial X}\right)S_{XR} + \frac{D_B k_T}{c_s}\left(\frac{\partial^2 C}{\partial X^2} + \frac{\partial^2 C}{\partial R^2} + \frac{1}{R+R'}\frac{\partial C}{\partial R}\right), \tag{5.15}$$

$$\frac{dC}{dt} = D_B\left(\frac{\partial^2 C}{\partial R^2} + \frac{\partial^2 C}{\partial X^2} + \frac{1}{R+R'}\frac{\partial C}{\partial R}\right) + \frac{D_B k_T}{T_{mean}}\left(\frac{\partial^2 T}{\partial R^2} + \frac{\partial^2 T}{\partial X^2} + \frac{1}{R+R'}\frac{\partial T}{\partial R}\right), \tag{5.16}$$

where S_{RR}, S_{XR}, S_{XX} represent stress components.

With conditions

$$\begin{aligned} W_1 &= 0 \quad \text{at} \quad R = -\chi, \\ W_2 &= 0 \quad \text{at} \quad R = +\chi, \end{aligned} \tag{5.17}$$

$$T = \begin{Bmatrix} T_1 \\ T_0 \end{Bmatrix} \quad \text{at} \quad R = \mp\chi, \tag{5.18}$$

$$C = \begin{Bmatrix} C_1 \\ C_0 \end{Bmatrix} \quad \text{at} \quad R = \mp\chi. \tag{5.19}$$

The transformations in relation between wave and laboratory frames as taken as:

$$\bar{r} = R, \quad \bar{x} = X - st, \quad \bar{w}_1 = W_1, \quad \bar{w}_2 = W_2 - s. \tag{5.20}$$

Dimensionless variables (x, r), velocity components (w_1, w_2), pressure p, temperature θ, peristaltic wall h, wave number δ, Reynolds number Re, thermal conductivity coefficient γ, viscosity coefficient β, amplitude b, Prandtl number Pr, curvature k, Brinkman number Br, time t^*, concentration ϕ, Schmidt number Sc, Soret number Sr, fluid parameter γ^*, Dufour number Du and permeability parameter Da are as follows:

$$x=\frac{\bar{x}}{\lambda},\qquad r=\frac{\bar{r}}{a},\qquad w_1=\frac{\bar{w}_1}{s},\qquad w_2=\frac{\bar{w}_2}{s},$$

$$p=\frac{a^2\bar{p}}{s\mu_o\lambda},\qquad \theta=\frac{T-T_o}{T_1-T_o},\qquad h=\frac{\chi}{a},\qquad \delta=\frac{a}{\lambda},$$

$$\beta=\beta'(T_1-T_o),\qquad \mathrm{Re}=\frac{\rho s a}{\mu_o},\qquad \gamma=\gamma'(T_1-T_o),\qquad b_1=\frac{b}{a},$$

$$\mathrm{Pr}=\frac{\mu_o c_p}{\kappa_o},\qquad Br=\frac{\mu_o^2 s}{\kappa_o(T_1-T_o)},\qquad k=\frac{R'}{a},\qquad \phi=\frac{C-C_o}{C_1-C_o},$$

$$Sr=\frac{\rho D_B K_T(T_1-T_o)}{\mu_o T_m(C_1-C_o)},\qquad Sc=\frac{\mu_o}{\rho D_B},\qquad Du=\frac{D_B K_T(C_1-C_0)}{c_p C_s \mu_o(T_1-T_0)},$$

$$\gamma^*=\frac{\eta s}{a},\qquad Da=\frac{K}{a^2}. \tag{5.21}$$

If ψ denotes the stream function then

$$w_1=-\frac{k\delta}{r+k}\frac{\partial\psi}{\partial x},w_2=\frac{\partial\psi}{\partial r}, \tag{5.22}$$

and implementing lubrication approach, one has

$$k\frac{\partial p}{\partial x}=-\frac{(k+r)(1-\beta\theta)}{2Da}\left(1-\frac{m\gamma^{*2}}{3!}\left(\frac{\partial^2\psi}{\partial r^2}-\frac{1}{(k+r)}\left(1+\frac{\partial\psi}{\partial r}\right)\right)^2\right)\left(1+\frac{\partial\psi}{\partial r}\right)$$

$$+\frac{1}{(k+r)}\frac{\partial}{\partial r}\left(S_{rx}(k+r)^2\right), \tag{5.23}$$

$$\frac{\partial p}{\partial r}=0, \tag{5.24}$$

$$\gamma\left(\frac{\partial\theta}{\partial r}\right)^2+(\gamma\theta+1)\left(\frac{\partial^2\theta}{\partial r^2}+\frac{1}{r+k}\frac{\partial\theta}{\partial r}\right)+Br\left(\frac{\partial^2\psi}{\partial r^2}-\frac{1}{(r+k)}\left(1+\frac{\partial\psi}{\partial r}\right)\right)S_{rx}$$

$$+\mathrm{Pr}\,Du\left(\frac{1}{r+k}\frac{\partial\phi}{\partial r}+\frac{\partial^2\phi}{\partial r^2}\right)=0, \tag{5.25}$$

$$\frac{1}{k+r}\frac{\partial \phi}{\partial r}+\frac{\partial^2 \phi}{\partial r^2}+SrSc\left(\frac{1}{k+r}\frac{\partial \theta}{\partial r}+\frac{\partial^2 \theta}{\partial r^2}\right)=0. \tag{5.26}$$

Eqns. (5.23) and (5.24) leads to

$$\frac{\partial}{\partial r}\left[\begin{array}{l}-\dfrac{(k+r)(1-\beta\theta)}{2Da}\left(1-\dfrac{m\gamma^{*2}}{3!}\left(\dfrac{\partial^2\psi}{\partial r^2}-\dfrac{1}{(k+r)}\left(1+\dfrac{\partial\psi}{\partial r}\right)\right)^2\right)\left(1+\dfrac{\partial\psi}{\partial r}\right)\\ +\dfrac{1}{(r+k)}\dfrac{\partial}{\partial r}\left(S_{rx}(r+k)^2\right)\end{array}\right]=0, \tag{5.27}$$

in which

$$S_{xr}=S_{rx}=\frac{1-\beta\theta}{2}\left(\frac{\partial^2\psi}{\partial r^2}-\frac{1}{(k+r)}\left(1+\frac{\partial\psi}{\partial r}\right)\right)\left(1-\frac{m\gamma^{*2}}{3!}\left(\frac{\partial^2\psi}{\partial r^2}-\frac{1}{(k+r)}\left(1+\frac{\partial\psi}{\partial r}\right)\right)^2\right). \tag{5.28}$$

Dimensionless conditions are

$$\psi=\mp F/2,\quad \frac{\partial\psi}{\partial r}=-1 \quad \text{at} \quad r=\mp h, \tag{5.29}$$

$$\theta=\left\{\begin{matrix}1\\0\end{matrix}\right\} \qquad \text{at} \quad r=\mp h, \tag{5.30}$$

$$\phi=\left\{\begin{matrix}1\\0\end{matrix}\right\} \qquad \text{at} \quad r=\mp h, \tag{5.31}$$

where

$$F=\int_{-h}^{h}\frac{\partial\psi}{\partial r}dr=\psi(h)-\psi(-h), \tag{5.32}$$

$$h=1+b_1\sin(2\pi x). \tag{5.33}$$

5.1.1 Entropy

The entropy in this case satisfies

$$S = -\frac{1}{\Theta_o^2}\mathbf{q}.\nabla T + \frac{1}{\Theta_o}\left(\begin{array}{c}\frac{\mu(T)}{2}\left(1-\frac{m}{3!}\left(\eta\left|\dot{G}\right|^2\right)^2\right)\left(\frac{\partial W_2}{\partial R}+\frac{R}{R'+R}\frac{\partial W_1}{\partial X}-\frac{W_2}{R'+R}\right)^2 \\ +\frac{D_B k_T}{\rho c_p c_s}\left(\frac{\partial^2 C}{\partial R^2}+\frac{\partial^2 C}{\partial X^2}-\frac{1}{R'+R}\frac{\partial C}{\partial R}\right)\end{array}\right). \quad (5.34)$$

It should be noticed that Eqn. (5.34) includes irreversibility because of transfer of heat, fluid friction and Dufour effects. Entropy generation in dimensionless form is

$$N_s = \left(\frac{\partial\theta}{\partial r}\right)^2 + \frac{\Lambda}{(\gamma\theta+1)}\left(\begin{array}{c}Br\frac{(1-\beta\theta)}{2}\left(-\frac{1}{(k+r)}\left(1+\frac{\partial\psi}{\partial r}\right)+\frac{\partial^2\psi}{\partial r^2}\right)^2\left(1-\frac{m\gamma^{*2}}{3!}\left(-\frac{1}{(k+r)}\left(1+\frac{\partial\psi}{\partial r}\right)+\frac{\partial^2\psi}{\partial r^2}\right)^2\right) \\ +\Pr Du\left(\frac{1}{k+r}\frac{\partial\varphi}{\partial r}+\frac{\partial^2\varphi}{\partial r^2}\right)\end{array}\right), \quad (5.35)$$

in which

$$S_G = \frac{\kappa(T)(T_1-T_o)^2}{\Theta_o^2 a^2}, \quad \Lambda = \frac{\Theta_o}{(T_1-T_o)}. \quad (5.36)$$

Bejan number (Be) indicating heat transfer irreversibility to total entropy is given by

$$Be = \frac{\left(\frac{\partial \theta}{\partial r}\right)^2}{\left(\frac{\partial \theta}{\partial r}\right)^2 + \frac{\Lambda}{(\gamma\theta+1)}\left(Br\frac{(1-\beta\theta)}{2}\left(-\frac{1}{(k+r)}\left(1+\frac{\partial \psi}{\partial r}\right)+\frac{\partial^2 \psi}{\partial r^2}\right)^2\left(1-\frac{m\gamma^{*2}}{3!}\left(-\frac{1}{(k+r)}\left(1+\frac{\partial \psi}{\partial r}\right)+\frac{\partial^2 \psi}{\partial r^2}\right)^2\right)\right)} \cdot$$
$$+\Pr Du\left(\frac{1}{k+r}\frac{\partial \varphi}{\partial r}+\frac{\partial^2 \varphi}{\partial r^2}\right) \qquad (5.37)$$

Clearly $Be \in [0,1]$.

5.2 Methodology

The modeled differential Eqns. (5.25) to (5.27) subject to the boundary conditions given in Eqns. (5.29) to (5.31) are computed numerically by Shooting method using the built-in command in Mathematica.

5.3 Analysis

This section is devoted to present physical description of axial velocity, temperature, concentration, entropy, Bejan number and heat flux at the upper wall for various parameters of interest.

5.3.1 Velocity

Figs. (5.1-5.4) show β, Da, k and γ^{*2} effects on axial velocity (w_2). Clearly velocity is maximum near centre of channel while it decays near upper wall where wall temperature being $T_0(<T_1)$. For higher β, an increase in amplitude is also noticed. It is due to the reason that μ and β have inverse relation. Thus for higher β, the viscosity decays and

consequently velocity enhances (see Fig. (5.1)). Fig. (5.2) witnesses that velocity enhances in the centre for higher Da. Since permeability parameter (K) has inverse relation with Da, thus by higher Da, there is less permeability. Consequently drag force reduces and velocity increases. Fig. (5.3) addresses response of curvature (k) on w_2. Further, velocity is less near the lower channel wall whereas it enhances in rest part of the channel. Moreover, velocity is symmetric about the centre line for straight channel. Fig. (5.4) is made to study effects of material parameter (γ^{*2}) on w_2. Velocity decrease at centre of the channel is noted for higher values of γ^{*2}.

5.3.2 Temperature

Variation of temperature (θ) for various pertinent parameters β, γ, Sr and Du is described through Figs. (5.5-5.8). Fig. (5.5) depicts that θ decays for increasing β. Fig. (5.6) presents that θ reduces by increasing γ. This is because of the reason that higher γ strengthen the material capability to diffuse or absorb heat. This occurs when fluid temperature is greater than wall temperature. Figs. (5.7) and (5.8) illustrate temperature (θ) response for increasing Soret (Sr) and Dufour (Du) effects respectively. Temperature amplifies for both variables. The reason for the same is that an increase in Sr or Du corresponds to viscosity decay and thus velocity enhances. Thus fast moving material particles with larger molecular vibration rise material temperature.

5.3.3 Concentration

Figs. (5.9) and (5.10) demonstrate reduction in concentration (ϕ) for larger Sr and Du.

Moreover ϕ also reduces when Sc is increased (see Fig. (5.11)). Schmidt number (Sc) is ratio of momentum diffusion to mass diffusion rates. Thus an increase in Sc corresponds to low mass diffusion thus concentration is reduced accordingly.

5.3.4 Entropy and Bejan Number

The influences of considered quantities β, γ, Sr and Du on entropy generation and Bejan number are revealed through Figs. (5.12) to (5.19). Figs. (5.12) and (5.14) are prepared to show the reaction of Ns for β and γ respectively. From these Figs., it is determined that in the middle of the channel there is no considerable change in Ns while it decays near the channel walls. The entropy and temperature are directly related. That's why these Figs. ensure decrease in temperature. Figs. (5.13) and (5.15) are captured to show the responses of Be for β and γ. Be behavior is opposite for increased values of larger β and γ. Figs. (5.16) and (5.18) show impacts of Sr and Du on Ns. It is noticed that Ns rises near the walls of channel for higher Du and Sr parameters whereas response of Be is opposite for these parameters (see Figs. (5.17) and (5.19)). It is clear that Be decreases for Sr while it enhances through Du.

5.3.5 Heat Transfer Coefficient

Heat transfer coefficient at the upper wall is $\frac{\partial h}{\partial r}\theta'(h)$. To show the effects of Soret and Dufour, heat transfer rate at the wall is sketched through bar charts in Figs. (5.20) and (5.21). Both Figs. show that heat transfer rate increases for higher Sr and Du.

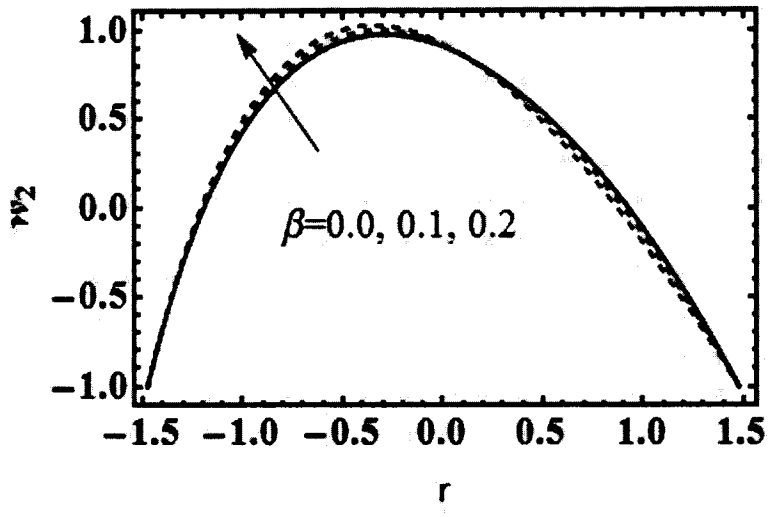

Fig. (5.1): Velocity profile for variable viscosity parameter $x = 0.3, \gamma = 0.02, k = 3,$ $Da = 1, Du = 0.5, Sr = 0.2, Ec = 2, \Pr = Sc = Sr = 0.5, \gamma^{*2} = 0.001.$

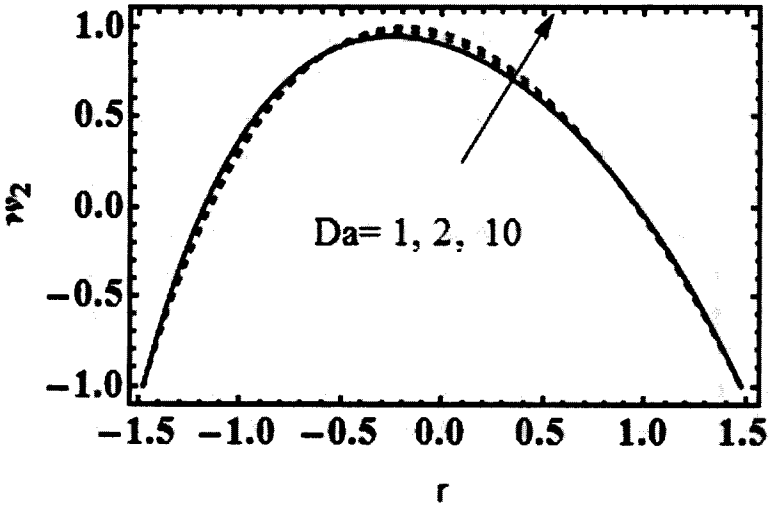

Fig. (5.2): Velocity profile for permeability parameters $x = 0.3, \beta = 0.001, \gamma = 0.02,$ $k = 3, Du = 0.5, Sr = 0.2, Ec = 2, \Pr = Sc = Sr = 0.5, \gamma^{*2} = 0.001.$

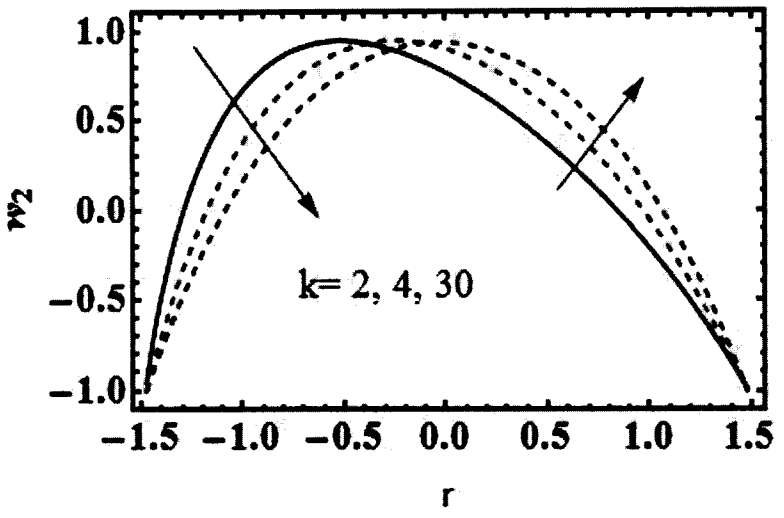

Fig. (5.3): Velocity profile for curvature parameter $x = 0.3, \beta = 0.001, \gamma = 0.02,$ $Da = 1, Du = 0.5, Sr = 0.2, Ec = 2, \Pr = Sc = Sr = 0.5, \gamma^{*2} = 0.001.$

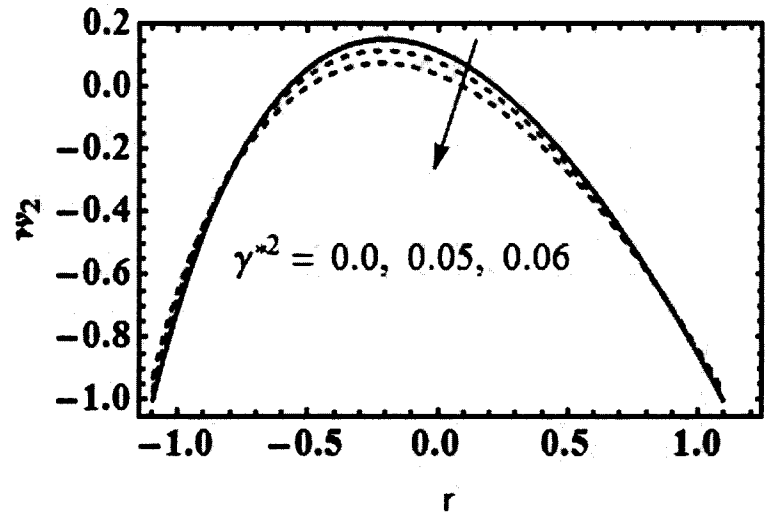

Fig. (5.4): Velocity profile for fluid parameter $x = 0.3, \beta = 0.001, \gamma = 0.02, k = 3,$ $Da = 1, Du = 0.5, Sr = 0.2, Ec = 2, \Pr = Sc = Sr = 0.5.$

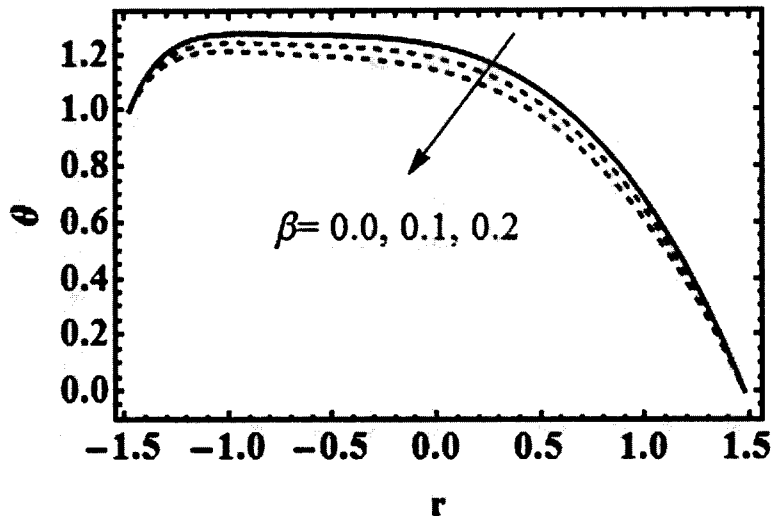

Fig. (5.5): Temperature profile for viscosity parameter $x = 0.3, \gamma = 0.02, k = 3,$ $Da = Du = 1, Sr = 0.2, \Pr = 0.4, Ec = 2, Sc = 0.5, Sr = 1, \gamma^{*2} = 0.003.$

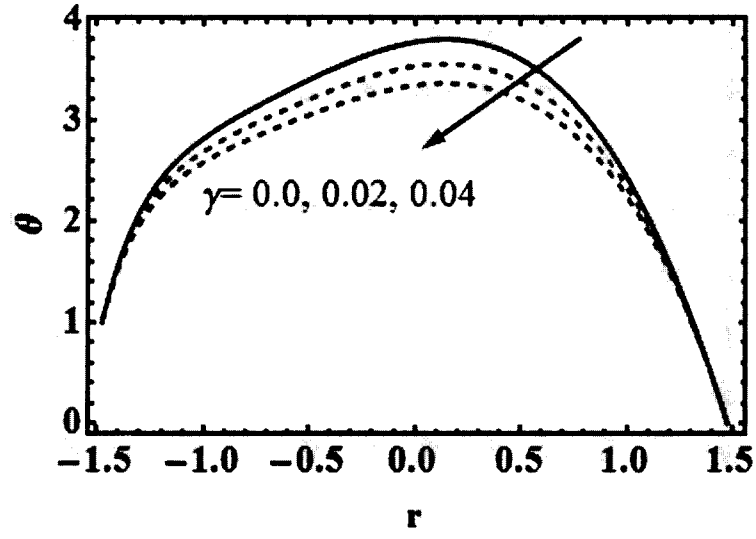

Fig. (5.6): Temperature profile for thermal conductivity parameter $x = 0.3, \beta = 0.01, k = 3,$ $Da = Du = 1, Sr = 0.2, \Pr = 0.4, Ec = 2, Sc = 0.5, Sr = 1, \gamma^{*2} = 0.003.$

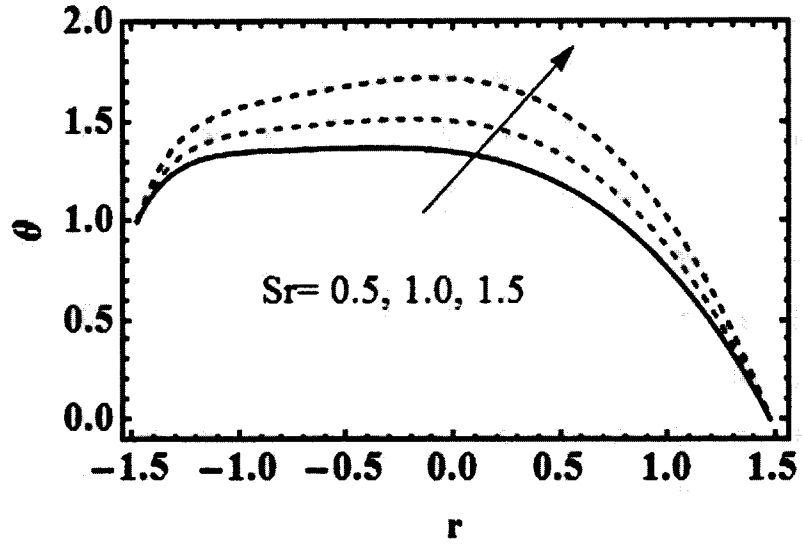

Fig. (5.7): Temperature profile for Soret parameter $x = 0.3, \beta = 0.01, \gamma = 0.02, k = 3,$ $Da = Du = 1, \Pr = 0.5, Ec = 2, Sc = 0.5, \gamma^{*2} = 0.0025.$

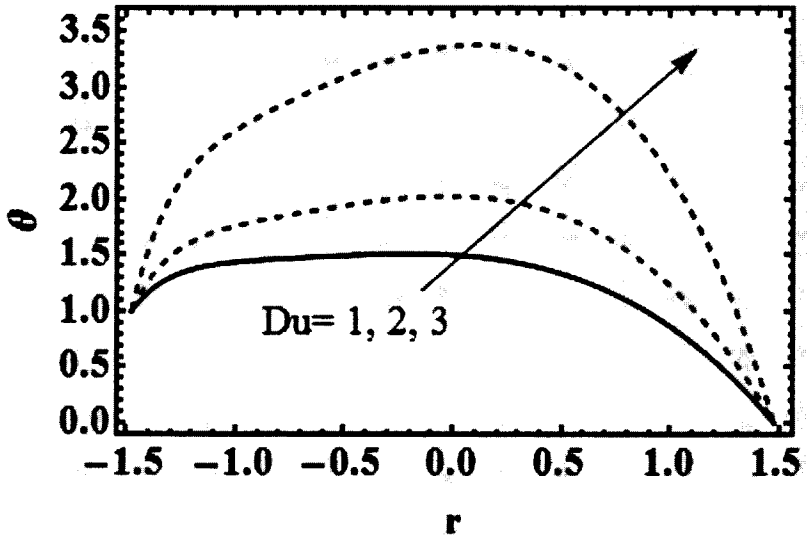

Fig. (5.8): Temperature profile for Dufour parameters $x = 0.3, \beta = 0.01, \gamma = 0.02, k = 3,$ $Da = 1, \Pr = 0.5, Ec = 2, Sc = 0.5, Sr = 0.5, \gamma^{*2} = 0.0025.$

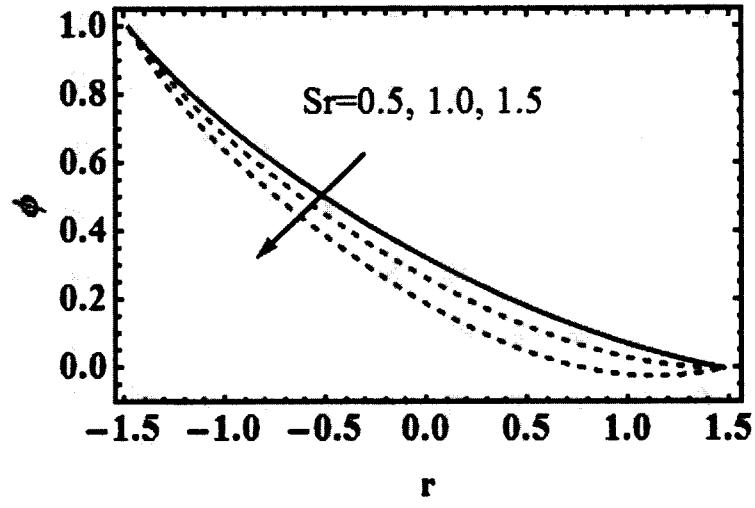

Fig. (5.9): Concentration profile for Soret parameter $x = 0.3, \beta = 0.1, \gamma = 0.02, k = 3, Da = 1,$ $Du = 2, \Pr = 0.5, Ec = 0.5, Sc = 0.5, \gamma^{*2} = 0.0025.$

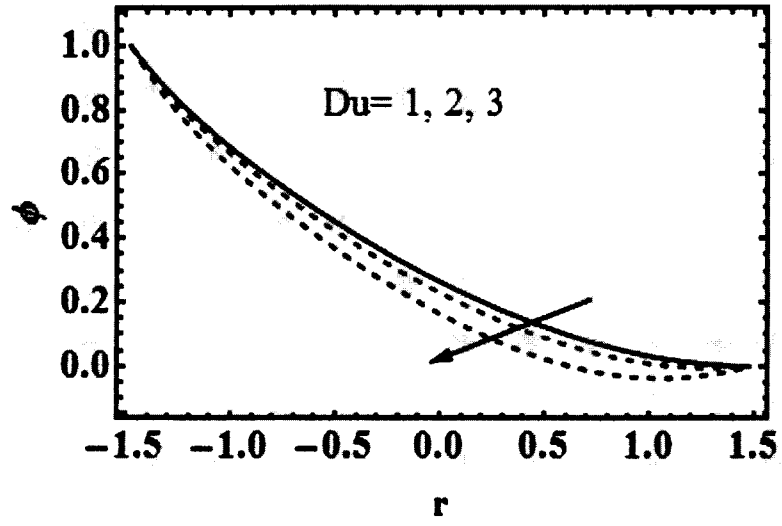

Fig. (5.10) : Concentration profile for Dufour parameter $x = 0.3, \beta = 0.1, \gamma = 0.02, k = 3,$ $Da = 1, Sr = 0.2, \Pr = 0.5, Ec = 0.5, Sc = 0.5, \gamma^{*2} = 0.0025.$

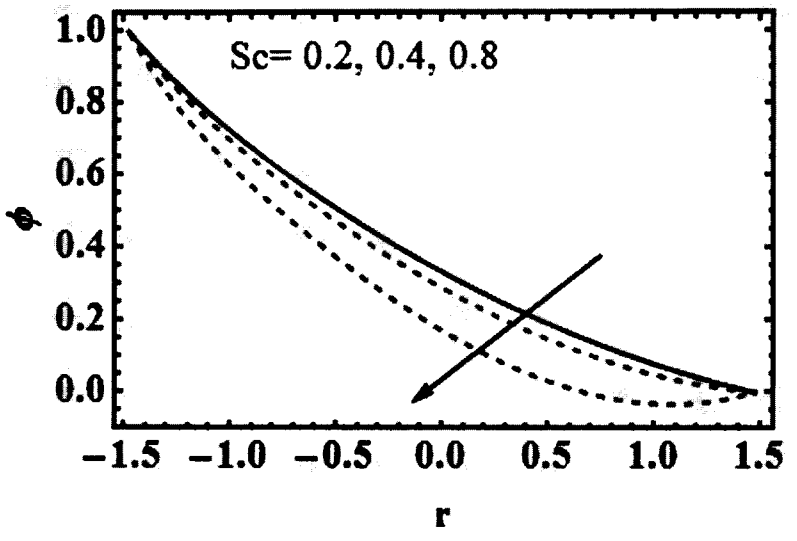

Fig. (5.11): Concentration profile for Schmidt parameter $x = 0.3, \beta = 0.1, \gamma = 0.02, k = 3, Da = 1,$ $Du = 0.5, Sr = 0.2, \Pr = 0.5, Ec = 2, \gamma^{*2} = 0.0025.$

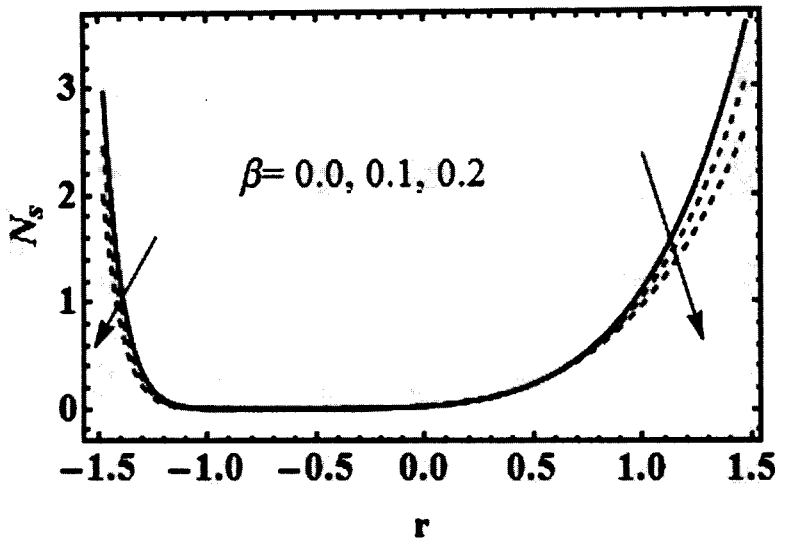

Fig. (5.12): Entropy for variable viscosity parameter $x = 0.3, \beta = 0.05, \gamma = 0.05, k = 3,$ $Da = Du = 1, Sr = 0.2, \Pr = 0.4, Ec = 2, Sc = 0.5, Sr = 0.5, \gamma^{*2} = 0.0025.$

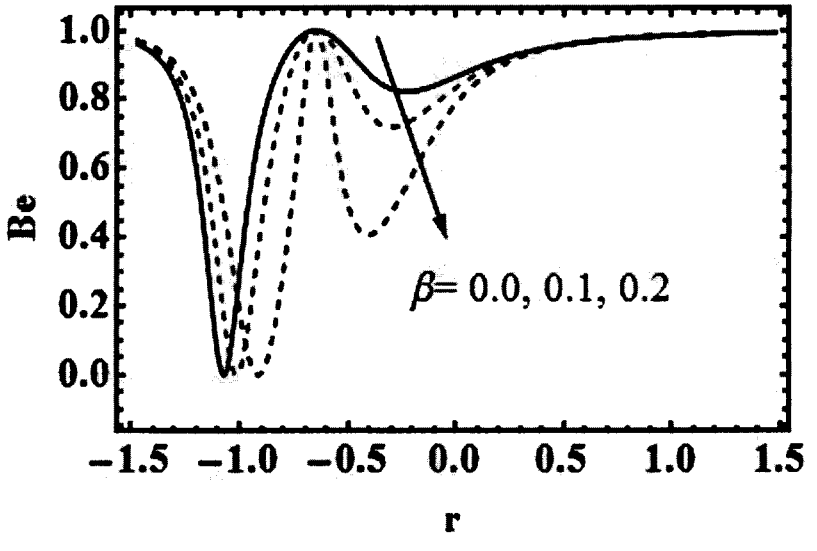

Fig. (5.13): Bejan number for variable viscosity parameter $x = 0.3, \beta = 0.05, \gamma = 0.05, k = 3,$ $Da = Du = 1, Sr = 0.2, \Pr = 0.4, Ec = 2, Sc = 0.5, Sr = 0.5, \gamma^{*2} = 0.0025.$

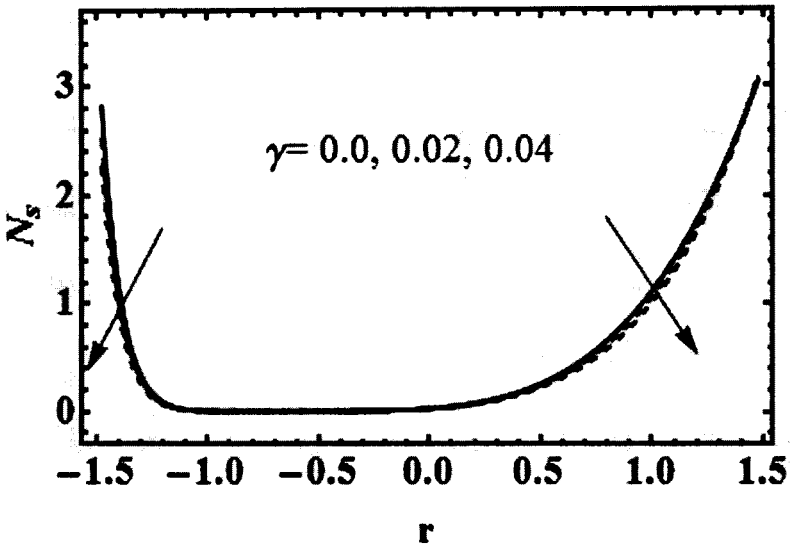

Fig. (5.14): Entropy for variable thermal conductivty coefiificient $x = 0.3, \beta = 0.05, \gamma = 0.05,$ $k = 3, Da = Du = 1, Sr = 0.2, \Pr = 0.4, Ec = 2, Sc = 0.5, Sr = 0.5, \Lambda = 0.01, \gamma^{*2} = 0.0025.$

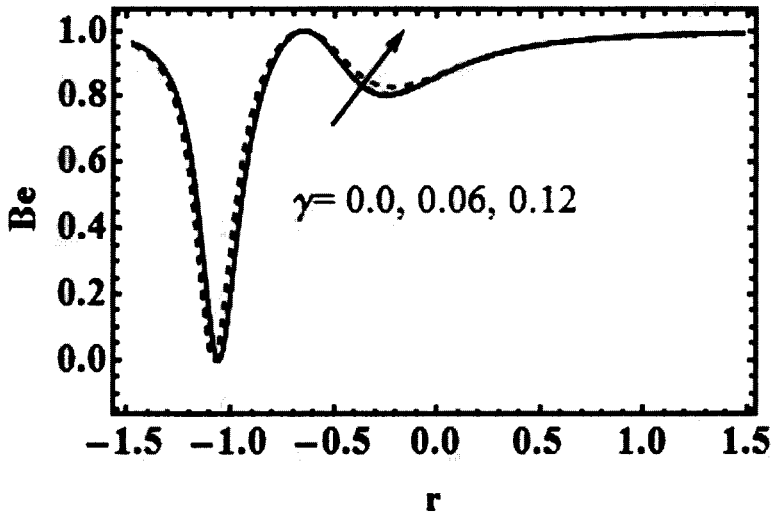

Fig. (5.15): Bejan number for variable thermal conductivty coefiificient $x = 0.3, \beta = 0.05, \gamma = 0.05,$ $k = 3, Da = Du = 1, Sr = 0.2, \Pr = 0.4, Ec = 2, Sc = 0.5, Sr = 0.5, \Lambda = 0.01, \gamma^{*2} = 0.0025.$

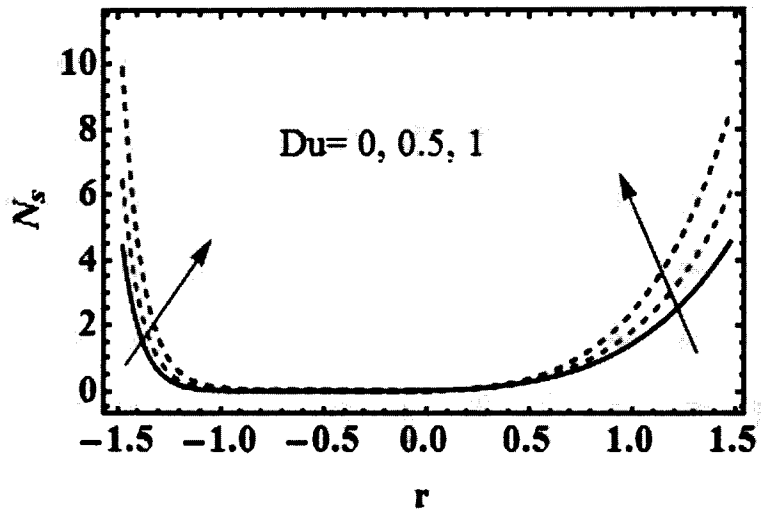

Fig. (5.16): Entropy for Dufur parameter with $x = 0.3, \beta = 0.04, \gamma = 0.05, k = 3,$ $Da = Du = 1, Sr = 0.3, \Pr = 0.5, Ec = 2, Sc = 0.5, Sr = 0.6, \Lambda = 0.01, \gamma^{*2} = 0.0025.$

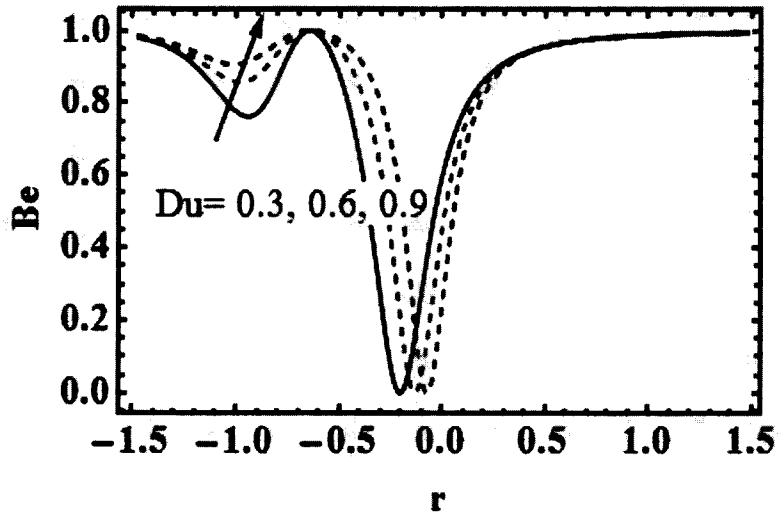

Fig. (5.17): Bejan number for Dufur parameter with $x = 0.3, \beta = 0.04, \gamma = 0.05, k = 3,$ $Da = Du = 1, Sr = 0.3, \Pr = 0.5, Ec = 2, Sc = 0.5, Sr = 0.6, \Lambda = 0.01, \gamma^{*2} = 0.0025.$

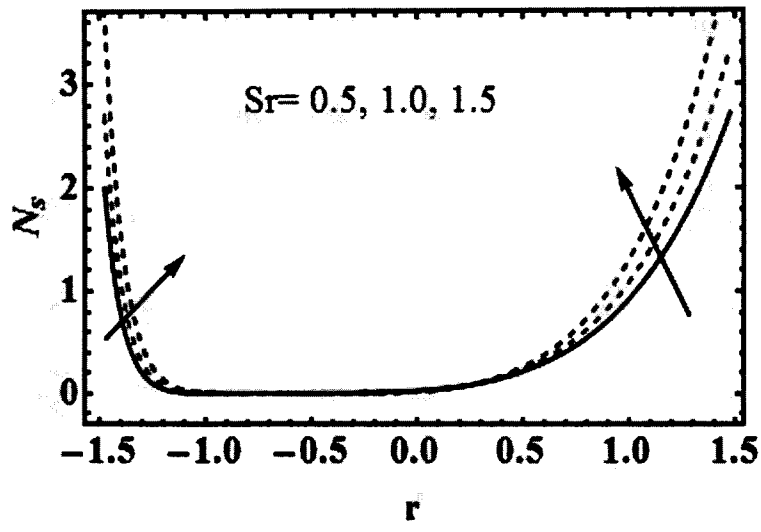

Fig. (5.18): Entropy for Soret coefiificient with $x = 0.3, \beta = 0.05, \gamma = 0.05, k = 3,$ $Da = Du = 1, Sr = 0.2, \Pr = 0.4, Ec = 2, Sc = 0.5, Sr = 0.5, \Lambda = 0.01, \gamma^{*2} = 0.0025.$

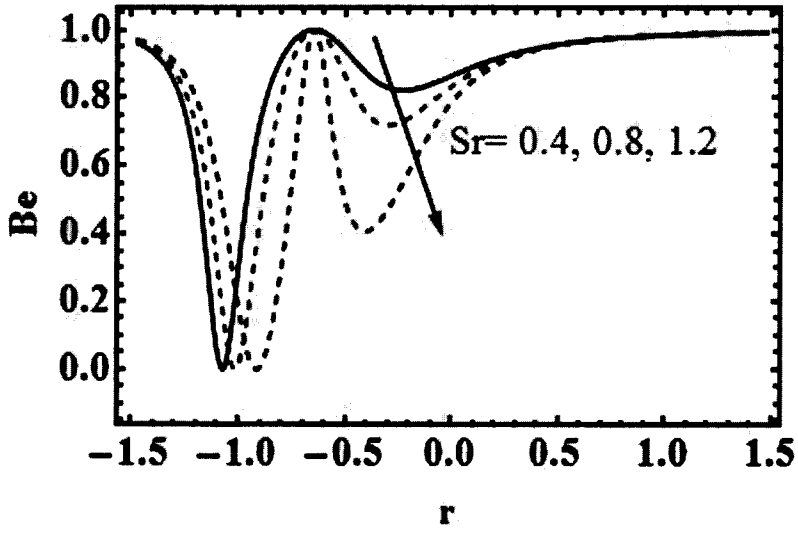

Fig. (5.19): Bejan number for Soret coefiificient with $x = 0.3, \beta = 0.05, \gamma = 0.05, k = 3,$ $Da = Du = 1, Sr = 0.2, \Pr = 0.4, Ec = 2, Sc = 0.5, Sr = 0.5, \Lambda = 0.01, \gamma^{*2} = 0.0025.$

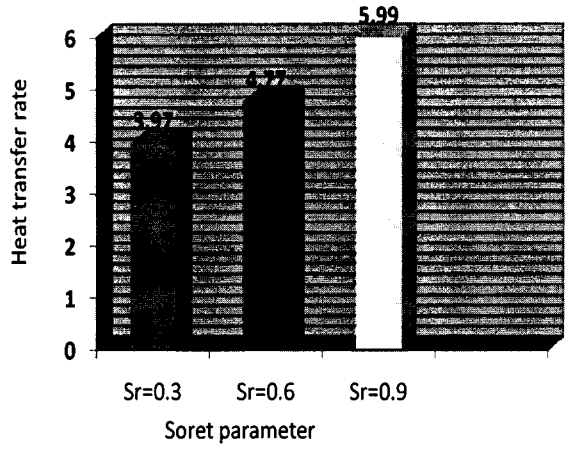

Fig. 5.20: Heat transfer rate for Soret parameter

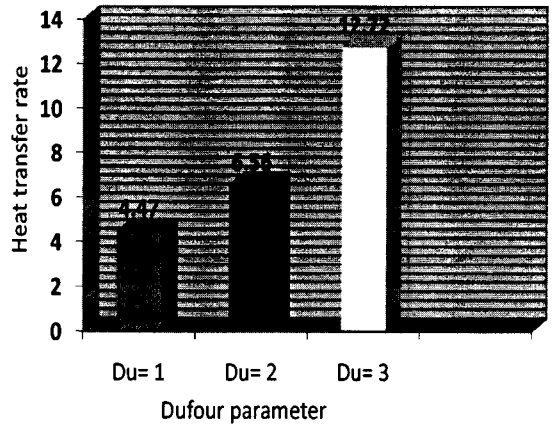

Fig. 5.21: Heat transfer rate for Dufour parameter

5.4 Conclusion

Soret and Dufour aspects on peristaltic flow of Sutterby fluid are examined. Main results are summarized below.

- There is decay in velocity in case of Sutterby fluid.
- Temperature reduces for increasing β and γ.
- Concentration decreases for both Soret and Dufour parameters.
- Entropy has parabolic trend and it is more near the upper wall than the lower wall due to difference in temperature at both walls.
- Total entropy has similar behavior for β and γ.
- Increasing behavior of entropy generation is noticed for both Soret and Dufour variables.
- Bejan number for Soret and Dufour variables is opposite when compared with entropy generation.
- Heat transfer rate behavior for both Soret and Dufour variables is qualitatively similar.

Chapter 6

Generation of Entropy in Peristaltic Activity of Third Grade Liquids under Magnetic Field

In this chapter the flow of third grade fluid is considered in curved geometry with the application of inclined magnetic field. Inclined magnetic field has rarely been used for curved channel. Heat equation has been undertaken with the effects of Joule heating, variable thermal conductivity and heat source/ sink. Non-linear radiation is accounted. Moreover, the entropy generation and Bejan number coupled with the effects of viscous dissipation, inclined magnetic field, heat source/ sink, non-linear thermal radiation and variable thermal conductivity are analyzed. The parameters of interest are graphically analyzed for entropy, Bejan number, temperature, velocity, stream lines and pressure gradient.

6.1 Mathematical Formulation

Peristaltic movement of third grade liquid is being analyzed in curved geometry. Width of curved channel is $2a$. This channel is coiled in a circle having radius $\left(R'\right)$. Components $\left(W_1, W_2\right)$ of velocity $\left(\mathbf{W}\right)$ are along the radial and axial directions (R, X) respectively. Inclined magnetic field of strength $\left(B_0\right)$ has been imposed with inclination $\left(\vartheta_0\right)$ with radius of the channel as defined in Eqn. (2.2), however, impact of induced magnetic field is

neglected because of the assumption of small magnetic Reynolds number. Thermal conductivity is assumed as function of temperature. Heat absorption coefficient and non-linear thermal radiation have also been incorporated in energy equation. Slip effects for velocity are applied at the channel walls. Convective conditions are entertained for heat. Waves are moving along the channel walls with speed (s), amplitude (a) and wavelength (λ) as in Fig. (2.1).

Geometry of such waves satisfies

$$R = \pm\chi = \pm\left[a + b\sin\left(\frac{2\pi}{\lambda}(X - st)\right)\right], \tag{6.1}$$

Governing equations for the considered problem are as

$$\nabla.\mathbf{W} = 0, \tag{6.2}$$

$$\rho\frac{d\mathbf{W}}{dt} = \nabla.\boldsymbol{\tau} - (\mathbf{J}\times\mathbf{B}), \tag{6.3}$$

$$\rho c_p\frac{dT}{dt} = \nabla.[\kappa(T)\nabla T] + tr(\mathbf{LS}) + \frac{\mathbf{J}.\mathbf{J}}{\sigma} - \nabla.\mathbf{q}_r + Q_0(T - T_0), \tag{6.4}$$

here, $\kappa(T)$ represents variable thermal conductivity of material, c_p specific heat, ρ density of fluid, $\mathbf{S}$ extra Stress tensor, $\boldsymbol{\tau}$ Stress tensor, Q_0 heat absorption parameter, $\mathbf{L}(=\text{grad}\,\mathbf{W})$ and radiative heat flux $(\mathbf{q}_r)$. According to Rosseland approximation, thermal radiation is

$$\mathbf{q}_r = -\frac{16T_0^3\sigma^*}{3k^*}(\nabla T), \tag{6.5}$$

in which $\sigma^*(=5.6697\times10^{-8}Wm^{-2}K^{-4})$ and k^* represent Stephan-Boltzmann constant and mean absorption coefficient respectively. Tensor for third grade fluid is written as

$$\boldsymbol{\tau} = -p\mathbf{I} + \mathbf{S}, \tag{6.6}$$

$$\mathbf{S} = \mu_0 \mathbf{B}_1 + \beta_1 \mathbf{B}_2 + \beta_2 \mathbf{B}_1^2 + \alpha_1 \left(tr\mathbf{B}_1^2\right)\mathbf{B}_1, \tag{6.7}$$

$$\mathbf{B}_1 = \mathbf{L}' + \mathbf{L}, \tag{6.8}$$

$$\mathbf{B}_2 = \left(\frac{\partial}{\partial t} + \mathbf{W}.\nabla\right)\mathbf{B}_1 + \mathbf{B}_1\mathbf{L} + \mathbf{L}'\mathbf{B}_1, \tag{6.9}$$

such that

$$\beta_1 \geq 0, \quad \alpha_1 \geq 0, \quad |\beta_1 + \beta_2| \leq \sqrt{24\mu\alpha_1}. \tag{6.10}$$

Component forms of Eqns. (6.2) to (6.4) are

$$\frac{R'}{R'+R}\frac{\partial W_2}{\partial X} + \frac{\partial W_1}{\partial R} + \frac{W_1}{R'+R} = 0, \tag{6.11}$$

$$\rho\left(\frac{dW_2}{dt} + \frac{W_1 W_2}{R+R'}\right) = \frac{R'}{R+R'}\left(\begin{array}{c} -\dfrac{\partial P}{\partial X} + \dfrac{1}{\left(R+R'\right)R'}\dfrac{\partial}{\partial R}\left(\left(R+R'\right)^2 S_{XR}\right) \\ +\dfrac{\partial S_{XX}}{\partial X} + \sigma B_0{}^2\left(W_1 \operatorname{Sin}\vartheta_0 \operatorname{Cos}\vartheta_0 - W_2 \operatorname{Sin}^2\vartheta_0\right) \end{array}\right), \tag{6.12}$$

$$\rho\left(\frac{dW_1}{dt} - \frac{W_2^2}{R+R'}\right) = -\frac{\partial P}{\partial R} + \left(\frac{R'}{R+R'}\right)\frac{\partial S_{XR}}{\partial X} - \frac{S_{XX}}{R+R'} + \frac{1}{R+R'}\frac{\partial}{\partial R}\left(\left(R+R'\right)S_{RR}\right)$$
$$+\sigma\frac{R'B_0{}^2}{R+R'}\left(W_2 \operatorname{Sin}\vartheta_0 \operatorname{Cos}\vartheta_0 - W_1 \operatorname{Cos}^2\vartheta_0\right), \tag{6.13}$$

$$\rho C_p \frac{dT}{dt} = \frac{\partial}{\partial R}\left(\kappa(T)\frac{\partial T}{\partial R}\right) - \frac{\kappa(T)}{R+R'}\frac{\partial T}{\partial R} + \frac{\partial}{\partial X}\left(\frac{\kappa(T)R'^2}{\left(R+R'\right)^2}\frac{\partial T}{\partial X}\right) - \frac{\partial W_2}{\partial R}\left(-S_{RR} + S_{XX}\right)$$
$$-\left(-\frac{\partial W_2}{\partial R} - \frac{R'}{R+R'}\frac{\partial W_1}{\partial X} + \frac{W_2}{R+R'}\right)S_{RX} + \left(\frac{\sigma R'B_0}{R'+R}\right)^2\left(W_1 \operatorname{Cos}\vartheta_0 - W_2 \operatorname{Sin}\vartheta_0\right)^2 + Q_0(T-T_0)$$
$$-\frac{16\sigma^* T_0^3}{3k^*}\left(-\frac{\partial^2}{\partial X^2} + \frac{1}{R+R'}\frac{\partial}{\partial R} - \frac{\partial^2}{\partial R^2}\right)T. \tag{6.14}$$

The imposed boundary conditions are

$$W_2 = 0, \qquad \text{at} \quad R = \pm\chi, \tag{6.15}$$

$$\left.\begin{aligned} \kappa_1 \frac{\partial T}{\partial R} &= -\beta_1' (T_1 - T) \quad \text{at} \quad R = -\chi, \\ \kappa_1 \frac{\partial T}{\partial R} &= -\beta_2' (T - T_0) \quad \text{at} \quad R = \chi, \end{aligned}\right\} \tag{6.16}$$

in which κ_1 is thermal conductivity of the walls and (β_1', β_2') Biot numbers.

The relation of transformations between wave (r^*, x^*) and laboratory (R, X) frames is shown as:

$$\bar{r} = R, \quad \bar{x} = X - st, \quad \bar{w}_1 = W_1, \quad \bar{w}_2 = W_2 - s. \tag{6.17}$$

Defining dimensionless variables (x, r), velocity components (w_1, w_2), curvature K, amplitude ratio b_1, pressure p, temperature θ, wave number δ, peristaltic wall $\bar{R}_1$, Reynolds number Re, components of extra stress tensor S_{ij}, variable thermal conductivity parameter β, Brinkman number Br, Prandtl number Pr, third grade fluid parameter β_3, Hartmann number H, radiation parameter R_d, heat absorption coefficient Q and thermal Biot parameters (β_1, β_2) as

$$(x, r) = \left(\frac{\bar{x}}{\lambda}, \frac{\bar{r}}{a}\right), \quad (w_1, w_2) = \left(\frac{\bar{w}_1}{s}, \frac{\bar{w}_2}{s}\right), \quad K = \frac{R'}{a}, \quad b_1 = \frac{b}{a}, \quad p = \frac{a^2 P}{s\mu_0 \lambda}, \quad \theta = \frac{T - T_0}{T_1 - T_0},$$

$$\delta = \frac{b}{\lambda}, \quad \bar{R}_1 = \frac{\bar{R}}{b}, \quad \text{Re} = \frac{\rho s a}{\mu_0}, \quad S_{ij} = \frac{a S_{ij}}{b\mu_0}, \quad \beta = \beta' (T_1 - T_0), \quad Br = \frac{\mu_0^2 s}{\kappa_0 (T_1 - T_0)},$$

$$\text{Pr} = \frac{\mu_0 c_p}{\kappa_0}, \quad \beta_3 = \frac{\alpha_1 s^2}{\mu_0 a^2}, \quad H = \sqrt{\frac{\sigma B_0^2 a^2}{\mu_0}}, \quad R_d = \frac{16\sigma^* T_0^3}{3k^*}, \quad Q = \frac{a^2 Q_o}{\kappa_o}, \quad \beta_1 = \frac{a\beta_1'}{\kappa_1},$$

$$\beta_2 = \frac{a\beta_2'}{\kappa_1}. \tag{6.18}$$

Velocities (w_1, w_2) as a stream function (ψ) can be defined as:

$$w_2 = \frac{\partial \psi}{\partial r}, \quad w_1 = -\delta\left(\frac{K}{r+K}\right)\frac{\partial \psi}{\partial x}. \tag{6.19}$$

Incompressibility condition in Eqn. (6.11) is fulfilled trivially; however, after applying lubrication technique, rest of the expressions can be written as:

$$K\frac{\partial p}{\partial x} = \frac{1}{r+K}\frac{\partial}{\partial r}\left((r+K)^2 S_{rx}\right) - \frac{H^2K^2\,\mathrm{Sin}^2\,\vartheta_0}{r+K}\left(\frac{\partial \psi}{\partial r}+1\right), \tag{6.20}$$

$$\frac{\partial p}{\partial r} = 0, \tag{6.21}$$

$$\begin{aligned}&(\beta\theta+1)\left(\frac{\partial^2\theta}{\partial r^2}+\frac{1}{r+K}\frac{\partial\theta}{\partial r}\right)+\beta\left(\frac{\partial\theta}{\partial r}\right)^2 - Br\left(-\frac{\partial^2\psi}{\partial r^2}+\frac{1}{r+K}\left(\frac{\partial\psi}{\partial r}+1\right)\right)S_{xr}\\ &+Q\theta + R_d\,\mathrm{Pr}\left(\frac{1}{r+K}\frac{\partial\theta}{\partial r}+\frac{\partial^2\theta}{\partial r^2}\right)+Br\frac{K^2H^2\,\mathrm{Sin}^2\,\vartheta_0}{(r+K)^2}\left(\frac{\partial\psi}{\partial r}+1\right)^2 = 0,\end{aligned} \tag{6.22}$$

Equations (6.20) and (6.21) imply that

$$\frac{\partial}{\partial r}\left(\frac{1}{(r+K)}\frac{\partial}{\partial r}\left(S_{rx}(r+K)^2\right) - \frac{K^2H^2\,\mathrm{Sin}^2\,\vartheta_0}{r+K}\left(\frac{\partial\psi}{\partial r}+1\right)\right) = 0, \tag{6.23}$$

$$S_{xr} = S_{rx} = \left(\frac{\partial^2\psi}{\partial r^2} - \frac{1}{r+K}\left(\frac{\partial\psi}{\partial r}+1\right)\right) + 2\beta_3\left(\frac{\partial^2\psi}{\partial r^2} - \frac{1}{r+K}\left(\frac{\partial\psi}{\partial r}+1\right)\right)^3, \tag{6.24}$$

$$h = 1 + b_1\,\mathrm{Sin}(2\pi x). \tag{6.25}$$

Now the dimensionless boundary conditions are

$$\psi = \mp F/2, \quad \frac{\partial \psi}{\partial r} = -1 \quad \text{at} \quad r = \mp h, \tag{6.26}$$

$$\left\{ \begin{aligned} &-\beta_1(\theta - 1) + \frac{\partial \theta}{\partial r} = 0, \quad \text{at} \quad r = -h, \\ &\beta_2 \theta + \frac{\partial \theta}{\partial r} = 0, \quad \text{at} \quad r = h. \end{aligned} \right\} \tag{6.27}$$

where

$$F = \int_{-h}^{h} \frac{\partial \psi}{\partial r} dr = \psi(h) - \psi(-h), \tag{6.28}$$

6.1.1 Entropy

Dimensional form of entropy production with the effects of viscous dissipation, variable thermal conductivity, Joule heating, heat absorption and non-linear thermal radiation is

$$S_{gen} = \frac{\kappa(T)}{\Theta_o^2}\left(\frac{dT}{dR}\right)^2 + \frac{1}{\Theta_o}\left[\left(-\frac{W_2}{\left(R+\bar{R}\right)} + \frac{\partial W_2}{\partial R} + \frac{\bar{R}}{\left(R+\bar{R}\right)}\frac{\partial W_1}{\partial X}\right) S_{RX} + Q_0(T - T_0) + \left(\frac{\sigma R' B_0}{\left(R+\bar{R}\right)}\right)^2 \left(W \operatorname{Cos} \vartheta_0 - W_2 \operatorname{Sin} \vartheta_0\right)^2 - \frac{16\sigma^* T_0^3}{3k^*}\left(-\frac{\partial^2}{\partial X^2} + \frac{1}{R+R'}\frac{\partial}{\partial R} - \frac{\partial^2}{\partial R^2}\right) T\right], \tag{6.29}$$

where Θ_o denotes the reference temperature. Non-dimensional form of entropy generation is

$$N_s = \frac{S_{gen}}{S_G} = \left(\frac{\partial\theta}{\partial r}\right)^2 + \frac{\Lambda}{1+\beta\theta}\left(\begin{array}{l} Br\left(S_{rx}\left(\frac{\partial^2\psi}{\partial r^2} - \frac{1}{r+K}\left(\frac{\partial\psi}{\partial r}+1\right)\right)\right) + \frac{Br\left(H^2\,\mathrm{Sin}^2\,\vartheta_0\right)K^2}{\left(r+K\right)^2}\left(\frac{\partial\psi}{\partial r}+1\right)^2 \\ +Q\theta + R_d\left(\frac{\partial^2\theta}{\partial r^2} + \frac{1}{r+K}\frac{\partial\theta}{\partial r}\right) \end{array}\right), \tag{6.30}$$

in which S_G and Λ are given by

$$S_G = \frac{\kappa(T)\left(T_1 - T_o\right)^2}{\Theta_o^2 b^2}, \quad \Lambda = \frac{\Theta_o}{\left(T_1 - T_o\right)}. \tag{6.31}$$

Bejan number (Be) defines irreversibility because of heat transfer to total irreversibility as:

$$Be = \frac{\left(\frac{\partial\theta}{\partial r}\right)^2}{\left(\frac{\partial\theta}{\partial r}\right)^2 + \frac{\Lambda}{1+\beta\theta}\left(\begin{array}{l} Br\left(\frac{\partial^2\psi}{\partial r^2} - \frac{1}{r+K}\left(\frac{\partial\psi}{\partial r}+1\right)\right)S_{rx} + \frac{BrK^2H^2\,\mathrm{Sin}^2\,\vartheta_0}{\left(r+K\right)^2}\left(\frac{\partial\psi}{\partial r}+1\right)^2 \\ +Q\theta + R_d\left(\frac{1}{r+K}\frac{\partial\theta}{\partial r} + \frac{\partial^2\theta}{\partial r^2}\right) \end{array}\right)}. \tag{6.32}$$

Here $0 \le Be \le 1$.

6.2 Methodology

As the problem under consideration is a non-linear system of differential equations; therefore, it is difficult to evaluate the exact solution of these equations. We calculate pressure gradient in Eqn. (6.20), and momentum in Eqn. (6.23)) by regular perturbation method for small parameter (β_3) of third grade material and energy Eqn. (6.22) is solved numerically. We define

$$\left.\begin{aligned} \frac{dp}{dx} &= \frac{dp_0}{dx} + \beta_3 \frac{dp_1}{dx} + O(\beta_3)^2, \\ \psi &= \psi_0 + \beta_3 \psi_1 + O(\beta_3)^2, \\ F &= F_0 + \beta_3 F_1 + O(\beta_3)^2, \\ S_{xr} &= S_{0xr} + \beta_3 S_{1xr} + O(\beta_3)^2. \end{aligned}\right\} \tag{6.33}$$

Putting (6.33) into Eqns. (6.20), (6.23), (6.24), (6.26) and (6.28) reduces the problem to the following zeroth and first order systems:

6.2.1 System at Zeroth Order

$$\frac{\partial}{\partial r}\left(\frac{1}{(r+K)}\frac{\partial}{\partial r}\left(S_{0xr}(r+K)^2\right) - \frac{K^2H^2\,\mathrm{Sin}^2\,\vartheta_0}{r+K}\left(\frac{\partial \psi_0}{\partial r}+1\right)\right) = 0, \tag{6.34}$$

$$\frac{dp_0}{dx} = \frac{1}{(r+K)K}\frac{\partial}{\partial r}\left(S_{0xr}(r+K)^2\right) - \frac{KH^2\,\mathrm{Sin}^2\,\vartheta_0}{r+K}\left(\frac{\partial \psi_0}{\partial r}+1\right), \tag{6.35}$$

in which

$$S_{0xr} = \left(\frac{\partial^2 \psi_0}{\partial r^2} - \frac{1}{(r+K)}\left(\frac{\partial \psi_0}{\partial r}+1\right)\right), \tag{6.36}$$

with boundary conditions

$$\psi_0 = \pm\frac{F_o}{2}, \quad \frac{\partial \psi_0}{\partial r} = -1, \quad \text{at} \quad r = \pm\chi. \tag{6.37}$$

6.2.2 First Order System

$$\frac{\partial}{\partial r}\left(\frac{1}{(r+K)}\frac{\partial}{\partial r}\left(S_{1xr}(r+K)^2\right) - \frac{K^2H^2\,\mathrm{Sin}^2\,\vartheta_0}{r+K}\left(\frac{\partial \psi_1}{\partial r}\right)\right) = 0, \tag{6.38}$$

$$\frac{dp_1}{dx} = \frac{1}{(r+K)K}\frac{\partial}{\partial r}\left(S_{1xr}(r+K)^2\right) - \frac{KH^2\,\mathrm{Sin}^2\,\vartheta_0}{r+K}\left(\frac{\partial \psi_1}{\partial r}\right), \tag{6.39}$$

$$S_{1xr}=\left(\frac{\partial^2\psi_1}{\partial r^2}-\frac{1}{(r+K)}\frac{\partial\psi_1}{\partial r}\right)+2\left(\frac{\partial^2\psi_0}{\partial r^2}-\frac{1}{(r+K)}\left(1+\frac{\partial\psi_0}{\partial r}\right)\right)^3, \tag{6.40}$$

with boundary conditions

$$\psi_1=\pm\frac{F_1}{2},\quad \frac{\partial\psi_1}{\partial r}=0,\quad \text{at}\quad r=\pm h. \tag{6.41}$$

6.3 Analysis

Effects of pertinent parameters i.e. Br, ϑ_0, β, Q, R_d, K, β_1, β_2, β_3 and H on temperature, total entropy, Bejan number, velocity, stream lines and pressure gradient are discussed and analyzed in this section.

6.3.1 Velocity

Axial velocity offers significant features of material flow response. Figs. (6.1-6.4) render the influence of velocity profile (w_2) within a curved channel subject to no-slip boundaries. It is noticed that parabolic trajectory is formed by velocity for pertinent parameters. However, velocity is not symmetric about central line $(r=0)$ due to curved channel. Fig. (6.1) portrays that velocity exhibits dual behavior for increasing values of material parameter (β_3). Velocity decays in the neighborhood of walls of the channel whereas it amplifies at centre of the channel. Fig. (6.2) represents the effect of K on w_2. For this parameter, the velocity also depicts dual behavior as in lower half it decays; whereas, it enhances in other half of the channel. Clearly, velocity is symmetric about $(r=0)$ for straight channel. Fig. (6.3) portrays that w_2 decreases near centre and increases near upper wall for higher value of Hartman number (H). As H corresponds to magnetic

force that is resistive force in nature; therefore, velocity drops off near the centre; however, it enhances in the vicinity of the upper channel due to curved configuration. In Fig. (6.4) inclination (ϑ_0) shows strength of magnetic force on velocity. It is evident from figure that magnetic force opposes fluid flow with more strength when it is perpendicular to flow direction $(\text{i.e. } \vartheta_0 = 90^o)$ and shows less resistance to flow when it is in the direction of the flow $(\text{i.e. when } \vartheta_0 \to 0^o)$.

6.3.2 Pressure Gradient

The impact of curvature, inclination of magnetic field and third grade material parameter on $\frac{dp}{dx}$ is revealed through Figs. (6.5-6.7). Fig. (6.5) depicts the effect of increasing K on pressure gradient. It is noted that $\frac{dp}{dx}$ increases at both the wider and narrower parts. Fig. (6.6) shows the response of pressure gradient for ϑ_0. $\frac{dp}{dx}$ rises by increasing ϑ_0. The highest pressure gradient is observed at $x = 0.75$. It indicates that flow can easily pass through centre of the channel. Fig. (6.7) illustrates that $\frac{dp}{dx}$ decreases at wider part of the channel for increasing β_3 whereas negligible change is seen at the narrow region.

6.3.3 Temperature

Figs. (6.8-6.14) have been prepared to show the impact of Brinkman number, inclination, radiation parameter, heat absorption parameter and Biot numbers on temperature profile (θ). Fig. (6.8) portrays effect of Brinkman number on θ. It is seen that θ increases with

the increase of Br. Reason to this increase is that frictional force enhances as fluid particles collide with each other and resultantly the kinetic energy increases. Conversion of kinetic energy into thermal energy takes place, because of which total temperature of the fluid rises. Fig. (6.9) depicts that by rising inclination of magnetic strength (ϑ_0) from 0^o to 90^o temperature increases and it becomes maximum when magnetic force acts in transverse direction of the fluid i.e. for $\vartheta_0 = 90^o$. In fact, the lines of magnetic field interact electrically with the liquid and generate Lorentz force. This force resists flow of the fluid thus converting kinetic energy into thermal energy. Resultantly, the temperature rises. Fig. (6.10) portrays the response of temperature for heat absorption coefficient (Q). Heat is absorbed for $Q > 0$ and emitted for $Q < 0$. Thus rise in temperature for $Q > 0$ is quite prominent. In Fig. (6.11) temperature reduces by rising the radiation parameter (R_d). The reason is that as R_d has inverse relation with heat absorption coefficient thus by increasing R_d, heat is radiated away and as a result temperature decreases. Impact of Biot numbers on temperature is depicted through Figs. (6.12) and (6.13). By increasing β_1, temperature decreases more rapidly near the lower wall as compared to the upper wall. Similarly, temperature drops down near the upper wall quickly in contrast with the lower wall by enhancing β_2. Fig. (6.14) clarifies the influence of thermal conductivity coefficient (β) on θ. It is seen that temperature lessens for higher value of β.

6.3.4 Entropy production and Bejan number

Entropy generation (Ns) and Bejan number (Be) are portrayed via Figs. (6.15-6.24) to illustrate the effect of thermal conductivity coefficient, Brinkman number, inclination of magnetic field, heat absorption parameter and non-linear thermal radiation parameter. Fig. (6.15) shows that entropy (Ns) decreases for β. In Fig. (6.16), Ns increases by enhancing Brinkman number $(Br\Lambda)$. As Brinkman number is conduction of heat due to viscous dissipation thus temperature enhances for this factor. Fig. (6.17) illustrates that entropy rises by increasing the angle of inclination (ϑ_0). By increasing θ_0, strength of magnetic field increases. Joule heating generates more heat resultantly entropy generation goes up. Figs. (6.18) and (6.19) show opposite behavior of entropy for Q and R_d. Entropy increases for heat absorption coefficient; however, it decreases for radiation parameter. It is also noticed that value of entropy is more near lower channel as compared to the upper channel wall. This is due to temperature gradient $(\text{as } (T_1 > T_0))$. It is also observed that change in entropy is less in the centre in contrast to the channel boundaries. Figs. (6.20-6.24) show the irreversibility caused by heat transfer (i.e. Bejan number) for various parameters. For higher β and R_d irreversibility due to heat diffusion is decreased; however, it increases for $Br\Lambda$, ϑ_0 and Q.

6.3.5 Trapping

Stream lines are presented to show the flow pattern of the material against parameters of interest. Trapping phenomenon for third grade material parameter (β_3), curvature

parameter (K) and inclination (θ_0) is expressed by plotting stream lines through Figs. (6.25-6.27). Figs. (6.25a-6.25c) show that bolus size increases in upper and lower half of the channel when β_3 is increased. Figs. (6.26a-6.26c) describe the influence of K on streamlines. It is noticed that by rising K, in upper half of the channel, bolus size reduces and moves in upward direction while in the lower half, bolus size increases and number of closed stream lines also increases. Figs. (6.27a-6.27c) portray increase in bolus size in lower half of the channel $\left(\text{for } 0^o \leq \vartheta_0 \leq 90^o\right)$.

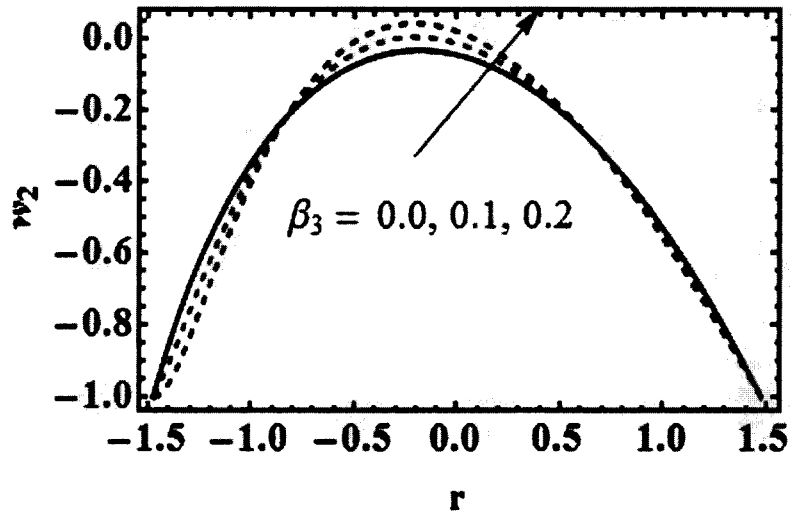

Fig. (6.1): w_2 for fluid parameter with $x = 0.3, a_1 = 0.5, K = 3,\ H = 1,\ \beta$=0.05, $\vartheta_0 = \frac{\pi}{4}$.

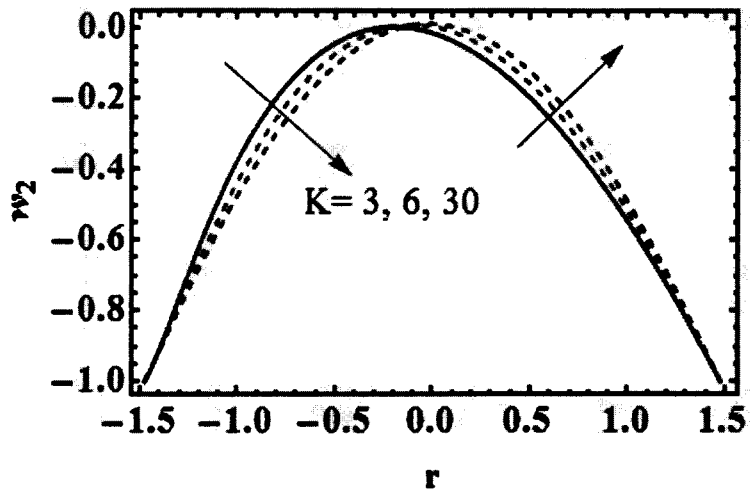

Fig. (6.2): w_2 for curvature parameter with $x = 0.3, a_1 = 0.5, H = 1,\ \beta$=0.05, $\beta_3 = 0.1, \vartheta_0 = \frac{\pi}{4}$.

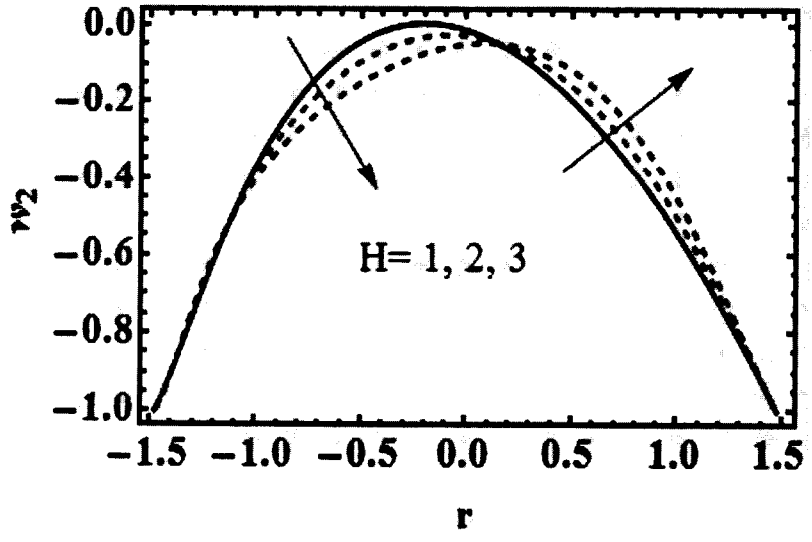

Fig. (6.3): w_2 for Hartman number with $x = 0.3, a_1 = 0.5, K = 3,\ \beta_3 = 0.1, \vartheta_0 = \frac{\pi}{4}$.

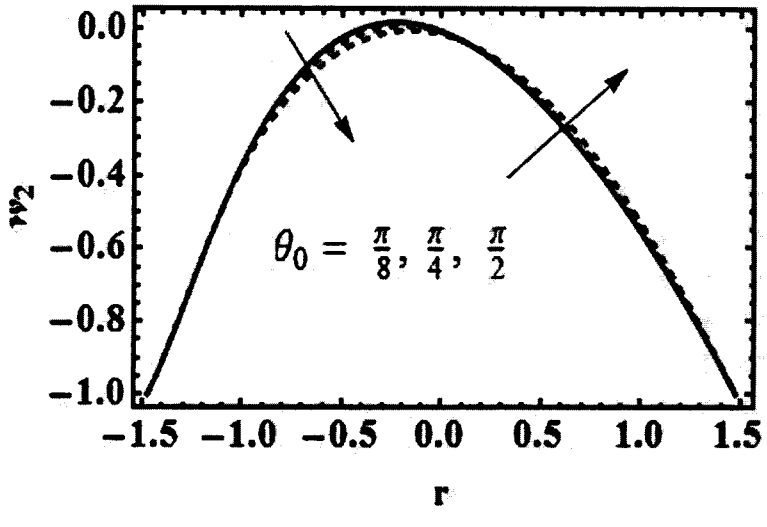

Fig. (6.4): w_2 for inclination of magnetic field with $x = 0.3, a_1 = 0.5, K = 3,\ H = 1, \beta_3 = 0.1$.

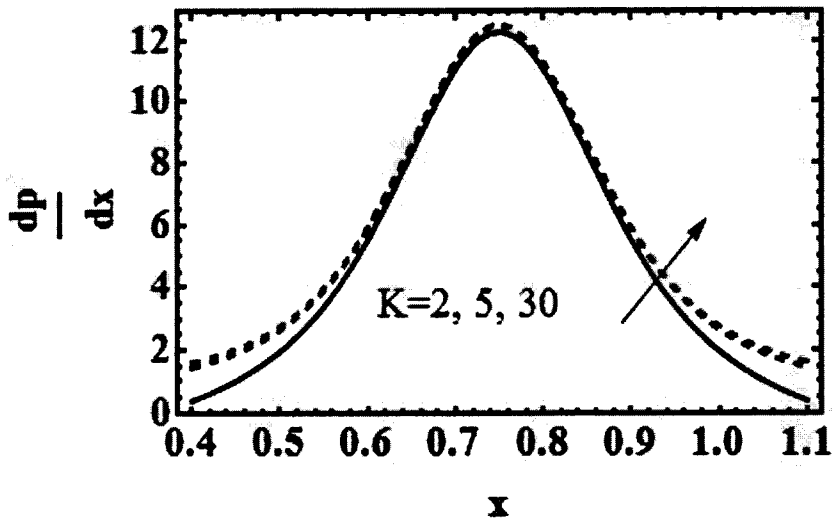

Fig. (6.5): $\frac{dp}{dx}$ for curvature parameter with $x = 0.3, a_1 = 0.5, H = 5, \beta_3 = 0.1, \vartheta_0 = \frac{\pi}{4}$.

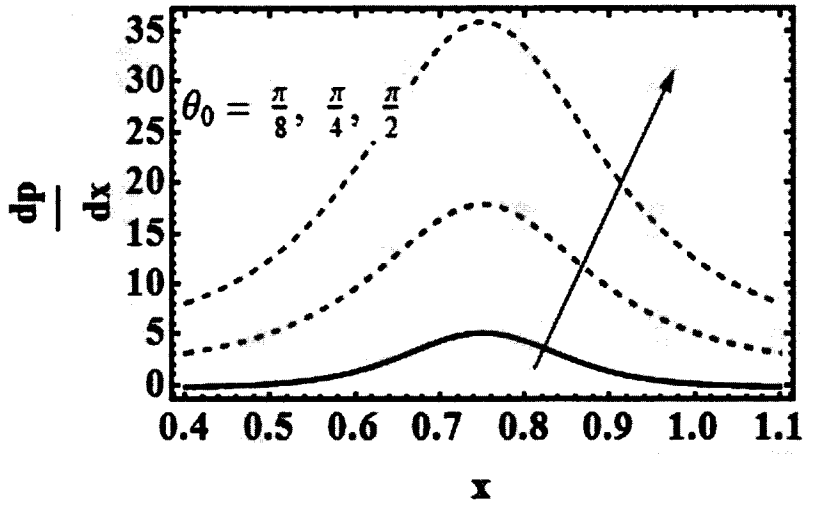

Fig. (6.6): $\frac{dp}{dx}$ for inclination of magnetic field with $x = 0.3, a_1 = 0.5, K = 3, H = 5, \beta_3 = 0.1$.

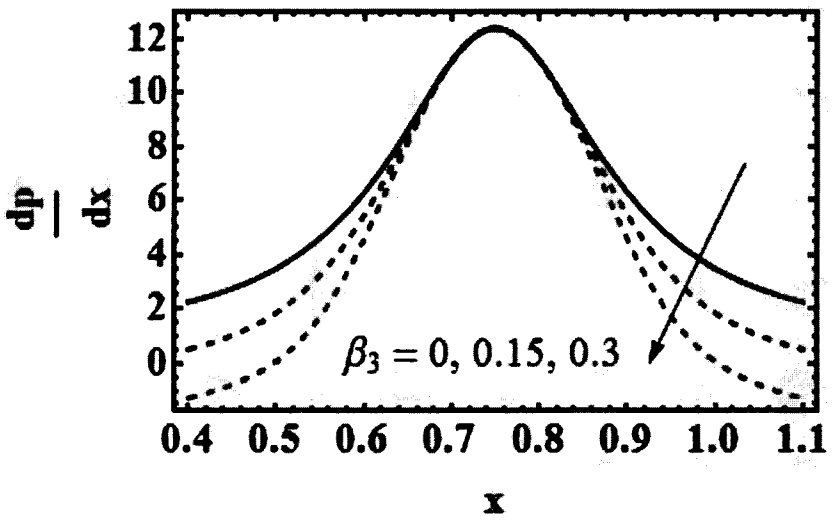

Fig. (6.7): $\frac{dp}{dx}$ for fluid parameter with $x = 0.3, a_1 = 0.5, K = 3,\ H = 5,\ \vartheta_0 = \frac{\pi}{4}$.

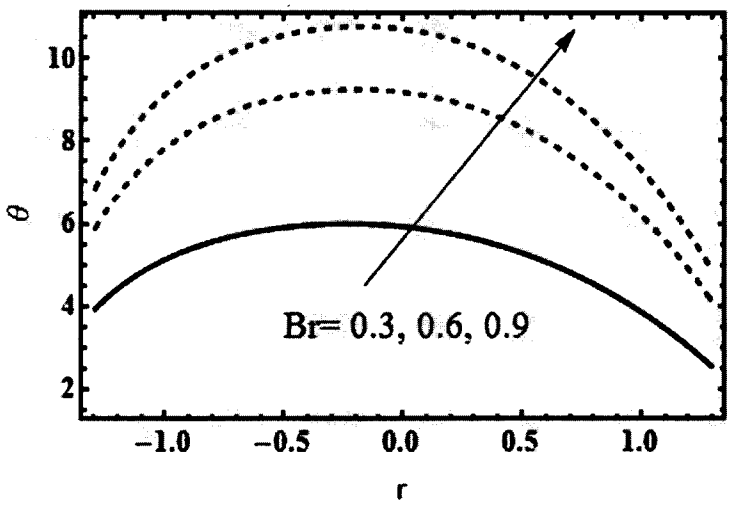

Fig. (6.8): Temperature for Brinkmann number with $x = 0.1, a_1 = 0.5, K = 3,\ H = 1,$ $\beta = \beta_3 = 0.1, \vartheta_0 = \frac{\pi}{4}, R_d = 0.2, \beta_1 = \beta_2 = 2, \Pr = Q = 0.5.$

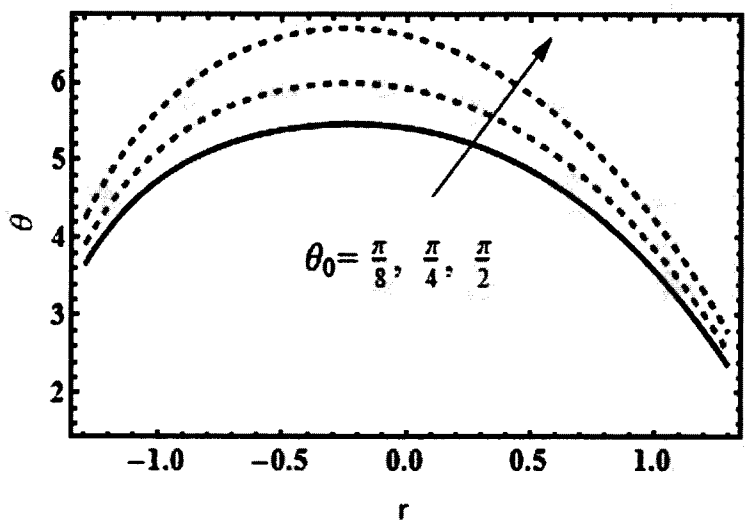

Fig. (6.9): Temperature for inclination of magnetic field with $x = 0.1, a_1 = 0.5, K = 3,$ $H = 1, \beta = \beta_3 = 0.1, R_d = 0.2, \beta_1 = \beta_2 = 2, \Pr = Q = 0.5.$

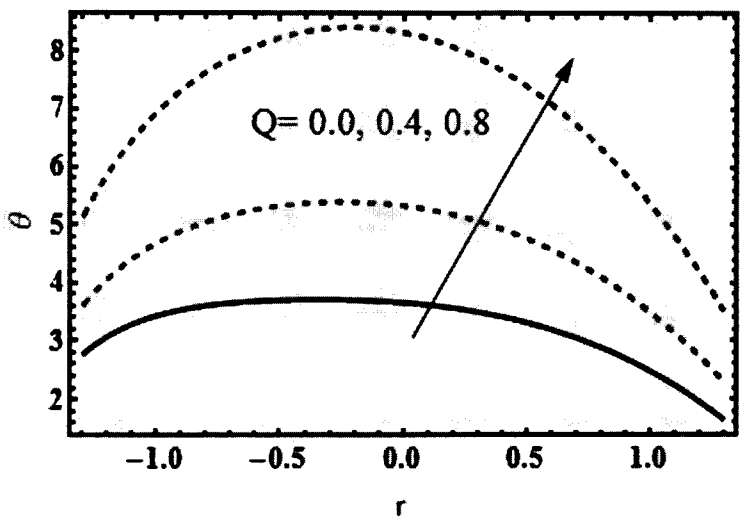

Fig. (6.10): Temperature for heat absorbtin parameter with $x = 0.1, a_1 = 0.5, K = 3,$ $H = 1, \beta = \beta_3 = 0.1, \vartheta_0 = \frac{\pi}{4}, R_d = 0.2, \beta_1 = \beta_2 = 2, Pr = Br = 0.3.$

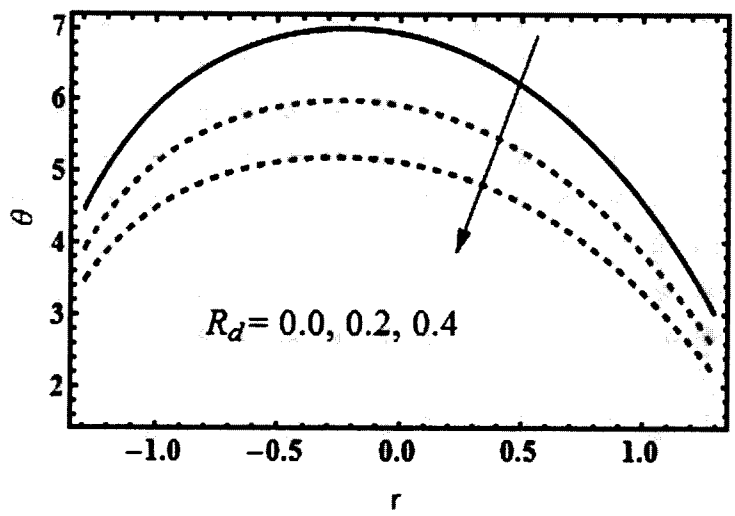

Fig. (6.11): Temperature for thermal radiation with $x = 0.1, a_1 = 0.5, K = 3,\ H = 1,$ $\beta=\beta_3 = 0.1, \vartheta_0 = \frac{\pi}{4}, \beta_1 = \beta_2 = 2, Q = Pr = Br = 0.3.$

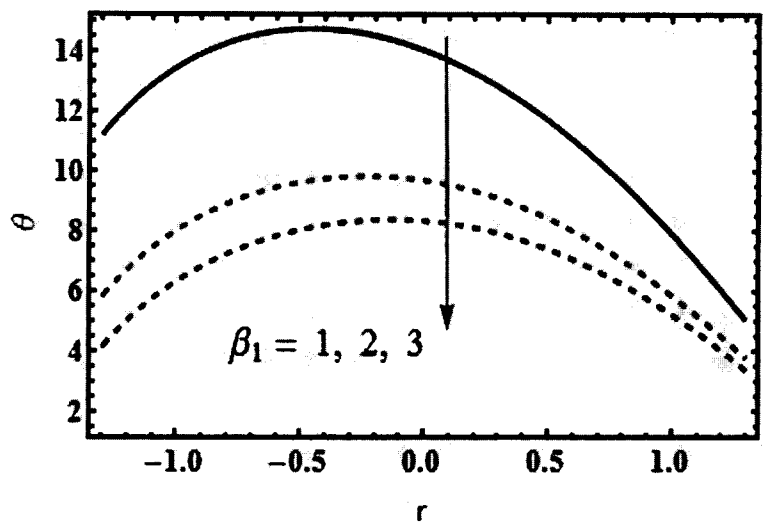

Fig. (6.12): Temperature for Biot number with $x = 0.1, a_1 = 0.5, K = 3,\ H = 1, \beta=0,$ $\beta_3 = 0.1, \vartheta_0 = \frac{\pi}{4}, R_d = 0.2, \beta_2 = 2, Q = 0.5, Pr = 1, Br = 0.3.$

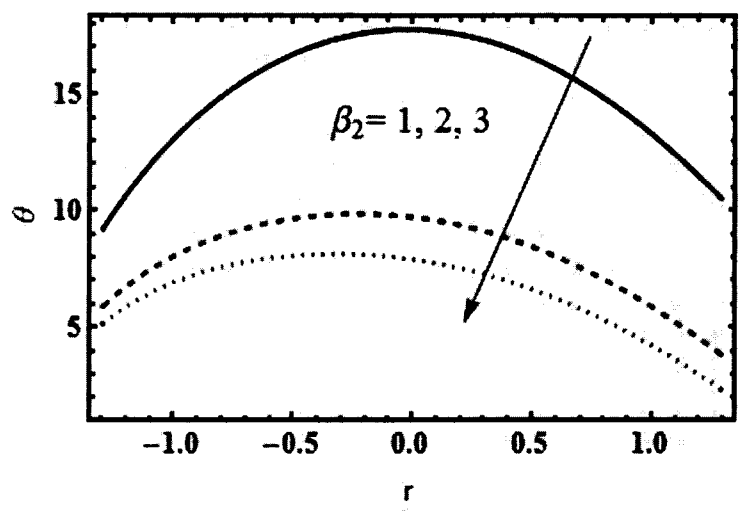

Fig. (6.13): Temperature for Biot number with $x = 0.1, a_1 = 0.5, K = 3,\ H = 1,\ \beta$=0,$\beta_3 = 0.1,$ $\vartheta_0 = \frac{\pi}{4}, R_d = 0.2, \beta_1 = 2, Q = 0.5, Pr = 1, Br = 0.3.$

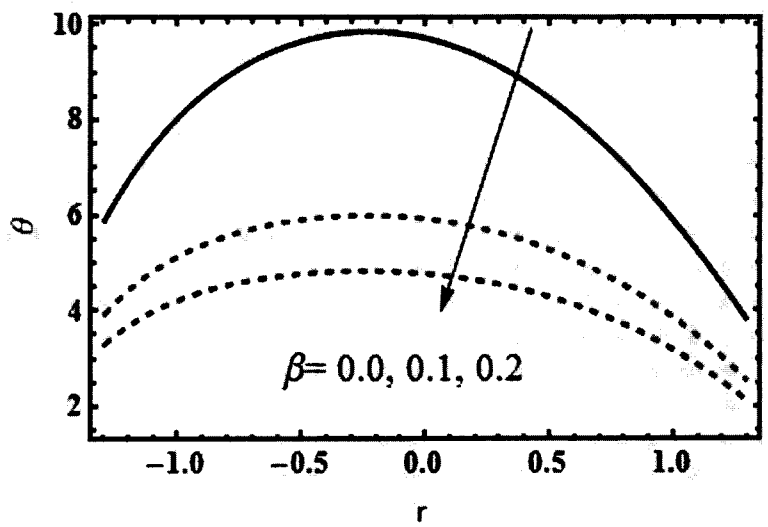

Fig. (6.14): Temperature for thermal conductivty parameter with $x = 0.1, a_1 = 0.5, K = 3,$ $H = 1, \beta_3 = 0.1, \vartheta_0 = \frac{\pi}{4}, R_d = 0.2, \beta_1 = \beta_2 = 2, Q = 0.5, Pr = 1, Br = 0.3.$

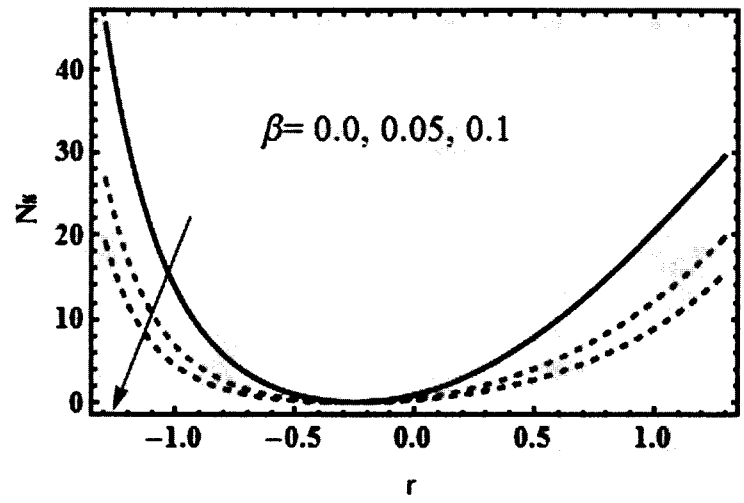

Fig. (6.15): *Ns* for thermal conductivity parameter with $x = 0.1, a_1 = 0.5, K = 3,\ H = 1,$ $\Lambda = 0.01, \beta_3 = 0.1, \vartheta_0 = \frac{\pi}{4}, R_d = 0.2, \beta_1 = \beta_2 = 2, Q = Pr = 0.5, Br = 0.3.$

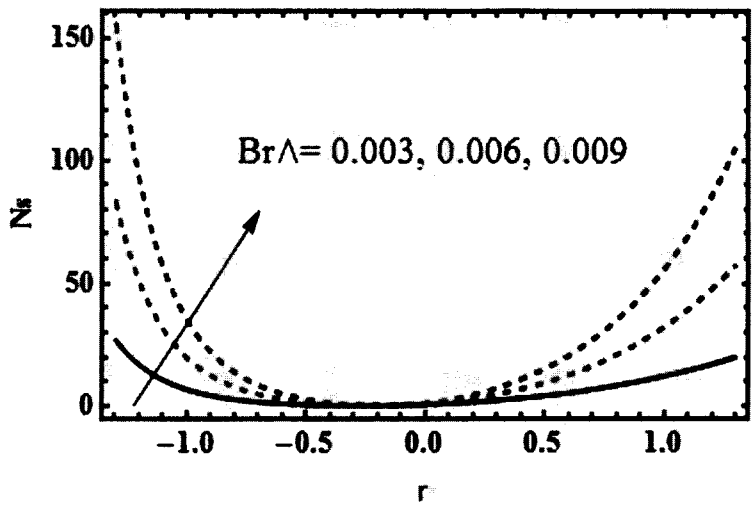

Fig. (6.16): *Ns* for Brinkmann number with $x = 0.1, a_1 = 0.5, K = 3,\ H = 1,$ β=0.05,$\Lambda = 0.01, \beta_3 = 0.1, \vartheta_0 = \frac{\pi}{4}, R_d = 0.2, \beta_1 = \beta_2 = 2, Q = Pr = 0.5.$

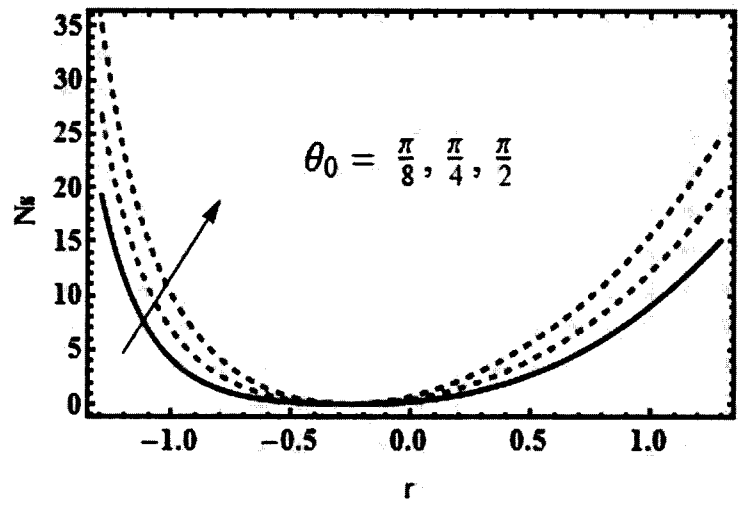

Fig. (6.17): *Ns* for inclination of magnetic field with $x = 0.1, \Lambda = 0.01, a_1 = 0.5, K = 3,$ $H = 1, \beta$=0.05,$\beta_3 = 0.1, R_d = 0.2, \beta_1 = \beta_2 = 2, Q = 0.5, Pr = 0.5, Br = 0.3.$

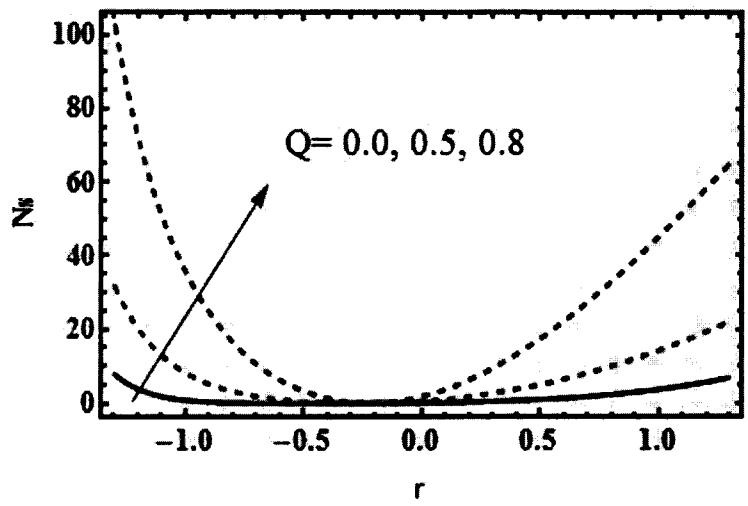

Fig. (6.18): *Ns* for heat absorbtion parameter with $x = 0.1, \Lambda = 0.01, a_1 = 0.5, K = 3, H = 1,$ β=0.05,$\beta_3 = 0.1, \vartheta_0 = \frac{\pi}{4}, R_d = 0.2, \beta_1 = \beta_2 = 2, Pr = 0.5, Br = 0.3.$

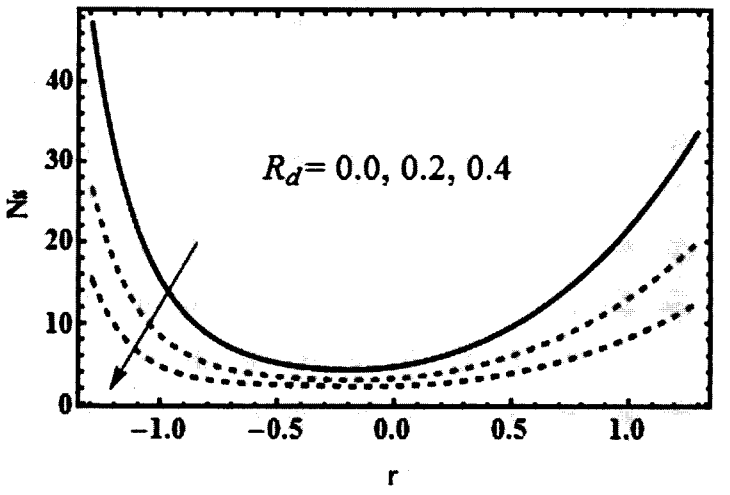

Fig. (6.19): *Ns* for radiation parameter with $x = 0.1, \Lambda = 0.01, a_1 = 0.5, K = 3,\ H = 1,\ \beta$=0.05, $\beta_3 = 0.1, \vartheta_0 = \frac{\pi}{4}, \beta_1 = \beta_2 = 2, Q = 0.5, Pr = 0.5, Br = 0.3.$

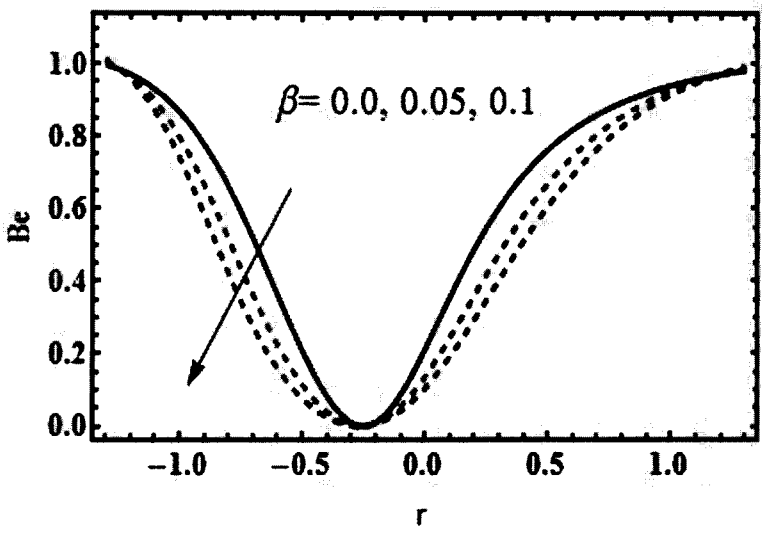

Fig. (6.20): *Be* for thermal conductivity parameter with $x = 0.1, a_1 = 0.5, K = 3,\ H = 1,$ $\Lambda = 0.01, \beta_3 = 0.1, \vartheta_0 = \frac{\pi}{4}, R_d = 0.1, \beta_1 = \beta_2 = 10, Q = 0.1, \mathrm{Pr} = 0.5, Br = 0.3.$

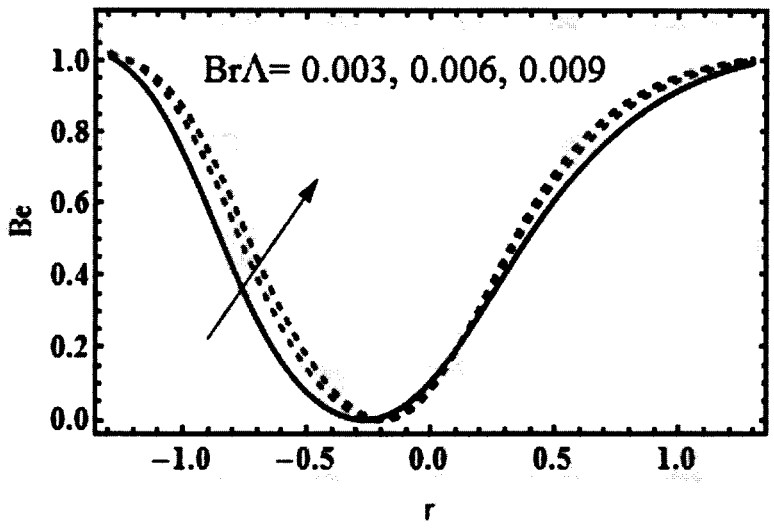

Fig. (6.21): *Be* for Brinkmann number with $x = 0.1, a_1 = 0.5, K = 3,\ H = 1,\ \beta$=0.05, $\Lambda = 0.01, \beta_3 = 0.1, \vartheta_0 = \frac{\pi}{4}, R_d = 0.1, \beta_1 = \beta_2 = 10, Q = 0.1, \Pr = 0.5.$

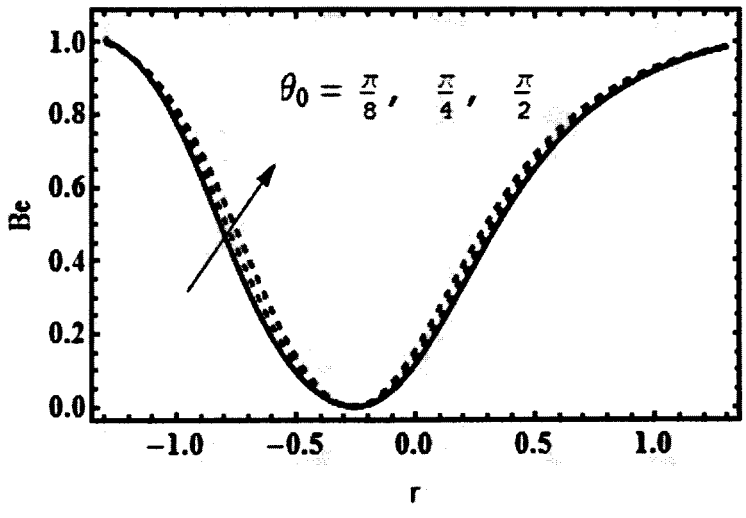

Fig. (6.22): *Be* for inclination of magnetic field with $x = 0.1, \Lambda = 0.01, a_1 = 0.5, K = 3,$ $H = 1,\ \beta$=0.05, $\beta_3 = 0.1, R_d = 0.2, \beta_1 = \beta_2 = 2, Q = 3, Pr = 0.1, Br = 0.3.$

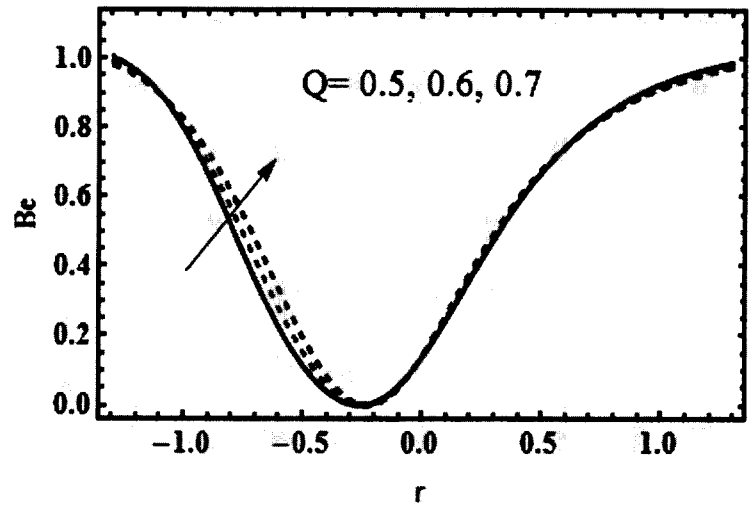

Fig. (6.23): *Be* for heat absorbtion parameter with $x = 0.1, \Lambda = 0.01, a_1 = 0.5, K = 3,$ $H = 1, \beta$=0.05,$\beta_3 = 0.1, \vartheta_0 = \frac{\pi}{4}, R_d = 0.2, \beta_1 = \beta_2 = 2, Pr = 0.1, Br = 0.3.$

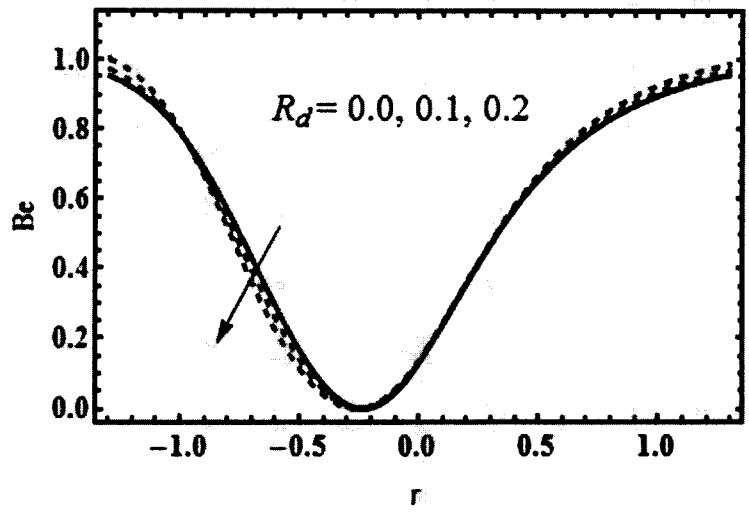

Fig. (6.24): Impact of radiation parameter on *Be* with $x = 0.1, \Lambda = 0.01, a_1 = 0.5, K = 3,\ H = 1,$ β=0.05,$\beta_3 = 0.1, \vartheta_0 = \frac{\pi}{4}, \beta_1 = \beta_2 = 2, Q = 0.5, Pr = 0.5, Br = 0.3.$

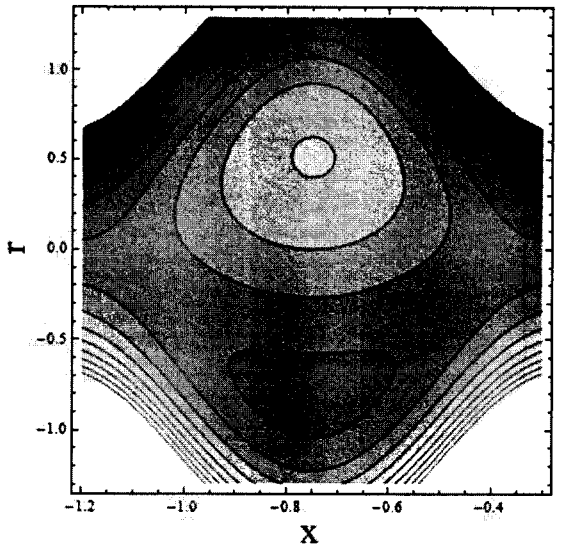

(a) $\beta_3 = 0.0$

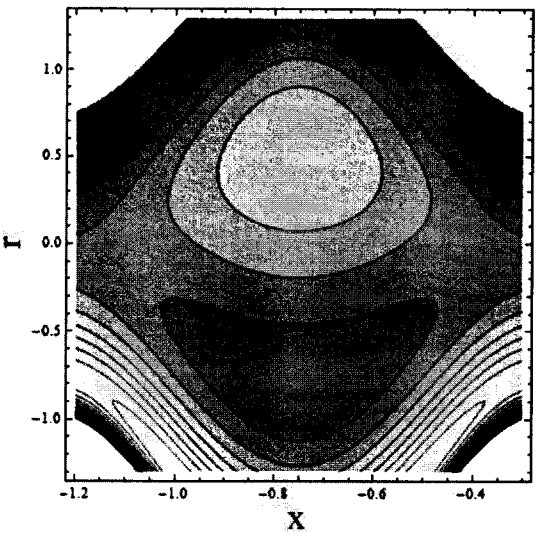

(b) $\beta_3 = 0.05$

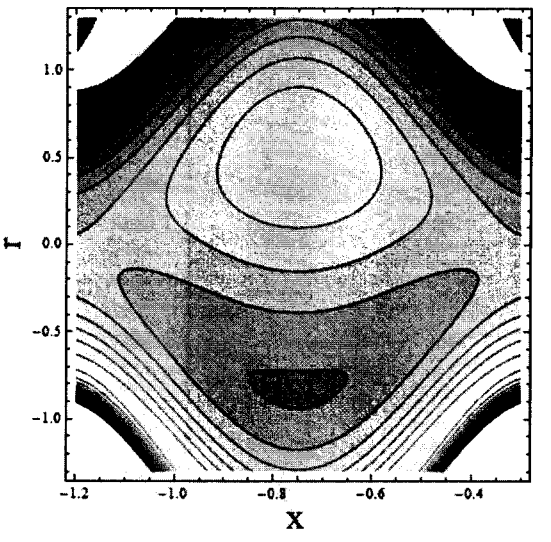

(c) $\beta_3 = 0.1$

Figs. (6.25a-6.25c): Streamlines for fluid parameter

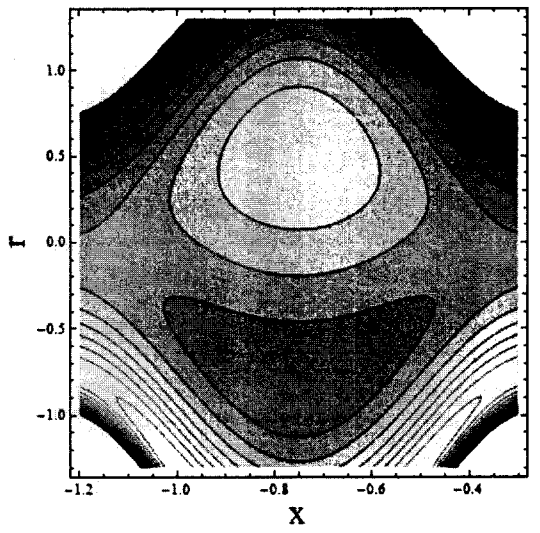

(a) $K = 3$

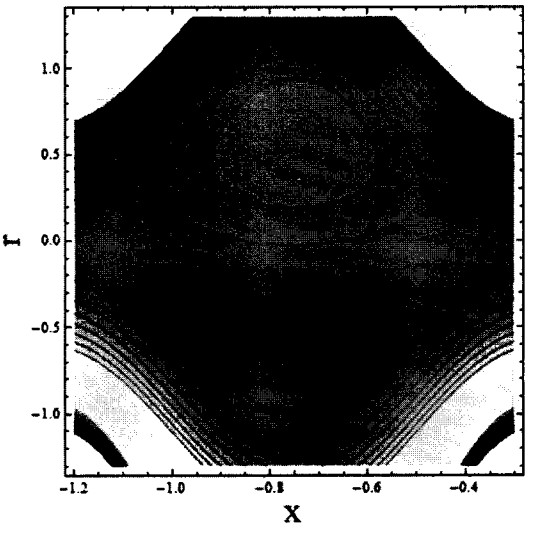

(b) $K = 6$

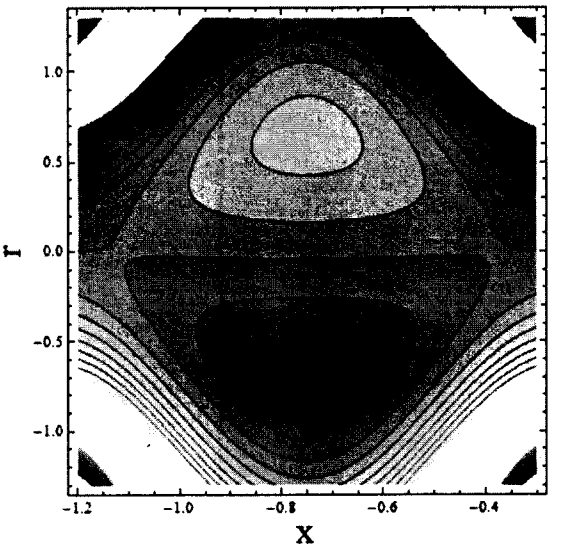

(c) $K = 30$

Figs. (6.26a-6.26c): Streamlines for curvature parameter

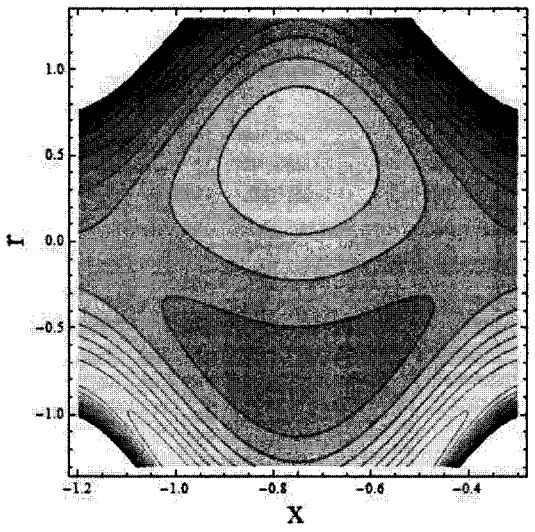

(a) $\theta_0 = \frac{\pi}{6}$

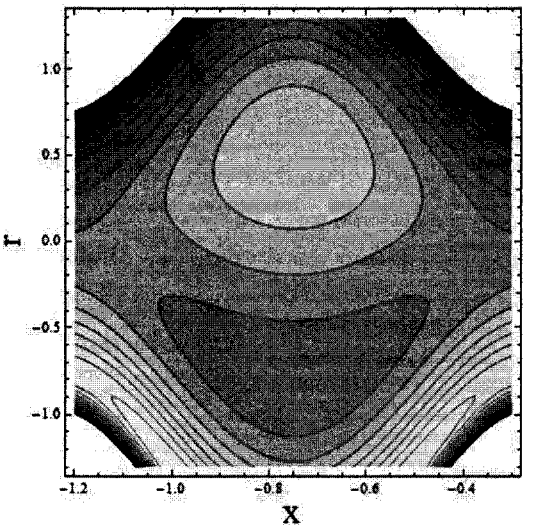

(b) $\theta_0 = \frac{\pi}{4}$

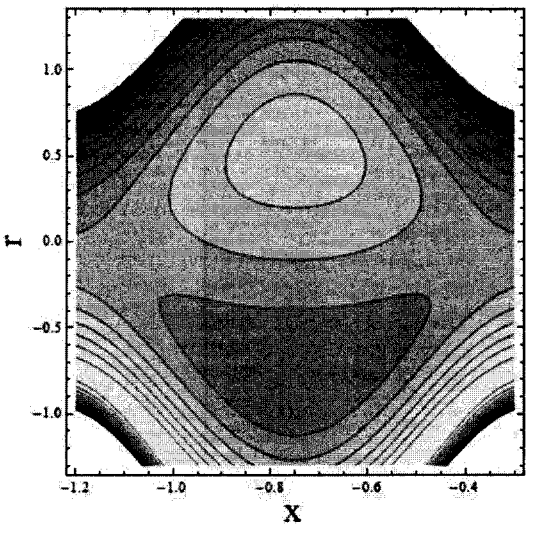

(c) $\theta_0 = \frac{\pi}{2}$

Figs. (6.27a-6.27c): Streamlines for inclination of magnetic field

6.4 Conclusion

This chapter discusses entropy production in peristaltic motion of third grade fluid with non-linear thermal radiation, magnetic field, variable thermal conductivity and heat source/ sink. The key points are listed below.

- Trend of the entropy generation is parabolic.
- Entropy generation is non-zero at the centre line $(r=0)$ and higher at lower wall in comparison with the upper wall due to temperature difference at both the boundaries.
- Temperature and Entropy boost up for the inclination and heat absorption parameters while these reduce for radiation and thermal conductivity parameters.
- Irreversibility caused by heat transfer is greater for inclination and Brinkman number.
- Velocity enhances at the centre of channel for larger material parameter whereas it decreases for Hartman number.

Chapter 7

Entropy Generation Analysis in Peristalsis of Sisko Fluid Subject to Variable Viscosity and Thermal Conductivity

Peristaltic flow of Sisko material with variable thermal conductivity and viscosity in curved configuration is analyzed. Entropy is also under consideration here to study the irregularities in heat transfer process. Problem is solved numerically. These solutions are utilized to plot the behaviors of quantities of interest against the pertinent parameters.

7.1 Mathematical Formulation

Here our aim is to inspect the entropy generation in peristalsis of Sisko material in a curved channel of width $2a$ coiled in circle with centre O and radius $R^{'}$. Components W_1 and W_2 of velocity are along radial (R) and axial (X) directions respectively. Both viscosity and thermal conductivity of Sisko material are taken as a function of space variable and temperature respectively. Fluid flow in the channel is due to propagation of waves with speed s, amplitude b and wavelength λ. Modeled problem is subjected to the no-slip boundary conditions. Transfer of heat is due to different wall temperatures T_0 and T_1 (such

that $T_0 > T_1$) and T_0 and T_1 are the temperature at upper and lower walls respectively.

Mathematical form of the wall geometry is

$$R = \pm\chi(X,t) = \pm\left[a + b\sin\left(\frac{2\pi}{\lambda}(X - st)\right)\right], \tag{7.1}$$

Flow expressions with considered assumptions are as follows:

$$R'\frac{\partial W_2}{\partial X} + \frac{\partial}{\partial R}\left((R' + R)W_1\right) = 0, \tag{7.2}$$

$$\rho\left(\frac{dW_2}{dt} + \frac{W_1 W_2}{R' + R}\right) = -\frac{\overline{R}}{(R' + R)}\frac{\partial P}{\partial X} + \frac{1}{(R' + R)^2}\frac{\partial}{\partial R}\left\{(R' + R)^2 S_{XR}\right\} + \frac{\overline{R}}{(R' + R)}\frac{\partial S_{XX}}{\partial X}, \tag{7.3}$$

$$\rho\left(\frac{dW_1}{dt} - \frac{W_2^2}{R' + R}\right) = -\frac{\partial P}{\partial R} + \frac{1}{(R' + R)}\frac{\partial}{\partial R}\left\{(R' + R)S_{RR}\right\} - \frac{S_{XX}}{(R' + R)} + \frac{\overline{R}}{(R' + R)}\frac{\partial S_{XR}}{\partial X}, \tag{7.4}$$

$$\rho C_p \frac{dT}{dt} = -\frac{\partial}{\partial R}\left(-\kappa(T)\frac{\partial T}{\partial R}\right) + \frac{\partial}{\partial X}\left(\frac{\kappa(T)R'^2}{(R' + R)^2}\frac{\partial T}{\partial X}\right) - \frac{\kappa(T)}{(R' + R)}\frac{\partial T}{\partial R} +$$
$$\left(\frac{\partial W_2}{\partial R} - \frac{W_2}{(R' + R)} + \frac{\overline{R}}{(R' + R)}\frac{\partial W_1}{\partial X}\right)S_{RX} + \frac{\partial W_2}{\partial R}(S_{RR} - S_{XX}). \tag{7.5}$$

Here P denotes pressure, ρ fluid density, S_{RR}, S_{XR}, S_{XX} stress components, C_p specific heat, $\kappa(T)$ temperature dependent thermal conductivity and T temperature.

Extra stress tensor $\mathbf{S}$ for Sisko fluid model that can be stated as follows [100]:

$$\mathbf{S} = \left(c + d\left|\frac{1}{2}tr(\mathbf{A})\right|^{n-1}\right)\mathbf{A}, \tag{7.6}$$

in which the first Rivilin-Erickson tensor is

$$\mathbf{A} = \text{grad}\,\mathbf{W} + \text{grad}\,\mathbf{W}', \tag{7.7}$$

Moreover, the parameters c and d represent the material parameters. Here, $n(\geq 0)$ is

power-law index for Sisko fluid model. For $(n<1)$ it shows shear thinning and $(n>1)$ shear thickening. In addition, for $\left(n=1,\ c=0,\ d=\mu \text{ or } c=\mu,\ d=0\right)$ the behavior of viscous liquid is found.

The boundary conditions are

$$W_2 = 0, \quad \text{at} \quad R = \pm\chi, \tag{7.8}$$

$$\left.\begin{aligned} \kappa_o \frac{\partial T}{\partial R} &= -\beta_1' \left(T_1 - T\right) \quad \text{at} \quad R = -\chi, \\ \kappa_o \frac{\partial T}{\partial R} &= -\beta_2' \left(T - T_0\right) \quad \text{at} \quad R = \chi, \end{aligned}\right\} \tag{7.9}$$

in which κ_0 is constant thermal conductivity at ambient temperature and $\left(\beta_1', \beta_2'\right)$ are Biot numbers. Space dependent viscosity is taken as follows:

$$\mu(R) = \mu_o \exp(-\alpha' R) \sqcup \mu_o \left(1 - \alpha' R\right), \tag{7.10}$$

where μ_o represents constant fluid viscosity and α' is variable viscosity coefficient. For $\alpha' = 0$, the present problem reduces to case of constant viscosity. Thermal conductivity is taken as temperature dependent in the form:

$$\kappa(T) = \kappa_o \left[1 + \beta' \left(T - T_0\right)\right], \tag{7.11}$$

in which β' is variable thermal conductivity coefficient. We consider the transformations relating to wave $\left(\bar{x}, \bar{r}\right)$ and laboratory $\left(X, R\right)$ frames as

$$\bar{x} = X - st, \quad \bar{r} = R, \quad \bar{w}_2 = W_2 - s, \quad \bar{w}_1 = W_1. \tag{7.12}$$

We now define dimensionless variables, velocities, pressure, temperature, wave number, peristaltic wall, Reynolds number, viscosity parameter, variable thermal conductivity

parameter, Brinkman number, Prandtl number, curvature, amplitude ratio, thermal Biot parameters and Sisko fluid parameter as

$$(x,r)=\left(\frac{\bar{x}}{\lambda},\frac{\bar{r}}{a}\right),\qquad (w_1,w_2)=\left(\frac{\bar{w}_1}{s},\frac{\bar{w}_2}{s}\right),\qquad p=\frac{a^2P}{s\mu_o\lambda},\qquad \theta=\frac{T-T_o}{T_1-T_o},$$

$$\delta=\frac{a}{\lambda},,\qquad h=\frac{\chi}{a},\qquad \mathrm{Re}=\frac{\rho sa}{\mu_o},\qquad \alpha=\frac{\alpha}{a},\qquad \beta=\beta'(T_1-T_o),$$

$$Br=\frac{\mu_o s^2}{\kappa_o(T_1-T_o)},\qquad \mathrm{Pr}=\frac{\mu_o C_p}{\kappa_o},\qquad k=\frac{R'}{a},\qquad b_1=\frac{b}{a},\qquad (\beta_1,\beta_2)=\left(\frac{a\beta_1'}{\kappa_0},\frac{a\beta_2'}{\kappa_0}\right),$$

$$\gamma^*=\frac{b}{a}\left(\frac{c}{d}\right)^{n-1}.$$

Velocities (w_1,w_2) through stream function (ψ) can be expressed below:

$$w_1=-\frac{k\delta}{r+k}\frac{\partial\psi}{\partial x},\quad w_2=\frac{\partial\psi}{\partial r}. \tag{7.13}$$

Incompressibility conditions is now trivially satisfied while other expressions after long wavelength and low Reynolds number give

$$\frac{k}{r+k}\frac{\partial p}{\partial x}=\frac{1}{(r+k)^2}\frac{\partial}{\partial r}\left((r+k)^2S_{rx}\right), \tag{7.14}$$

$$\frac{\partial p}{\partial r}=0, \tag{7.15}$$

$$\beta\left(\frac{\partial\theta}{\partial r}\right)^2+(1+\beta\theta)\left(\frac{\partial^2\theta}{\partial r^2}+\frac{1}{r+k}\frac{\partial\theta}{\partial r}\right)+Br\left(\frac{\partial^2\psi}{\partial r^2}-\frac{1}{(r+k)}\left(\frac{\partial\psi}{\partial r}+1\right)\right)S_{rx}=0. \tag{7.16}$$

Eqns. (7.14) and (7.15) implies

$$\frac{\partial}{\partial r}\left[\frac{1}{(r+k)}\frac{\partial}{\partial r}\left((r+k)^2S_{rx}\right)\right]=0, \tag{7.17}$$

$$3\frac{\partial S_{rx}}{\partial r}+(r+k)\frac{\partial^2 S_{rx}}{\partial r^2}=0, \tag{7.18}$$

$$S_{rx}=\left(\frac{\partial^2\psi}{\partial r^2}-\frac{1}{(r+k)}\left(\frac{\partial\psi}{\partial r}+1\right)\right)\left[(1-\alpha r)+\gamma^*\left(\frac{\partial^2\psi}{\partial r^2}-\frac{1}{(r+k)}\left(\frac{\partial\psi}{\partial r}+1\right)\right)^{n-1}\right], \tag{7.19}$$

and $p=p(x)$.

Dimensionless boundary conditions are

$$\left.\begin{aligned}&\psi=\pm F/2,\quad \frac{\partial\psi}{\partial r}=-1 \quad \text{at} \quad r=\pm h,\\ &\frac{\partial\theta}{\partial r}-\beta_1(\theta-1)=0, \qquad \text{at} \quad r=-h,\\ &\frac{\partial\theta}{\partial r}+\beta_2\theta=0, \qquad\quad \text{at} \quad r=h,\end{aligned}\right\} \tag{7.20}$$

where

$$F=\int_{-h}^{h}\frac{\partial\psi}{\partial r}dr=\psi(h)-\psi(-h), \tag{7.21}$$

$$h=1+b_1\sin(2\pi x). \tag{7.22}$$

Heat transfer rate in non-dimensional form is

$$Z=\frac{\partial h}{\partial x}\frac{\partial\theta(h)}{\partial r}. \tag{7.23}$$

7.1.1 Entropy

Entropy equation in dimensional form is as follows:

$$S_{gen}=\frac{\kappa(T)}{\Theta_o^2}\left(\frac{dT}{dR}\right)^2+\frac{1}{\Theta_o}\left[\left(\frac{\partial W_2}{\partial R}-\frac{W_2}{(\bar{R}+R)}+\frac{\bar{R}}{(\bar{R}+R)}\frac{\partial W_1}{\partial X}\right)S_{RX}+\frac{\partial W_2}{\partial R}(S_{RR}-S_{XX})\right], \tag{7.24}$$

where Θ_o denotes the reference temperature and second term in Eqn. (7.24) is for viscous

dissipation.

Dimensionless form of entropy generation thus becomes

$$N_s = \frac{S_{gen}}{S_G} = \left(\frac{\partial \theta}{\partial r}\right)^2 + \frac{Br.\Lambda}{1+\beta\theta}\left(\frac{\partial^2 \psi}{\partial r^2} - \frac{1}{r+k}\left(\frac{\partial \psi}{\partial r}+1\right)\right) S_{rx}, \tag{7.25}$$

in which N_s shows Entropy generation parameter, S_G entropy generation characteristic and Λ temperature difference parameter. S_G and Λ are given by

$$S_G = \frac{\kappa(T)\left(T_1 - T_o\right)^2}{\Theta_o^2 a^2}, \quad \Lambda = \frac{\Theta_o}{\left(T_1 - T_o\right)}. \tag{7.26}$$

Eqn. (7.24) represents that entropy generation is a combination of irreversibility processes known as heat transfer irreversibility $\left(S_{gen}\right)_T$ and fluid friction irreversibility $\left(S_{gen}\right)_F$. Mathematically Bejan number Be is written as

$$Be = \frac{\left(S_{gen}\right)_T}{\left(S_{gen}\right)_T + \left(S_{gen}\right)_F}. \tag{7.27}$$

It is clear that $0 \le Be \le 1$. Here $Be = 0$ corresponds to dominance of fluid friction effects while $Be = 1$ shows high irreversibility due to heat transfer. Furthermore, $Be = 1/2$ implies the same contribution for both.

7.2 Methodology

We have non-linear system of differential equations and thus cannot be evaluated exactly. Hence we solve velocity Eqn. (7.14) and heat equation (7.16) subject to its boundary conditions (7.20) is solved numerically by NDSolve command in Mathematica. This command solves differential equation by Shooting method.

7.3 Analysis

This section includes the physical interpretation of axial velocity, pumping characteristics temperature and entropy generation for pertinent quantities.

7.3.1 Velocity

Figs. (7.1-7.3) display α, γ^* and k effects on w_2. It is observed from Fig. (7.1) that space dependent viscosity yields more resistance to fluid flow near lower wall. As a result the amplitude of axial velocity w_2 decreases where flowing fluid has less resistance in the vicinity of upper wall and so axial velocity increases for α. Fig. (7.2) depicts the response of w_2 for increasing γ^*. Here w_2 has opposite outcome near upper and lower boundaries respectively. Fig. (7.3) illustrates curvature k impacts on w_2. This Fig. reveals that symmetry of axial velocity is disturbed due to increasing k.

7.3.2 Temperature

This subsection is devoted to represent temperature θ via r for different sundry parameters α, β, β_1, β_2, γ^* and Br through Figs. (7.4-7.9). From Fig. (7.4) it is seen that for larger viscosity parameter α the temperature decays. Influence of β on θ dominates and θ decreases (see Fig. (7.5)). It is due to the fact that β enlarges the fluid ability to disperse or soak up heat. This happens when wall temperature is less than the fluid temperature. Figs. (7.6-7.7) exhibit effects of Biot numbers β_1, β_2 on θ. Temperature decreased when β_1 and β_2 are increased. Fig. (7.8) illustrates the response of θ for larger fluid parameter γ^*. It is evident through this plot that temperature rises when γ^* enhances.

Fig. (7.9) represents temperature (θ) for Brinkman number (Br). Through this Fig. it is revealed that temperature is maximum for an enhancement in Br. This shows prominent effect of viscosity in Brinkman number which opposes the fluid flow. Due to resistance in flow the collision of fluid particles increases and particles lose their energy and as a result temperature enhances.

7.3.3 Entropy Generation

This subsection is made to interpret the physical behavior of entropy generation and Bejan number for various pertinent considered quantities (i.e. α, β, γ^* and $Br\Lambda$). For this purpose Figs. (7.10-7.17) are presented. Figs. (7.10) and (7.11) are made to see the influences of α and β on Ns respectively. It is clear from these Figs. that Ns decays in the vicinity of channel walls when α and β increase. No doubt entropy (Ns) and temperature have direct relation. Thus these Figs. ensure the decay of temperature. Influence of fluid parameter γ^* can be seen via Fig. (7.12). This plot reveals that an increase in γ^* leads to more entropy. Fig. (7.13) depicts the effect of $Br\Lambda$ on Ns. Physically dimensionless number $Br\Lambda$ explains the viscous effects and has direct proportion to square of velocity. Thus an enhancement in $Br\Lambda$ corresponds to higher entropy. Figs. (7.14) and (7.15) addresses the influences of parameters α and β on Bejan number Be respectively. It is evident that Be has similar behavior for both α and β. Response of Brinkman number $Br\Lambda$ on Be is illustrated through Fig. (7.16). This figure describes that Be increases for higher $Br\Lambda$. Impact of fluid parameter on Bejan number is shown in the Fig. (7.17). Clearly Bejan number enhances for fluid parameter.

7.3.4 Heat Transfer Rate

Bar charts are presented in Figs. (7.18) and (7.19) to illustrate the change in heat transfer rate for pertinent parameters Br and β. Fig. (7.18) shows increase in heat transfer rate as Br enhances. It is due to the dominant characteristic of viscosity in heat equation. Fig. (7.19) gives that heat transfer rate is decreased when variable thermal conductivity parameter increased.

7.3.5 Trapping and Pumping

Trapping phenomenon is found significant in problems regarding peristalsis. It creates in the form a fluid mass called bolus which circulates internally and it is enclosed by streamlines. The propagating peristaltic waves push such type of bolus forward with the same velocity as that of waves. Trapping has importance in fluid transportation via peristalsis. Figs. (7.20-7.22) are made to depict the streamlines nature for various parameters involved in the present analysis. Figs. (7.20a-7.20c) show streamlines behavior for viscosity parameter α. In this figure bolus size decay in the upper half however it expands in the lower half of peristaltic channel for increasing α. Streamlines for γ^* can be depicted through Figs. (7.21a-7.21c). It is found for higher γ^* bolus expands near both wall of channel. Figs. (7.22a-7.22c) show effect of k on streamlines. It is clear from these figures that behavior of bolus is opposite in upper and lower channels. In the upper half bolus contracts while in lower half it expands.

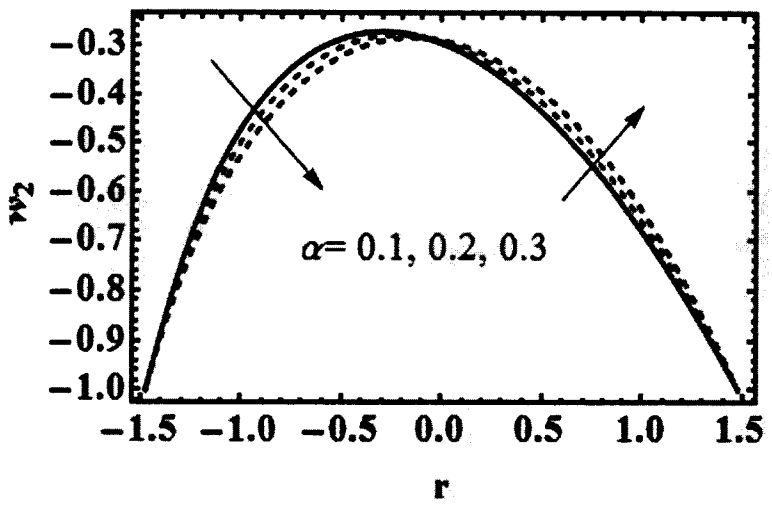

Fig. 7.1: Velocity for viscosity parameter with $x = 0.3, a_1 = 0.5, k = 2, \gamma^* = 0.1$.

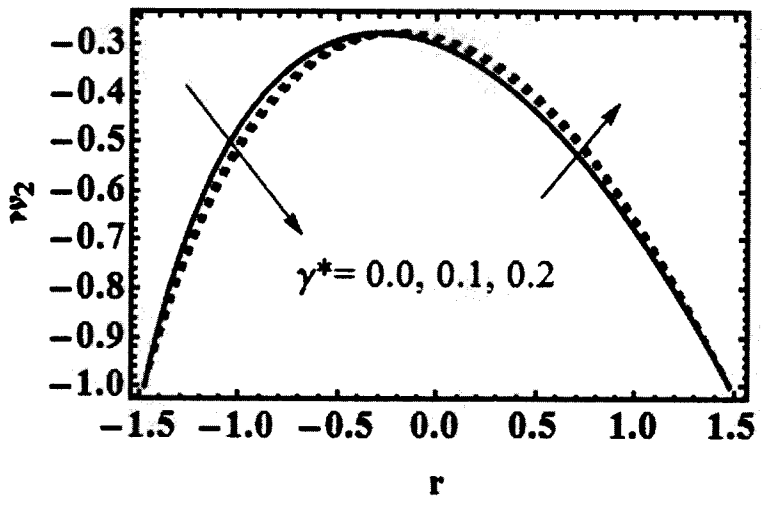

Fig. (7.2): Velocity for Sisko fluid with $x = 0.3, a_1 = 0.5, k = 2, \alpha = 0.1$.

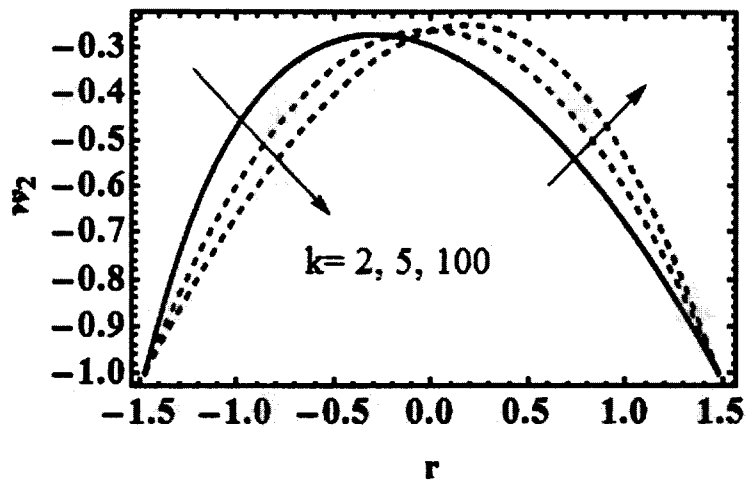

Fig. (7.3): Velocity for curvature parameter with $x = 0.3, a_1 = 0.5, \gamma^* = 0.1, \alpha = 0.1$.

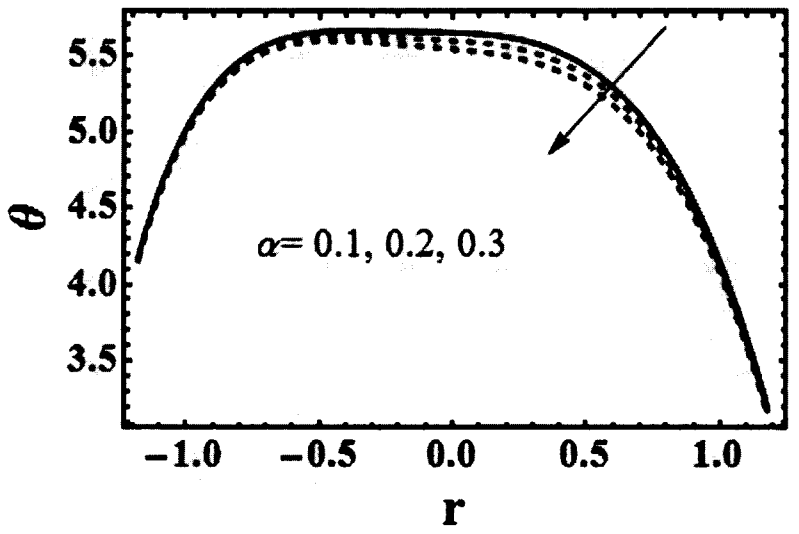

Fig. (7.4): Temperature for viscocity with $a_1 = 0.3, k = 2, \gamma^* = 0.1, Br = 1, \beta = 0.1, \beta_1 = \beta_2 = 2$.

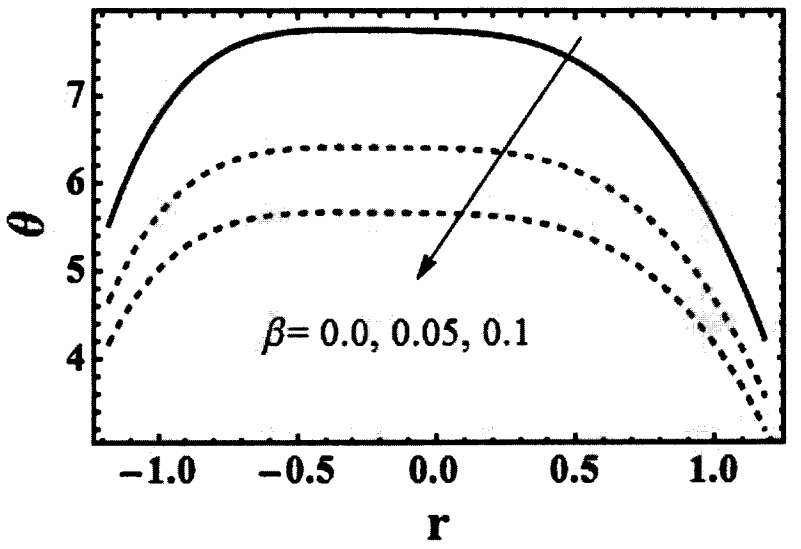

Figs. (7.5): Temperature for thermal conductivity with $a_1 = 0.3, k = 2, \gamma^* = 0.1, Br = 1, \alpha = 0.1, \beta_1 = \beta_2 = 2.$

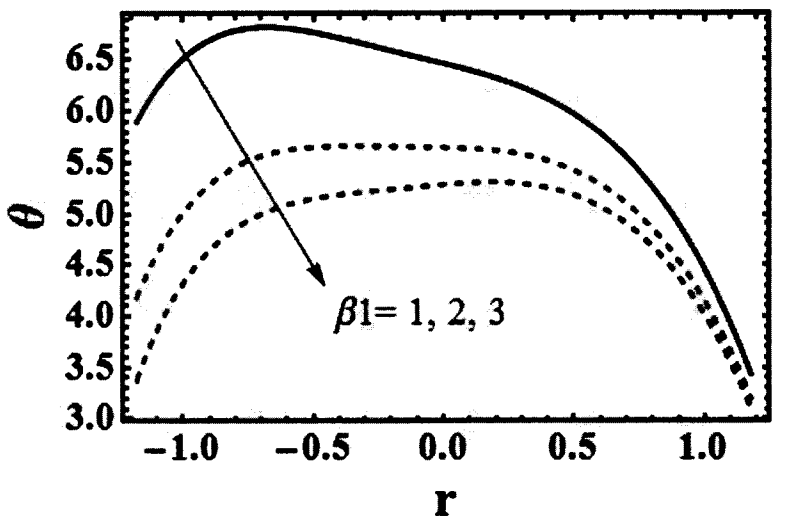

Fig. (7.6): Temperature for fluid parameter with $a_1 = 0.3, k = 2, Br = 1, \alpha = \beta = 0.1, \beta_1 = \beta_2 = 2.$

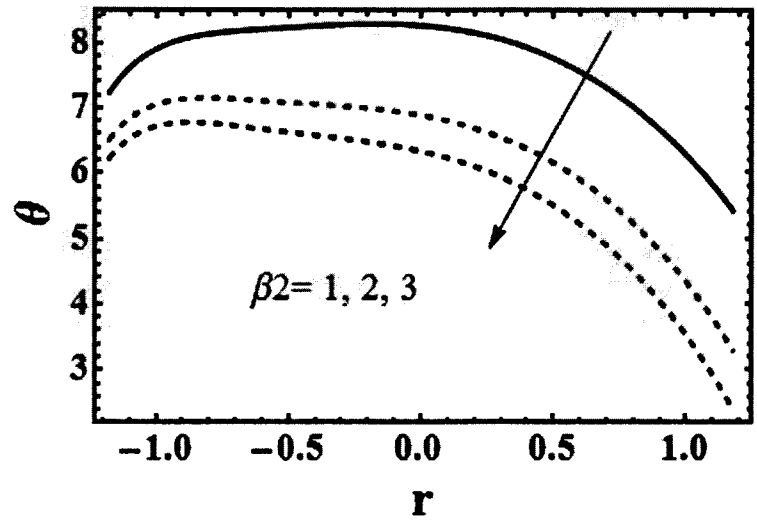

Fig. (7.7): Temperature for Biot coefficent with $a_1 = 0.3, k = 2, \gamma^* = 0.1, Br = 1, \alpha = \beta = 0.1, \beta_2 = 2.$

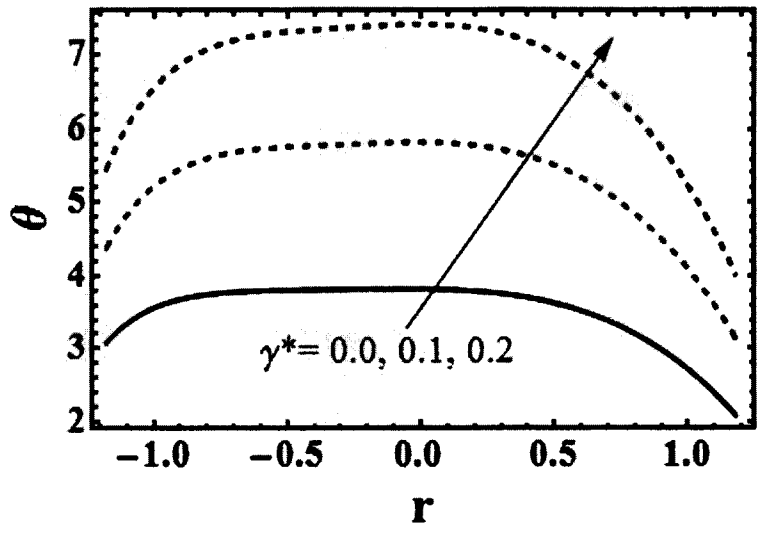

Fig. (7.8): Temperature for Biot coefficent with $a_1 = 0.3, k = 2, \gamma^* = 0.1, Br = 1, \alpha = \beta = 0.1, \beta_1 = 2.$

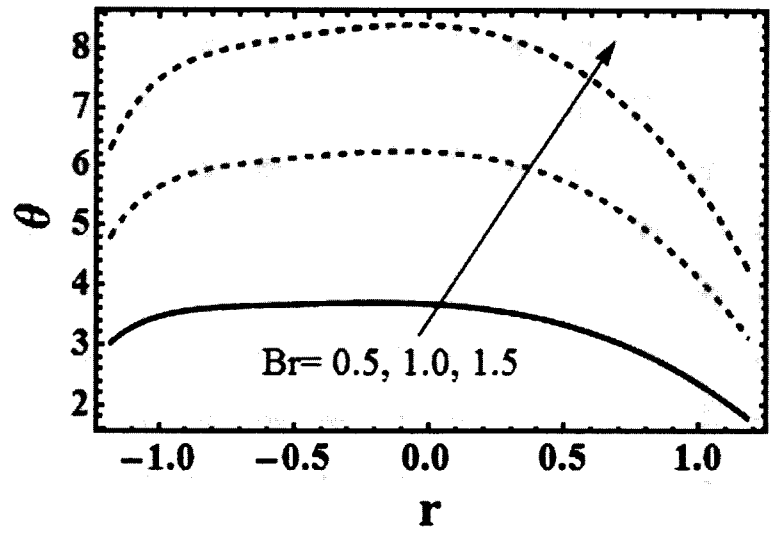

Fig. (7.9): Temperature for Brinkmann number with $a_1 = 0.3, k = 2,\ \gamma^* = 0.1, \alpha = \beta = 0.1, \beta_1 = \beta_2 = 2.$

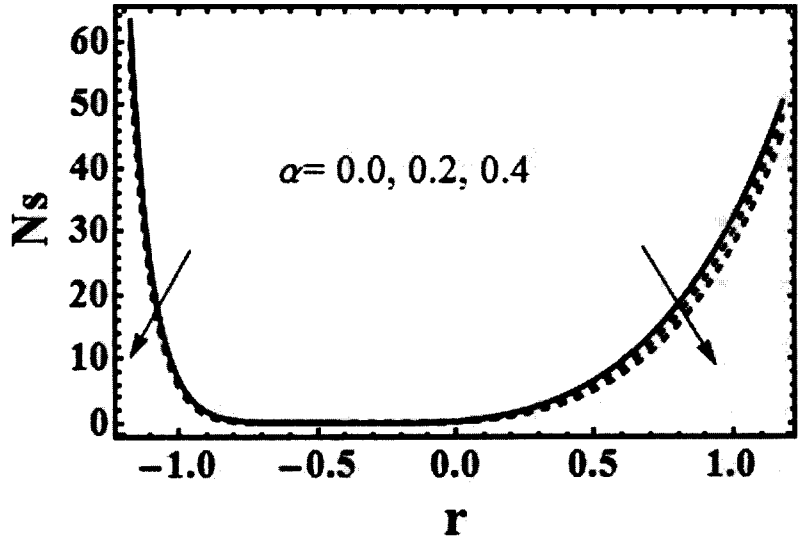

Fig. (7.10): Entropy for viscocity with $a_1 = 0.3, k = 2, \gamma^* = 0.1, Br = 1, \Lambda = 0.01,$ $\beta = 0.1, \beta_1 = \beta_2 = 1.$

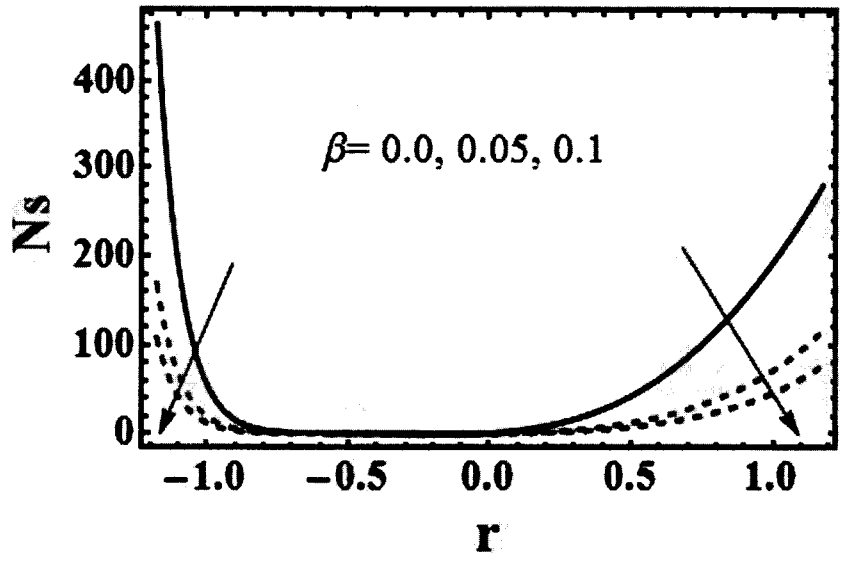

Fig. (7.11): Entropy for thermal conductivity with $a_1 = 0.3, k = 2, \gamma^* = 0.1, Br = 1,$ $\Lambda = 0.01, \alpha = 0.1, \beta_1 = \beta_2 = 1.$

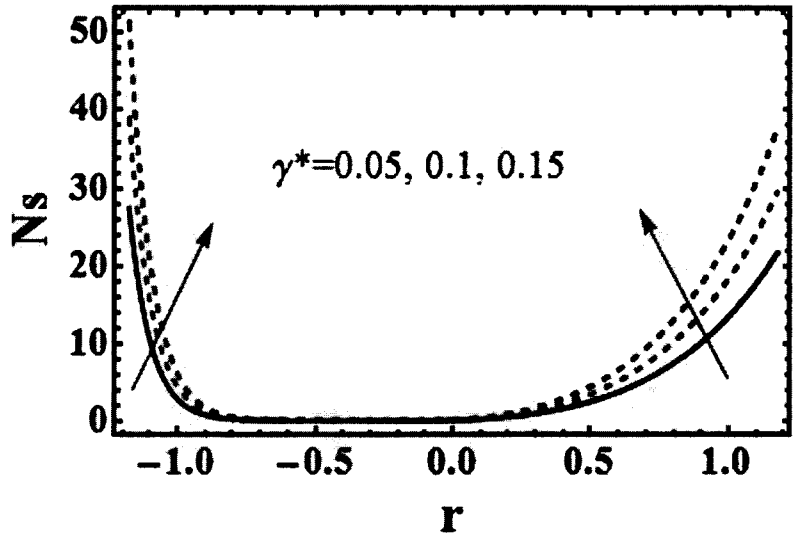

Fig. (7.12): Entropy for fluid parameter with $a_1 = 0.3, k = 2, Br = 1,$ $\Lambda = 0.01, \alpha = \beta = 0.1, \beta_1 = \beta_2 = 1.$

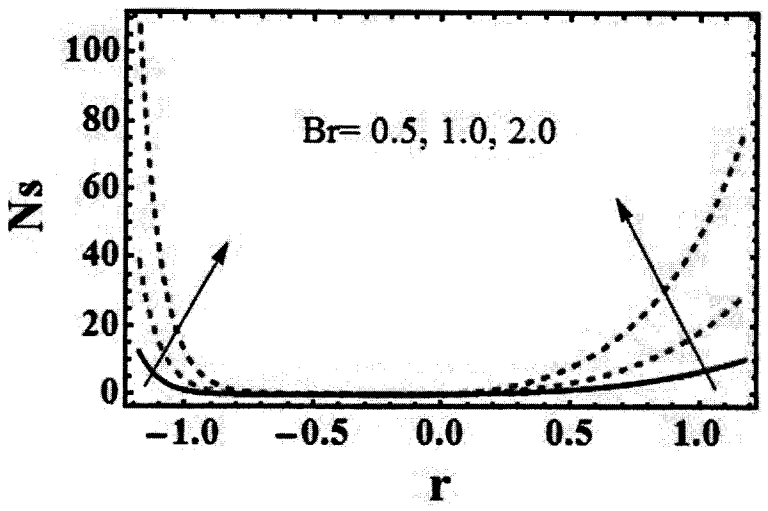

Fig. (7.13): Entropy for Brinkmann number with $a_1 = 0.3, k = 2, \gamma^* = 0.1,$ $\Lambda = 0.01, \alpha = \beta = 0.1, \beta_1 = \beta_2 = 1.$

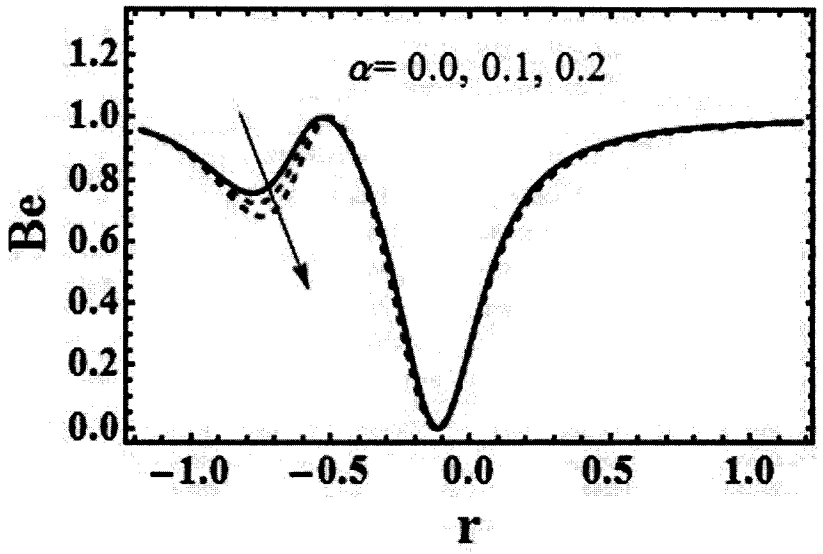

Fig. (7.14): Bejan number for viscosity parameter with $a_1 = 0.3, k = 2, \gamma^* = 0.1, Br = 1,$ $\Lambda = 0.1, \beta = 0.1, \beta_1 = \beta_2 = 2.$

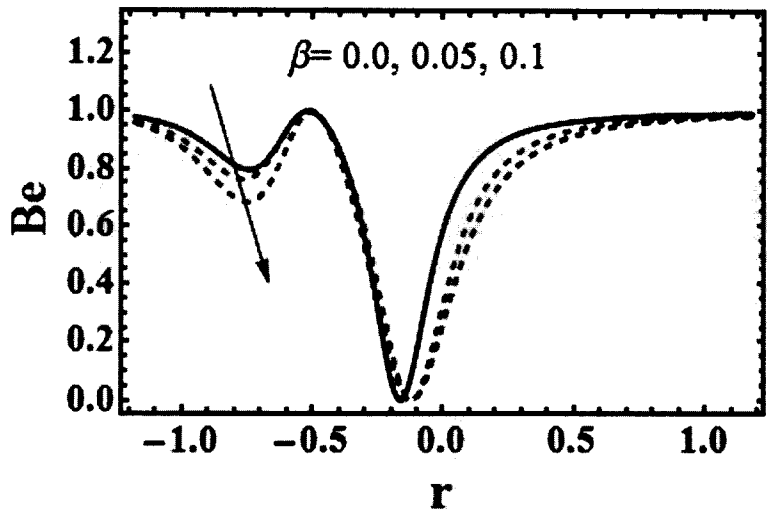

Fig. (7.15): Bejan number for thermal conductivity coefficentwith $a_1 = 0.3, k = 2, \gamma^* = 0.1,$ $Br = 1, \Lambda = 0.1, \alpha = 0.1, \beta_1 = \beta_2 = 2.$

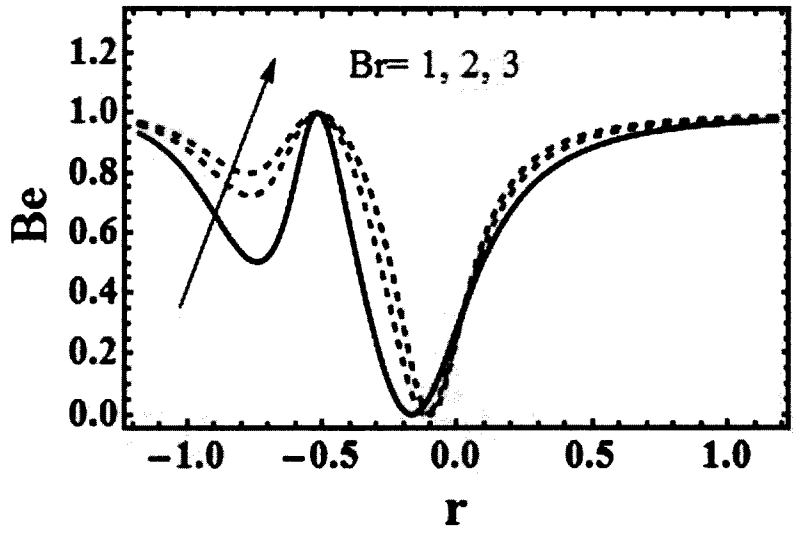

Fig. (7.16): Bejan number for Brinkman number with $a_1 = 0.3, k = 2, \gamma^* = 0.1,$ $\Lambda = 0.1, \alpha = \beta = 0.1, \beta_1 = \beta_2 = 2.$

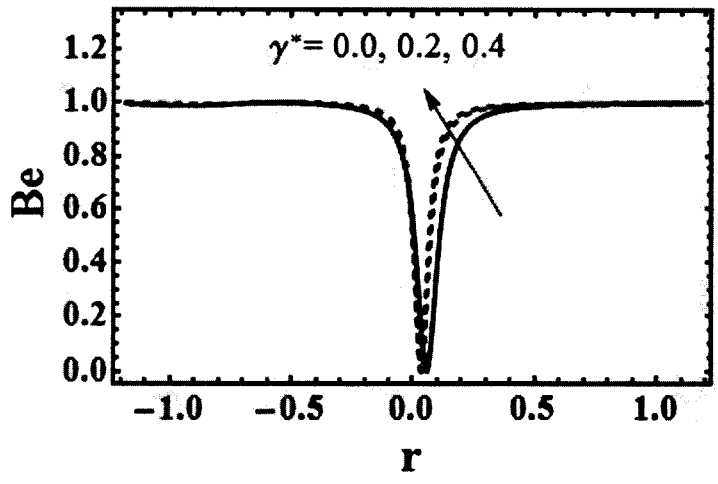

Fig. (7.7)g

Fig. (7.17): Bejan number for fluid parameter with $a_1 = 0.3, k = 2, Br = 1,$ $\Lambda = 0.1, \alpha = \beta = 0.1, \beta_1 = \beta_2 = 2.$

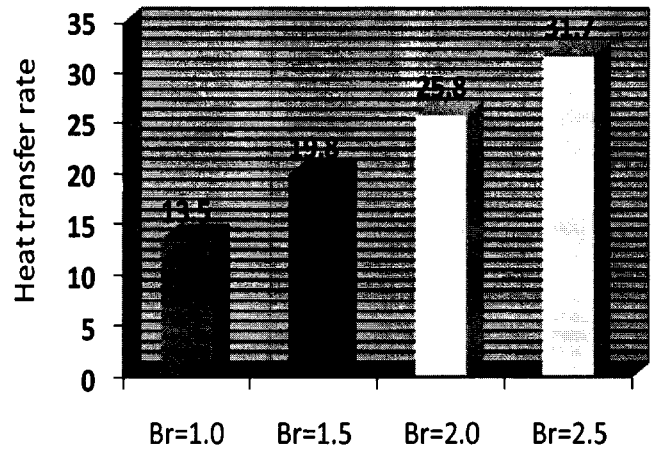

Fig. (7.18): Heat transfer rate for Brinkman number with $a_1 = 0.3, k = 3, \gamma^* = 0.1, \Lambda = 0.1,$ $\alpha = \beta = 0.1, \beta_1 = \beta_2 = 2.$

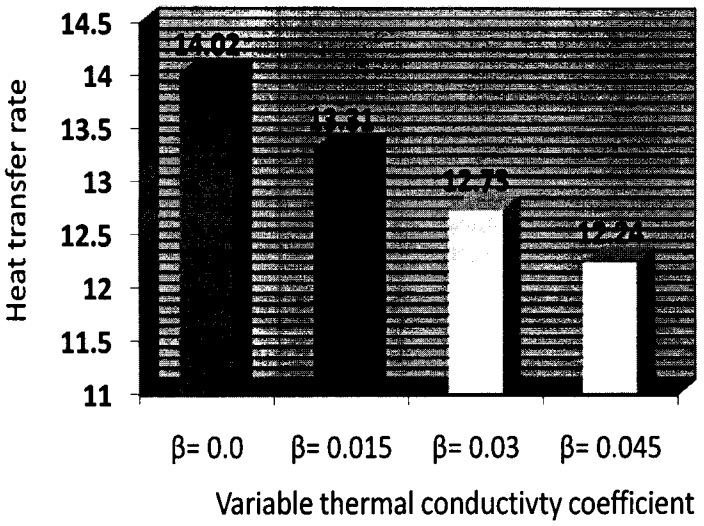

Fig. (7.19): Heat transfer rate for thermal conductivty parameter with $a_1 = 0.3, k = 3,$ $\gamma^* = 0.1, Br = 1, \Lambda = 0.1, \alpha = 0.1, \beta_1 = \beta_2 = 2.$

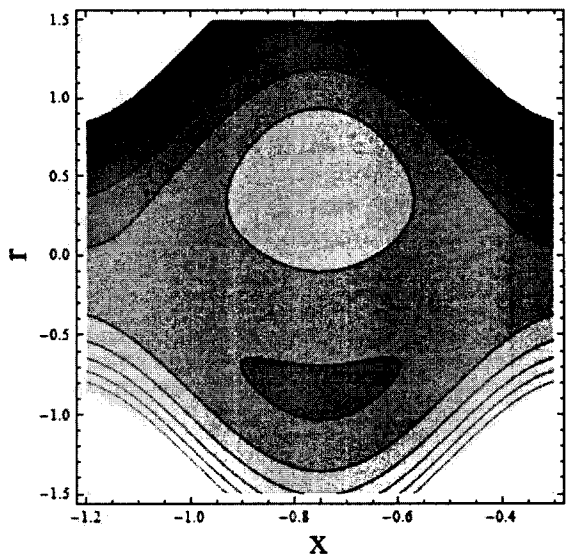

(a): $\alpha = 0.0$

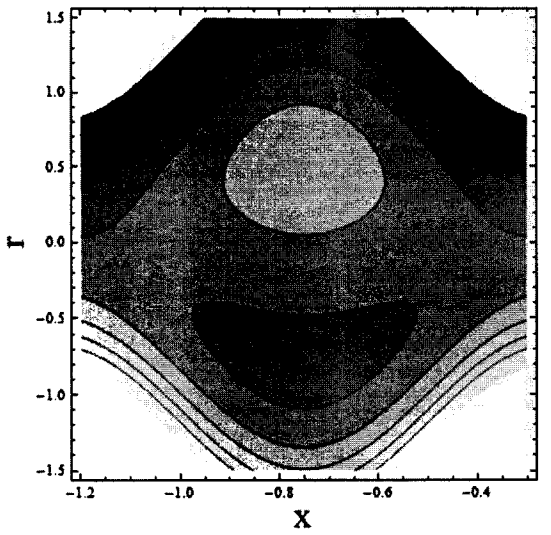

(b): $\alpha = 0.1$

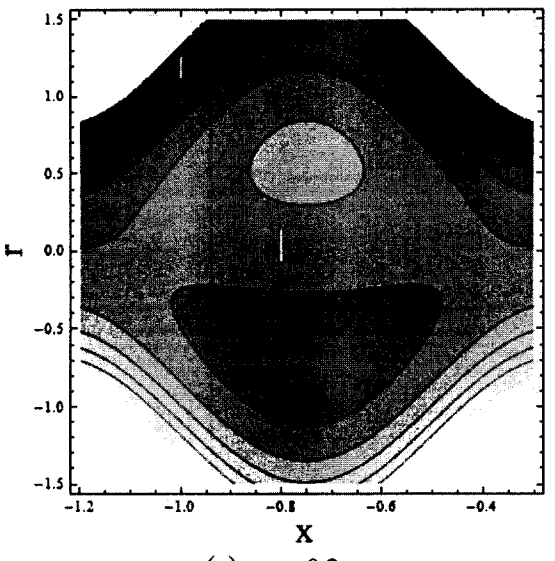

(c): $\alpha = 0.2$

Figs. (7.20a-7.20c): Streamlines for variable viscosity coefficient

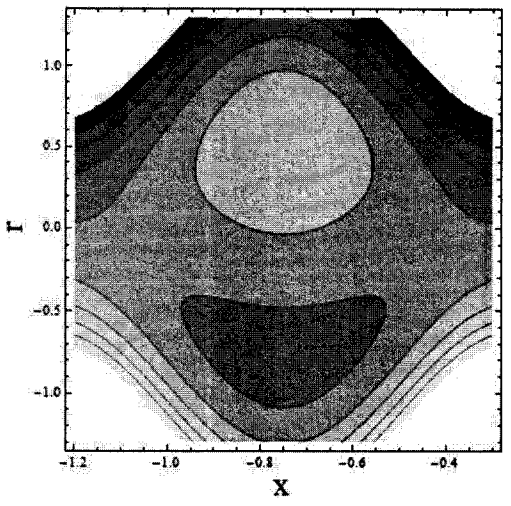

(a): $\gamma^* = 0.0$

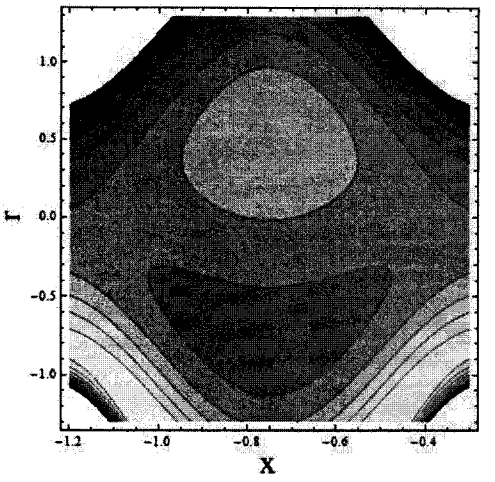

(b): $\gamma^* = 0.1$

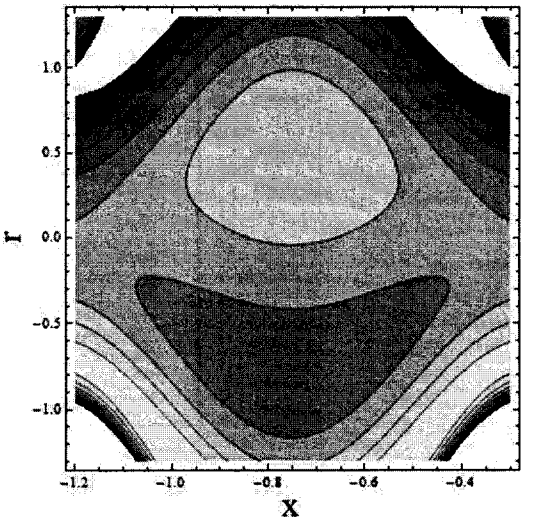

(c): $\gamma^* = 0.2$

Figs. (7.21a-7.21c): Streamlines for Sisko fluid parameter

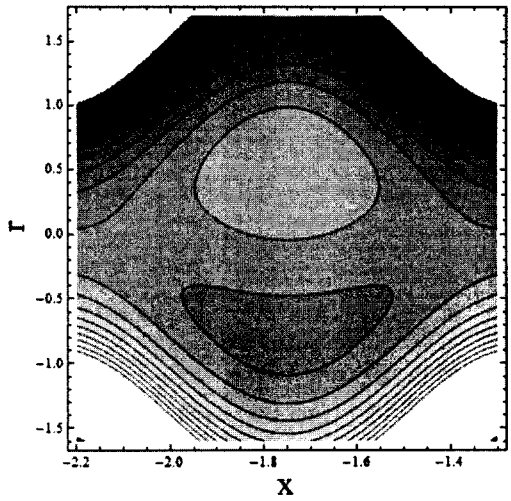

(a): $k = 3$

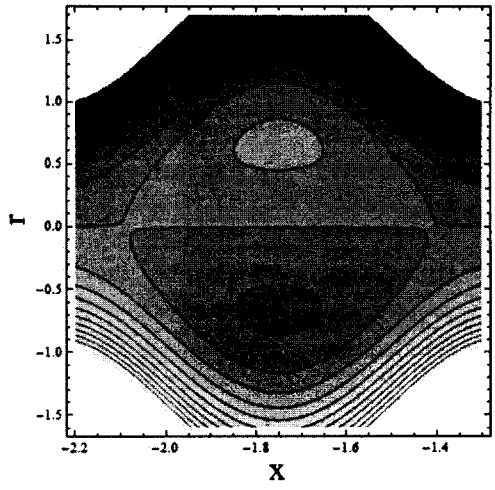

(b): $k = 10$

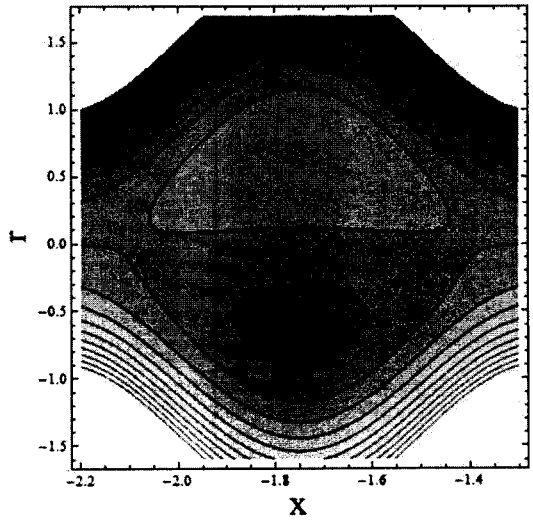

(c): $k = 30$

Figs. (7.22a-7.22c): Streamlines for curvature parameter

7.4 Conclusion

The worth mentioning outcomes of the modeled problem are presented below.

- Similar response of axial velocity has been reported for increasing for α and k.
- Variable viscosity and thermal conductivity parameters (α and β) are responsible for temperature reduction while Sisko fluid parameter γ^* enhances the fluid temperature.
- Minimum irreversibility (i.e. entropy) is observed in case of variable viscosity and thermal conductivity.
- Variation in Bejan number is found same for both α and β.
- Present result is reduced to viscous fluid when $\gamma^* = 0$ and $n = 1$.

Chapter 8

Electro-Thermal Transportation of Carreau Fluids Through Peristalsis in a Curved Micro-Channel

In this chapter the modeling of electroosmotic Carreau liquid flow through a microchannel in curved configuration is studied. Fluid flow is because of both the peristaltic pumping and electro osmosis effects. Energy equation is developed by viscous dissipation. Long wavelength and small Reynolds number are chosen to simplify related expressions. These equations are further solved by numerical technique. In addition, EDL phenomenon is experienced by the channel because of zeta potential. Solution of the electric potential function is obtained analytically by employing Debye-Hückel approximation. Effects of Helmholtz-Smoluchowski velocity, curvature, ratio of zeta potential, inverse EDL thickness and Joule heating parameters on temperature, velocity and trapping characteristics are presented and analyzed through graphical results.

8.1 Mathematical Formulation

We intend to investigate peristaltic flow of non-Newtonian incompressible fluid model within microchannel in curved geometry. Unperturbed width of the channel is $2c$, radius of curvature is $\bar{R}$ and it has centre O. Components of velocity

$\mathbf{W} = \left(W_1(X,R,t), W_2(X,R,t)\right)$ are taken along curvilinear coordinates (R,X). Here X lies along with centre line of microchannel while R is perpendicular to it (See Fig. 8.1). Flow in curved channel is due to both motility of wall that is transverse deflection of sinusoidal wave and electro-kinetic force (body force). An electric field $(\mathbf{E})$ is imposed to walls of micro channel.

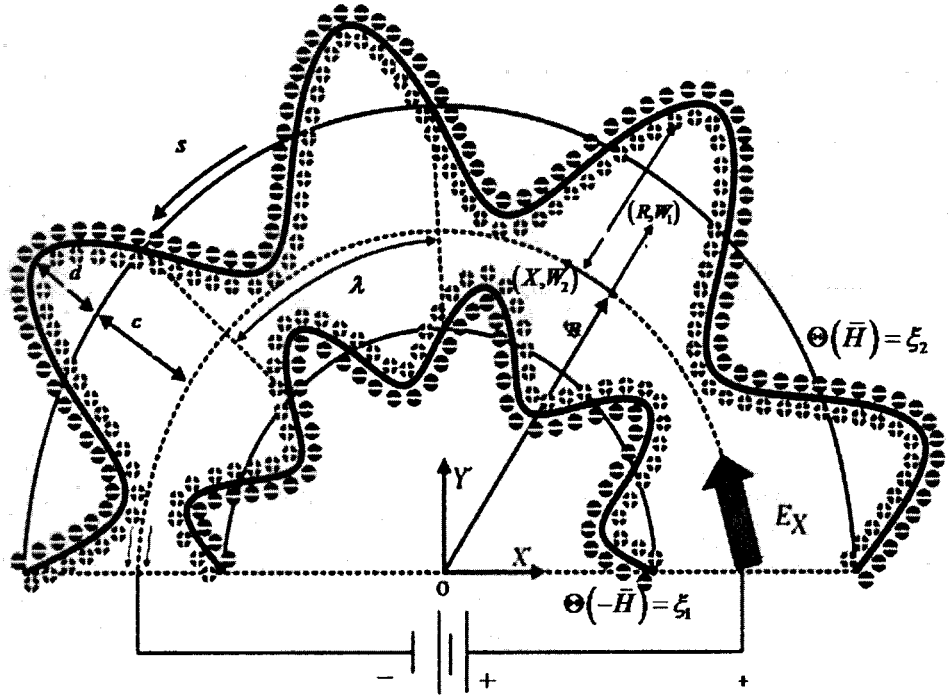

Fig. 8.1: Geometry of problem

The wall shape is defined as:

$$R = \mp\bar{H}(X,t) = \mp\left(c - d\cos^2\left(\frac{X - st}{\lambda}\right)\right), \tag{8.1}$$

here $\bar{H}$ represents radial distance of the wave from centre line, d wave amplitude, λ

wavelength and s wave speed. The wavelength λ of micro-curved channel is assumed to be much larger than half width of channel such that $\frac{c}{\lambda} \beth 1$. No-slip conditions for momentum equation at the boundaries are taken and temperature on walls is T_0.

Cauchy stress tensor $(\boldsymbol{\tau})$ for Carreau fluid model is

$$\boldsymbol{\tau} = \mathbf{S} - PI, \tag{8.2}$$

$$\mathbf{S} = \left(\mu_\infty + (\mu_0 - \mu_\infty)\left(1 + \left(\kappa \left| \dot{\mathbf{G}} \right| \right)^2 \right)^{\frac{n-1}{2}} \right) \dot{\mathbf{G}}, \tag{8.3}$$

where $\mathbf{S}$ denotes extra stress tensor, I identity tensor, P pressure, (μ_0, μ_∞) initial and infinite shear rate viscosity, $|\dot{G}| = \sqrt{\frac{1}{2} trace(\mathbf{A}_1^2)}$ trace. The first Rivlin–Ericksen tensor $(\mathbf{A}_1)$ is

$$\mathbf{A}_1 = (div\mathbf{W})^t + (div\mathbf{W}). \tag{8.4}$$

Eqn. (8.3) can also be written as:

$$\mathbf{S} \approx \mu_0 \left(1 + \frac{(n-1)\kappa^2}{2} \left| \dot{\mathbf{G}} \right|^2 \right) \dot{\mathbf{G}}, \tag{8.5}$$

$$S_{XX} \approx \mu_0 \left(1 + \frac{(n-1)\kappa^2}{2} \left(\left(2\frac{\partial W_1}{\partial R} \right)^2 + \left(\frac{\partial W_2}{\partial R} + \frac{R}{\bar{R}+R}\frac{\partial W_1}{\partial X} - \frac{W_2}{\bar{R}+R} \right)^2 \right)^{\frac{n-1}{2}} \right) \left(2\frac{\partial W_1}{\partial R} \right),$$

$$S_{XR} \approx \mu_0 \left(1 + \frac{(n-1)\kappa^2}{2} \left(\left(2\frac{\partial W_1}{\partial R} \right)^2 + \left(\frac{\partial W_2}{\partial R} + \frac{R}{\bar{R}+R}\frac{\partial W_1}{\partial X} - \frac{W_2}{\bar{R}+R} \right)^2 \right)^{\frac{n-1}{2}} \right) \left(\frac{\partial W_2}{\partial R} + \frac{R}{\bar{R}+R}\frac{\partial W_1}{\partial X} - \frac{W_2}{\bar{R}+R} \right),$$

$$S_{RR} \approx \mu_0 \left(1 + \frac{(n-1)\kappa^2}{2} \left(\left(2\frac{\partial W_1}{\partial R} \right)^2 + \left(\frac{\partial W_2}{\partial R} + \frac{R}{\bar{R}+R}\frac{\partial W_1}{\partial X} - \frac{W_2}{\bar{R}+R} \right)^2 \right)^{\frac{n-1}{2}} \right) \left(-2\frac{\partial W_1}{\partial R} \right).$$

Viscous fluid can be achieved by putting $n=0$ in Eqn. (8.5) .

Conservation equations for momentum and energy for Carreau incompressible fluid coupled with body force that is produced by action of imposed electric field on free ion in EDL have the following expressions [111, 112]:

$$\frac{\bar{R}}{\bar{R}+R}\frac{\partial W_2}{\partial X}+\frac{\partial W_1}{\partial R}+\frac{W_1}{\bar{R}+R}=0, \tag{8.6}$$

$$\rho\left(\frac{\partial W_2}{\partial t}+(\mathbf{W}.\nabla)W_2+\frac{W_1W_2}{\bar{R}+R}\right)=-\frac{\bar{R}}{(R+\bar{R})}\frac{\partial P}{\partial X}+\frac{1}{(R+\bar{R})^2}\frac{\partial}{\partial R}\left(S_{XR}(R+\bar{R})^2\right)$$
$$+\frac{\bar{R}}{(R+\bar{R})}\frac{\partial S_{XX}}{\partial X}+\rho_e E_X, \tag{8.7}$$

$$\rho\left(\frac{\partial W_1}{\partial t}+(\mathbf{W}.\nabla)W_1-\frac{W_2^{\,2}}{\bar{R}+R}\right)=-\frac{\partial P}{\partial R}+\frac{1}{(R+\bar{R})}\frac{\partial}{\partial R}\left(S_{RR}(R+\bar{R})\right)-\frac{S_{XX}}{(R+\bar{R})}$$
$$+\frac{\bar{R}}{(R+\bar{R})}\frac{\partial S_{XR}}{\partial X}+\rho_e E_R, \tag{8.8}$$

$$\rho C_p\left(\frac{\partial T}{\partial t}+(\mathbf{W}.\nabla)T\right)=\kappa\left(\frac{\partial^2 T}{\partial R^2}+\frac{1}{(R+\bar{R})}\frac{\partial T}{\partial R}+\frac{\bar{R}^2}{(R+\bar{R})^2}\frac{\partial^2 T}{\partial X^2}\right)-\frac{\partial W_1}{\partial R}(S_{XX}-S_{RR})$$
$$+\left(\frac{\partial W_2}{\partial R}+\frac{\bar{R}}{(R+\bar{R})}\frac{\partial W_1}{\partial X}-\frac{W_2}{(R+\bar{R})}\right)S_{XR}, \tag{8.9}$$

with the boundaries conditions:

$$\begin{aligned} &W_2=0,\quad T=T_0 \quad \text{at} \quad R=-\bar{H},\\ &W_2=0,\quad T=T_0 \quad \text{at} \quad R=\bar{H}. \end{aligned} \tag{8.10}$$

Here ρ denotes density, components S_{XX}, S_{XY}, S_{YY} of the extra stress tensor $\mathbf{S}$, C_p specific heat and T material temperature. Here the body force $(\mathbf{F})$ is due to imposed external electric field defined as:

$$\mathbf{F} = \rho_e \mathbf{E} = \rho_e \left(E_X \vec{e}_X + E_R \vec{e}_R \right), \tag{8.11}$$

in which ρ_e is net charge density defined as:

$$\rho_e \equiv ze\left(n_+ - n_-\right), \tag{8.12}$$

with z ionic valence and $n_{\mp}$ are respective number densities of ions and counter co-ions. The electric field and electro-osmotic flow are related by:

$$\mathbf{E} = -\nabla\Theta = \frac{\bar{R}}{R+\bar{R}} \frac{\partial\Theta}{\partial X} \vec{e}_X + \frac{\partial\Theta}{\partial R} \vec{e}_R, \tag{8.13}$$

in which Θ shows electric potential. By electrostatics theory, electric potential is given by expression of Poisson equation as:

$$\nabla^2\Theta = -\frac{\rho_e}{\varepsilon} = -\frac{ze\left(n_+ - n_-\right)}{\varepsilon}, \tag{8.14}$$

subject to boundary conditions as symmetric zeta potential at curved micro channel walls are:

$$\Theta\left(-\bar{H}\right) = \xi_1, \quad \Theta\left(\bar{H}\right) = \xi_2. \tag{8.15}$$

The Nernst-Planck equation for the curved configuration in the absence of chemical reactions is given by

$$\frac{dn_{\pm}}{dt} = D_{\pm}\left(\nabla^2 n_{\pm}\right) \pm \frac{n_{\pm} D_{\pm} e}{T_0 k_b} \left[\frac{\bar{R}}{\left(\bar{R}+R\right)} \frac{\partial}{\partial X} \left(\frac{\bar{R} n_{\pm}}{\left(\bar{R}+R\right)} \frac{\partial\Theta}{\partial X} \right) + \frac{1}{\left(\bar{R}+R\right)} \frac{\partial}{\partial R} \left(\left(\bar{R}+R\right) n_{\pm} \frac{\partial\Theta}{\partial R} \right) \right], \tag{8.16}$$

in which k_b denotes Boltzmann constant, T_0 absolute temperature and D diffusivity of an ionic species.

In laboratory frame, flow phenomena are taken as unsteady while it is steady according to wave frame of reference $(\bar{r}, \bar{x})$. The relationship between the laboratory and wave frames

is:

$$\bar{r}=R,\ \bar{x}=X-st,\ \bar{w}_2(\bar{x},\bar{r})=W_2(X,R,t)-s,\ \bar{w}_1(\bar{x},\bar{r})=W_1(X,R,t). \tag{8.17}$$

We define dimensionless parameters: (r,x) radial and axial variables, p pressure, (u,v) velocity components, δ wave number, d_1 wave amplitude, θ temperature, Re Reynolds number, h dimensionless radial distance of centerline from the wave, k curvature, Br Brinkman number, Pr Prandtl number, m' Debye-Hückel parameter, U'_{HS} Helmholtz-Smoluchowski velocity, R_ξ ratio of zeta potential, Γ Carreau fluid parameter and Θ_0 thermal potential are defined as follows:

$$\begin{aligned}
&(r,x)=\left(\frac{\bar{r}}{c},\frac{\bar{x}}{\lambda}\right), \quad p=\frac{c^2P}{s\mu_0\lambda}, \quad (w_1,w_2)=\left(\frac{\bar{w}_1}{s},\frac{\bar{w}_2}{s}\right), \quad \delta=\frac{c}{\lambda},\\
&d_1=\frac{d}{c}, \quad \theta=\frac{T-T_0}{T_0}, \quad \mathrm{Re}=\frac{sc}{\upsilon}, \quad h=\frac{\bar{H}}{c},\\
&k=\frac{\bar{R}}{c}, \quad Br=\frac{\mu_0 s^2}{\kappa T_0}, \quad \mathrm{Pr}=\frac{\mu C_p}{\kappa}, \quad m'=mc,\\
&\phi=\frac{\Theta}{\Theta_0}, \quad \xi_1'=\frac{\xi_1}{\Theta_0}, \quad \xi_2'=\frac{\xi_2}{\Theta_0}, \quad U'_{HS}=-\frac{\varepsilon\Theta_0 E_x}{\mu s},\\
&R_\xi=\frac{\xi_2}{\xi_1}, \quad \Gamma=\frac{s\kappa}{c}, \quad \Theta_0=\frac{k_bT_0}{ze}.
\end{aligned} \tag{8.18}$$

The fundamental equations (8.6-8.9) and (8.14) are first transformed in wave frame and then the non-dimensional forms are

$$\frac{\delta k}{k+r}\frac{\partial w_2}{\partial x}+\frac{\partial w_1}{\partial r}+\frac{w_1}{k+r}=0, \tag{8.19}$$

$$\begin{aligned}
&\mathrm{Re}\left(-\delta\frac{\partial w_2}{\partial x}+\frac{\delta(w_2+1)k}{(k+r)}\frac{\partial v}{\partial x}+w_1\frac{\partial v}{\partial r}+\frac{w_1(w_2+1)}{k+r}\right)=-\frac{k}{(k+r)}\frac{\partial p}{\partial x}+\frac{1}{(k+r)^2}\frac{\partial}{\partial r}\left(S_{xr}(k+r)^2\right)\\
&+\frac{\delta k}{(k+r)}\frac{\partial S_{xx}}{\partial x}+U'_{HS}\left(\delta^2\frac{k^2}{(k+r)^2}\frac{\partial^2\phi}{\partial x^2}+\frac{1}{(k+r)}\frac{\partial}{\partial r}\left((k+r)\frac{\partial\phi}{\partial r}\right)\right),
\end{aligned} \tag{8.20}$$

$$\mathrm{Re}\,\delta\left(-\delta\frac{\partial w_1}{\partial x}+\frac{\delta k}{(k+r)}\frac{\partial w_1}{\partial x}+w_1\frac{\partial w_1}{\partial r}+\frac{(w_2+1)^2}{k+r}\right)=-\frac{\partial p}{\partial r}+\delta\frac{1}{r+k}\frac{\partial}{\partial r}\left(S_{rr}(k+r)\right)$$

$$+\frac{k\delta^2}{(k+r)}\frac{\partial S_{xx}}{\partial x}+U'_{HS}\frac{\delta^2 k}{(k+r)}\left(\delta^2\frac{k^2}{(k+r)^2}\frac{\partial^2\phi}{\partial x^2}+\frac{1}{(k+r)}\frac{\partial}{\partial r}\left((k+r)\frac{\partial\phi}{\partial r}\right)\right), \tag{8.21}$$

$$\mathrm{Re}\,P_r\left(-\delta\frac{\partial\theta}{\partial x}+\frac{\delta k(w_2+1)}{(r+k+r)}\frac{\partial\theta}{\partial x}+w_1\frac{\partial\theta}{\partial r}\right)=\frac{\partial^2\theta}{\partial r^2}+\frac{1}{r+k}\frac{\partial\theta}{\partial r}+\frac{\delta^2k^2}{(r+k)^2}\frac{\partial^2\theta}{\partial x^2}$$

$$+Br\frac{\partial w_1}{\partial r}(S_{xx}-S_{rr})+Br\left(\frac{\partial w_2}{\partial r}+\frac{\delta k}{(r+k)}\frac{\partial w_1}{\partial x}-\frac{w_2+1}{(r+k)}\right)S_{xr}, \tag{8.22}$$

$$\frac{\delta^2k^2}{(k+r)^2}\frac{\partial^2\phi}{\partial x^2}+\frac{\partial^2\phi}{\partial r^2}+\frac{1}{(k+r)}\frac{\partial\phi}{\partial r}-m^2\left(\frac{n_+-n_-}{2}\right)=0, \tag{8.23}$$

and

$$S_{xx}\approx 2\delta\mu_0\left(\frac{s}{c}\right)\left(1+\frac{(n-1)\Gamma^2}{2}\left[\left(2\frac{\partial w_1}{\partial r}\right)^2+\left(\frac{\partial w_2}{\partial r}+\frac{\delta k}{r+k}\frac{\partial w_1}{\partial x}-\frac{w_2+1}{r+k}\right)^2\right]^{\frac{n-1}{2}}\right)\left\{\frac{\partial w_1}{\partial r}\right\},$$

$$S_{xr}\approx \mu_0\left(\frac{s}{c}\right)\left(1+\frac{(n-1)\Gamma^2}{2}\left[\left(2\frac{\partial w_1}{\partial r}\right)^2+\left(\frac{\partial w_2}{\partial r}+\frac{\delta k}{r+k}\frac{\partial w_1}{\partial x}-\frac{w_2+1}{r+k}\right)^2\right]^{\frac{n-1}{2}}\right)\left\{\frac{\partial w_2}{\partial r}+\frac{\delta k}{r+k}\frac{\partial w_1}{\partial x}-\frac{w_2+1}{r+k}\right\}, \tag{8.24}$$

$$S_{rr}\approx -2\delta\mu_0\left(\frac{s}{c}\right)\left(1+\frac{(n-1)\Gamma^2}{2}\left[\left(2\frac{\partial w_1}{\partial r}\right)^2+\left(\frac{\partial w_2}{\partial r}+\frac{\delta k}{r+k}\frac{\partial w_1}{\partial x}-\frac{w_2+1}{r+k}\right)^2\right]^{\frac{n-1}{2}}\right)\left\{\frac{\partial w_1}{\partial r}\right\},$$

in which $m\left(=\sqrt{\frac{2n_0(cze)^2}{T_0k_b\varepsilon}}\right)$ is Debye-Hückel parameter related to the thickness of Debye layer. The dimensionless boundary conditions are:

$$\begin{aligned} &w_2=-1, \quad \text{at} \quad r=\pm h,\\ &\theta=0, \quad \text{at} \quad r=\pm h,\\ &\phi(-h)=\xi_1', \quad \phi(h)=\xi_2'. \end{aligned} \tag{8.25}$$

The Nerst-Planck Eqn. (8.16) in dimensionless form is:

$$Pe\,\delta^2\left((w_1+1)\frac{k}{(k+r)}\frac{\partial n_{\mp}}{\partial x}+w_2\frac{\partial n_{\mp}}{\partial r}\right)=\left(\frac{\delta^2k^2}{(k+r)^2}\frac{\partial^2 n_{\mp}}{\partial x^2}+\frac{\partial^2 n_{\mp}}{\partial r^2}+\frac{1}{(k+r)}\frac{\partial n_{\mp}}{\partial r}\right)$$
$$\pm\left(\frac{\delta^2k}{r+k}\frac{\partial}{\partial x}\left(\frac{n_{\mp}k}{(r+k)}\frac{\partial\phi}{\partial x}\right)+\frac{1}{(r+k)}\frac{\partial}{\partial r}\left(n_{\mp}(r+k)\frac{\partial\phi}{\partial r}\right)\right), \tag{8.26}$$

in which Pe is magnitude of Peclet number. In the above equation $Pe\,\delta^2\to 0$, thus we arrived at:

$$\frac{\partial^2 n_{\mp}}{\partial r^2}+\frac{1}{(r+k)}\frac{\partial n_{\mp}}{\partial r}=\mp\frac{1}{(r+k)}\frac{\partial}{\partial r}\left(n_{\mp}(r+k)\frac{\partial\phi}{\partial r}\right), \tag{8.27}$$

with boundary conditions:

$$n_{\pm}(\phi=0)=1,\qquad \text{and}\quad \frac{\partial n_{\pm}}{\partial r}=0,\qquad \text{at}\quad \frac{\partial\phi}{\partial r}=0. \tag{8.28}$$

Exact solution of the above problem is:

$$n_{\mp}=\exp(\pm\phi). \tag{8.29}$$

The Eqns. (8.23) and (8.29) under lubrication theory assumption we get:

$$\frac{\partial^2\phi}{\partial r^2}+\frac{1}{(r+k)}\frac{\partial\phi}{\partial r}-m^2\sinh\phi=0. \tag{8.30}$$

The ion distribution and electric potential are independent of the velocity of the fluid. The above Eqn. (8.30) can be linearized by apply Debye Hückel assumption. This implies

$$\frac{\partial^2\phi}{\partial r^2}+\frac{1}{(r+k)}\frac{\partial\phi}{\partial r}-m^2\phi=0, \tag{8.31}$$

subject to boundary condition:

$$\phi(-h)=\xi_1',\quad \phi(h)=\xi_2'. \tag{8.32}$$

The analytical solution of the Eqn. (8.31) subject to boundary conditions (8.32) is:

$$\phi(x,r)=\xi_1'\left(\frac{L_2-R_\xi L_1}{I_1L_2-I_2L_1}I_0\left(m(k+r)\right)+\frac{R_\xi I_1-I_2}{I_1L_2-I_2L_1}L_0\left(m(k+r)\right)\right), \tag{8.33}$$

in which

$$I_1=I_0\left(m(k-h)\right),\quad I_2=I_0\left(m(k+h)\right),\quad L_1=L_0\left(m(k-h)\right),\quad L_2=L_0\left(m(k+h)\right). \tag{8.34}$$

In which I_0 and L_0 are respective modified Bessel functions of 1st and 2nd kind having order zero.

Equations (8.19-8.22) under assumption of lubrication theory, eliminating pressure gradient and utilizing $w_2=\frac{\partial\psi}{\partial r}$, $w_1=-\delta\frac{k}{k+r}\frac{\partial\psi}{\partial x}$, we reached at

$$\frac{\partial}{\partial r}\left(\frac{1}{(r+k)}\frac{\partial}{\partial r}\left(S_{xr}(r+k)^2\right)+U_{HS}'\frac{\partial}{\partial r}\left((r+k)\frac{\partial\phi}{\partial r}\right)\right)=0, \tag{8.35}$$

$$\frac{1}{k+r}\frac{\partial\theta}{\partial r}+\frac{\partial^2\theta}{\partial r^2}+Br\left(\frac{\partial v}{\partial r}-\frac{v+1}{(k+r)}\right)S_{xr}=0, \tag{8.36}$$

in which

$$S_{xr}\approx\mu_0\left(\frac{s}{c}\right)\left[1+\frac{(n-1)\Gamma^n}{2}\left[\frac{\partial^2\psi}{\partial r^2}-\frac{1}{k+r}\left(1+\frac{\partial\psi}{\partial r}\right)\right]^{\frac{(n-1)}{2}}\right]\left(\frac{\partial^2\psi}{\partial r^2}-\frac{1}{k+r}\left(1+\frac{\partial\psi}{\partial r}\right)\right), \tag{8.37}$$

subject to the boundary conditions:

$$\begin{aligned}&\psi=\pm\frac{F}{2},\quad \frac{\partial\psi}{\partial r}=-1. \quad \text{at} \quad r=\pm h,\\ &\theta=0 \quad \text{at} \quad r=\pm h.\end{aligned} \tag{8.38}$$

8.2 Analysis

The modeled differential Eqns. (8.35-8.36) subject to boundary conditions (8.38) are solved

by numerical technique using NDSolve command in Mathematica 11 software. Results have been presented below. These results are drawn for the pertinent parameters of interest like curvature effects of micro-channel, Carreau fluid model effects, electro-osmotic velocity effects, inverse EDL thickness effects, influence of zeta potential ratio and impact of Joule heating (electric dissipation) on velocity, trapping phenomena and temperature.

8.2.1 Velocity

One of the most significant characteristics in fluid flow is to evaluate the velocity of fluid through curved microchannel. Figs. (8.2-8.6) are prepared to analyze the flow characteristics for significant parameters. Furthermore, a comparison of the viscous and non-Newtonian fluid model is also presented. In these Figs., dual behavior of velocity is seen in the microchannel and it changes near the central point. Figs. 8.2(a, b) show the effects of curvature parameter on velocity profile. It is seen that velocity decreases for higher values of k at the lower region of micro-channel; however, reverse behavior is observed for the upper half of the channel. Moreover, velocity is maximum near the centre of the channel and it is symmetric at the axial location $(x=0)$ for straight channel. Through Figs. 8.2(a) and (b), it is observed that trend of velocity versus curvature parameter for viscous fluid is the same when compared with Carreau fluid. However, velocity is parabolic in shape for viscous fluid and has sharp edge near the centre for Carreau fluid.

Fig. 8.3(a, b) illustrate the effects of electro-osmotic velocity $\left(U_{HS}^{'}\right)$ for both viscous and non-Newtonian fluids on velocity profile. Electro osmotic velocity is imperative parameter of problem in hand. $U_{HS}^{'}$ has a direct relationship with externally applied electric field E_x.

It is negative by definition as $U_{HS}^{'}\left(=-\frac{\varepsilon\Theta_0 E_x}{\mu s}\right)$. Different values of this parameter are considered for constant fluid viscosity, permittivity and applied electrical potential, while applied axial electric field is changed to get a variation in velocity profile. Here $\left(U_{HS}^{'}=-1\right)$ means that direction of applied electric field and direction of flow are same and $\left(U_{HS}^{'}=1\right)$ indicates that direction of electric field and direction of the flow are opposite. While $\left(U_{HS}^{'}=0\right)$ corresponds to case of peristaltic transport of non-Newtonian fluid through curved geometry when electro osmotic effects are not considered. From Fig. 8.3(a), it is observed that velocity manifests when values of electro-osmotic velocity move from negative to positive in lower half of micro-channel. However, trend of velocity is reversed for the upper half of micro-channel. In Fig. 8.3(b), trend of velocity is the same for viscous and Carreau fluid qualitatively. In addition, with the change in electro-osmotic velocity, variation in viscous fluid is larger than Carreau fluid model.

Scrutiny of Fig. 8.4(a) depicts that with a significant increase in $m^{'}$, remarkable enhancement in axial velocity at lower half of channel occurs. On other hand, such an elevation for $m^{'}$ is resulted in deceleration at upper micro-channel not exactly at the centre but little beyond the centerline. Electro-osmotic parameter has an inverse relation with Debye length. Obviously, decrease in Debye length that corresponds to enhanced value of $m^{'}$, raises electrical potential (see Ref. [111]). By varying $m^{'}$, velocity distribution is controlled effectively.

Impact of zeta potential ratio $\left(R_{\xi}^{'}\right)$ on velocity is investigated through Figs. 8.5(a, b) by

taking different values of $R_{\xi}^{'}(=-1,-0.5,0.5,1)$. Here, $R_{\xi}^{'}=1$ means that potential at both the walls are equal and $R_{\xi}^{'}=0.5$ corresponds that zeta potential at upper wall is half of lower wall etc. Through these Figs., it is revealed that velocity increases by increasing zeta potential ratio ranging from $R_{\xi}^{'}=-1$ to 1 in the region $r<0$, and converse behavior is observed for the region $r>0$. In Figs. 8.5(a) and (b), a contrast of viscous and non-Newtonian fluid model is presented. In this comparison it is concluded that behavior of velocity for both the fluid models are alike. However, velocity changes significantly in the case of viscous fluid. Fig. (8.6) is portrayed to reveal the effects of Carreau fluid parameter (Γ) on velocity. It is depicted through this Fig. that velocity decays in the lower region of the micro-channel whereas reverse trend is achieved in the upper region by increasing Γ. Velocity in the vicinity of the centre of channel remains unchanged. However, the change in the entire channel is not so predominant.

8.2.2 Trapping

In peristalsis, one of the very interesting phenomena of trapping occurs. In this phenomenon, behaviors of stream lines are analyzed which present a very clear picture of flow pattern. In fluid movement, these contours plots have intrinsic flow characteristics which is known as trapping. In trapping, closed paths (called circulation) are formed by some centre stream lines which depicts smooth movement of fluid. Analysis of trapping phenomena for non-Newtonian fluid flow subject to external applied electric field is illustrated in Figs. (8.7-8.9).

The effect of inverse EDL parameter $(m^{'})$ to trapping is scrutinized via Figs. (8.7a-8.7c).

The smaller values of m' (i.e. when EDL thickness is more), bolus in size and shape are different in both halves of the channel. Moreover it is seen that bolus size also varies by varying EDL thickness. For large m' (i.e. decreasing thickness of EDL wall), bolus in number and size decreases in the lower region.

The impact of curvature parameter (k) to trapping is investigated through Figs. (8.8a-8.8c). The smaller values of curvature portray stronger curvature of micro-channel and when $(k \to \infty)$ the special case of straight channel is achieved. In Figs. 8.8(a, b), for small values of (k), it is noticed that number of trapping bolus is larger in upper half and less in the lower half. Moreover, in lower half trapping bolus is elliptical in shape. In these Figs., it is clear that for $(k = 1.2, 3)$, bolus is asymmetric in upper and lower halves of the micro-channel. However, when we move from curved to straight channel, trapping bolus is more symmetric in both halves of the channel.

Figs. (8.9a-8.9c) are prepared to demonstrate the effects of electric filed (U'_{HS}). In these Figs., it is observed that sizes of trapping bolus in both halves are different and asymmetric. It is also noted that trapping streamlines are more when electric field and flow direction are same i.e. $(U'_{HS} = -1)$ and less in number when electric filed direction and flow direction are opposite i.e. $(U'_{HS} = 1)$. In Fig. 8.9(b), when electro-osmotic effects are not present i.e. $(U'_{HS} = 0)$, the number of trapped streamlines are more in upper half and less in the lower half of the channel.

8.2.3 Temperature

Figs. (8.10-8.14) are prepared to demonstrate the development in temperature profile in the channel with variation of Helmholtz-Smoluchowski velocity $\left(U_{HS}^{'}\right)$, curvature parameter $\left(k\right)$, inverse Electric Double Layer thickness parameter $\left(m\right)$ and Carreau fluid parameter $\left(\Gamma\right)$. A comparison of viscous and Carreau fluid model is also made for various parameters. It is clear from the Figs. (8.10-8.14) that temperature profiles are homogenous in contrast with axial velocity profiles. Here trend of temperature distribution is parabolic in the curved channel and maximum value of the temperature occurs in the central part of the channel. Fig. 8.10(a, b) depict variation in temperature profile via r by varying $U_{HS}^{'}$. From these Figs. it is revealed that temperature decays by increased values of $U_{HS}^{'}$. In these Figs., when viscous fluid is compared with Carreau model, same behavior for temperature is observed for both fluids. However, for Carreau model temperature varies rapidly than viscous fluid. Figs. 8.11(a, b) indicate curvature parameter effects on temperature distribution for both fluid models. For smaller values of k, (for stronger curvature channel), a significant rise in temperatures is noted in the micro-channel. Whereas for larger values of k, (for straighter channel geometries) temperature reduces, it means cooling produces in the straighter channel. In stronger curved channel, peak in temperature appears is in the upper half plane whereas, for straighter geometries, it appear in the central part of the channel. Fig. 8.12(a, b) exhibits temperature distribution against $m>0$. Heating is produced by lower EDL thickness however cooling is encouraged Carreau fluid parameter by higher electrical double layer thickness in the micro-channel. Fig. (8.13)

depict temperature profile for Carreau fluid parameter (Γ). It is evident from the Fig. temperature boosts up significantly for even the small variation in Γ. It shows that heating is encouraged by Carreau fluid when it is compared with viscous fluid $(\Gamma = 0)$. Enhancement in temperature is also evident in the Figs. (8.11-8.13)(b) for Carreau model. From the results of temperature distribution, it can be concluded that trend of temperature profile versus pertinent parameters $\left(U_{HS}^{'}, k, m\right)$ are the same for both fluid models however temperature rises significantly in case of Carreau fluid.

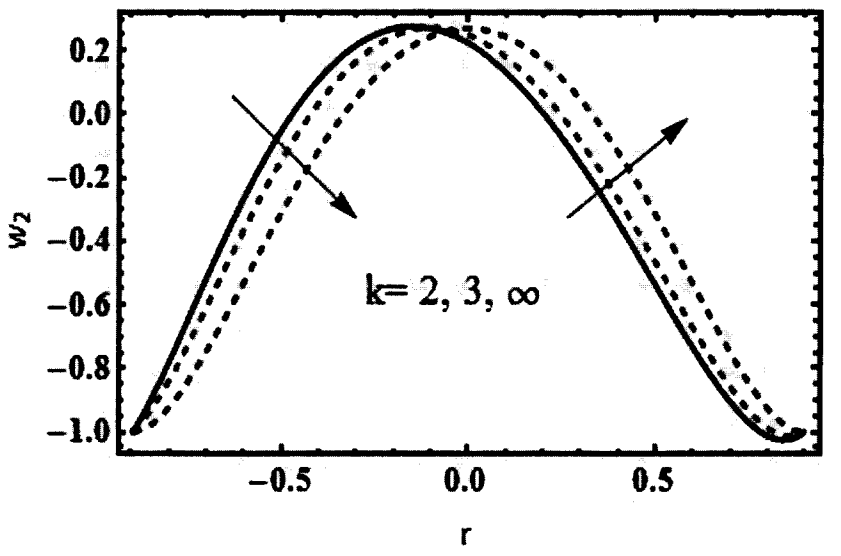

(a)

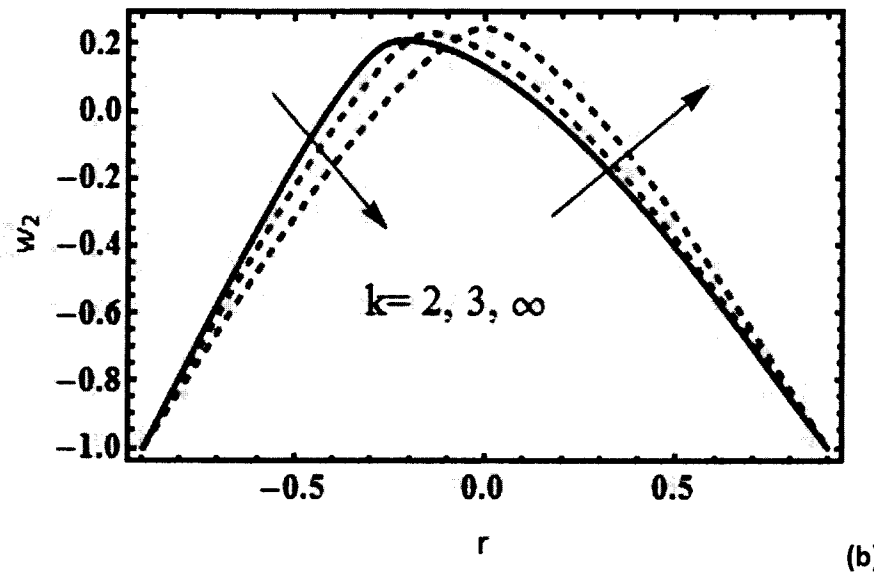

(b)

Fig. (8.2): Velocity distribution for variation of curvature parameter

(a) for viscous fluid $(n = 0)$ (b) for Carreau fluid $(n = 2)$ with other coefficients

$$d_1 = 0.3, U'_{HS} = -1, \varphi = 1.5, R_\xi = 1, m = 5, \beta = 0.1, \ \Gamma = 0.4, \alpha = 0.2 .$$

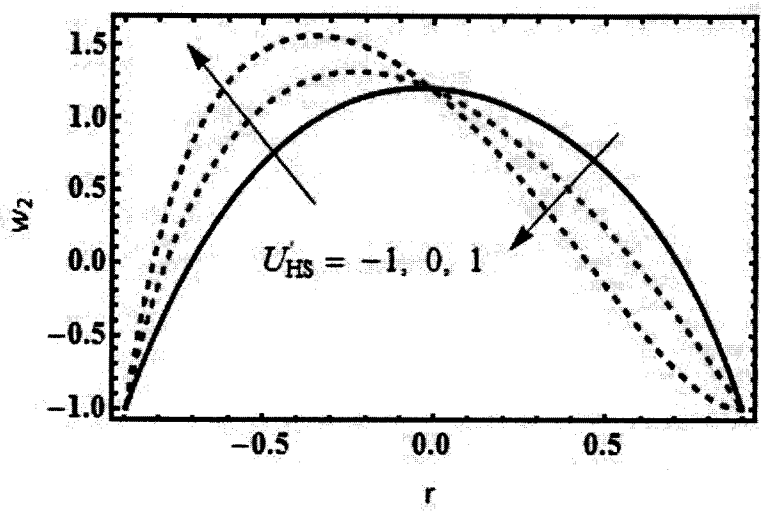

(a)

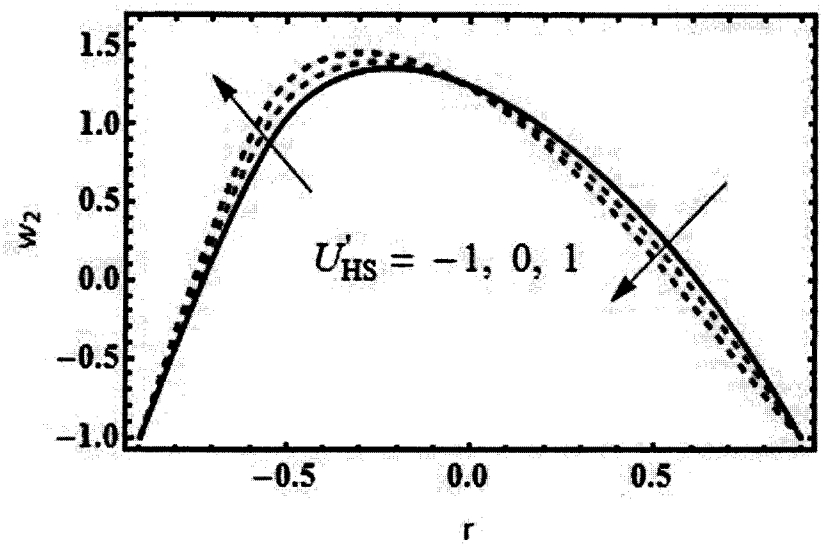

(b)

Fig. (8.3): Velocity distribution for variation of $U_{HS}^{'}$

(a) for viscous fluid $(n = 0)$ (b) for Carreau fluid $(n = 2)$ with other coefficients

$d_1 = 0.3, \varphi = 3, m = 5, R_\xi = 1, k = 1.2, \beta = 0.1, \Gamma = 0.2, \alpha = 0.2.$

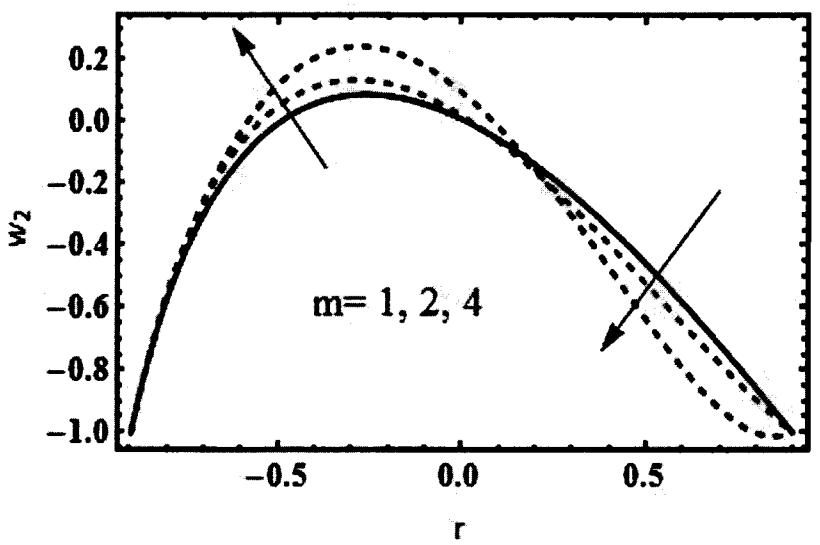

(a)

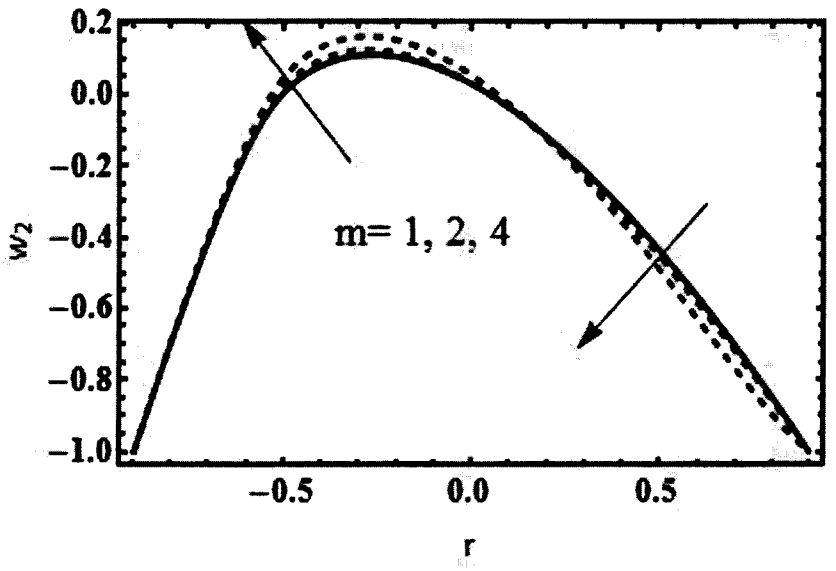

(b)

Fig. (8.4): Velocity distribution for variation of inverse EDL parameter

(a) for viscous fluid $(n=0)$ (b) for Carreau fluid $(n=2)$ with other coefficients

$R=1, d_1=0.3, U'_{HS}=-1, R_\xi=1, \varphi=1.5, k=1.2, \beta=0.1, \Gamma=0.2, \alpha=0.2.$

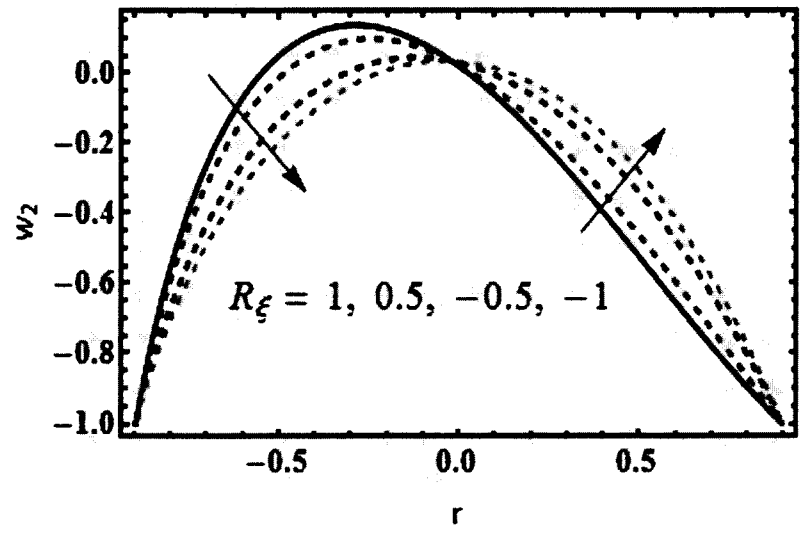

(a)

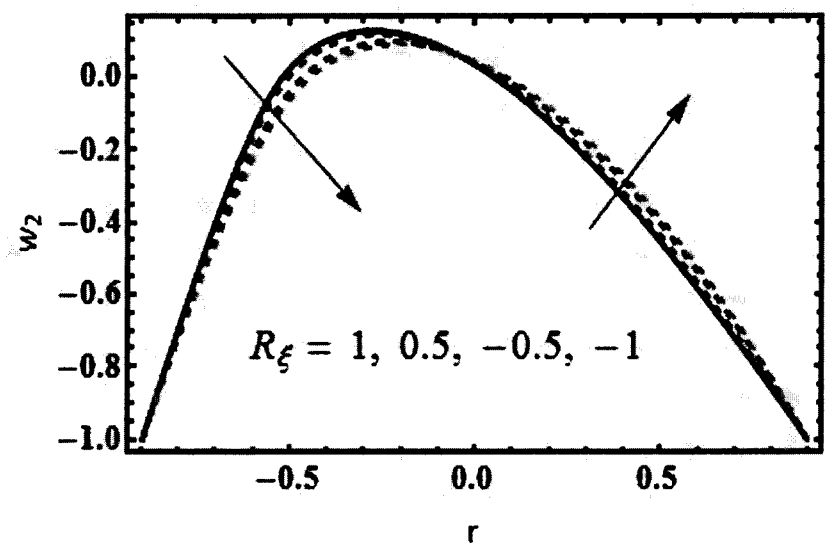

(b)

Fig. (8.5a): elocity distribution for variation of potential ratio parameter

(a) for viscous fluid $(n = 0)$ (b) for Carreau fluid $(n = 2)$ with other coefficients

$d_1 = 0.3, U'_{HS} = -1, \varphi = 1.5, m = 2, k = 1.2, \beta = 0.1, \Gamma = 0.2, \alpha = 0.2.$

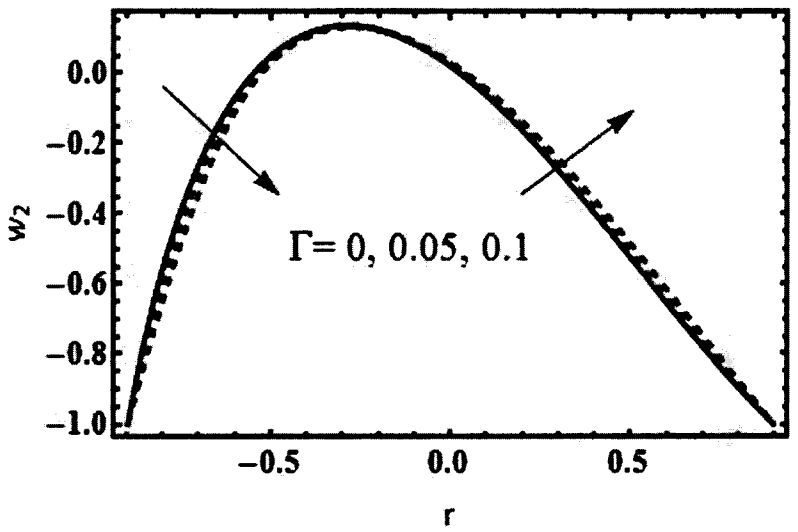

Figs. 8.6: Velocity distribution for variation of Carreau fluid parameter with other coefficients

$d_1 = 0.3, R_\xi = 1, \varphi = 1.5, m = 2, k = 1.2, \beta = 0.1, U'_{HS} = -1, \alpha = 0.2.$

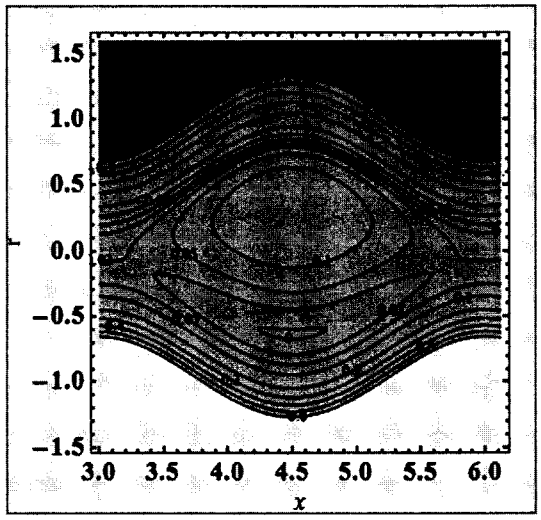

(a): m=1

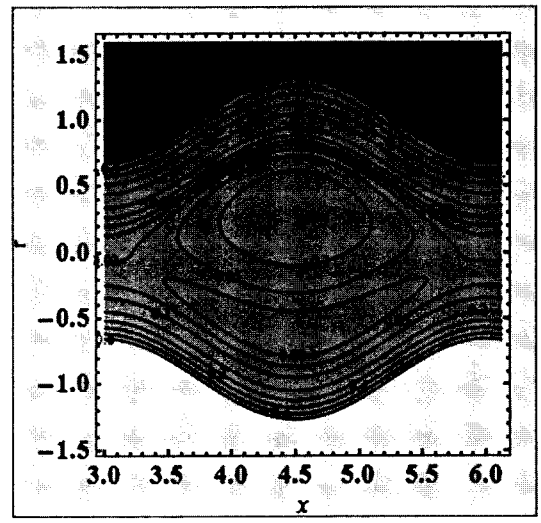

(b): m=2

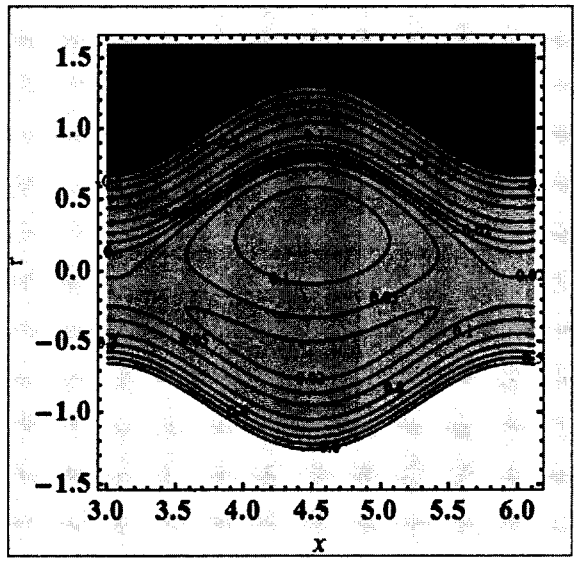

(c): m=3

Figs. (8.7a-8.7c): Stream lines for various values of inverse EDL parameter for Carreau fluid flow with other coefficients $d_1 = 0.3, R_\xi = 0.5, \varphi = 1.7, k = 1.5, \beta = 0.1, U'_{HS} = 1, \Gamma = 0.3, n = 2, \alpha = 0.2.$

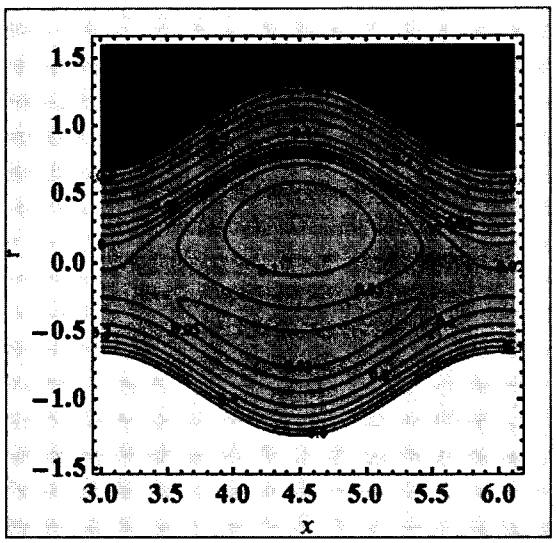

(a): k=1.3

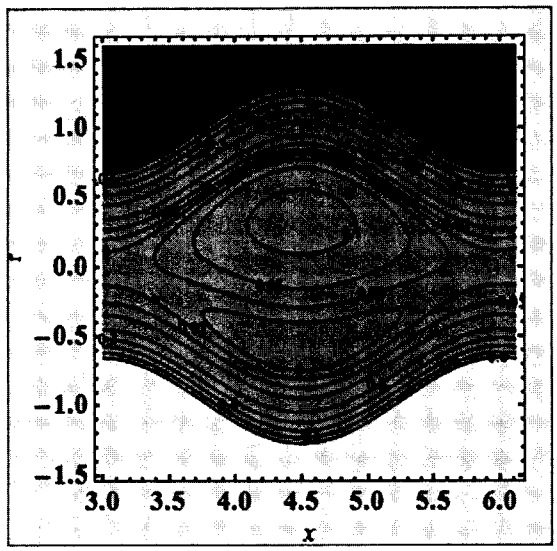

(b): k=3.0

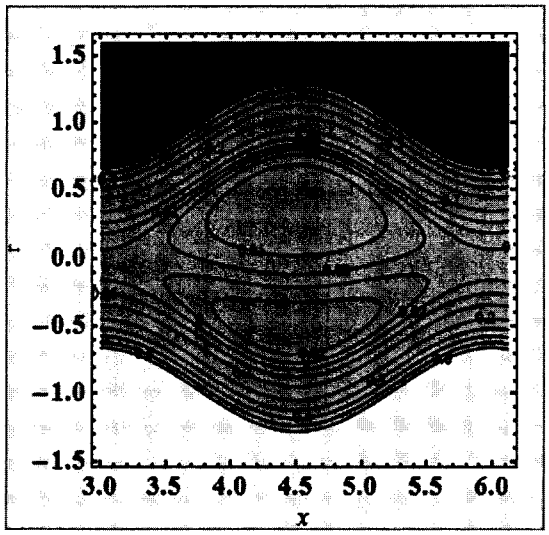

(c): k=100

Figs. (8.8a-8.8c): Stream lines for various values of curvature parameter for Carreau fluid flow with other coefficients $d_1 = 0.3, m = 2, R_\xi = 0.5, \varphi = 1.7, \beta = 0.1, U'_{HS} = 1, \Gamma = 0.3, n = 2, \alpha = 0.2$.

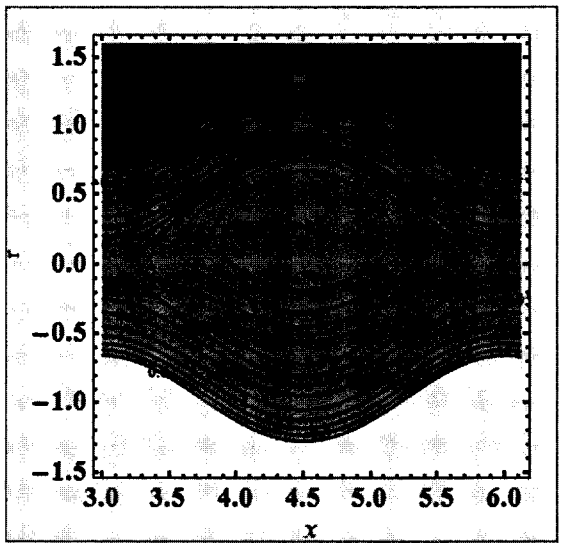

(a): $U'_{HS} = -1$

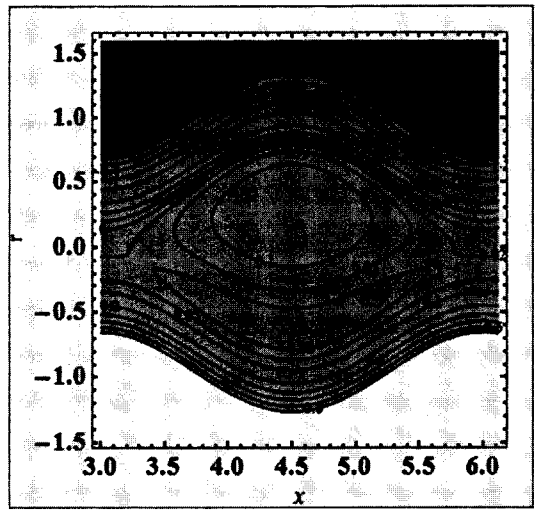

(b): $U'_{HS} = 0$

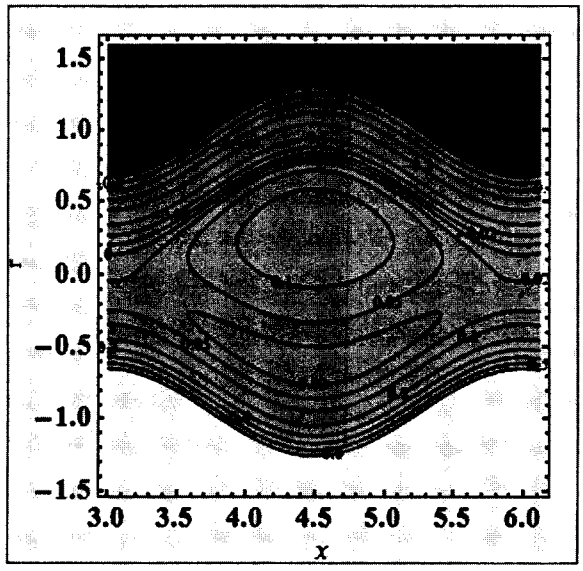

(c): $U'_{HS} = 1$

Figs. (8.9a-8.9c): Stream lines for various values of U'_{HS} for Carreau fluid flow with other coefficients $d_1 = 0.3, m = 3, R_\xi = 0.5, \varphi = 1.7, k = 1.5, \beta = 0.1, \Gamma = 0.3, n = 2, \alpha = 0.2.$

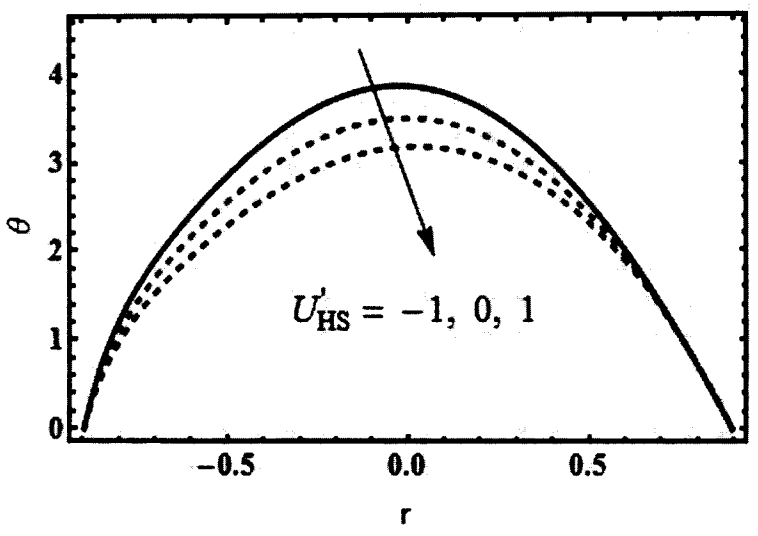

(a)

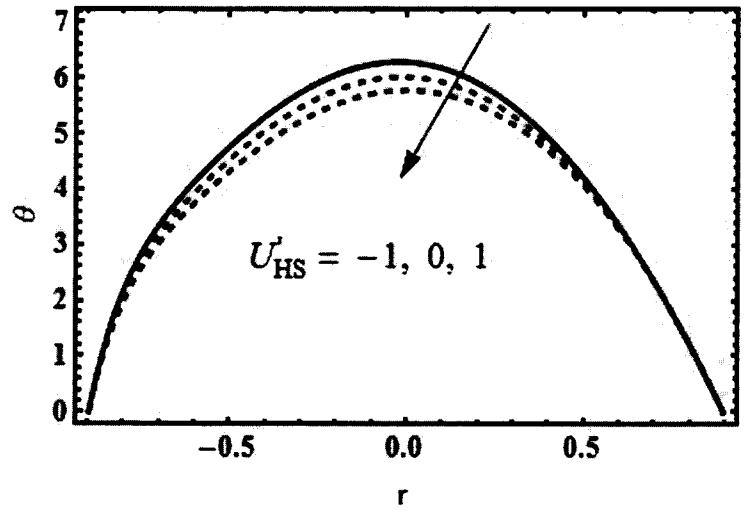

(b)

Fig. 8.10: Temperature distribution for variation of $U_{HS}^{'}$

(a) for viscous fluid $(n=0)$ (b) for Carreau fluid $(n=2)$ with other coefficients

$d_1 = 0.3, m = 1, \varphi = 3, k = 1.2, R_\xi = 1, \beta = 0.1, \Gamma = 0.08, \alpha = 0.2, \Pr = Br = 1, m = 2.$

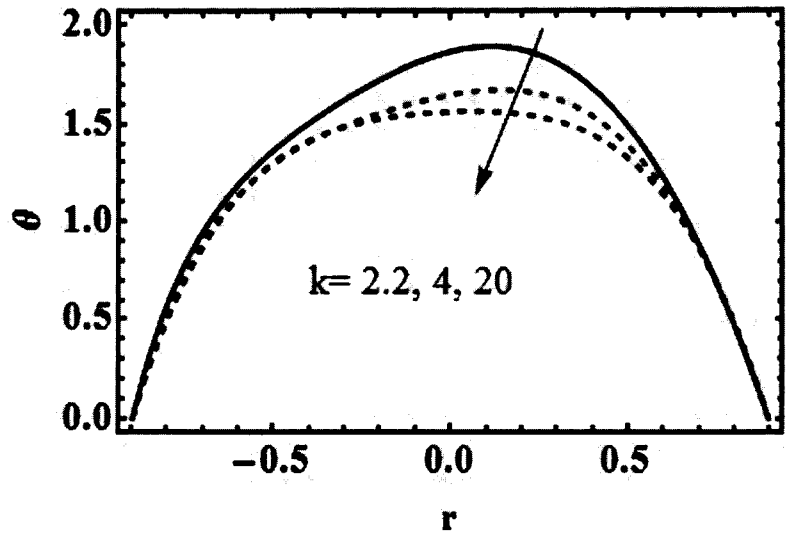

(a)

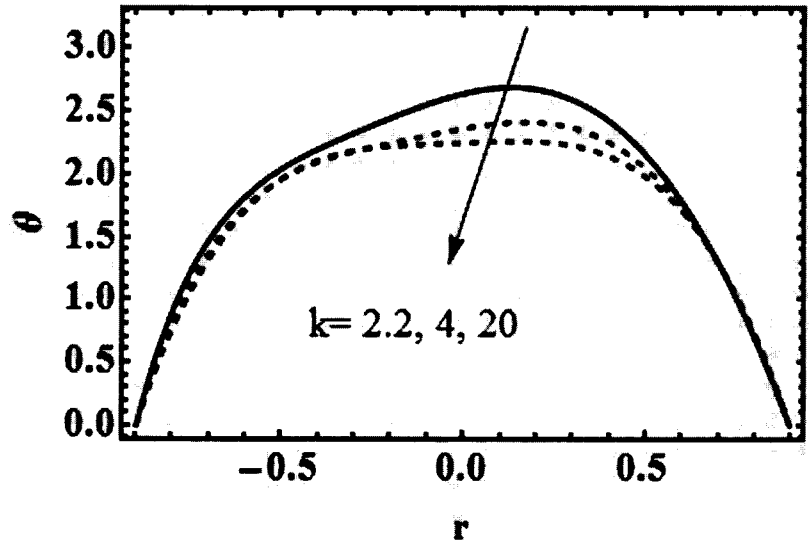

(b)

Fig. 8.11: Temperature distribution for variation of curvature parameter (a) for viscous fluid $(n = 0)$ (b) for Carreau fluid $(n = 2)$ with other coefficients $d_1 = 0.3, U'_{HS} = -1, \varphi = 3, S = 1, R_\xi = 1, \beta = 0.1, \Gamma = 0.08,\ \alpha = 0.2, \Pr = 1, m = 2.$

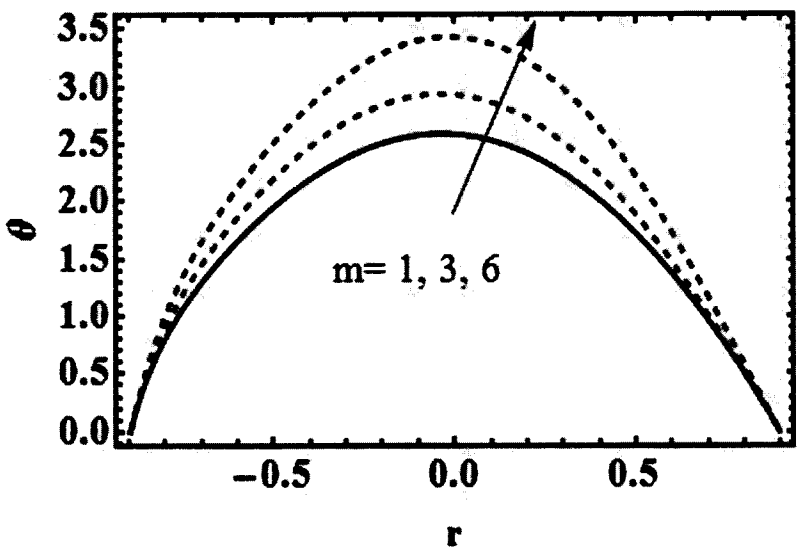

(a)

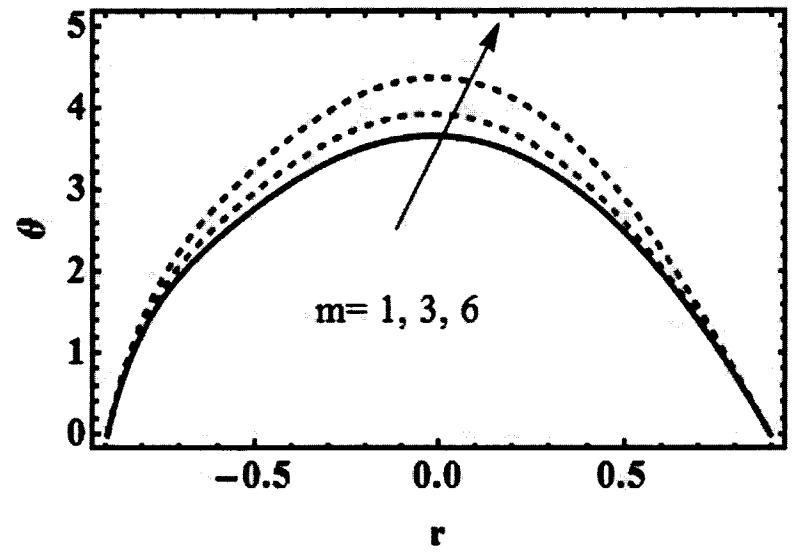

(b)

Fig. 8.12: Temperature distribution for variation of inverse EDL parameter (a) for viscous fluid $(n=0)$ (b) for Carreau fluid $(n=2)$ with other coefficients

$d_1 = 0.3, U'_{HS} = -1, \varphi = 3, k = 1.2, R_\xi = 1, \beta = 0.1, \Gamma = 0.08,\ \alpha = 0.2, \Pr = Br = 1, S = 1$

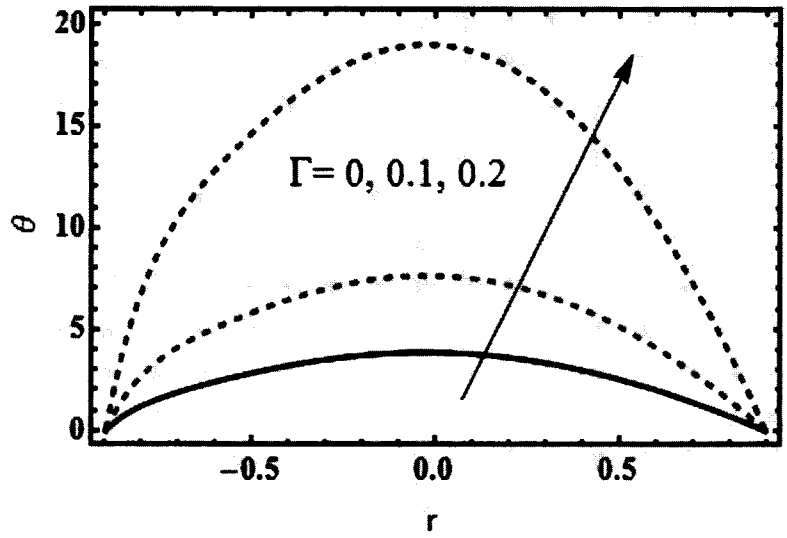

Fig. 8.13: Temperature distribution for variation of Carreau fluid parameter with other coefficients

$d_1 = 0.3, n = 2, U'_{HS} = -1, \varphi = 3, k = 1.2, R_\xi = 1, \beta = 0.1, \alpha = 0.2, \Pr = Br = 1, m = 2.$

8.3 Conclusions

This chapter addresses Carreau fluid flow in a curved microchannel via peristaltic pumping with electric field as a body force. The boundaries of the channel are subject to low zeta potential. key observations are mentioned below.

- Velocity shows dual response in the channel for various parameters due to curvature effects.
- Carreau fluid parameter is responsible to enhance the magnitude of temperature.
- Temperature rises for inverse EDL thickness parameters.
- Temperature is more in curved channel than straight geometry.
- Trend of velocity and temperature is similar qualitatively for both viscous and non-Newtonian fluids.

Chapter 9

Conclusions

This thesis discusses peristaltic transport of non-Newtonian fluid in curved geometry with the effects of variable physical properties of the materials. Heat and mass transfer effects are considered. Entropy is also modeled and investigated for various important quantities of interest.

In chapter one, brief introduction and applications of peristalsis are presented. Literature survey and fundamental equations of fluid mechanics are discussed.

In chapter two peristaltic movement of Jeffrey fluid with variable thermal conductivity and viscosity are addressed. Inclined magnetic field is applied to the flow. It is noted that axial velocity shows dual response for various parameter. Temperature decays for higher values of thermal conductivity and viscosity coefficients. Moreover, temperature is higher for curved channel in comparison to the straight channel. It is also found that entropy increases for increasing inclination of magnetic field.

Chapter three addresses heat and mass transport in peristaltic flow of MHD third grade fluid through curved channel. Soret and Dufour effects are examined. Chemical reaction with activation energy is also attended. It is found that velocity increases for temperature dependent viscosity parameter. Temperature increases for Dufour parameter whereas concentration reduces for Soret variable. For higher activation energy parameter, concentration also

increases.

Chapter four studied peristaltic transport of Sutterby fluid in curved configurations. Inclined magnetic field is also imposed. Energy expression is modeled with effects of viscous dissipation, non-linear thermal radiation and variable thermal conductivity. Entropy generation is also modeled. It is concluded that velocity decreases in lower half of the channel for higher values of Hartmann number and curvature parameter. Entropy is minimum for higher thermal conductivity and radiation parameters. Brinkman number is responsible for increases in heat transfer rate.

In chapter five non-Darcy resistance in peristaltic transport of Sutterby fluid is addressed. Soret and Dufour features have been retained. It is observed that velocity decay for Sutterby fluid parameter. Concentration decreases for both Soret and Dufour parameters while entropy increases for these variables.

Entropy generation for thermal radiation, heat absorption coefficient, variable thermal conductivity and magnetic field effects are examined in chapter six. Third grade material flow by peristalsis in curved configuration has been considered. It is noted that velocity enhances at the centre of channel for larger fluid parameter whereas it decreases for Hartman number. Trend of entropy generation is parabolic. Temperature and entropy boost up for inclination and heat absorption parameters while these reduce for radiation and thermal conductivity parameters.

In Chapter seven peristaltic flow of Sisko material is modeled with variable characteristics of thermal conductivity and viscosity via curved configuration. Entropy is also under

consideration to study irregularities in heat transfer process. It is observed that for larger thermal conductivity parameter the temperature decays whereas it increases for Sisko fluid parameter. Irregularity in heat transfer is found minimum through entropy generation for larger viscosity and thermal conductivity.

Chapter eight presents modeling of electroosmotic Carreau liquid flow through a microchannel in curved geometry. Velocity shows dual behavior for different parameters in the curved microchannel and is asymmetric near the centre due to curvature effects. Temperature decreases for EDL thickness however reversed holds for electric dissipation parameter.

Finally, it is concluded that this study will provide remarkable applications in different fields of life as peristalsis has prime importance in the fields of physiology, industries and engineering.

References

1. Latham TW, Fluid motion in a peristaltic pump, [MS thesis]. MIT, Cambridge. 1966.
2. Burns JC and Parkes T, Peristaltic motion, Journal of Fluid Mechanics. 29 (1967) 731-743.
3. Shapiro AH, Jaffrin MY and Weinberg SL, Peristaltic pumping with long wavelengths at low Reynolds number, Journal of Fluid Mechanics. 37 (1969) 799-825.
4. Yin FCP and Fung YC, Comparison of theory and experiment in peristaltic transport, Journal of Fluid Mechanics. 47 (1971) 93-112.
5. Barton C and Raynor S, Peristaltic flow in tubes. The Bulletin of mathematical biophysics, 30 (1968) 663-680.
6. Lew HS, Fung YC and Lowenstein CB, Peristaltic carrying and mixing of chyme in the small intestine (an analysis of a mathematical model of peristalsis of the small intestine), Journal of Biomechanics. 4 (1971) 297-315.
7. Tong P and Vawter D, An analysis of peristaltic pumping. Journal of Applied Mechanics, 39 (1972) 857-862.
8. Li CH, Peristaltic transport in circular cylindrical tubes, Journal of Biomechanics, 3 (1970) 513-523.
9. Mittra TK and Prasad SN, Interaction of peristaltic motion with Poiseuille flow, Bulletin of Mathematical Biology, 36 (1974) 127-141.
10. Liron N. On peristaltic flow and its efficiency, Bulletin of Mathematical Biology. 38 (1976) 573-596.

11. Jaffrin MY, Inertia and streamline curvature effects on peristaltic pumping, International Journal of Engineering Science., 11 (1973) 681-699.

12. Gupta BB and, Seshadri V, Peristaltic pumping in non-uniform tubes, Journal of Biomechanics. 9 (1976) 105-109.

13. Vishnyakov VI, Pavlov KB and Romanov AS. Peristaltic flow of a non-Newtonian viscoplastic liquid in a slot channel. Journal of Engineering Physics. 31 (1976) 1078-1082.

14. Manero O Mena B and Valenzuela R, Further developments on non-Newtonian flow in oscillating pipes, Rheologica Acta, 17 (1978) 693-697.

15. Srivastava LM, Srivastava VP and Sinha SN, Peristaltic transport of a physiological fluid, Biorheology. 20 (1983) 153-166.

16. Böhme G and Friedrich R. Peristaltic flow of viscoelastic liquids. Journal of Fluid Mechanics. 128 (1983) 109-122.

17. Srivastava LM and Srivastava VP, Peristaltic transport of a two-layered model of physiological fluid, Journal of Biomechanics. 15 (1982) 257-265.

18. Takabatake S and Ayukawa K, Numerical study of two-dimensional peristaltic flows, Journal of Fluid Mechanics. 122 (1982) 439-465.

19. Pozrikidis C. A study of peristaltic flow, Journal of Fluid Mechanics, 180 (1987) 515-527.

20. Li M and Brasseur JG, Non-steady peristaltic transport in finite-length tubes, Journal of Fluid Mechanics. 248 (1993) 129-151.

21. Rao R and Mishra M, Nonlinear and curvature effects on peristaltic flow of a viscous fluid in an asymmetric channel, Acta Mechanica. 168 (2004) 35-59.

22. Mekheimer KS, Peristaltic transport of a Newtonian fluid through a uniform and non-uniform annulus, Arabian Journal for Science and Engineering. 30 (2005) 69-83.

23. Provost AM, Schwarz WH, A theoretical study of viscous effects in peristaltic pumping, Journal of Fluid Mechanics. 279 (1994) 177-195.

24. Mekheimer KS, Shankar BM and Abo-Elkhair RE, Effects of Hall current and permeability on the stability of peristaltic flow, SN Applied Sciences. 1 (2019) 1-9.

25. Tariq H, Khan AA and Zaman A, Theoretical analysis of peristaltic viscous fluid with inhomogeneous dust particles, Arabian Journal for Science and Engineering. 46 (2021) 31-39.

26. Raju KK and Devanathan R, Peristaltic motion of non-Newtonian, Part-I, Rheologica acta. 11 (1972) 170-178.

27. Raju KK and Devanathan R, Peristaltic motion of non-Newtonian, Part-I: Viscoelastic. Rheologica acta. 13 (1974) 944-948.

28. Siddiqui AM and Schwarz WH, Peristaltic pumping of a third order fluid in a planer channel, Rheologica acta. 32 (1993) 47-56.

29. Siddiqui AM, Provost A and Schwarz WH, Peristaltic flow of a second order fluid in tubes, Journal of Non-Newtonian Fluid Mechanics. 53 (1994) 257-284.

30. Srivastava LM, Peristaltic transport of a couple-stress fluid, Rheologica Acta. 25 (1986) 638-641.

31. Hayat T, Wang Y, Siddiqui AM, Hutter K and Asghar S, Peristaltic transport of a third order fluid in a circular cylindrical tube, Mathematical Models and Methods in Applied Sciences. 12 (2002) 1691-1706.

32. Hayat T, Wang Y, Siddiqui AM and Hutter K, Peristaltic motion of Johnson Segalman fluid in a planar channel, Mathematical Problems in Engineering. 1 (2003) 01-23.

33. Wang Y, Hayat T and Hutter K, Peristaltic flow of a Johnson-Segalman fluid through a deformable tube, Theoretical and Computational Fluid Dynamics. 21 (2007) 369-380.

34. Haroun MH, Effect of Deborah number and phase difference on peristaltic transport of a third-order fluid in an asymmetric channel, Comm. Non-linear Sci. Numer. Simul. 8 (2007) 1464-1480.

35. Ali N and Hayat T, Peristaltic motion of a Carreau fluid in an asymmetric channel, Applied Mathematics and Computation. 193 (2007) 535-552.

36. Hayat T, Khan AA, Bibi F, Farooq S, Activation energy and non-Darcy resistance in magneto peristalsis of Jeffrey material, Journal of Physics and Chemistry of Solids. 2019;129:155-61.

37. Hayat T, Aslam N, Khan MI, Khan MI and Alsaedi A, Physical significance of heat generation/absorption and Soret effects on peristalsis flow of pseudoplastic fluid in an inclined channel, Journal of Molecular Liquids. 275 (2019) 599-615.

38. Hino T and Yanagimachi R, Active peristaltic movements and fluid production of the mouse oviduct: their roles in fluid and sperm transport and fertilization, Biology of reproduction. 101 (2019) 40-49.

39. Babu VR, Peristaltic flow of Bingham fluid in an inclined tube. International Journal of Engineering Development and Research. 7 (2019) 127 -132.

40. Formato G, Romano R, Formato A, Sorvari J, Koiranen T, Pellegrino A and Villecco F, Fluid-Structure Interaction Modeling Applied to Peristaltic Pump Flow Simulations. Machines. 7 (2019): doi.org/10.3390/machines7030050

41. Reddappa B, Parandhama A and Sreenadh S, Peristaltic transport of conducting Williamson fluid in a porous channel, International Journal of Mathematics and Computer Science. 10 (2019) 277-288.

42. Sato H, Kawai T, Fujita T and Okabe M. Two dimensional peristaltic flow in curved channels. The Japan Society of Mechanical Engineering. B. 66 (2000) 679-85.

43. Ali Ali N, Sajid M and Hayat T, Long wavelength flow analysis in a curved channel, Zeitschrift für Naturforschung A. 65 (2010) 191-106.

44. Ali N, Sajid M, Abbas Z and Javed T, Non-Newtonian fluid flow induced by peristaltic waves in a curved channel. European Journal of Mechanics-B/Fluids, 29 (2010) 387-394.

45. Hayat T, Noreen S and Alsaedi A, Effect of an induced magnetic field on peristaltic flow of non-Newtonian fluid in a curved channel, Journal of Mechanics in Medicine and Biology. 12 (2012): 1250058.

46. Hina S, Hayat T, Mustafa M, Aldossary OM and Asghar S, Effect of wall properties on the peristaltic flow of a third grade fluid in a curved channel, Journal of Mechanics in Medicine and Biology. 12 (2012): 1250067.

47. Ramanamurthy JV, Prasad KM and Narla VK, Unsteady peristaltic transport in curved channels, Physics of Fluids. 25 (2013): 091903.

48. Narla VK, Prasad KM and Ramanamurthy JV, Peristaltic motion of viscoelastic fluid with fractional second grade model in curved channels, Chinese journal of chemical engineering. 25 (2013): 582390.

49. Hayat T, Abbasi FM, Ahmad B and Alsaedi A, Peristaltic transport of Carreau-Yasuda fluid in a curved channel with slip effects, PloS one. 9 (2014): e95070.

Abbasi FM, Alsaedi A and Hayat T, Peristaltic transport of Eyring-Powell fluid in a curved channel, Journal of Aerospace Engineering. 27 (2017): 04014037.

50. Hina S, Mustafa M and Hayat T, Peristaltic motion of Johnson-Segalman fluid in a curved channel with slip conditions, PloS one. 9 (2014): e114168.
51. Hina S, Mustafa M, Hayat T and Alotaibi ND, On peristaltic motion of pseudoplastic fluid in a curved channel with heat/mass transfer and wall properties, Applied Mathematics and Computation. 263 (2015) 378-391.
52. Ahmed R, Ali N, Al-Khaled K, Khan SU and Tlili I, Finite difference simulations for non-isothermal hydromagnetic peristaltic flow of a bio-fluid in a curved channel: applications to physiological systems, Computer Methods and Programs in Biomedicine. 195 (2020): 105672.
53. Hayat T, Rafiq M, Alsaadi F and Ayub M, Soret and Dufour effects on peristaltic transport in curved channel with radial magnetic field and convective conditions, Journal of Magnetism and Magnetic Materials. 405 (2016) 358-369.
54. Asghar Z, Ali N, Ahmed R, Waqas M and Khan WA, A mathematical framework for peristaltic flow analysis of non-Newtonian Sisko fluid in an undulating porous curved channel with heat and mass transfer effects, Computer methods and programs in biomedicine. 182 (2019):105040.
55. Nawaz S, Hayat T and Alsaedi A, Analysis of entropy generation in peristalsis of Williamson fluid in curved channel under radial magnetic field, Computer methods and programs in biomedicine. 180 (2019):105013.

56. Tanveer A, Hayat T and Alsaedi A, Peristaltic flow of MHD Jeffery nanofluid in curved channel with convective boundary conditions: a numerical study, Neural Computing and Applications. 30 (2018) 437-446.

57. Hayat T, Farooq S and Alsaedi A, Mixed convection peristaltic motion of copper-water nanomaterial with velocity slip effects in a curved channel, Computer Methods and Programs in Biomedicine. 142 (2017) 117-128.

58. Stud VK, Sephon GS and Mishra RK, Pumping action on blood flow by a magnetic field, Bulletin of Mathematical Biology. 39 (1977): doi: 10.1007/BF02462917

59. Srivastava LM and Agrawal RP, Oscillating flow of a conducting fluid with a suspension of spherical particles, Journal of Applied Mechanics. 47 (1980) 196.

60. Mekheimer KS, Peristaltic flow of blood under effect of a magnetic field in a non-uniform channels. Applied Mathematics and Computation, 153 (2004) 763-777.

61. Krzeminski SK, Smialek M and Wlodarczyk M, Numerical analysis of peristaltic MHD flows, IEEE Transactions on Magnetics. 36 (2000) 1319-1324.

62. Afifi NAS and Gad NS, Interaction of peristaltic flow with pulsatile magneto-fluid through a porous medium, Acta Mechanica. 149 (2001) 229-237.

63. Mekheimer KS and Al-Arabi TH, Nonlinear peristaltic transport of MHD flow through a porous medium, International Journal of Mathematics and Mathematical Sciences. 26 (2033) 1663-1682.

64. El Naby AEHA, El Misery AEM and El Kareem MA, Effects of a magnetic field on trapping through peristaltic motion for generalized Newtonian fluid in channel, Physica A: Statistical Mechanics and its Applications. 367 (2006) 79-92.

65. Hayat T, Khan M, Siddiqui AM and Asghar S, Non-linear peristaltic flow of a non-Newtonian fluid under effect of a magnetic field in a planar channel, Communications in Nonlinear Science and Numerical Simulation. 12 (2007) 910-919.

66. Hayat T and Ali N, Peristaltically induced motion of a MHD third grade fluid in a deformable tube, Physica A: Statistical Mechanics and its Applications. 370 (2006) 225-239.

67. Hayat T, Afsar A, Khan M and Asghar S, Peristaltic transport of a third order fluid under the effect of a magnetic field, Computers and Mathematics with Applications. 53 (2007) 1074-1087.

68. Mekheimer KS, Peristaltic flow of blood under effect of a magnetic field in a non-uniform channels, Applied Mathematics and Computation. 153 (2004) 763-777.

69. Mekheimer KS and Elmaboud YA, Peristaltic flow through a porous medium in an annulus: application of an endoscope, Applied Mathematics & Information Sciences. 2 (2008) 103-121.

70. Tanveer A, Khan M, Salahuddin T, Malik MY and Khan F, Theoretical investigation of peristaltic activity in MHD based blood flow of non-Newtonian material, Computer Methods and Programs in Biomedicine. 187 (2020):105225.

71. Tanveer A, Hayat T, Alsaedi A and Ahmad B, Heat transfer analysis for peristalsis of MHD Carreau fluid in a curved channel through modified Darcy law, Journal of Mechanics. 35 (2019) 527-535.

72. Hayat T, Bibi F, Farooq S and Khan AA, Nonlinear radiative peristaltic flow of Jeffrey nanofluid with activation energy and modified Darcy's law, Journal of the Brazilian Society of Mechanical Sciences and Engineering. 41 (2019):1-11.

73. Farooq S, Hayat T and Ahmad B, A theoretical analysis for peristalsis of Casson material with thermal radiation and viscous dissipation, Thermal Science. 23 (2019) 3351-3364.

74. Farooq S, Hayat T, Khan MI and Alsaedi A, Entropy generation minimization (EGM) in magneto peristalsis with variable properties, Computer Methods and Programs in Biomedicine. 186 (2020):105045.

75. Khan WA, Farooq S, Kadry S, Hanif M, Iftikhar FJ and Abbas SZ, Variable characteristics of viscosity and thermal conductivity in peristalsis of magneto-Carreau nanoliquid with heat transfer irreversibilities, Computer Methods and Programs in Biomedicine. 190 (2020):105355.

76. Vajravelu K, Radhakrishnamacharya G and Radhakrishnamurty V, Peristaltic flow and heat transfer in a vertical porous annulus with long wave approximation, International Journal of Non-Linear Mechanics. 42 (2007) 754-759.

77. Ali N, Sajid M, Javed T and Abbas Z, Heat transfer analysis of peristaltic flow in a curved channel, International Journal of Heat and Mass Transfer. 53 (2010) 3319-3325.

78. Srinivas S and Kothandapani M, The influence of heat and mass transfer on MHD peristaltic flow through a porous space with compliant walls, Applied Mathematics and Computation. 213 (2009) 197-208.

79. Hayat T, Hina S and Ali N, Simultaneous effects of slip and heat transfer on the peristaltic flow, Communications in Nonlinear Science and Numerical Simulation. 15 (2010) 1526-1537.

80. Ellahi R, Bhatti MM and Vafai K, Effects of heat and mass transfer on peristaltic flow in a non-uniform rectangular duct, International Journal of Heat and Mass Transfer. 71 (2014) 706-719.

81. Sinha A, Shit GC and Ranjit NK, Peristaltic transport of MHD flow and heat transfer in an asymmetric channel: Effects of variable viscosity, velocity-slip and temperature jump, Alexandria Engineering Journal. 54 (2015) 691-704.

82. Vaidya H, Rajashekhar C, Manjunatha G, Prasad KV, Makinde OD and Sreenadh S, Peristaltic motion of non-Newtonian fluid with variable liquid properties in a convectively heated nonuniform tube: Rabinowitsch fluid model, Journal of Enhanced Heat Transfer. 26 (2019) doi: 10.1615/JEnhHeatTransf.2019029230

83. Manjunatha G, Rajashekhar C, Vaidya H, Prasad KV and Divya BB, Heat transfer analysis on peristaltic transport of a Jeffery fluid in an inclined elastic tube with porous walls, International Journal of Thermofluid Science and Technology. 7 (2020): 20070101.

84. Bejan A, Second law analysis in heat transfer, Energy. 5 (1980) 720–732.

85. Bejan A, Entropy generation minimization: the method of thermodynamic optimization of finite-size systems and finite-time processes., New York: CRC Press; 2013. p. 1996.

86. Souidi F, Ayachi K and Benyahia N, Entropy generation rate for a peristaltic pump, Journal of Non-Equilibrium Thermodynamics. 34 (2009) 171-194.

87. Abbas MA, Bai Y, Rashidi MM and Bhatti MM, Analysis of entropy generation in the flow of peristaltic nanofluids in channels with compliant walls, Entropy. 2016;18:90.

88. Rashidi M, Bhatti, M. Abbas M and Ali M, Entropy generation on MHD blood flow of nanofluid due to peristaltic waves, Entropy.18 (2016): doi.org/10.3390/e18040117

89. Hayat T, Rafiq M, Ahmad B and Asghar S, Entropy generation analysis for peristaltic flow of nanoparticles in a rotating frame, International Journal Heat and Mass Transfer. 108 (2017) 1775-1786.

90. Khan MI, Qayyum S, Hayat T and Alsaedi A, Entropy generation minimization and statistical declaration with probable error for skin friction coefficient and Nusselt number Chinese Journal of Physics. 56 (2018) 1525-1546.

91. Farooq S, Hayat T, Alsaedi and Asghar S, Mixed convection peristalsis of carbon nanotubes with thermal radiation and entropy generation. Journal of Molecular Lliquids. 250 (2018) 451-467.

92. Afridi MI, Qasim M and Makinde OD, Entropy generation due to heat and mass transfer in a flow of dissipative elastic fluid through a porous medium, Journal of Heat Transfer. 141 (2019): doi.org/10.1115/1.4041951

93. Noreen S, Abbas A and Hussanan A, Entropy Generation via Ohmic Heating and Hall Current in Peristaltically-Flowing Carreau Fluid, Entropy. 21 (2019): doi: 10.3390/e21050529

94. Khan MI, Farooq S, Hayat T, Shah F and Alsaedi A. Numerical simulation for entropy generation in peristaltic flow with single and multi-wall carbon nanotubes. International Journal of Numerical Methods for Heat & Fluid Flow. 29 (2019) 4684-4705.

95. Nawaz S, Hayat T and Alsaedi A, Analysis of entropy generation in peristalsis of Williamson fluid in curved channel under radial magnetic field, Computer Methods and Programs in Biomedicine. 180 (2019): 105013.

96. Reddy MVS and Reddy DP, Peristaltic pumping of a Jeffrey fluid with variable viscosity through a porous medium in a planar channel, International Journal of Mathematical Archive. 1 (2010) 42-54.

97. Ali N, Hussain Q, Hayat T and Asghar S, Slip effects on the peristaltic transport of MHD fluid with variable viscosity, Physics Letter A. 372 (2008) 1477-1489.

98. Eldabe NTM, El-Sayed MF, Ghaly AY and Sayed MH, Mixed convective heat and mass transfer in a non-Newtonian fluid at a peristaltic surface with temperature dependent viscosity, Archive of Applied Mechanice. 78 (2008) 599-624.

99. Tanveer A, Hayat T and Alsaed A, Variable viscosity in peristalsis of Sisko fluid, Applied Mathematics and Mechanics (English Edition). 39 (2018) 501-512.

100. Q. Hussain, S. Asghar, T. Hayat and A. Alsaedi, Heat transfer analysis in peristaltic flow of MHD Jeffrey fluid with variable thermal conductivity, Applied Mathematics Mechanics. 36 (2015) 499-516.

101. Hussain Q, Latif T, Alvi N and Asghar S, Nonlinear radiative peristaltic flow of hydromagnetic fluid through porous medium, International Journal of Results in Physics. 9 (2018) 121-134.

102. Hayat T, Abbasi FM, Ahmad B and Alsaedi A, MHD mixed convective peristaltic flow with variable viscosity and thermal conductivity, Sains Malaysiana. 43 (2014) 1583-1590.

103. Hussain Q, Asghar S, Hayat T and Alsaedi A, Peristaltic transport of hydromagnetic Jeffrey fluid with temperature dependent viscosity and thermal conductivity, International Journal of Biomathematics. 9 (2015): 1650029.

104. Latif T, Alvi N, Hussain Q and Asghar S, Variable properties of MHD third order fluid with peristalsis. International Journal of Results in Physics. 6 (2016) 963-972.

105. Abbasi F, Hayat T and Ahmad B, Hydromagnetic peristaltic transport of variable Viscosity fluid with heat transfer and porous medium, Journal of Applied Mathematics and Information Sciences. 10 (2016) 2173-2181.

106. Tripathi D, Sharma A and Bég OA, Electrothermal transport of nanofluids via peristaltic pumping in a finite micro-channel: Effects of Joule heating and Helmholtz-Smoluchowski velocity, International Journal of Heat and Mass Transfer. 111 (2017) 138-149.

107. Tripathi D, Sharma A and Bég OA, Joule heating and buoyancy effects in electro-osmotic peristaltic transport of aqueous nanofluids through a microchannel with complex wave propagation, Advanced Powder Technology. 29 (2018) 639-653.

108. Narla VK, Tripathi D and Sekhar GR, Time-dependent analysis of electroosmotic fluid flow in a microchannel, Journal of Engineering Mathematics. 114 (2019) 177-196.

109. Narla VK, Tripathi D and Bég OA, Electro-osmosis modulated viscoelastic embryo transport in uterine hydrodynamics: mathematical modeling, Journal of Biomechanical Engineering. 141 (2019) doi.org/10.1115/1.4041904

110. Narla VK and Tripathi D, Electroosmosis modulated transient blood flow in curved microvessels: Study of a mathematical model. Microvascular Research. 123(2019) 25-34.

111. Narla VK, Tripathi D and Bég OA, Analysis of entropy generation ain biomimetic electroosmotic nanofluid pumping through a curved channel with joule dissipation, Thermal Science and Engineering Progress. 15 (2020):100424.